Utah State University

DigitalCommons@USU

All Graduate Theses and Dissertations

Graduate Studies

5-2013

The Phosphoramidase Compentency of Prototypical Phosphatase Catalytic Motifs

Mark P. Haney

Follow this and additional works at: https://digitalcommons.usu.edu/etd

Part of the Biochemistry Commons

Recommended Citation

Haney, Mark P., "The Phosphoramidase Compentency of Prototypical Phosphatase Catalytic Motifs" (2013). *All Graduate Theses and Dissertations*. 1483.
https://digitalcommons.usu.edu/etd/1483

This Dissertation is brought to you for free and open access by the Graduate Studies at DigitalCommons@USU. It has been accepted for inclusion in All Graduate Theses and Dissertations by an authorized administrator of DigitalCommons@USU. For more information, please contact digitalcommons@usu.edu.

UtahStateUniversity
MERRILL-CAZIER LIBRARY

THE PHOSPHORAMIDASE COMPETENCY OF PROTOTYPICAL PHOSPHATASE CATALYTIC MOTIFS

by

Mark P. Haney

A dissertation submitted in partial fulfillment
of the requirements for a degree

of

DOCTOR OF PHILOSOPHY

in

Chemistry

Approved:

Alvan C. Hengge Major Professor	Lisa M. Berreau Committee Member
Cheng-Wei Tom Chang Committee Member	Bradley S. Davidson Committee Member
Daren P. Cornforth Committee Member	Mark R. McLellan Vice President for Research and Dean of the School of Graduate Studies

UTAH STATE UNIVERSITY
Logan, Utah

2013

Copyright © Mark P. Haney

All Rights Reserved

ABSTRACT

The Phosphoramidase Competency of Prototypical Phosphatase Catalytic Motifs

by

Mark P. Haney, Doctor of Philosophy

Utah State University, 2013

Major Professor: Dr. Alvan C. Hengge
Department: Chemistry and Biochemistry

The discovery that phosphorylation of proteins occurs on nitrogen by particular kinases raises the question of whether a separate class of phosphoramidases also exists, or if known phosphatases carry out the hydrolysis of phosphoramidates. The phosphoramidase activity of a number of phosphatases with different catalytic motifs was studied using the substrates *N*-phenylphosphoramidate (*N*-phPAM) and phosphoryl imidazole (PIm). The phosphatases assayed were: the protein tyrosine phosphatase YopH; alkaline phosphatase; the dual-specificity phosphatase VHR; prostatic acid phosphatase, PAcP; PHPT1, the only known phosphohistidine phosphatase; and the serine/threonine phosphatases λPP and PP1. The catalytic efficiencies, k_{cat}/K_M ($s^{-1}M^{-1}$), were compared for the respective phosphoramidase and phosphatase activities for each enzyme. Ratios of catalytic efficiencies $(k_{cat}/K_M)/(k_{cat}/K_M)$ of *p*NPP over PIm are: YopH – 27; AP – 4.1; VHR – 0.22; PAcP – 1.6; AP – 0.51; and PHPT1 – 0.00007. λPP catalyzed hydrolysis of PIm, although kinetic constants could not be obtained. PP1 exhibited no phosphoramidase activity. The results show that most phosphatase catalytic motifs display catalytic promiscuity by cleaving both phosphoesters and phosphoramidates, but with a pronounced preference for one substrate type versus the other.

(199 pages)

Public Abstract

The Phosphoramidase Competency of Prototypical Phosphatase Catalytic Motifs

Mark P. Haney

Utah State University, 2013

Phosphorylation of proteins is ubiquitous. Phosphorylation can activate proteins, deactivate proteins, assist in signaling, or serve other roles depending upon the biochemical pathway. Attaching phosphate to proteins is accomplished by enzymes called kinases; removing phosphate from proteins is accomplished by enzymes called phosphatases. Cells must regulate their biochemical pathways, and the antipodal roles of kinases and phosphatases represent the yin-yang of phosphorylation.

Phosphorylation of proteins is known to occur on serine, threonine, and tyrosine. This creates a phosphoester bond. Phosphoester bonds have a phosphorus-oxygen (P-O) bond. The ability of phosphatases to cleave such phosphoester bonds is well studied. Phosphorylation of proteins is also known to occur on lysine, arginine, and histidine. This creates a phosphoramidate bond. Phosphoramidate bonds have a phosphorus-nitrogen (P-N) bond. The ability of phosphatases to cleave such phosphoramidate bonds is not well studied. The research herein involved a side-by-side comparison of the abilities of the known phosphatases to cleave the P-O bond of *p*NPP and the P-N bonds of *N*-phenyl phosphoramidate and phosphoryl imidazole.

The enzymes selected were well-studied phosphatases possessing a catalytic motif representative of a class of enzymes. The phosphatases assayed were: the protein tyrosine phosphatase YopH; alkaline phosphatase; the dual-specificity phosphatase VHR; prostatic acid phosphatase, PAcP; PHPT1, the only known phosphohistidine phosphatase; and the serine/threonine phosphatases λPP and PP1. The catalytic efficiencies, k_{cat}/K_M ($s^{-1}M^{-1}$), were compared for the respective phosphoramidase and phosphatase activities for each enzyme. Ratios of catalytic efficiencies $(k_{cat}/K_M)/(k_{cat}/K_M)$ of *p*NPP over PIm are: YopH – 27; AP – 4.1; VHR – 0.22; PAcP – 1.6; AP – 0.51; and PHPT1 – 0.00007. λPP catalyzed hydrolysis of PIm, although kinetic constants could not be obtained. PP1 exhibited no phosphoramidase activity. The results show that most phosphatase catalytic motifs display catalytic promiscuity by cleaving both phosphoesters and phosphoramidates, but with a pronounced preference for one substrate type versus the other.

DEDICATION

To my wife Stefanie, who has supported me in this endeavor. And to my daughter, Mica, and son, Thorin, who have taught me about life as I have taught them.

ACKNOWLEDGMENTS

Money to run a lab and pay graduate students doesn't fall from the sky like manna from heaven. The professor has to chase it down. Hours thinking up projects, digging through the literature, and getting preliminary results precede any grant application. Once that's done, there's the stress of writing the application, submitting it, and God willing, actually getting the funds. The agencies providing funds are filled with people who expect results for the funds. So having the money doesn't mean less stress. It's just a different kind of stress.

When I started graduate school my faculty advisor wasn't the head of the chemistry department. Sometime during my tenure as a student he became the department head. This had to be more stress.

During the past five years I felt stress to get results. My first year's project took almost an entire year and resulted in nothing but experience. Nature decided my efforts were to be rewarded with a null result. I moved to a different project that had some literature background, but there were many unanswered questions. Two of the biggest questions were: 1) how is the experiment actually to be conducted, and 2) is the experiment even doable? It took me the better part of two years to figure out the answer to question 1, all the while question 2 was nagging at my mind. So, for three years I was having quite a bit of stress. I'm not deeply religious, but was praying a lot.

The stress I felt was mine. During this time I did not feel unduly pressured by Prof. Hengge to get results. He found the money, he owned the lab, he needed results, he was the department head, he had some stress.

We both came to the chemistry building in the morning, he did his job, I did mine. We both had stress. Like a good boss he insulated me from the stresses he was having related to my research. I focused on the science. I focused on the results. I focused on classes. I focused on TA duties. I was able to focus on what I was supposed to be focusing on because my boss was a good boss. Thanks boss. I noticed the things you did for me, even when I wasn't around.

My committee is comprised of people who helped polish a rough-around-the-edges Jarhead. With the exception of Prof. Cornforth, I've been a student in each member's class. During my cumulative exams, orals, and dissertation proofs I received no quarter. But, I knew I wouldn't and put my efforts into each event. It made me smarter. I've received good feedback, and in the process have become more professional in science. I am thankful for the help and advice of my committee.

My last acknowledgments must go to the staff in the chemistry building, Geri, Margaret, and LuAnn, as well as the staff in the School of Graduate Studies. There's a bureaucracy that must be adhered to. If the bureaucracy runs smoothly the organization runs smoothly. Flexibility in the bureaucracy is caused by people willing to work with me. I've seen a lot of bureaucratic flexibility, and a lot of smooth administration, both of which reflect good people doing their jobs well. Again, that's helped me focus on my job. Thanks.

Mark P. Haney

CONTENTS

Page

ABSTRACT ……………………………………………………………….……iii

PUBLIC ABSTRACT ………………………………………………………… v

DEDICATION ……………………………………………………..………vi

ACKNOWLEDGMENTS ……………………………………………...…vii

LIST OF TABLES ……………………………………………………....xii

LIST OF FIGURES ……………………………………………………....xiv

LIST OF ABBREVIATIONS…………………………………………………..xix

CHAPTER

1. INTRODUCTION ……………………………………………………….1

1.1 Background ……………………………………………………1
1.2 The Enzymes ……………………………………………………3

1.2.1 PHPT1……………………………………………………….3
1.2.2 YopH ……………………………………………………5
1.2.3 VHR……………………………………………………….11
1.2.4 PAcP ……………………………………………………14
1.2.5 λPP & PP1 …………………………………………………18
1.2.6 AP …………………………………………………………24

1.3 Comparisons between Phosphomonoesters and Phosphoramidates ….28

1.3.1 Relative Rates of Phosphomonoester versus Phosphoramidate Hydrolysis ……………………………...28
1.3.2 Hydrolysis Proceeds via Pre-equilibrium……………………32
1.3.3 LFER Values for Aryl Monoesters and Phosphoramidates Vary as a Function of Ionization ……………………………34
1.3.4 Metals ……………………………………………………37
1.3.5 Geometry …………………………………………………40
1.3.6 Phosphorylated Amino Acids ………………………………41
1.3.7 Substrates used in Study …………………………………….42
1.3.8 Considerations for Benchtop Handling Phosphoramidates…44

2. MATERIALS AND METHODS ……………………………………………45

2.1 Initial Considerations ……………………………………………45
2.2 Synthetic Protocols ……………………………………………46

2.2.1 General Procedures ……………………………………………46
2.2.2 *p*NPP, disodium salt ……………………………………………47
2.2.3 *N*-phenyl phosphoramidate ……………………………………………48
2.2.4 Tribenzyl phosphite ……………………………………………48
2.2.5 Dibenzyl N-phenyl phosphoramidate ……………………………………………50
2.2.6 *N*-phPAM triethyl ammonium salt ……………………………………………51
2.2.7 *N*-phPAM sodium salt ……………………………………………52
2.2.8 Phosphoimidazole ……………………………………………52
2.2.9 Diphosphoimidazole ……………………………………………53
2.2.10 Monophosphoimidazole ……………………………………………54

2.3 Enzyme Preparation ……………………………………………55

2.3.1 Human PHPT1 ……………………………………………55
2.3.2 YopH ……………………………………………58
2.3.3 Alkaline Phosphatase ……………………………………………59
2.3.4 λPP ……………………………………………61

2.4 Substrate-Dependent Experimental Techniques and Mathematical Analysis ……………………………………………63

2.4.1 *p*NPP ……………………………………………63
2.4.2 *N*-phPAM ……………………………………………64
2.4.3 PIm ……………………………………………65

2.4.3.1 Specific Protocols for PIm Assays ……………………………………………67

2.5 Enzymatic Assays ……………………………………………68

2.5.1 PHPT1 ……………………………………………68
2.5.2 YopH ……………………………………………69
2.5.3 VHR ……………………………………………70
2.5.4 PAcP ……………………………………………70
2.5.5 λPP ……………………………………………71
2.5.6 PP1γ ……………………………………………73
2.5.7 AP ……………………………………………74

2.6 Titration of *N*-phPAM ……………………………………………74

2.7 Computer Modeling of Substrates into Active Sites …………………..75

3. RESULTS …………………………………………………………..……77

3.1 Overall Experimental Results ………………………………………….77
3.2 Results by Enzyme ……………………………………………………..79

3.2.1 PHPT1 ………………………………………………………79
3.2.2 YopH ……………………………………………………… 79
3.2.3 VHR ………………………………………………………..82
3.2.4 PAcP ………………………………………………………..85
3.2.5 λPP and PP1 ………………………………………………..89
3.2.6 AP …………………………………………………………..91

4. DISCUSSION………………… ………………………………………………..103

4.1 Discussion of Overall Experimental Results …………………………103
4.2 Discussion of Results by Enzyme …………………………………….106

4.2.1 PHPT1 ………………………………………………………106
4.2.2 YopH ……………………………………………………….109
4.2.3 VHR ………………………………………………………..113
4.2.4 hPAcP ………………………………………………………117
4.2.5 λPP & PP1 …………………………………………………119
4.2.6 AP …………………………………………………………..121

5. CONCLUSIONS ……………………………………………….......124

5.1 Summary of Phosphoramidase vs. Phosphatase Activities ………….124
5.2 Computer Modeling …………………………………………………….125
5.3 Major Conclusions …………………………………………………….128
5.4 Future Study in the Field of Phosphoramidates and Phosphoramidases ……………………………………………….130

REFERENCES ……………………………………………………………………….131

APPENDIX …………………………………………………………………………..142

CURRICULUM VITAE …………………………………………………...……176

LIST OF TABLES

Table Page

1-1 A side by side comparison of the enzymes used in this study……………………..3

1-2 Phosphoramidate Brønsted values as a function of leaving group type and pK_a….35

1-3 β_{nuc} values for the hydrolysis of DNPP, bis-DNPP, *p*NPP, phosphopyridine, and phosphoacetate………………………………………………………………….. 36

1-4 Hydrolytic rates (s^{-1}) for *p*NPP^{2-}, phosphopicoline$^-$, and PIm^- in the presence of metals……………………………………………………………………..……38

2-1 Published inhibition values with P_i for enzymes used in this study………………46

3-1 The k_{cat}, K_M, and k_{cat}/K_M values measured for the hydrolysis of *p*NPP, *N*-phPAM, and PIm by the enzymes used in this study…………….………….77

3-2 Literature values for the catalytic pH optimum of the enzymes used in this study..78

3-3 Kinetic literature values for *E. coli* AP at pH 8.0………………………………..99

4-1 Ratio of second order rate constants (*p*NPP/PIm) by enzyme…………….….….103

4-2 Percent protonation of the substrate before catalysis versus percent protonation of the free leaving group in solvent……………………………………………..105

4-3 Kinetic results for PHPT1……………………………………………………..107

4-4 Comparison of distances between PHPT1 crystal structure with P_i and computer models with *p*NPP and PIm……………………………………………………..110

4-5 Kinetic results for YopH………………………………………………………110

4-6 Comparison of distances between YopH crystal structure with vanadate and computer models with *p*NPP and PIm………………………………………..114

4-7 Kinetic results for VHR. ……………………………………………………115

4-8 Comparison of distances between VHR crystal structure with sulfate and computer models with *p*NPP and PIm…………………………………………116

4-9 Kinetic results for PAcP……………………………………………………….118

4-10 Comparison of distances between PAcP crystal structure with phosphate and computer models with *p*NPP and PIm……………………………………..…119

4-11 Comparison of distances between λPP crystal structure with sulfate and computer models with *p*NPP and PIm…………………………………………..121

4-12 Kinetic results for AP……………………………………………………….123

4-13 Comparison of distances between *E. coli* AP crystal structure with phosphate and computer models with *p*NPP and PIm…………………………………….123

A1 Excel spreadsheet for the data entry of the hydrolysis of PIm by PAcP. ………. 169

LIST OF FIGURES

Figure Page

1-1 The catalytic motif of PHPT1. ……………………………………………………...4

1-2 Overall structure of PHPT1 (PDB 2OZW), A, with active site enlarged, B……...5

1-3 Active site of PHPT1 (PDB 2OZW) with bound phosphate as viewed from above phosphate……………………………………………………………………….6

1-4 Active site of PHPT1 (PDB 2OZW) with bound phosphate as viewed laterally toward phosphate………………………………………………………………….7

1-5 Overall structure of YopH (PDB 2I42)…………………………………………...8

1-6 The active site of YopH (PDB 2I42)……………………………………….......8

1-7 Active site of YopH (PDB 2I42) with bound vanadate as viewed from above vanadate……………………………………………………………………...9

1-8 Active site of YopH (PDB 2I42) with bound vanadate as viewed laterally toward vanadate; vanadate cannot be seen because active site is buried……………….... 9

1-9 Catalytic motif of Protein Tyrosin Phosphatases as represented by YopH……... 10

1-10 Overall structure of VHR (PDB 1VHR) with sulfate bound at the active site….. 12

1-11 The active site of VHR (PDB 1VHR) with bound sulfate…………………….... 12

1-12 Active site of VHR (PDB 1VHR) with bound sulfate as viewed from above sulfate………………………………………………………………………..… 13

1-13 Active site of VHR (PDB 1VHR) with bound sulfate as viewed laterally toward sulfate………………………………………………………………………. 13

1-14 Catalytic subunit of hPAcP (PDB 1ND6) with bound phosphate…………….... 15

1-15 Active site of hPAcP with bound phosphate……………………………………..16

1-16 The unreactive form of PAcP’s phosphoenzyme intermediate…………………..16

1-17 Catalytic motif of Histidine Acid Phosphatases as represented by PAcP………. 17

1-18 Active site of PAcP (PDB 1ND6) with bound phosphate as viewed from above phosphate………………………………………………………………….... 17

1-19 Active site of PAcP (PDB 1ND6) with bound phosphate as viewed laterally toward phosphate…………………………………………….…………….. 18

1-20 λPP with sulfate bound in coordination mode A (see figure 1-21)(PDB 1G5B).. 20

1-21 λPP active site with sulfate bound in coordination mode A…………………...... 20

1-22 λPP active site with sulfate bound in coordination mode B…………………….. 21

1-23 λPP active site with sulfate bound in coordination mode C…………………….. 21

1-24 Catalytic motif of λPP wherein a metal-coordinated hydroxide is the Nucleophile…………………………………………………………………..... 23

1-25 Catalytic motif of λPP wherein a bridging hydroxide is the nucleophile……….. 23

1-26 Catalytic motif of λPP wherein metal-coordinated hydroxide deprotonates a nucleophilic water……………………………………………………………….. 24

1-27 Structure of *E. coli* AP with phosphate bound (PDB 1ED8)……………………. 25

1-28 Active site of *E. coli* AP……………………………………………………… 25

1-29 Active site of AP (PDB 1ED8) with bound phosphate as viewed from above phosphate…………………………………………………………………….. 26

1-30 Active site of AP (PDB 1ED8) with bound phosphate as viewed laterally toward phosphate…………………………………………………………………….... 26

1-31 Catalytic motif of alkaline phosphatase as represented by *E. coli* AP…….……. 28

1-32 Hydrolytic rates as a function of pH for phosphomonoesters………………….... 29

1-33 Hydrolytic rates as a function of pH for phosphoramidates……………………… 30

1-34 Species represented in Figures 1-32 and 1-33………………………………….... 30

1-35 Hydrolytic mechanism of alkyl phosphomonoester monoanions and dianions… 31

1-36 Hydrolytic mechanism of neutral alkyl phosphomonoesters…………………… 32

1-37 Pre-equilibrium protonation of the bridging atom………………………………. 32

1-38 Ionization states of phosphoramidates………………………………………….. 33

1-39 Transition state in the hydrolysis of phosphomonoester dianions………………. 36

1-40 Transition state in the hydrolysis of phosphopyridine monoanions……………. 37

1-41 Magnesium is catalytic under alkaline conditions……………………………… 38

1-42 Zinc catalyzes hydrolysis of PIm by bringing reactants in proximity…………... 39

1-43 3D structure of *p*NPP as the dianion, left, and monoanion, right……………….. 40

1-44 Bond and electron domain geometries of the bridging nitrogen for N-methyl phosphoramidate (A&B), *N*-phPAM (C), phosphopyridine (D), and PIm (E)..…41

1-45 Substrates and leaving groups with pK_as………………………………………... 43

2-1 Synthesis of *p*NPP…………………………………………………………..… 48

2-2 General synthetic scheme for *N*-phenyl phosphoramidate……………………….. 49

2-3 Synthesis of tribenzyl phosphite……………………………………………….50

2-4 Synthesis of Dibenzyl *N*-phenyl phosphoramidate……………………………..51

2-5 Synthesis of *N*-phPAM triethyl ammonium salt……………………...……….52

2-6 General synthetic scheme for phosphoimidazole………………………………….53

2-7 Synthesis diphosphoimidazole…………………………………………………54

2-8 Synthesis of monophosphoimidazole…………………………………………...55

2-9 SDS-PAGE of PHPT1…………………………………………………………58

2-10 SDS-PAGE of YopH…………………………………………………………… 59

2-11 SDS-PAGE of AP……………………………………………………….…..... 61

2-12 SDS-PAGE of λPP………………………………………………………….……63

2-13 UV/Vis profile for PIm versus Im, both at 1 mM……………………………...65

2-14 1H NMR Time course for the hydrolysis of PIm by PAcP ……………………..66

2-15 Titration curve showing ^{31}P shift (ppm) of *N*-phPAM as a function of pH………75

3-1 Predominant protonation states of the substrates at the experimental pH………….. 78

3-2 Phosphate bound in the active site of PHPT1……………………………………..… 80

3-3 *p*NPP bound in the active site of PHPT1 as modeled in Acclerys………………… 80

3-4 PIm bound in the active site of PHPT1 as modeled in Acclerys………………….. 81

3-5 Vanadate bound in the active site of YopH……………………………………..... 82

3-6 *p*NPP bound in the active site of YopH as modeled in Acclerys……………….... 83

3-7 PIm bound in the active site of YopH as modeled in Acclerys…………………… 83

3-8 *p*NPP bound in the active site of YopH with the WPD llop removed as modeled in Acclerys……………………………………………………………………… 84

3-9 PIm bound in the active site of YopH with the WPD loop removed as modeled in Acclerys………………………………………………………………………. 84

3-10 Sulfate bound in the active site of VHR…………………………………………. 85

3-11 *p*NPP bound in the active site of VHR as modeled in Acclerys………………….. 86

3-12 PIm bound in the active site of VHR as modeled in Acclerys…………………… 86

3-13 Phosphate bound in the active site of PAcP……………………………………. 87

3-14 *p*NPP bound in the active site of PAcP as modeled in Acclerys………………... . 88

3-15 PIm bound in the active site of PAcP as modeled in Acclerys…………………... 88

3-16 Double reciprocal plot with λPP…………………………………….………. 90

3-17 λPP with bound sulfate in coordination mode B, boxes A and B (PDB 1G5B)……………………………………………………….……... 92

3-18 λPP with *p*NPP as modeled in Acclerys, boxes A and B………………………. 93

3-19 λPP with PIm as modeled in Acclerys, boxes A and B………………...…….. 94

3-20 Sulfate bound in active site……………………………………………..…….. 95

3-21 *p*NPP bound in active site of λPP as modeled in Acclerys………….………… 96

3-22 PIm bound in active site of λPP as modeled in Acclerys………….……… 97

3-23 PP1 active site with phosphate…………………………………………………...... 97

3-24 PP1 active site with *p*NPP as modeled in Acclerys……………………………… 98

3-25 PP1 active site with PIm as modeled in Acclerys……………………..………. 98

3-26 Phosphate bound in active site of AP (PDB 1ED8)……………………………… 99

3-27 *p*NPP bound in active site of AP as modeled in Acclerys………………………… 100

3-28 PIm bound in active site of AP as modeled in Acclerys………………..……… 100

3-29 Phosphate bound in active site of AP (PDB 1ED8)……………………..……. 101

3-30 *p*NPP bound in active site of AP as modeled in Acclerys………………………… 101

3-31 PIm bound in active site of AP as modeled in Acclerys………………………... 102

5-1 Selective dephosphorylation of a protein…………………………….………..129

A1 Proton NMR spectrum of *p*NPP …………………………………………………143

A2 ^{31}P NMR spectrum of *p*NPP …………………………………………………… 144

A3 Proton NMR spectrum of tri-benzyl phosphite ……………………………….. 145

A4 ^{31}P NMR spectrum of tri-benzyl phosphite ……………………………………. 146

A5 ^{31}P NMR spectrum of tri-benzyl phosphite ……………………………………. 147

A6 Proton NMR spectrum of dibenzyl *N*-phPAM ………………………………… 148

A7 Proton NMR spectrum of dibenzyl *N*-phPAM ………………………………… 149

A8 ^{31}P NMR spectrum of dibenzyl *N*-phPAM …………………………………… 150

A9 Proton NMR spectrum of *N*-phPAM triethyl ammonium salt ………………… 151

A10 ^{31}P NMR spectrum of *N*-phPAM triethyl ammonium salt …………………..… 152

A11 Proton NMR spectrum of *N*-phPAM sodium salt …………………………….. 153

A12 ^{31}P NMR spectrum of *N*-phPAM sodium salt ……………………………….... 154

A13 Proton NMR spectrum of di-phospho imidazole ……………………………… 155

A14 ^{31}P NMR spectrum of di-phospho imidazole …………………………………. 156

A15 Proton NMR spectrum showing the reaction of DPI to PIm ………………….. 157

A16 ^{31}P NMR spectrum showing the reaction of DPI to MPI ……………………… 158

A17 Proton NMR spectrum of imidazole ………………………………………... 159

A18 Proton NMR spectrum of pyrazine …………………………………………….. 160

A19 Proton NMR spectrum of PIm with pyrazine standard in the coaxial tube ……. 161

A20 Proton NMR spectrum of PIm with pyrazine standard in the coaxial tube ……. 162

A21 ^{31}P NMR spectrum of PIm …………………………………………………. 163

A22 Plot of the data in Table A1. Curvature can be seen in the data. ……………... 170

A23 The hydrolysis of PIm by PHPT1 at pH 8.5 …………………………………… 171

A24 A dataset entered into Scientist. ……………………………………………….. 172

A25 A mathematical model inputted into Scientist. ………………………………… 172

A26 A Scientist parameter set. ……………………………………………………… 173

A27 The data spreadsheet will display calculated values ………………………….. 174

A28 A Micromath chart of the raw and fitted data. ………………………………… 174

LIST OF ABBREVIATIONS

Abbreviation	Expanded Form or Meaning
AMP	Adenosine monophosphate
AP	Alkaline phosphatase
^oC	Degrees Celcius
$CDCl_3$	Deuterated chloroform
DMSO	Dimethyl sulfoxide
DNA	Deoxyribose nucleic acid
DNPP	Di-nitrophenylphosphate
DTT	Di-thiothreitol
EDTA	Ethylenediaminetetraacetic acid
GMP	Guanosine monophosphate
HCl	Hydrochloric acid
HEPES	4-2-hydroxyethyl-1-piperazineethanesulfonic acid
His tag	Histidine tag
HPLC	High Performance Liquid Chromatography
IPTG	Isopropyl β-D-1 thiogalactopyranoside
k_{cat}	Catalytic rate constant
kDa	kilo Dalton
K_i	Inhibition constant
KIE	Kinetic Isotope Effect
K_M	The Michaelis constant
λPP	Lambda phosphatase

LFER	Linear Free Energy Relationship
MHz	Mega Hertz
mNBP	meta-nitrobenzylphosphate
NMR	Nuclear magnetic resonance
N-phPAM	N-phenylphosphoramidate
OD	Optical density
PAcP	Prostatic acid phosphatase
PCA	pyridine-2-carbaldoxime
PHPT1	Protein histidine phosphatase 1
P_i	Inorganic phosphate
PIm	Phosphoryl Imidazole
pNP	*para*-nitrophenol
*p*NPP	*para*-nitrophenylphosphate
PP1	Protein phosphatase 1
PTP	Protein tyrosine phosphatase
RCF	Relative centrifugal force
TCEP	*tris*-c-carboxyethylphosphine
TEV	Tobacco etch virus
Tris	*tris*(hydroxymethyl)aminomethane
UV/Vis	Ultraviolet/Visible
VHR	Vaccinia H1 related protein.
VH1	Vacinna H1
V_{max}	The maximum velocity of an enzymatic reaction

YopH	*Yersinia* outer protein H
WPD	W – tryptophan, P – proline, D – aspartic acid.

CHAPTER 1

INTRODUCTION

1.1 Background

Protein phosphorylation occurs on histidine,[1-6] lysine,[5,7-9] and arginine,[5,10-12] and such phosphoramidates have been shown to account for as much as 76% of protein phosphorylation as compared to 24% for phosphoesters.[7] Therefore, phosphoramidases should be prevalent in the proteome. Yet, only a single phosphoramidase is known. While other phosphoramidases may remain undiscovered, another possibility is that existing phosphoester phosphatases are catalytically promiscuous, cleaving phosphoramidates in addition to their native phosphoester substrates.

Articles published in 1955 and 1957 reported enzymes with both phosphomonoester phosphatase and phosphoramidase activities.[13,14] The reports predate amino acid sequencing and protein crystallography.[15,16] Based on the biological source and method of isolation, one of these enzymes was probably prostatic acid phosphatase, PAcP, while the other may have been alkaline phosphatase, AP. If so, these reports would be among the first to indicate that phosphoester phosphatases cleave phosphoramidates.

There appears to be a single report of an enzyme that is completely specific for a phosphoramidate.[17] Purified rat brain extracts yielded a 30 kDa enzyme that was termed 6-phospholysine phosphatase. It catalyzed the hydrolysis of phospholysine and ammonium phosphoramidate, but was unable to catalyze the hydrolysis of AMP, GMP, *p*NPP, or phosphohistidine. The report did not include an amino acid sequence, even though this technique was commonly available at the time of the report. Identification of the enzyme was based mainly upon elution behavior of the enzyme during size exclusion and ion exchange chromatography. The absence of a sequence prevents definitive assignment of the enzyme to a class; that the enzyme was a previously, or subsequently, reported enzyme cannot be ruled out. No additional reports of studies with this enzyme have appeared in the literature.

The above literature reports show some enzymes catalyze hydrolysis of phosphoesters and phosphoramidates, while in another case, an enzyme is completely specific for a phosphoramidate. From a biological perspective, both results are potentially beneficial to a cell.[18] If a cell can accomplish multiple tasks with a single protein it will reduce the energy expended in the synthesis of multiple proteins. On the other hand, control of biochemical pathways is crucial, and high substrate specificity allows a cell to maintain tight control of a pathway. If an enzyme is specific for either a phosphomonoester or phosphoramidate substrate, it must be due to the active site and catalytic mechanism, herein referred to as the motif.

The purpose of the research herein was to determine if known phosphatase motifs cleave both P-O and P-N bonds, or if enzymes exist specifically with phosphoramidase activity. Because enzymes within a class share the same catalytic motif, well-characterized enzymes from the known phosphomonoester phosphatases are used to represent the different classes. Each enzyme was assayed with phosphoramidates and a phosphoester. Successful catalytic hydrolysis of both substrate types does not mean that all enzymes within the class are promiscuous; it only indicates that the motif is able to act on both bond types.

1.2 The Enzymes

This chapter provides a review of the motifs present in selected phosphomonoesterases and a phosphoramidase. A synopsis of the enzymes is provided in Table 1-1. Enzymes are selected for use in this study because they possess a catalytic core representative of the enzyme class and are well-characterized. After reviewing the enzymes, uncatalyzed phosphomonoester and phosphoramidate hydrolysis is reviewed.

Table 1-1. A side by side comparison of the enzymes used in this study.

Phosphatase class	**Enzyme used**	**Substrate Specificity**	**Acid, base, and metal catalysis**	**Covalent intermediate formed with:**
Histidine Phosphatases	Phosphohistidine phosphatase 1	phosphohistidine	General base	No covalent intermediate
Protein Tyrosine Phosphatases	*Yersenia* outer protein H	phosphotyrosine	General acid/base	Cys403
Dual specificity Phosphatases	VH1 related protein	phosphotyrosine phosphoserine phosphothreonine	General acid/base	Cys124
Histidine acid phosphatases	Prostatic acid phosphatase	non-specific	General acid/base	His12
Serine/threonine specific phosphatases	Lambda phosphatase	phosphoserine phosphothreonine	Two divalent Metals	No covalent intermediate
Alkaline Phosphatases	*E. coli* AP	non-specific	One Mg(II) and two Zn(II)	Ser102

1.2.1 hPHPT1 (human protein histidine phosphatase 1)

Relatively recently, the phosphoramidase, protein histidine phosphatase 1, PHPT1, was isolated and characterized.[19] PHPT1 is a mammalian protein found in liver and brain cells. This relatively small 14 kDa enzyme possess 125 amino acids and is a monomer. Presently, it is the sole representative of the phosphoramidase class. It has displayed the ability to hydrolyze phosphorylated histidine residues in proteins and peptides.[2]

PHPT1 is believed to use general base catalysis (Figure 1-1). His53 deprotonates water, which acts as a nucleophile. The histidine leaving group departs with concomitant generation of inorganic phosphate, P_i.[20] Although mutation of other amino acids in the active site cause reduced activity, only the mutation of H53 results in complete loss of catalytic activity.[20,21] The H53A mutant binds P_i four times more strongly than the wild type, K_d = 0.28 mM versus 1.1 mM for H53A vs WT, respectively.[20]

The pH optimum for hydrolysis of *p*NPP by PHPT1 is 8, although activity is present from pH 5.6 to 10.6.[20] NMR studies indicate the general base, His53, remains un-protonated throughout the pH range.[20] The crystal structure with bound phosphate shows no residues in the active site that could act as a general acid to activate the substrate. The NMR result, crystal structure, mutational study, and failure of the enzyme to exchange ^{18}O with P_i are all consistent with the proposed mechanism.[20]

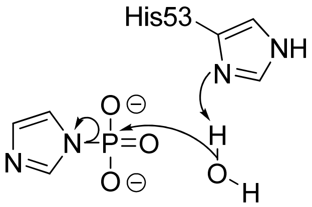

Figure 1-1. The catalytic motif of PHPT1. His53 deprotonates a nucleophilic water molecule. Protonation of the leaving group is not effected by the enzyme.

The overall structure of the enzyme consists of two α-helices and six β-strands. There is one active site and it is well exposed to the solvent (Figures 1-2, 1-3, and 1-4).

Binding of the phosphate moiety is effected via hydrogen bond interactions with the peptide backbone and electrostatic interaction with Lys21 (Figure 1-2B).

1.2.2 YopH (*Yesinia* outer protein H)

Protein Tyrosine Phosphatases, PTPs, have a conserved segment of 250 amino acids that form the catalytic domain.[22] The signature motif for PTPs is (I/V)VHCXAGXGR(S/T)G.[22] In this study, YopH is the selected representative of the PTP, class of enzymes. It possesses the catalytic domain and motif of the PTP family.

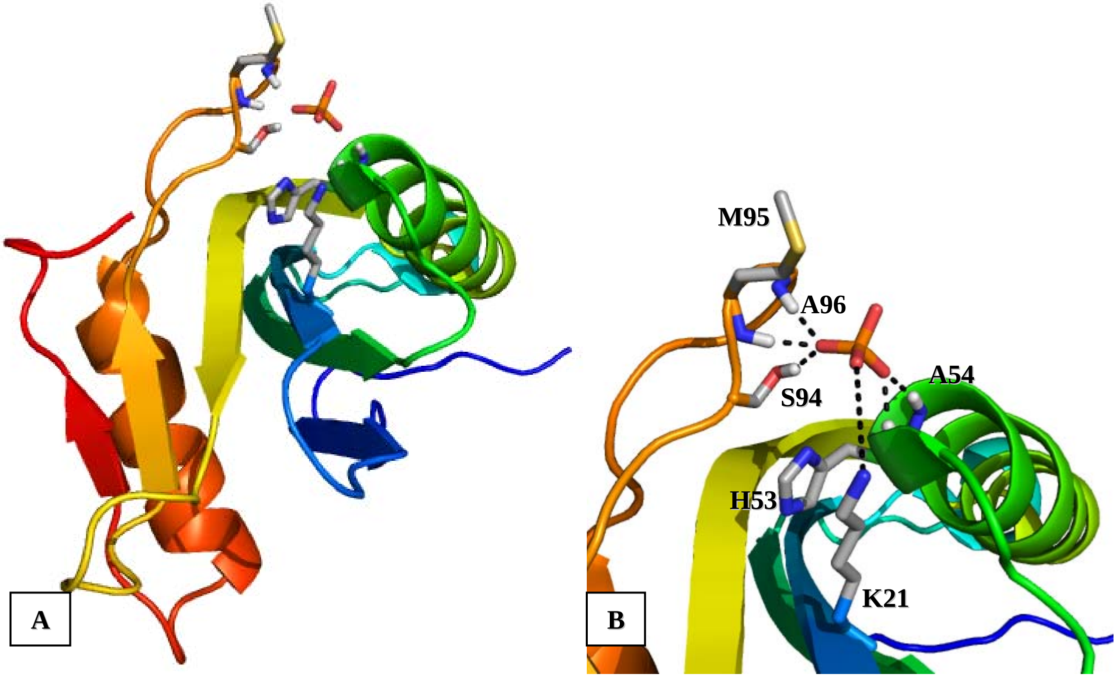

Figure 1-2. A) overall structure of PHPT1 (PDB 2OZW) B) with active site enlarged. Phosphate is bound to the enzyme through hydrogen bonding with His53, Ala54, Ser94, Met95, Ala96 and electrostatic interaction with Lys21.

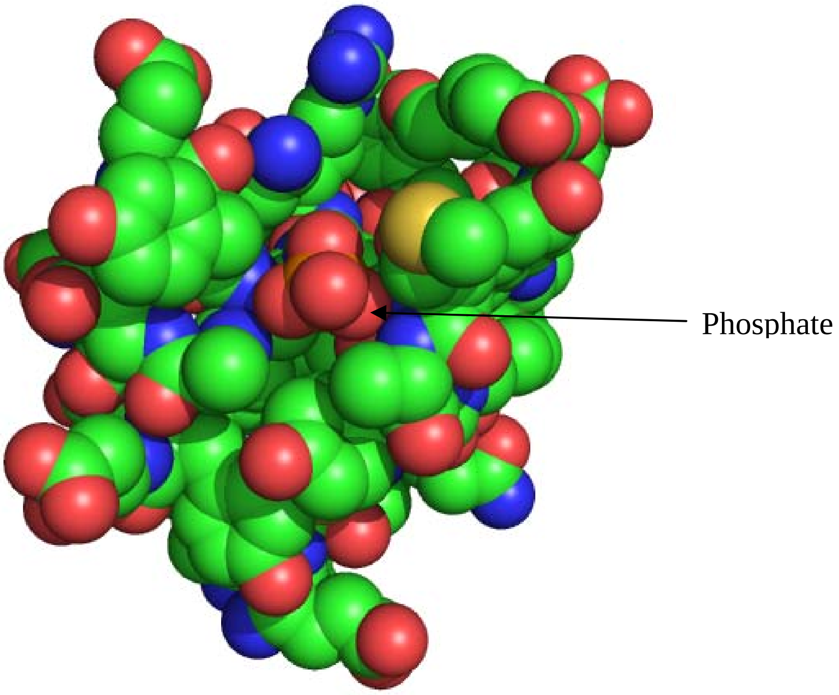

Figure 1-3. Active site of PHPT1 (PDB 2OZW) with bound phosphate as viewed from above phosphate. Active site is approximately 14 Å long, 9.2 Å wide, and 6.9 Å high. Space filling models illustrate possible interactions of amino acid residues near the active site with the substrate. The substrates used in this study are geometrically different, as will be covered in **1.3.5**, and the potential for interactions may be seen with these models. Color scheme: green represents carbon, red represents oxygen, blue represents nitrogen, yellow represents sulfur, orange represents phosphorus. This color scheme will be maintained in further figures.

The 50.8 kDa wild type protein from *Yersenia pestis* has 468 amino acids and is a monomer. YopH is secreted by *Yersenia* bacteria as a component of the pathogenic process.

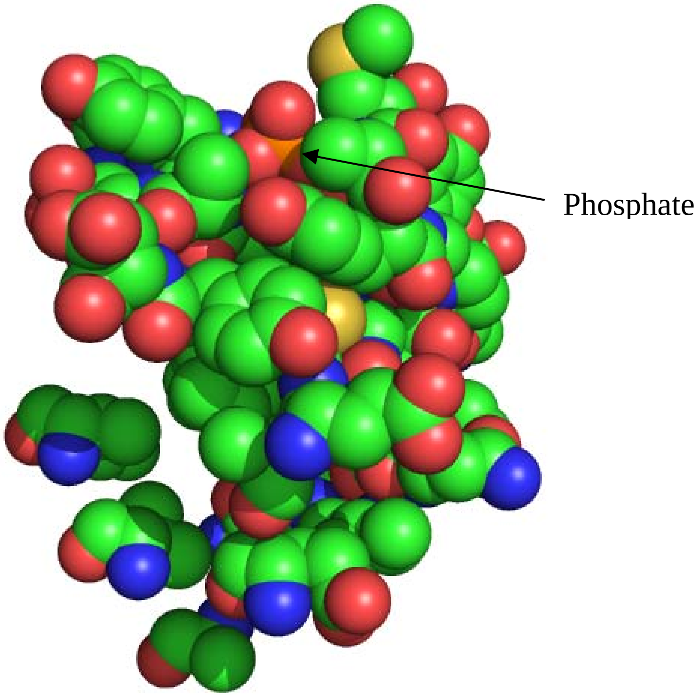

Figure 1-4. Active site of PHPT1 (PDB 2OZW) with bound phosphorus as viewed laterally toward phosphate.

The overall structure of YopH consists of seven α-helices and eight β-sheets (Figure 1-5). The active site is separated from the solvent when the WPD loop is closed. Binding of the phosphate moiety is via interactions with the protein backbone and electrostatic interactions with Arg409, a conserved residue in PTPs and dual-specificity phosphatases, and Arg404 (Figure 1-6).[23,24] The active site is deep, requiring phosphorylated species to be long enough to enter (Figures 1-7 and 1-8). This is a possible explanation for YopH's specificity for phosphotyrosine in lieu of phosphoserine and phosphothreonine.[25]

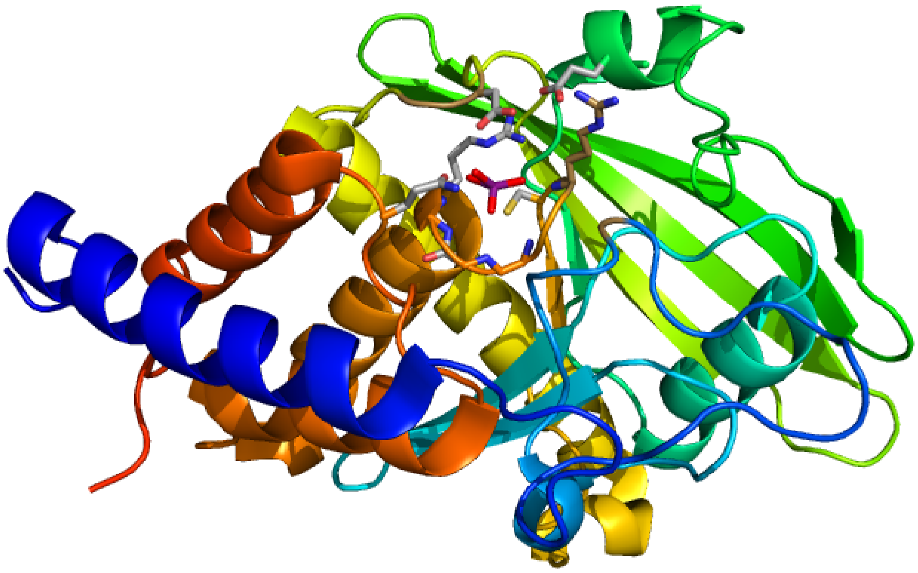

Figure 1-5. Overall structure of YopH (PDB 2I42). Bound vanadate is shown in purple near the top of the image.

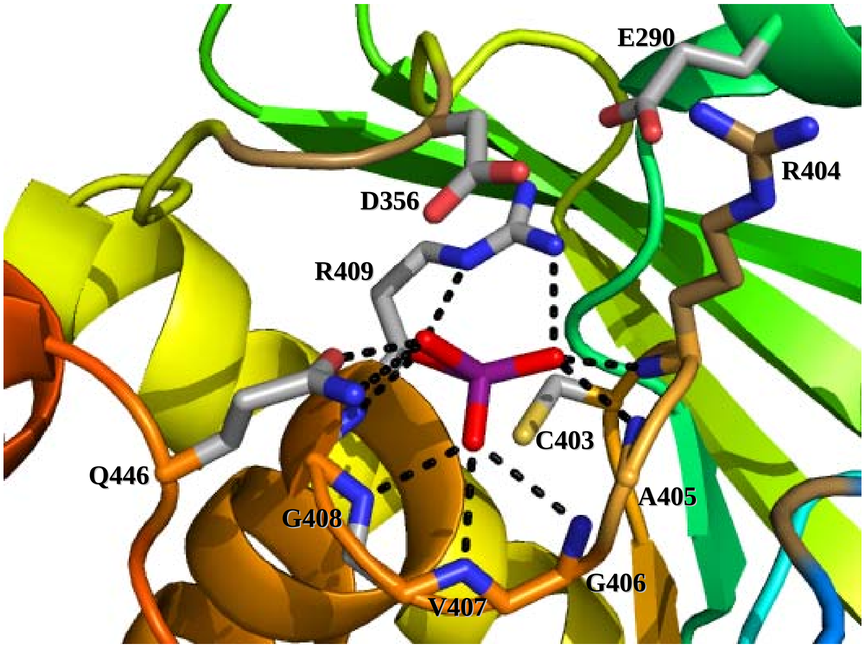
E290
R404
D356
R409
C403
Q446
A405
G408
G406
V407

Figure 1-6. The active site of YopH (PDB 2I42). Vanadate is shown in purple/red.

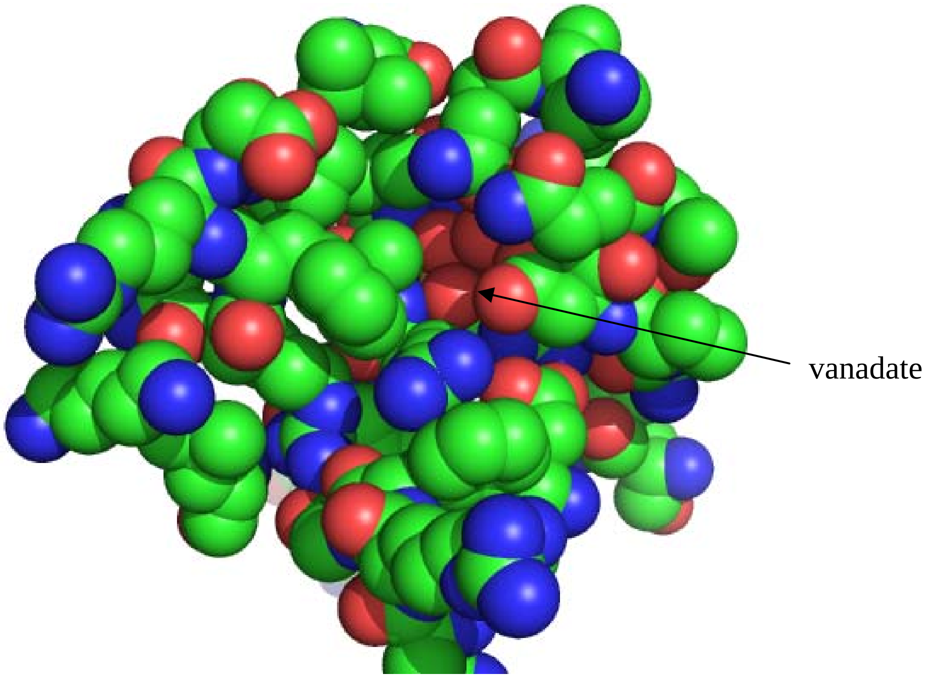

Figure 1-7. Active site of YopH (PDB 2I42) with bound vanadate as viewed from above vanadate.

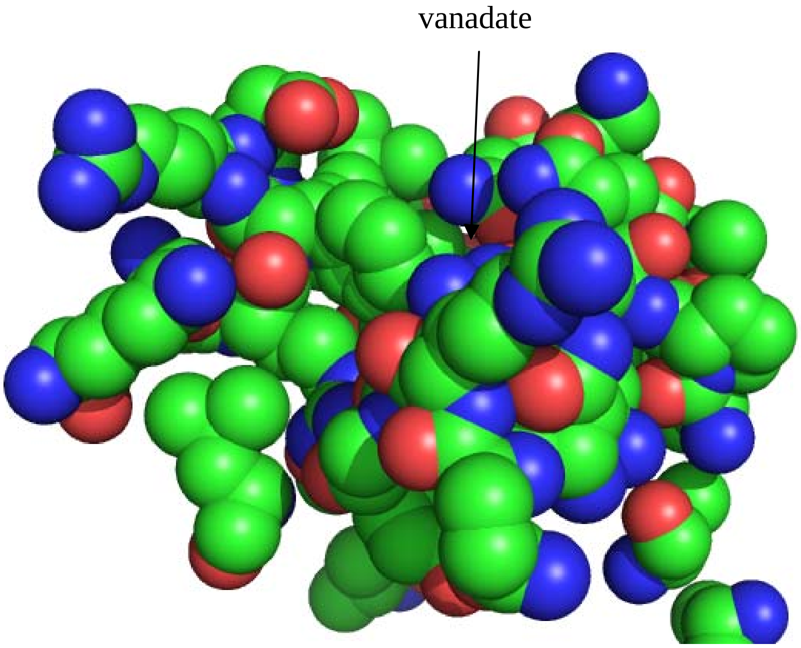

Figure 1-8. Active site of YopH (PDB 2I42) with bound vanadate as viewed laterally toward vanadate; vanadate cannot be seen because active site is buried. With WPD loop closed, the active site is separated from solvent.

PTPs effect catalysis via formation of a cysteine-phosphate intermediate (Figure 1-9).[22-24,26-35] The cysteine involved has a pK_a of approximately 4.7.[36] YopH has a pH optimum between 5.0 and 5.5.[26] PTPs display a bell-shaped pH profile due to the pK_a of the cysteine nucleophile and an aspartic acid residue that acts as a general acid/base.[37] The aspartic acid residue is part of a flexible WPD loop. It acts as a general acid, providing a proton to stabilize charge on the leaving group.[23] The same residue then acts as a general base to deprotonate the nucleophilic water that breaks the phosphorus-sulfur bond.

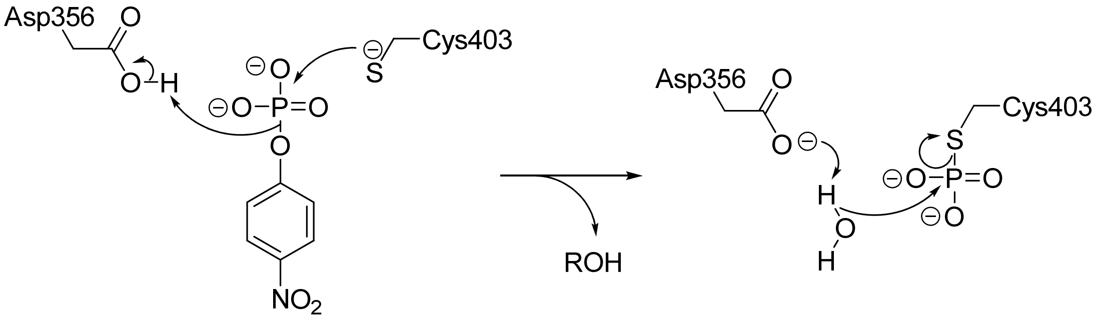

Figure 1-9. Catalytic motif of protein tyrosine phosphatases as represented by YopH.

In the catalytic mechanism, the substrate enters the active site as the dianion. In a synchronous fashion, cysteine attacks phosphorus, cleaving the P-O bond and generating the phosphoenzyme intermediate, while the general acid protonates the leaving group. Water attacks phosphorus, being deprotonated by the general base. In assays with phosphomonoesters, phosphoryl transfer is rate limiting.[28,30,38-40] This motif is shared by dual-specificity phosphatases, the difference being that the general acid/base is not on a flexible WPD loop.

Timing of leaving group protonation is dependent upon the pK_a of the leaving group,[31,41] which determines the extent of bond fission in the transition state; this mirrors the behavior of substrates in uncatalyzed reactions.[37] As will be seen in 1.3.2, protonation of the leaving group is important in the cleavage of P-O bonds.

Mutant D356N's k_{cat} is ~ 10^4 fold lower than the wild type.[22] That the mutant retains some catalytic ability is an indication that YopH uses factors in addition to general acid/base chemistry to effect catalysis.

1.2.3 VHR (Vaccinia H1-Related Dual-Specificity Phosphatase)

In this project VHR was used as a representative member of the dual-specificity phosphatases, DSPs. It has been assigned two enzyme commission numbers, one identifying it as a protein tyrosine phosphatase, 3.1.3.48, and another identifying it as a dual-specificity phosphatase, DSP, 3.1.3.16. This enzyme is known to catalyze the hydrolysis of phosphoserine, phosphothreonine, and phosphotyrosine substrates. It shares the same conserved motif as the PTPs.[42] VHR is a human protein, although VH1 is encoded from the virus which is used to inoculate against smallpox. VHR is a 20 kDa enzyme with 184 amino acids and is monomer.

Like the PTPs its catalytic motif involves formation of a cysteine-phosphate intermediate, which in VHR involves cysteine 124.[38,42-45] The cysteine involved has a pK_a of approximately 5.5.[46] VHR's pH optimum is between 5.5 and 6.0.[44] Unlike the PTPs, in DSPs the general acid-base, Asp92 in VHR, is not positioned on a flexible loop.

Binding of the substrate's phosphate moiety is through hydrogen bonding with the protein backbone and electrostatic interactions with Arg130, directly analogous to interactions seen with other enzymes in the PTP family (Figures 1-10 and 1-11). VHR has a shallower active site cleft than YopH, an explanation for its dual-specificity (Figures 1-12 and 1-13). With departure of the substrate's leaving group, a

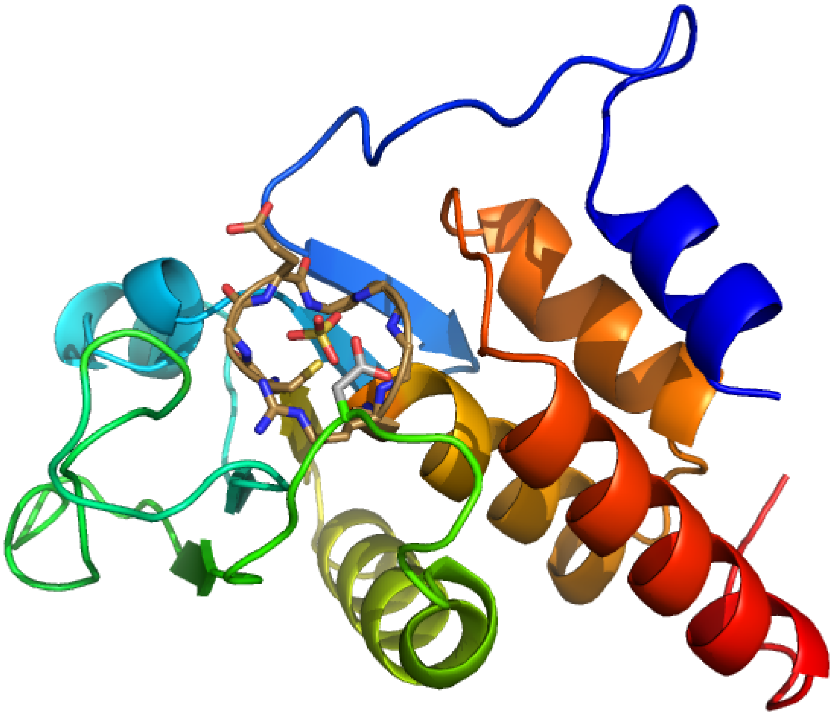

Figure 1-10. Overall structure of VHR (PDB 1VHR) with sulfate bound at the active site.

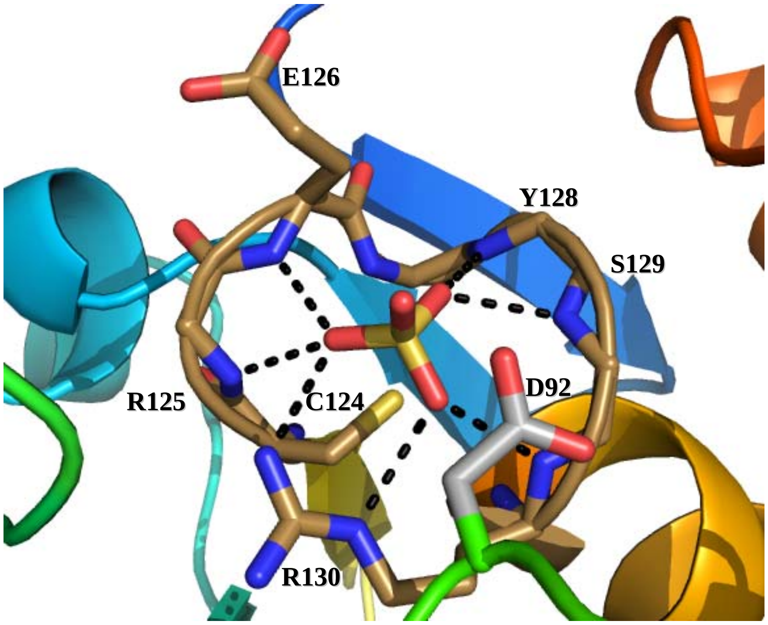
E126
Y128
S129
R125
C124
D92
R130

Figure 1-11. The active site of VHR (PDB 1VHR) with bound sulfate. Potential hydrogen bonds with a distance greater than 3.0 Å were not considered.

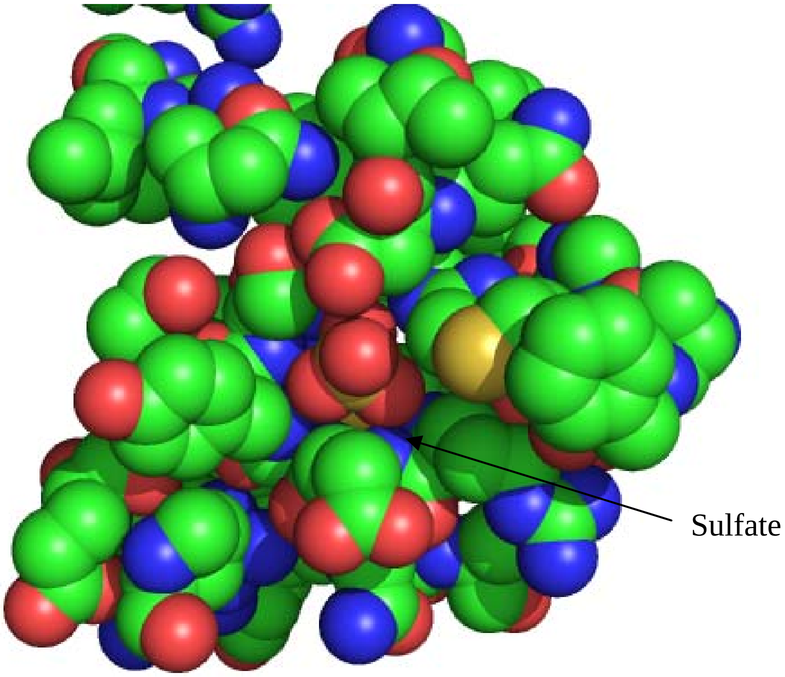

Figure 1-12. Active site of VHR (PDB 1VHR) with bound sulfate as viewed from above sulfate.

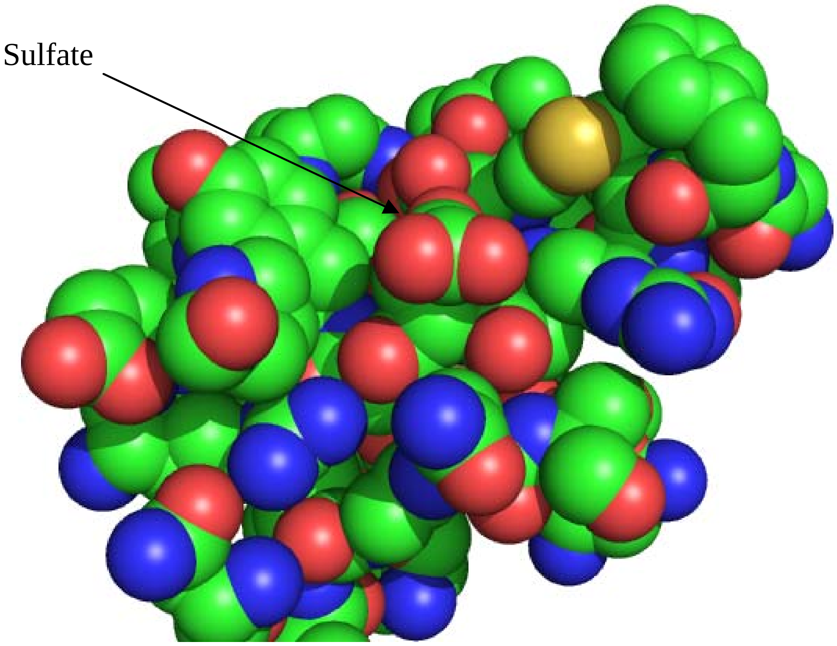

Figure 1-13. Active site of VHR (PDB 1VHR) with bound sulfate as viewed laterally toward sulfate.

phosphoenzyme intermediate is formed. It is the breakdown of this phosphoenzyme intermediate that is the rate limiting step in VHR catalyzed hydrolysis.[42]

In a side by side comparison between Protein Tyrosine Phosphatase 1, PTP1, and VHR, using substituted aromatic phosphoesters, k_{cat} values for PTP1 show dependence upon the geometry of the substrate, while VHR's values do not. The authors conclude that "the active site structure of the VHR protein phosphatase appears to be more accommodating than that of PTP1."[43] This observation may prove prescient when considering geometrical differences between phosphomonoesters and phosphoramidates.

1.2.4 hPAcP (human prostatic acid phosphatase)

The acid phosphatases hydrolyze phosphate esters at low pH. These phosphatases are found in many organisms, yeast, bacteria, mammals, and involve different phosphoester substrates, e.g. glucose-1-phosphate, phytic acid, and phosphorylated amino acids. The enzymes share a conserved sequence RH(G/N)XRX(P/A/S). Like the PTPs and DSPs, the histidine acid phosphatases form a covalent phosphoenzyme intermediate; in this case the phosphoenzyme intermediate is phosphohistidine in lieu of phosphocysteine. Prostatic acid phosphatase, PAcP, possesses the conserved motif and forms the phosphohistine intermediate.[47-50] PAcP is the representative of the histidine acid phosphatase class of enzymes for the research herein.

PAcP is expressed in mammalian prostates. Its up-regulation was used as a marker for prostate cancer, although such application has ceased. Significant research has been devoted to PAcP, reflecting its previous medical use.

This 41 kDa protein has 386 amino acids. *In vivo* it is a glycosylated homodimer.[48] Each monomer has an α/β domain with a seven-strand β-sheet with α-

helices on both sides, and an α-helix domain (Figure 1-14). Binding of the phosphate moiety is accomplished through hydrogen bonding with active site residue His257, and electrostatic interactions with conserved residues Arg11, Arg15, and Arg79 (Figure 1-15).[48,49]

PAcP has a broad pH optimum from 3 to 5.5, with a limb showing reduced activity in the basic pH region.[47,48,51] The strong activity in the acidic range is a reflection of the “enzymes specificity for the monoanionic form of the substrate.”[47] The basic limb is a result of deprotonation of the phosphoenzyme intermediate; the neutral form of the intermediate is less reactive than the cationic form (Figure 1-16).[47]

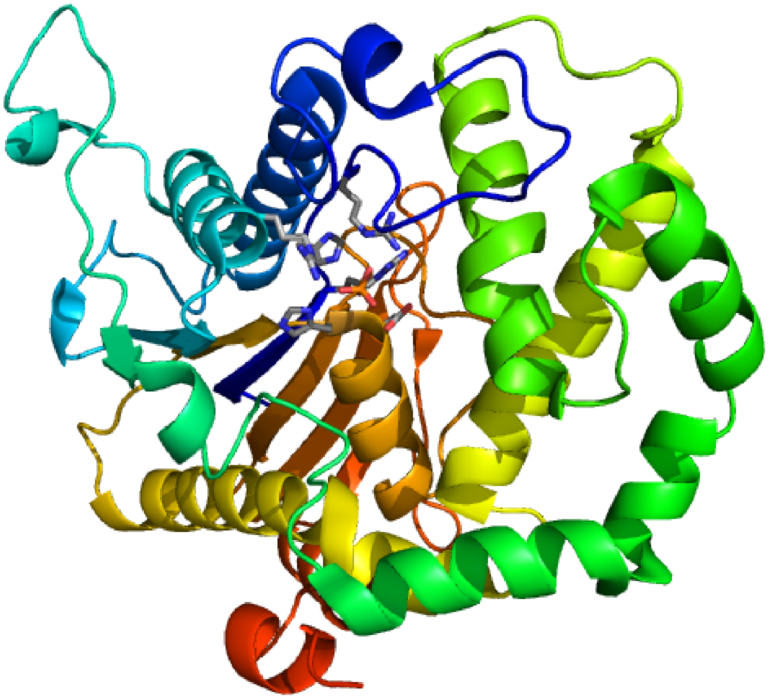

Figure 1-14. Catalytic subunit of hPAcP (PDB 1ND6) with bound phosphate.

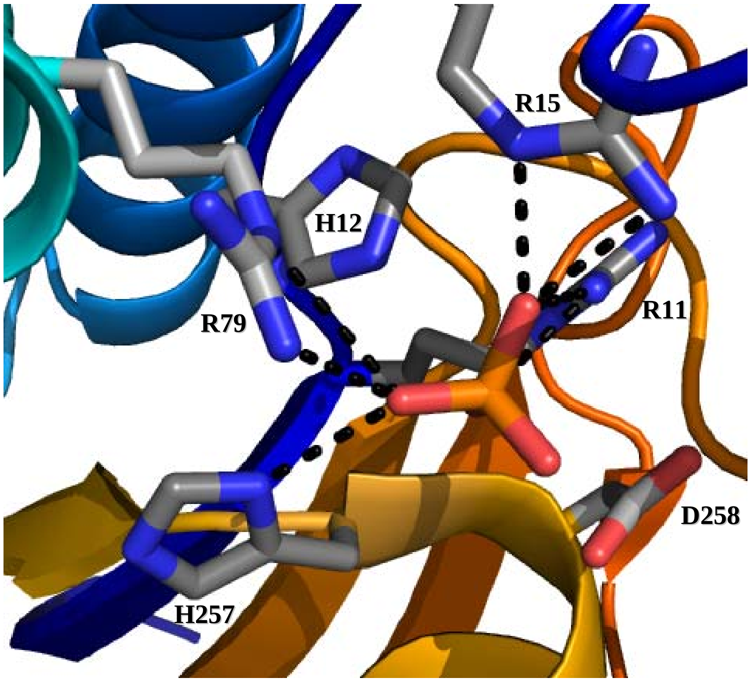

Figure 1-15. Active site of hPAcP with bound phosphate.

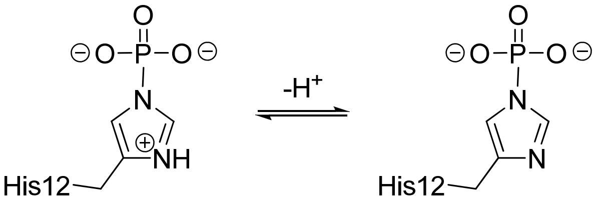

Figure 1-16. The basic limb of the pH rate profile is due to formation of the unreactive, dianionic form of the phosphoenzyme intermediate (right).

A conserved aspartic acid acts as a general acid and base to donate a proton to the leaving group and subsequently deprotonate a nucleophilic water (Figure 1-17). Attack on the phosphorus by water cleaves the histidine-phosphorus bond, regenerating the enzyme's active site. The substrate is surrounded by amino acid residues (Figures 1-18 and 1-19). Breakdown of the phosphoenzyme intermediate is rate limiting.[47,51,52]

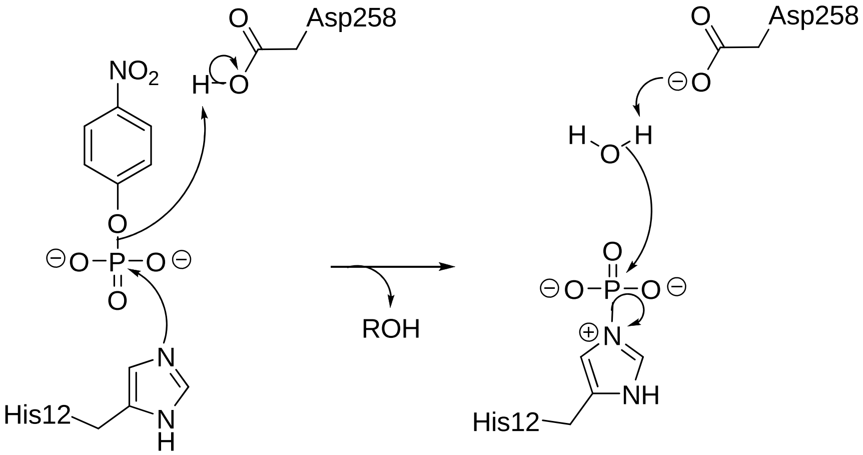

Figure 1-17. Catalytic motif of Histidine Acid Phosphatases as represented by PAcP. Nucleophilic histidine attacks phosphorus, while a general acid protonates the leaving group. In a subsequent step, water attacks phosphorus, being deprotonated by the general base.

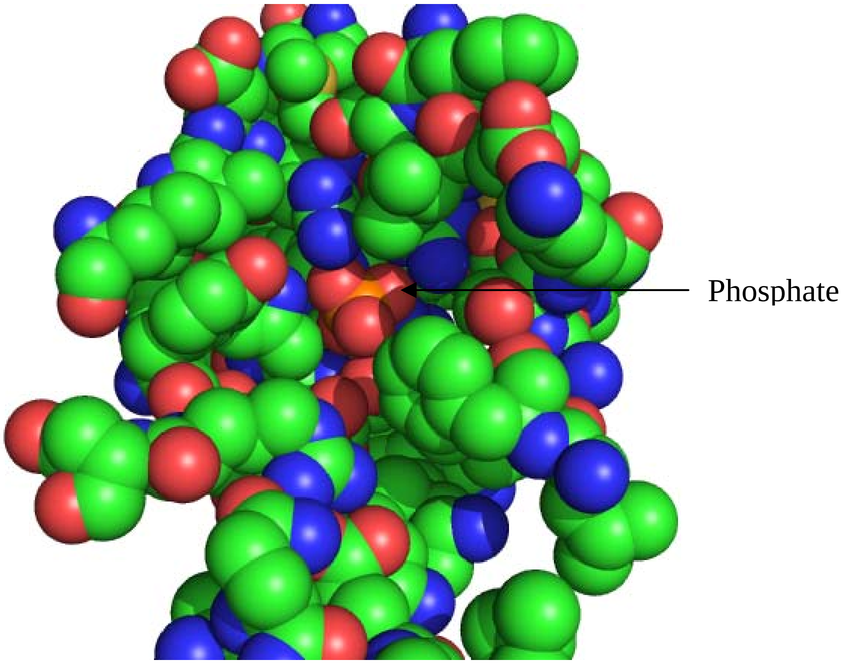

Figure 1-18. Active site of PAcP (PDB 1ND6) with bound phosphate as viewed from above phosphate. The active site is constricted.

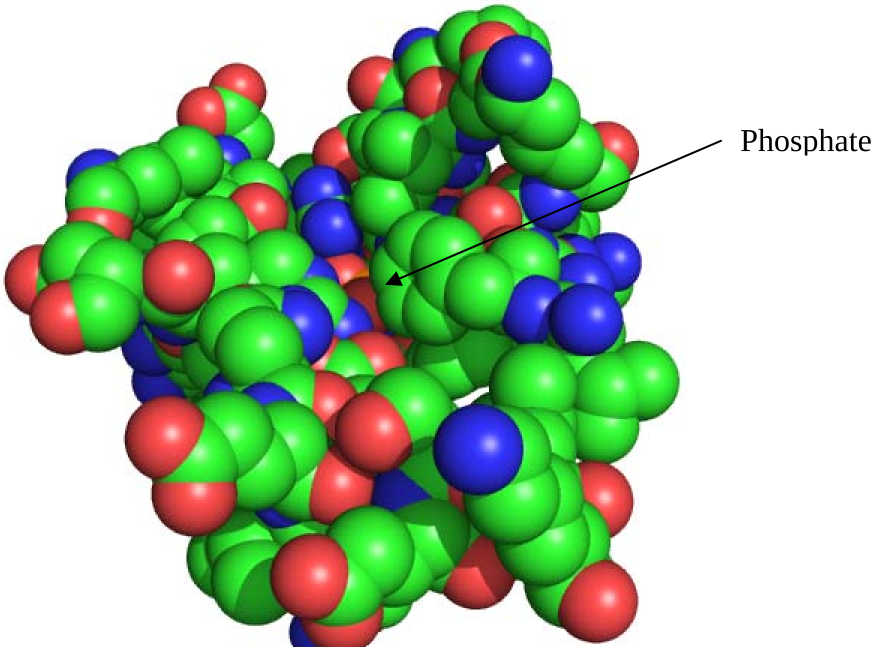

Figure 1-19. Active site of PAcP (PDB 1ND6) with bound phosphate as viewed laterally toward phosphate.

Two mutants showed complete loss of activity, H12A and R11A. Aside from facilitating binding, R11 may also play a role in the protonation of H12. D258A caused a reduction of k_{cat}/K_M by two orders of magnitude. That catalysis was not completely stopped indicates other general acid/base sources are available.[50]

1.2.5 λPP (lambda phosphatase) and PP1 (protein phosphatase)

Metalloenzymes used in this study included λPP, PP1, and AP. Both λPP and PP1 are members of the serine/threonine specific phosphatases and possess the same catalytic motif. Lambda phosphatase is encoded by the lambda virus, a bacteriophage. λPP has the minimal catalytic core of the protein phosphatases, PP, and is the representative of the protein phosphatase class of enzymes for this study.

The PP family of enzymes possesses the conserved motif **D**X**H**(X)$_n$G**D**XXD(X)$_m$G**N**-HD/E. The active sites of the protein phosphatases use two metal ions per active site.[53] Different phosphatases within the family have different divalent metal ion dependencies, with Mn, Fe, Co, Ni, Cu, and Zn being common. Depending upon the phosphatase, the active site metals may be the same or may be different metals. Identities of the native metal ions for most phosphatases within the PP family have not been determined.

λPP is a 221 amino acid, 25 kDa monomeric protein.[54] Each active site possesses two of the same metal ions *in vitro* (Figures 1-20 through 1-23).[54-65] The overall structure consists of two β-sheets, one 4-stranded and one 6-stranded, and six α-helices (Figure 1-20). X-ray crystal structures revealed sulfate bound in three modes, hereinafter referred to as coordination modes A, B, and C.[54] In modes A and B, a water molecule is interposed between the tetrahedral sulfate and Arg53 (Figures 1-21 and 1-22). One oxyanion is coordinated directly to Mn_2, while another oxyanion has a water molecule blocking coordination to Mn_1. In coordination mode C, three of the sulfate oxyanions are able to coordinate directly to Mn_1 and Mn_2, with one of the oxygens forming a bridge between the metals (Figure 1-23). In this mode, no water is interposed between the sulfate oxyanions and the metals. Whether or not each of the binding modes represents a catalytically functional mode has not been determined. The crystal structures show λPP demonstrates significant flexibility in its binding sulfate within the active site, and a large part of this flexibility involves water.

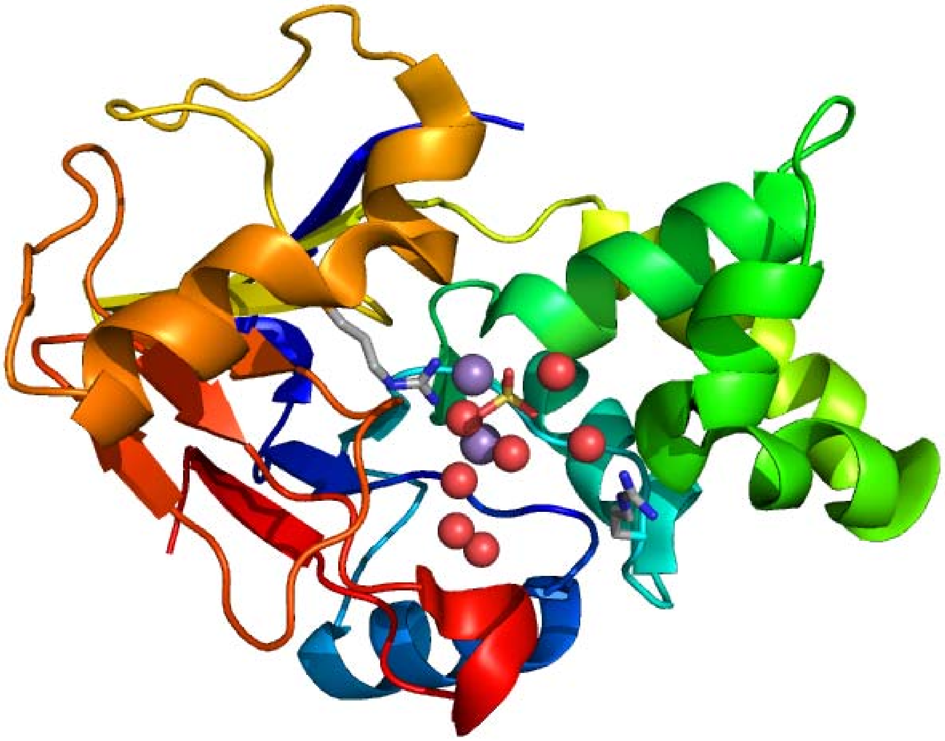

Figure 1-20. λPP with sulfate bound in coordination mode A (see figure 1-21)(PDB 1G5B). Two Mn^{2+} ions shown in purple, water shown in red.

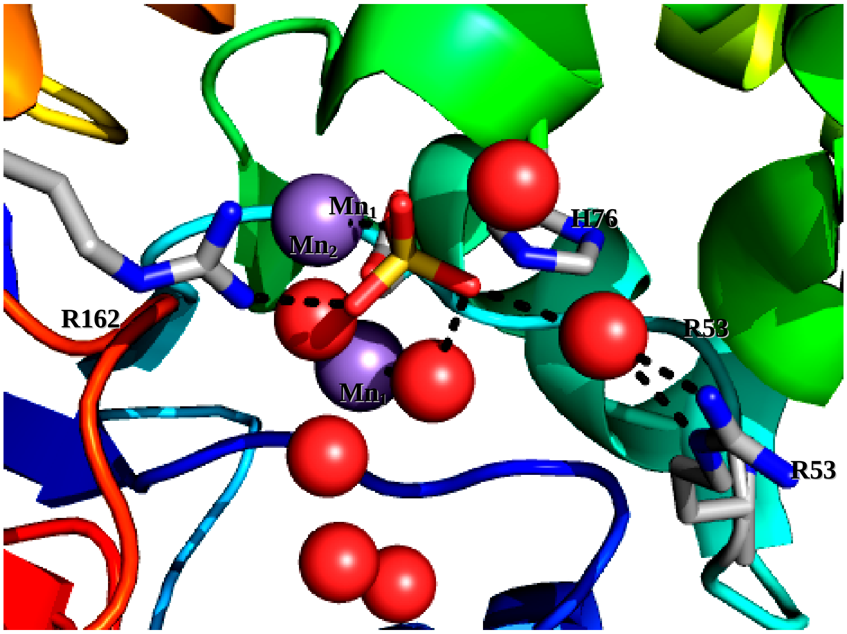
Mn$_1$
Mn$_2$
H76
R162
R53
Mn$_1$
R53

Figure 1-21. λPP active site with sulfate bound in coordination mode A. Red spheres are water.

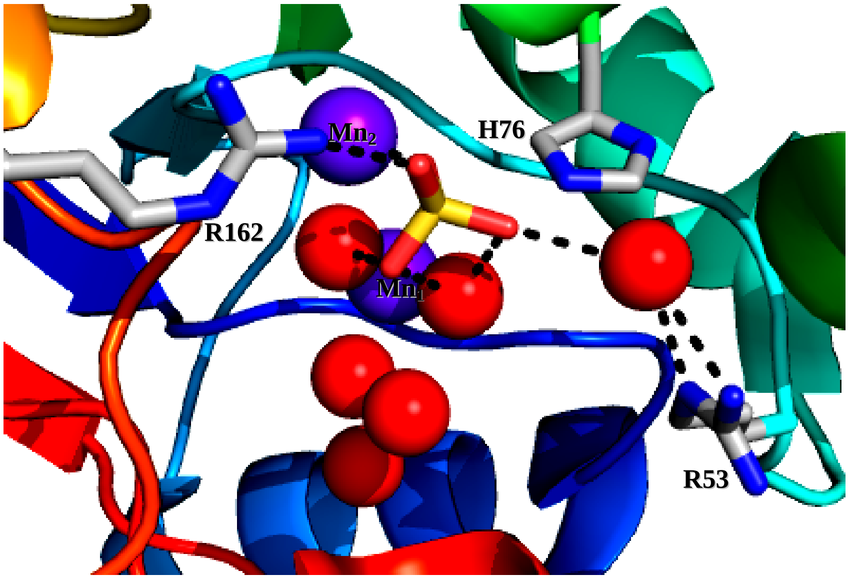

Figure 1-22. λPP active site with sulfate bound in coordination mode B.

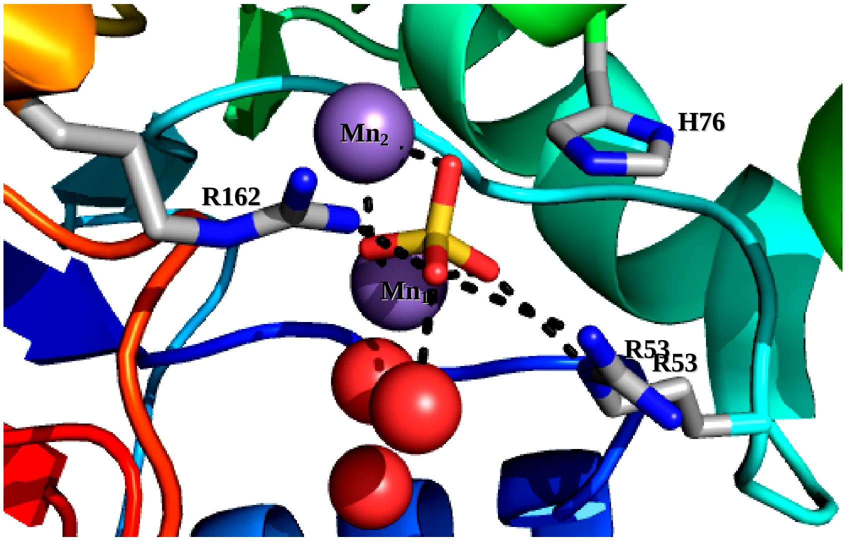

Figure 1-23. λPP active site with sulfate bound in coordination mode C.

λPP dephosphorylates proteins and peptides phosphorylated on serine, threonine, and tyrosine; it is unable to dephosphorylate the simple phosphorylated amino acids phosphoserine, phosphothreonine, or phosphotyrosine.[60] The enzyme has phosphodiesterase activity, being able to hydrolyze bis-*p*-nitrophenyl phosphate, $k_{cat} = 44$ s^{-1}, $K_M = 10$ mM; the same experiment yielded a k_{cat} of 47 s^{-1}, $K_M = 5.0$ mM for the monoester *p*NPP.[66] The diesterase activity coupled with the inability of the enzyme to hydrolyze phosphorylated serine, threonine, or tyrosine has led to speculation that λPP's native substrates might not be phosphomonoesters, but phosphodiesters.[66]

Greatest activity is shown when Mn(II) is present, although activity with Ni(II) is similar, $\text{activity}_{Ni}/\text{activity}_{Mn} = 0.83$.[53,60] The k_{cat}/K_M pH optimum for λPP hydrolysis of *p*NPP is pH 7.8, while the greatest k_{cat} is shown at pH 8.5.[56] The acidic limb of λPP's bell shaped pH profile is due to a nucleophilic metal-bound water molecule. The basic limb is likely due to deprotonation of His76 which may assist in substrate binding.[56]

The two metal atoms are not held equally in the active site. For λPP with Mn^{2+}, K_d1 is 2 μM, while K_d2 is 160 μM.[59,67] K_d2 is higher than manganese concentrations that would be found in a cell. As a result, it has been postulated that phosphate substrates enter the active site bound to manganese.[59] The K_{sp} for manganese phosphate is 3.17×10^{-8},[68] so the suggestion that phosphate substrates form complexes with manganese before entering the active site is reasonable.

Studies have not definitively determined the catalytic mechanism of the PP family of enzymes. Once the substrate is bound, three catalytic possibilities exist.[37] A metal-coordinated hydroxide could be a nucleophile, attacking the substrates phosphorus (Figure 1-24). A bridging hydroxide could be a nucleophile, attacking the substrate's phosphorus (Figure 1-25). Or, a metal-coordinated hydroxide could act as a general base, deprotonating a nucleophilic water (Figure 1-26). In either case, the rate limiting step for λPP catalysis with *p*NPP as the substrate is cleavage of the phosphoester bond.[56]

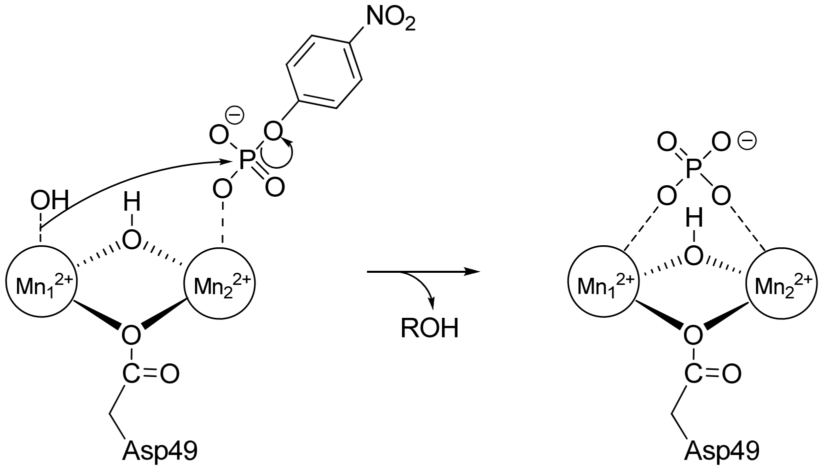
NO2
O
O
P
O
O
OH
H
O
Mn1 2+
Mn2 2+
O
C=O
Asp49
ROH
O
O
P
O
O
H
O
Mn1 2+
Mn2 2+
O
C=O
Asp49

Figure 1-24. Catalytic motif of λPP wherein a metal-coordinate hydroxide is the nucleophile.

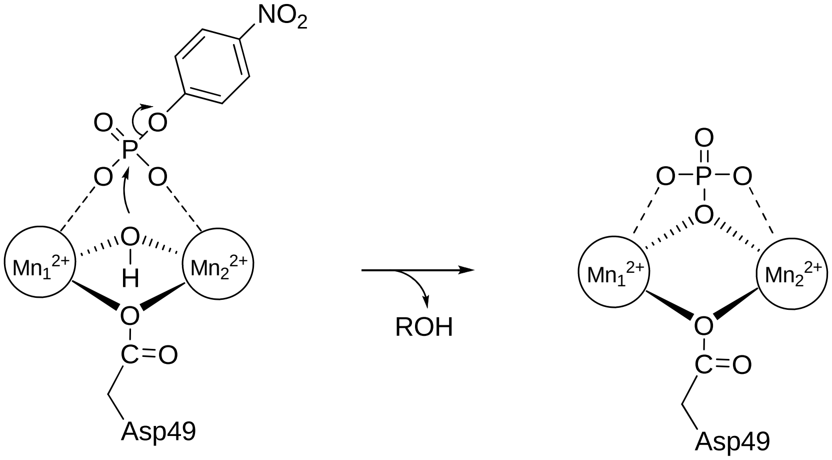
NO2
O
O
P
O
O
O
H
Mn1 2+
Mn2 2+
O
C=O
Asp49
ROH
O
O-P-O
O
Mn1 2+
Mn2 2+
O
C=O
Asp49

Figure 1-25. Catalytic motif of λPP wherein a bridging hydroxide is the nucleophile.

Mutation of a conserved histidine residue, H76 in λPP, results in lowered k_{cat} with little change in K_M. The role of this histidine is not clear. It could function to bind the substrate through a salt bridge, act as a general acid to protonate departing leaving groups, or act as a general base to deprotonate the nucleophilic metal-coordinated

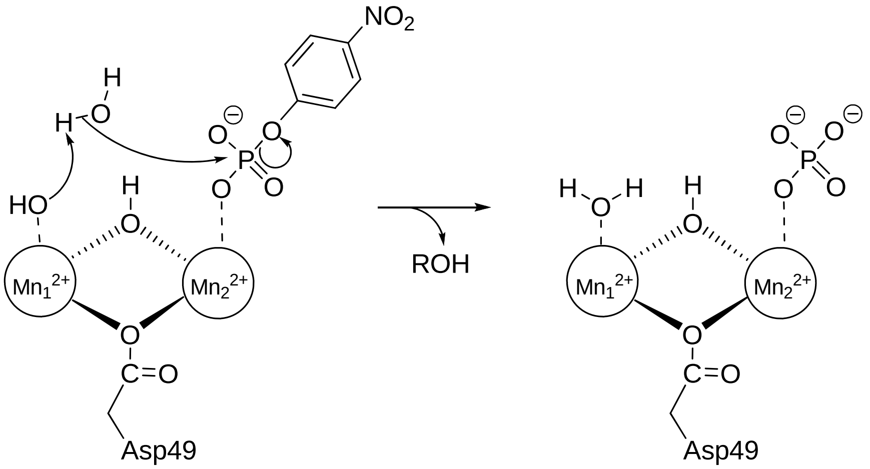

Figure 1-26. Catalytic motif of λPP wherein metal-coordinated hydroxide deprotonates a nucleophilic water.

water.[37] Arginines 53 and 162 are also important for activity. Crystal structures show these residues playing a role in binding and possibly substrate orientation in modes A, B, and C.

1.2.6 AP (Alkaline Phosphatase)

The other metalloenzyme used in this study was alkaline phosphatase. AP is ubiquitous in organisms, being found in bacteria and higher organisms. It is found in most organs in mammals. Because it has been extensively studied and has the catalytic core representative of this class of enzymes, *E. coli* AP was chosen to represent this class of enzymes.

E. coli AP is a 47 kDa, 449 amino acid homodimeric enzyme. The catalytic motif involves three metals, two Zn^{2+} and one Mg^{2+} (Figures 1-27 and 1-28).[69-79] The overall structure of *E. coli* AP consists of a 10-stranded β-sheet surrounded by 15 α-helices, with a second 3-stranded β-sheet and an α-helix outside the core structure.[80] The active site is well hydrated in crystal structures, which show the active site is also highly exposed to solvent (Figures 1-27 and 1-28).

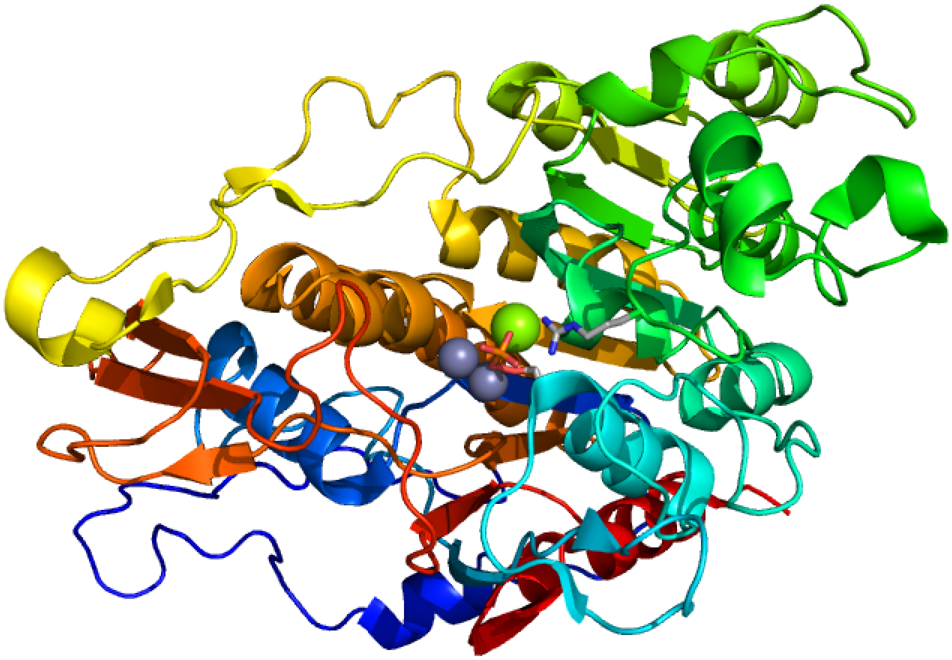

Figure 1-27. Structure of *E. coli* AP with phosphate bound (PDB 1ED8). Active site metals form a catalytic triad.

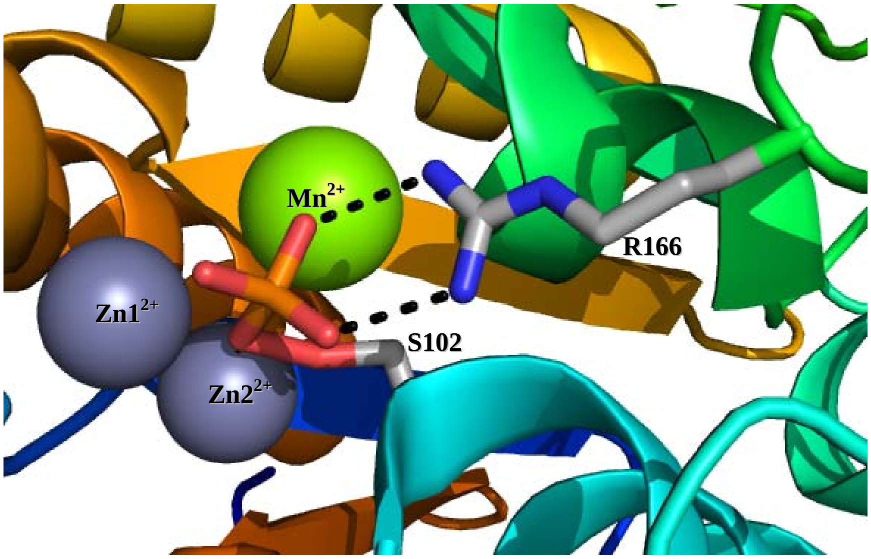

Figure 1-28. Active site of *E. coli* AP.

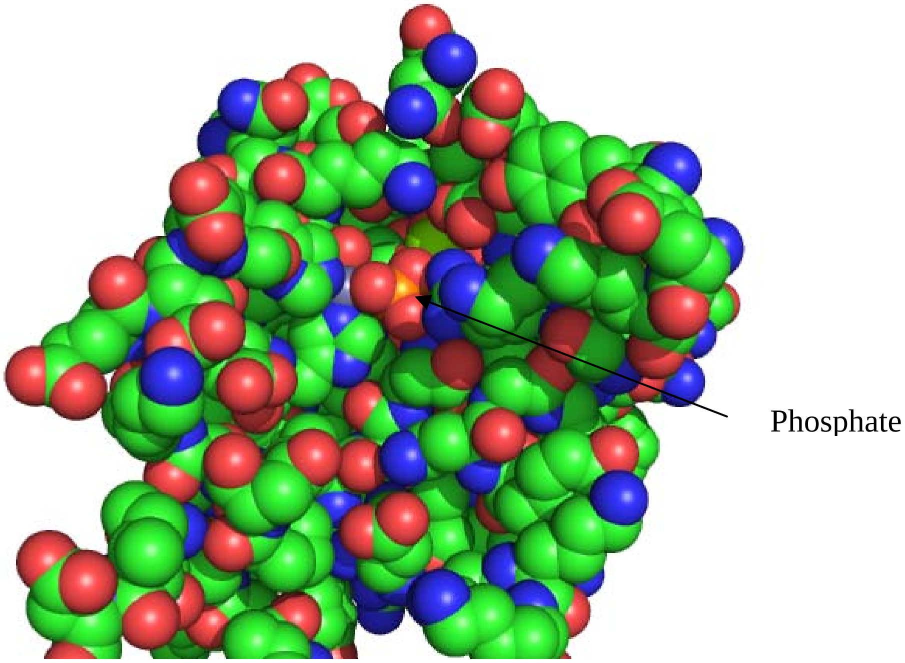

Figure 1-29. Active site of AP (PDB 1ED8) with bound phosphate as viewed from above phosphate.

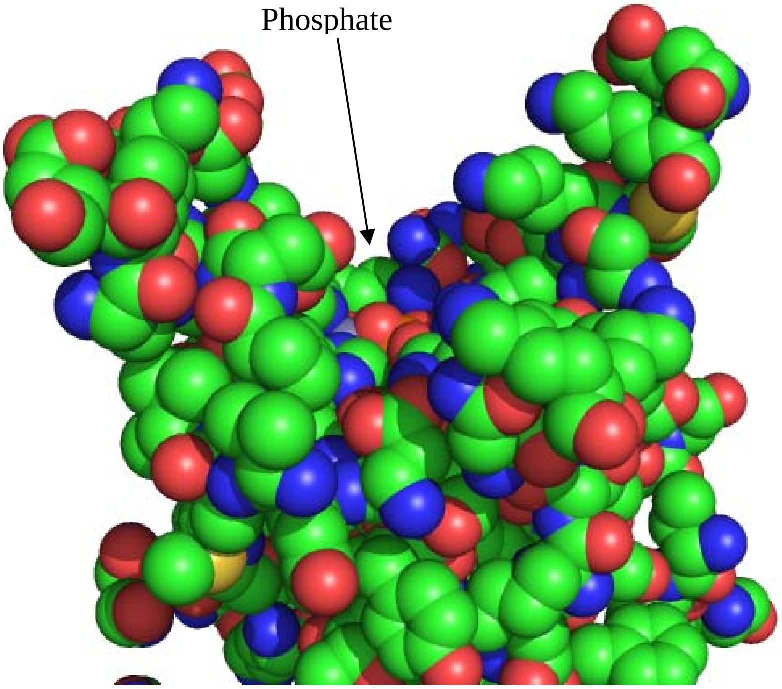

Figure 1-30. Active site of AP (PDB 1ED8) with bound phosphate as viewed laterally toward phosphate.

The pH optimum is substrate dependent, but the optimal pH is always alkaline. The acidic limb of AP's bell-shaped pH profile is a reflection of the substrates pK_a. The basic limb is driven by factors within the enzyme that affect binding, possibly blocking of the active site by a zinc-coordinated water molecule.[73] *E. coli* AP has a pH optimum of between 9.0 and 9.5 with *p*NPP.

The zinc ions bind the substrate, bring the nucleophilic serine close to the electrophilic phosphorus, lower the pK_a of serines hydroxyl moiety, and stabilize charge buildup on the leaving group (Figure 1-31). The magnesium ion coordinates a general base hydroxide that deprotonates the serine nucleophile; it may also assist in the necessary geometry of the active site. Arg166 forms electrostatic interactions with the substrates phosphate moiety, assisting in substrate binding. Breakdown of the phosphoenzyme intermediate is the rate limiting step of catalysis below pH 7.5, while release of P_i is rate limiting above pH 7.5.[37,73,80-82]

AP has been called a non-specific phosphatase as it is able to catalyze the hydrolysis of a variety of substrates, including phosphomonoesters, phosphodiesters, phosphotriesters, phosphonates, and phosphoramidates. Research has demonstrated its ability to catalyze hydrolysis of phospholysine substrates.[11,12] As will be reviewed, phosphoramidates are relatively stable under alkaline conditions, the same conditions where AP demonstrates its greatest catalytic efficiency.

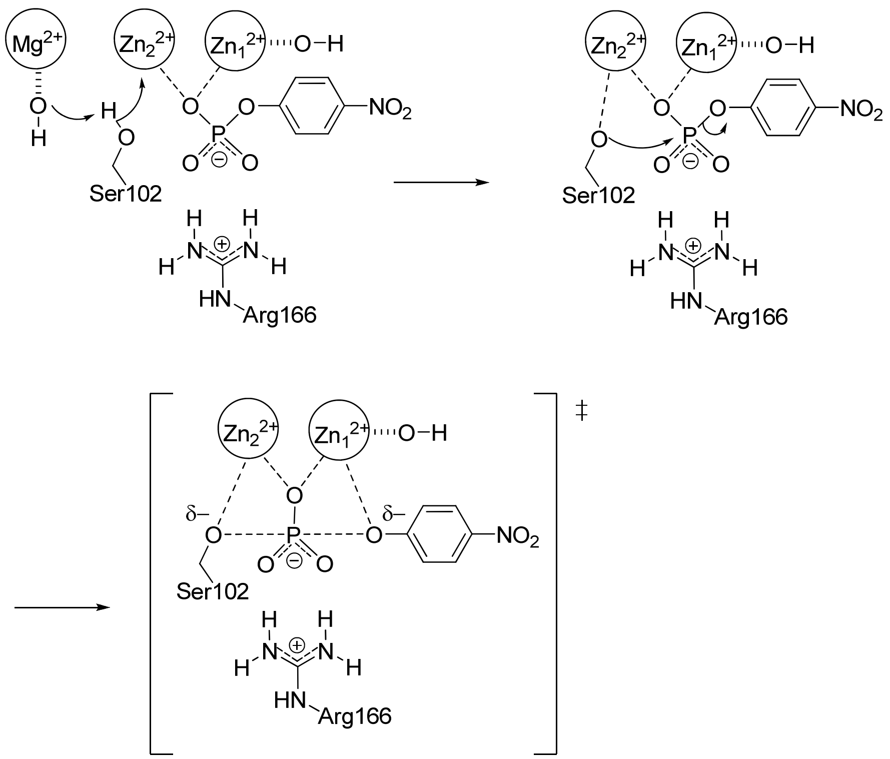

Figure 1-31. Catalytic motif of alkaline phosphatase as represented by *E. coli* AP.

1.3 Comparisons between Phosphomonoesters and Phosphoramidates

1.3.1 Relative Rates of Phosphomonoester versus Phosphoramidate Hydrolysis

Mechanisms for non-enzymatic cleavage of phosphoester bonds have been intensely studied since the 1950's. The non-enzymatic research laid the groundwork for later enzymatic studies, as scientists realized enzymatic and non-enzymatic hydrolysis must share some mechanistic similarities.[83]

The hydrolysis profiles as a function of pH for selected phosphomonoesters and phosphoramidates are provided (Figures 1-32 and 1-33). The data is a collection from the literature, and hydrolytic rates were collected at different temperatures.[2,83-91] A direct comparison of rates is not appropriate where different experimental temperatures were used. However, the profiles are indicative of the mechanism of hydrolysis.

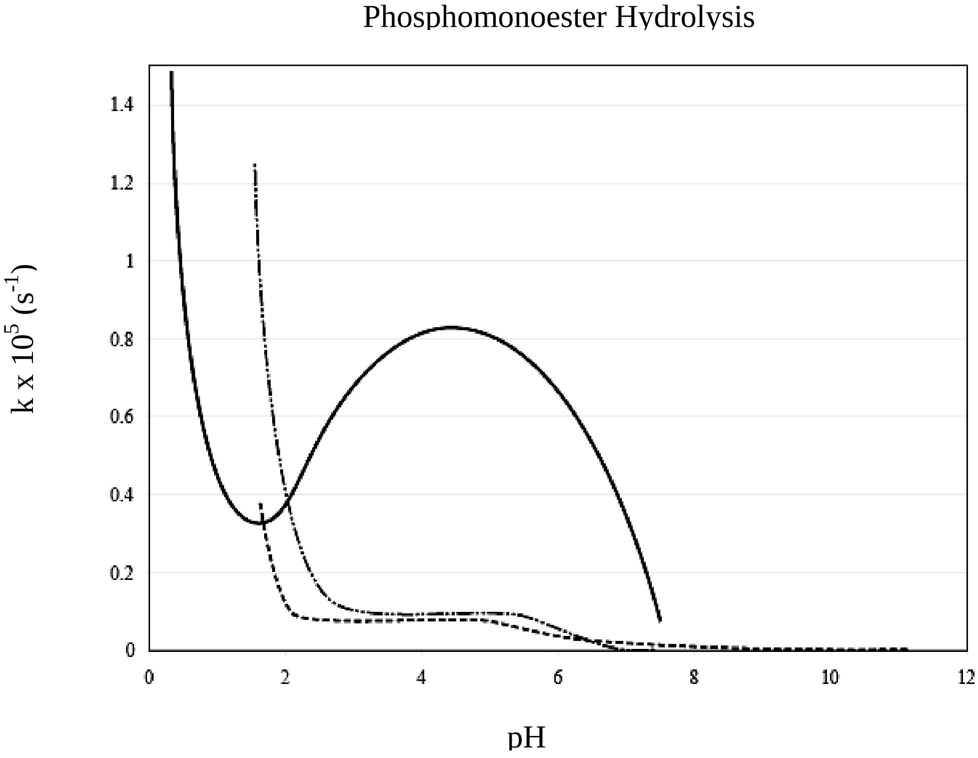

Figure 1-32. Hydrolytic rates as a function of pH for phosphomonoesters. ——— Methyl phosphate[85] (**1**) at 100 °C , ------------ *para*-nitrophenyl phosphate[88] (**2**), *p*NPP, at 37 °C, -·-·-·- benzyl phosphate[90] (**3**) at 76 °C. Plots from literature were scanned, digitized with PlotDigitize, overlaid in Excel, and the resulting graphic refined Photoshop.

Even when hydrolyzed at lower temperatures, hydrolytic rates are higher for phosphoramidates (Figure 1-32) than phosphomonoesters (Figure 1-33). For the phosphoesters and phosphoramidates shown in Figures 1-32 and 1-33, increases in proton concentration tend to cause higher rates of hydrolysis, although there are troughs with some species as pH decreases. The exceptions to the trend are N-methyl

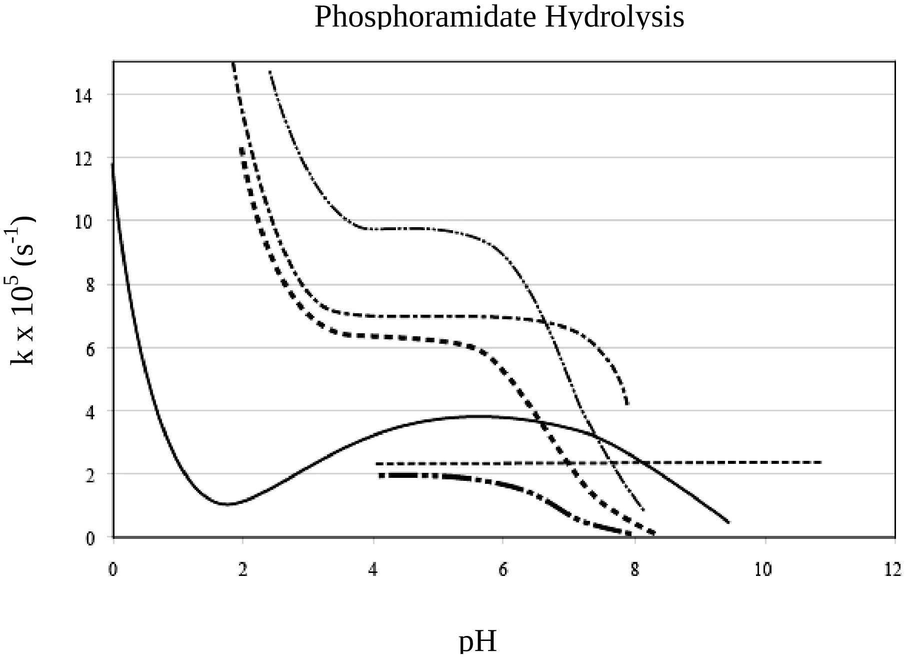

Figure 1-33. Hydrolytic rates as a function of pH for phosphoramidates.

▬▪▬▪ PIm[91] (**4**) and ┅┅┅┅ NMePIm[91] (**5**), 40 °C; —··—··— *N*-phPAM[86] (**6**), 20 °C; -·-·-·- Ammonium PA[87] (**7**), 36 °C; - - - - *N-p*-chloroPAM[86] (**8**), 20 °C; ——— *N-p*-chloroPAM[86] in 50% dioxane, 20 °C. Rate constants for *N-p*-chloroPAM are x10^3. Plots from literature were scanned, digitized with PlotDigitize, overlaid in Excel, and the resulting graphic refined in Photoshop.

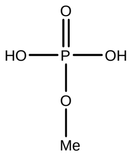

1

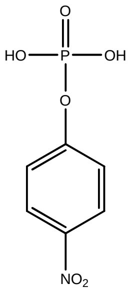

2

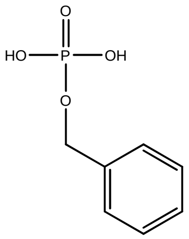

3

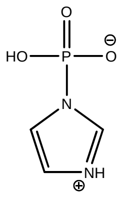

4

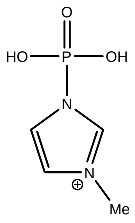

5

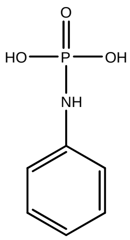

6

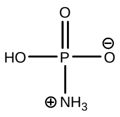

7

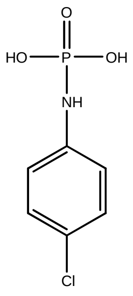

8

Figure 1-34. Species represented in Figures 1-32 and 1-33. Protonation state will vary as a function of pH.

phosphoimidazole which hydrolyzes in a pH independent manner,[91,92] and N-p-chlorophosphoramidate in 50% dioxane.[86] Phosphoramidate bonds are more labile under acidic conditions than phosphoesters, while both species exhibit least hydrolysis under mildly alkaline conditions.

The location of a proton(s) during phosphomonoester hydrolysis can be inferred from pK_as.[93] The overall hydrolytic rate constant at a given pH is given by (1.1):[94]

$$k_o = k_N[N] + k_M[M] + k_D[D] \tag{1.1}$$

where [N], [M], and [D] are the mole fractions of the neutral, monoanion, and dianion of a phosphomonoester species, as calculated from the Henderson-Hasselbalch equation, respectively. The pH rate profiles are a reflection of equation 1.1. It is apparent that for both phosphomonoesters and phosphoramidates $k_N > k_M > k_D$.

Isotopic studies with ^{18}O showed that the monoanions and dianions of alkyl phosphomonoesters cleave at the bridging P-O bond, whereas the neutral and cationic species cleave predominantly at the C-O bond (Figures 1-35 and 1-36).[94] For the enzymes studied, cleavage does not occur at the C-X (X = N or O) bond. Therefore, comparisons of uncatalyzed versus enzyme-catalyzed reactions can be limited to comparisons with monoanionic and dianionic hydrolysis.

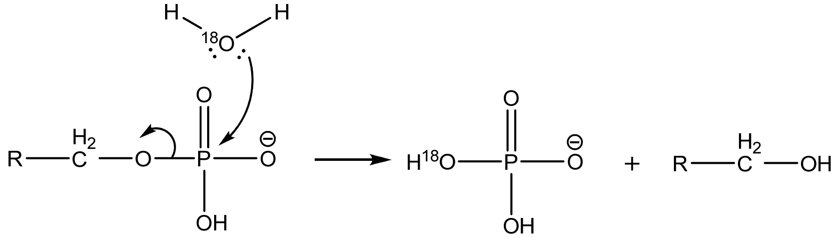

Figure 1-35. Hydrolytic mechanism of alkyl phosphomonoester monoanions and dianions. Cleavage is at the P-O bond.

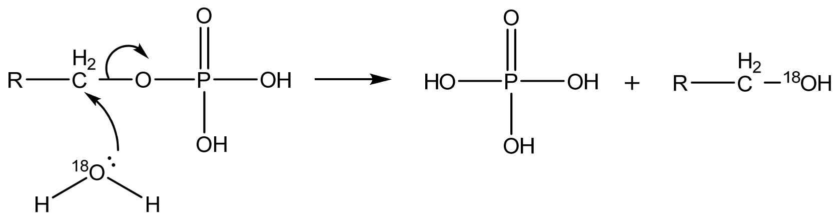

Figure 1-36. Hydrolytic mechanism of neutral alkyl phosphomonoesters. Cleavage is predominantly at the C-O bond.

1.3.2 Hydrolysis Proceeds via Pre-equilibrium

Monoanions hydrolyze faster than dianions because they are able to undergo a pre-equilibrium protonation of the bridging atom (Figure 1-37). Protonation of the bridging atom places charge on the leaving group and makes the P-O_{bridge} bond more labile.

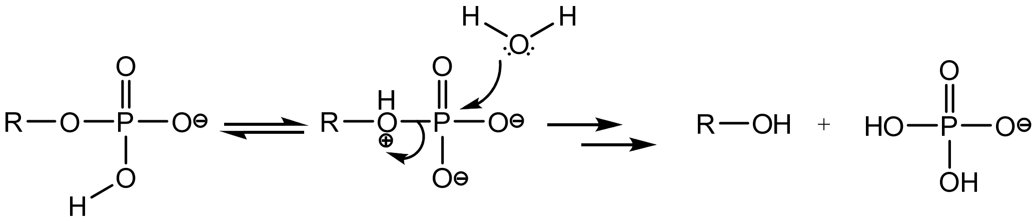

9

10

Figure 1-37. Pre-equilibrium protonation of the bridging atom.

Monoanionic phosphoramidates may exist as either zwitterions, **12**, **13**, and **16**, or non-zwitterions, **11**. ^{31}P NMR experiments indicate **15** is not a predominant form in aqueous media.[91] Phosphopyridine cannot exist as a dianion; it must exist as a monoanion, **13**, or a neutral species, **14**.

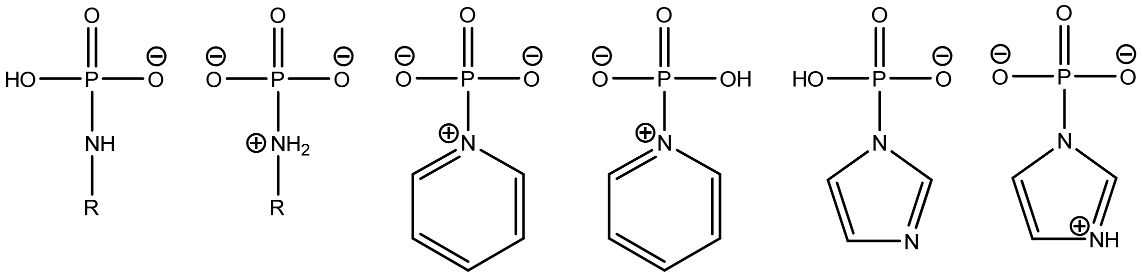

11 **12** **13** **14** **15** **16**

R – H, alkyl, or aryl.

Figure 1-38. Ionization states of phosphoramidates.

Rationalization for phosphoramidate hydrolysis being faster than phosphomonoester hydrolysis can be provided by comparing the predominate monoanionic form. Monoanionic phosphomonoesters exist predominantly with the non-bridging atom protonated, as with **9**. Monoanionic phosphoramidates can exist predominantly with the bridging atom charged or sharing charge, as with **12**, **13**, **14**, and **16**, although some species can exist without the bridging nitrogen protonated, as with **11**. Pre-equilibrium is not necessary with **12**, **13**, **14**, and **16**, as the leaving group is already activated by charge.

Confirmation that the bridging nitrogen is protonated in phosphoramidates as expected by the pK_a of the leaving group (Table A1) is provided by studies with heats of ionization[95] and ^{31}P NMR.[91] Phosphoramidate hydrolysis profiles (Figure 1-30) show inflections close to the pK_as of the leaving groups. N-methylphosphoryl imidazole is charged under all conditions and shows no inflection, a further confirmation that charge on the leaving group affects the profile.

Since the zwitterion is the reactive species, phosphoramidate substrates that enter the enzyme active site as zwitterions may illuminate how the motif is handling the substrate. The phosphoramidate substrate will not need to have the leaving group activated, whereas phosphomonoesters with a pK_a greater than 5.5 need the leaving group to be activated during hydrolysis.

It will be seen that several enzymatic motifs use residues as a general acids to effect protonation of the leaving group. This technique matches the non-enzymatic hydrolysis in that protonation of the leaving group is important as demonstrated by the faster hydrolysis of the monoanion form of monoesters.

1.3.3 LFER Values for Aryl Monoesters and Phosphoramidates Vary as a Function of Ionization

As covered above, existence of a cationic bridging atom greatly enhances hydrolysis. This phenomenon is reflected in LFER values with phosphomonoesters and phosphoramidates.

β_{LG} values for the hydrolysis of aryl phosphomonoester dianions demonstrate sensitivity of the reaction to the leaving group, $\beta_{LG} = -1.23$.[96-98] Leaving groups able to stabilize charge hydrolyze faster, whereas those that cannot stabilize charge hydrolyze slower. Phosphomonoester monoanion hydrolysis has less sensitivity to the leaving group, $\beta_{LG} = -0.27$,[99] as a proton exists that can participate in pre-equilibrium,

Phosphoramidate hydrolysis can display sensitivity or insensitivity to the leaving group, depending upon the nature of the nitrogenous species. Those species with a leaving group pK_a below the pK_a of the phosphate moiety display insensitivity to the nature of the leaving group (Table 1-2). As with phosphomonoester monoanions, these phosphoramidates will readily exchange the proton from the non-bridging oxygen to the bridging atom, forming the reactive species. Substituted pyridines are charged and sensitive to substituents that can stabilize the charge. Phosphoramidates wherein the leaving group pK_a is above the pK_a of the phosphate moiety are also charged and sensitive to substituents that can stabilize the charge. Available β_{nuc} values are in agreement with the β_{LG} values, in that species displaying sensitivity to the leaving group have little sensitivity to the nucleophile (Table 1-3).

PIm does not correspond with any of the Brønsted slopes in Table 1-2. Upon protonation the imidazolium moiety can delocalize positive charge within the ring which holds two nitrogens. This gives PIm much greater stability than analogous phosphorylated pyridines.

Table 1-2. Phosphoramidate Brønsted values showing dependence on leaving group as a function of leaving group type and leaving group pK_a.[100]

Leaving Group	pK_a	β_{LG}	Leaving Group	pKa	β_{LG}	Leaving Group	pK_a	β_{LG}
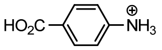	2.54	0.2	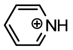	5.37	-1.11	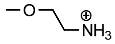	9.61	-0.90
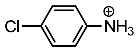	4.07		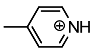	6.21		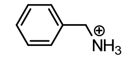	9.33	
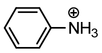	4.69		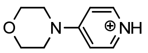	8.53		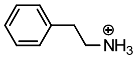	9.83	
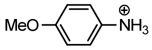	5.44		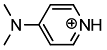	9.39		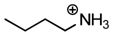	10.77	
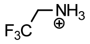	5.7					⊕ NH3	9.38	

LFER data does not indicate whether or not the transition state involves complete cleavage of the P-X bond, i.e. formation of metaphosphate. Stereochemical inversion was found in the hydrolysis of the dianion of 2,4-dinitrophenyl phosphate and the monoanion of phenyl phosphate; this demonstrated metaphosphate does not form as an intermediate.[103,104] Tempered with the lack of racemization, hydrolysis for

Table 1-3. β_{nuc} values for the hydrolysis of DNPP, bis-DNPP,[101] *p*NPP,[99] phosphopyridine, and phosphoacetate.[102]

Hydrolyzing Species	Cation	Attacking Species	β_{nuc}
*p*NPP^{2-}	None	Substituted pyridines	0.18
	0.33 M Mg^{2+}	Substituted pyridines	0.17
	0.33 M Ca^{2+}	Substituted pyridines	0.21
Phosphopyridine^{-}	None	Oxygen nucleophiles	0.24
	0.33 M Mg^{2+}	Oxygen nucleophiles	0.25
Ammonium phosphoramidate^{-}	None	Substituted pyridines	0.22
3-methoxypyridine^{-}	None	Substituted pyridines	0.17
Isoquinoline-*N*-phosphoramidate^{-}	None	Substituted pyridines	0.2
4-morpholinopyridine	None	Substituted pyridines	0.22

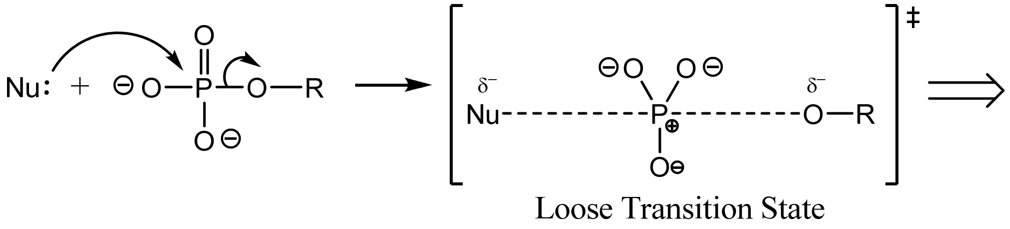

Figure 1-39. Transition state in the hydrolysis of phosphomonoester dianions. Hydrolysis proceeds via a concerted reaction with a loose transition state.

phosphomonoester dianions must proceed via a S_N2 type mechanism with a loose transition state (Figure 1-39).

Three lines of evidence demonstrate that phosphopyridine hydrolysis is also concerted, with a S_N2 type mechanism (Figure 1-40): 1 - phosphopyridine hydrolysis was found to be second order; 2 – decreases in $-\beta_{LG}$ were concurrent with increasing strength of the nucleophile; and 3 – a plot of rate versus pK_{nuc} shows a positive slope.[105] It is a reasonable assumption that other phorphoramidates also undergo hydrolysis with a concerted, loose transition state, but experimental data to support such an assumption is not available.

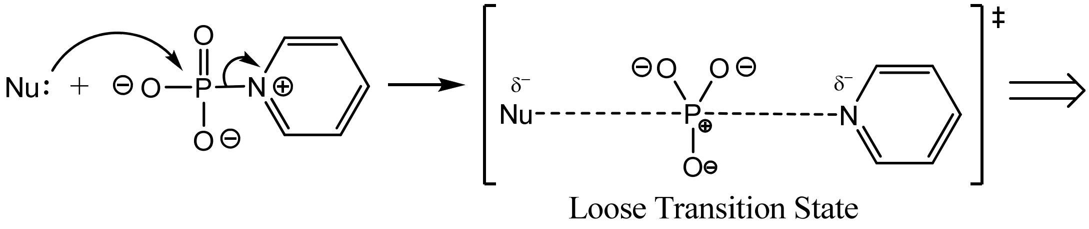

Figure 1-40. Transition state in the hydrolysis of phosphopyridine monoanions. Hydrolysis proceeds via a concerted reaction with a loose transition state. Charge on the pyridine in the transition state will change from positive to neutral. δ^- was drawn to indicate charge is less positive than in ground state.

1.3.4 Metals

Divalent magnesium and calcium cause little change in β_{nuc} or β_{LG} values for reactions of *p*NPP^{2-} or phosphorylated pyridines. For phosphorylated pyridines $\beta_{LGwater}$ = -1.05, while β_{LG} in the presence of 0.33 M Mg^{2+} = -1.02,[99] indicating Mg^{2+} causes no change in the associative character of the transition state (Table 1-2). Yet, the presence of such metals can have different effects upon hydrolytic rates that are compound specific (Table 1-4). Reflecting their nature as Lewis acids, metals have catalytic interactions with negatively charged leaving groups in the transition state.[37,99] With phosphorylated pyridines such interactions are not available. The metals still interact with the non-bridging oxygens, and do so in an anti-catalytic manner.

Under more alkaline conditions, pH 9.1 versus 8.0, magnesium accelerates hydrolysis of phosphoramidates. A metal-coordinated hydroxide is generated, which is a stronger nucleophile than water. The oxygens of the phosphate moiety can coordinate to magnesium, bringing the hydroxide in close proximity to the phosphorus (Figure 1-41).

The combined effects of generation of a strong nucleophile and intramolecularity serve to facilitate catalysis.[37,106]

Table 1-4. Hydrolytic rates (s^{-1}) for *p*NPP dianion, phosphopicoline monoanion,[106] and PIm monoanion[107] in the presence of metals.

	Temp (^oC)	pH	Rate (Rate enhancement)			
Species			No metal	Mg^{2+}	Ca^{2+}	Zn^{2+}
pNPP^{2-}	39.2	9.1	1.7×10^{-8}	1.4×10^{-8} *a* (0.8)	4.8×10^{-8} *a* (2.8)	
Phospho-$Picoline^{-}$	25	8.0	1.6×10^{-3}	1.2×10^{-3} *a* (0.8)	*	
	25	9.1	1.6×10^{-3}	2.4×10^{-3} *a* (1.5)	*	
PIm^{-}	40.1	5.1	1.73×10^{-5}	1.18×10^{-5} *a* (0.7)	1.45×10^{-5} *b* (0.8)	
PIm^{-}	81.6	4.5	2.00×10^{-5}			1.45×10^{-5} *c* (0.7)

*Rate constant could not be calculated from apparent rate constant because K_a for MPP with Ca^{2+} was not determined. However, adjusted rate constant would be lower than apparent rate constant, indicating Ca^{2+} is inhibitory. *a* – 0.33 M for metal, *b* – 0.117 M for metal, *c* – 0.12 M for metal.

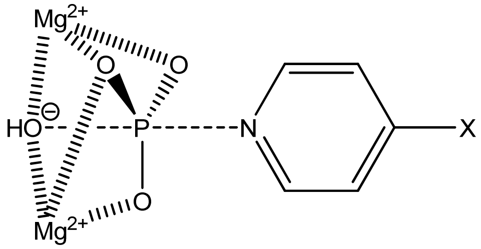

Figure 1-41. Magnesium is catalytic under alkaline conditions.

Zinc coordination lowers the pK_a of water from 15.7 to 9.5. Depending upon the number and types of ligands it can lower the pK_a further to between 5 and 9.[108,109] Variability of the resulting pK_a of water results in flexibility of the resulting hydroxide. Coordinated water with a low pK_a can be readily deprotonated, making it a much better nucleophile than water with a higher pK_a.

If the coordinated water is to serve as a general base an enzyme's coordination sphere may be tailored to generate a metal coordinated hydroxide with a pK_a to match the compound that must be deprotonated by the hydroxide. This may give the enzyme greater specificity for substrates. In general, hydroxyl species that can access zinc's coordination sphere will experience a lowered pK_a, including serine. AP's S102 has a pK_a of less than 5.5, a reflection of its coordination to zinc.

Zinc is able to form catalytic mononuclear and dinuclear complexes. A mononuclear complex has been observed with Zn^{2+}, pyridine-2-carbaldoxime, and PIm (Figure 1-42). An entropy change from -5.2 eu for the uncatalyzed reaction to -28.3 eu for the catalyzed reaction is observed. The Zn^{2+}-PCA catalyzed reaction is $1x10^3$ times faster for PIm.[91] In addition, dinuclear Zn^{2+} complexes catalyze the cleavage of 2-hydroxypropyl-4-NPP and RNA. In these reactions entropic advantages occur.[37,91] It is obvious that one of the roles of zinc is to bring the reactants together.

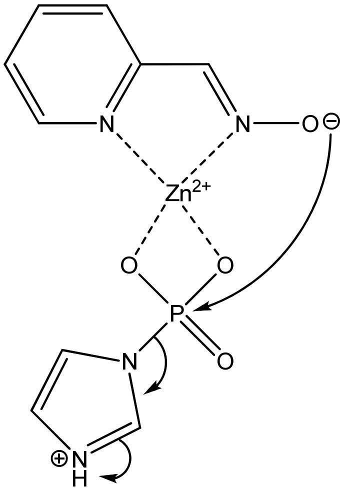

Figure 1-42. Zinc catalyzes hydrolysis of PIm by bringing reactants in close proximity.

1.3.5 Geometry

All phosphomonoesters contain a sp^3 hybridized bridging oxygen with bent bond geometry and two pairs of non-bonding electrons that yield a tetrahedral electron domain geometry (Figure 1-43). Phosphoramidates can form significantly more bond and electron domain geometries, with each geometry having potentially different effects on substrate catalysis.

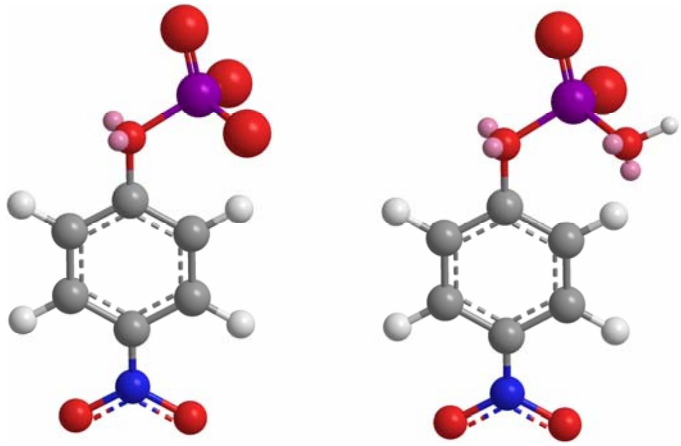

Figure 1-43. 3D structure of *p*NPP as the dianion, left, and monoanion, right. Color scheme is: grey – carbon, white – hydrogen, blue – nitrogen, red – oxygen, purple – phosphorus, pink – electron lone pair. This color scheme will be maintained in further 3D structures of small molecules.

Bridging nitrogens of phosphoramidates may be sp^3 hybridized, with the possibility of one hydrogen and one lone pair, or two hydrogens and no lone pairs. With two hydrogens bond geometry is bent and electron domain geometry is tetrahedral (Figure 1-44 A). With one hydrogen, bond geometry is trigonal pyramidal while the electron domain geometry is tetrahedral (Figure 1-44 B and C). If the bridging nitrogen is sp^2 hybridized, bond geometry is trigonal planar with the non-bonding electrons participating in aromaticity within the ring (Figure 1-44 D and E). For imidazole, protonation of N3 will have no effect on bond or electron domain geometry.

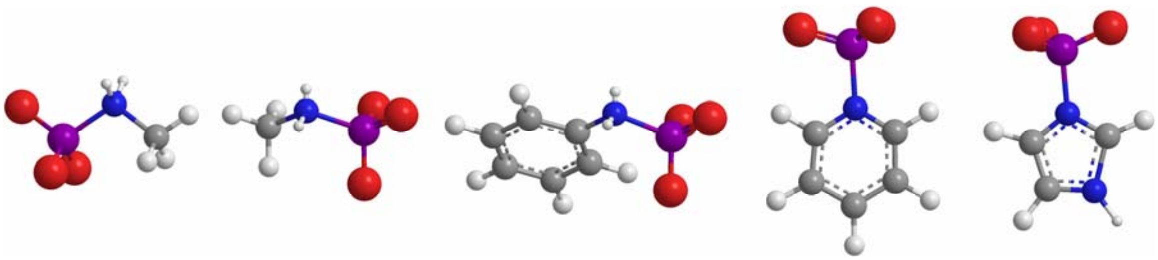

A
Bent,
tetrahedral

B
Trigonal
pyramidal,
tetrahedral

C
Trigonal
pyramidal,
tetrahedral

D
Trigonal planar,
aromatic/trigonal
planar

E
Trigonal planar,
aromatic/trigonal
planar

Figure 1-44. Bond and *electron domain* geometries of the bridging nitrogen for N-methyl phosphoramidate (A & B), *N*-phPAM (C), phosphopyridine (D), and PIm (E).

For PIm, as the pH decreases, protonation occurs on the imidazole moiety,[91] most likely on the non-bridging nitrogen. Protonation of the bridging nitrogen would result in loss of aromaticity.

The information presented heretofore is not a complete review of what is known about phosphomonoester and phosphoramidate hydrolysis. What has been presented provides comparisons between phosphomonoesters and phosphoramidates. An examination of physiological substrates has been readied with this information as background.

1.3.6 Phosphorylated Amino Acids

Amino acids that can form phosphoesters are serine, threonine, and tyrosine, while those that can form phosphoramidates are lysine, arginine, and histidine. Phospholysine and phosphoarginine are the most labile of these phosphorylated species. Much justification for instability can be attributed to pK_a. At physiological pH, phospholysine and phosphoarginine will be protonated on the bridging nitrogen. Only phosphohistidine will exhibit stability due to its pK_a being slightly below physiological. It will require a slightly acidic environment to activate the imidazole leaving group.

As mentioned previously, different enzyme classes have different catalytic motifs. Some motifs protonate the bridging oxygen as part of catalysis. A case could arise wherein a phosphoramidate with an already protonated and charged sp^3 bridging nitrogen binds at the active site. The nitrogen cannot accept another proton before breaking the P-N bond; it may only be protonated during or after cleavage of the bond. What affect timing has on protonation of the bridging atom and enzyme catalysis is uncertain. Also covered were the effects of divalent metals on non-enzymatic catalysis of phosphoramidates. What affect these same metals have on phosphoramidate catalysis when enzyme-bound is uncertain. The geometries of phosphoesters and phosphoramidates can be similar with sp^3 nitrogens, or quite different, as with sp^2 nitrogens. What affect these differences have on enzyme catalysis is uncertain. With the differences between phosphomonoesters and phosphoramidates identified, it cannot then be anticipated that all motifs will catalyze hydrolysis of phosphoesters and phosphoramidates. Differences in the two types of substrates may be sufficient to prevent catalytic promiscuity. On the other hand, there are similarities in the substrates that may allow enzymes to hydrolyze both phosphomonoesters and phosphoramidates.

1.3.7 Substrates used in Study

Small molecule substrates used in this study are *p*NPP, *N*-phPAM, and PIm. The ester bond of *p*NPP closely resembles that of phosphotyrosine, although the electron withdrawing nitro group of *p*NPP helps stabilize charge on the bridging oxygen during hydrolysis. *N*-phPAM is isoelectronic and isosteric with *p*NPP; it is isosteric with phospholysine.

PIm is analogous to phosphohistidine, but differs in the lack of an alkyl substituent at C4. In phosphorylation of histidine, preference is to nitrogen 3 simply because it is less hindered. This point is not trivial, as kinases are selective for which nitrogen is phosphorylated. PHPT1 demonstrated specificity in dephosphorylating nitrogen 3 over nitrogen 1.[2]

The predominant protonation state of the substrates is determined by the assay pH and pK_a (Figure 1-45) *N*-phPAM was determined to have a pK_a of 7.05[110] with protonation occurring on the phosphate oxygen.

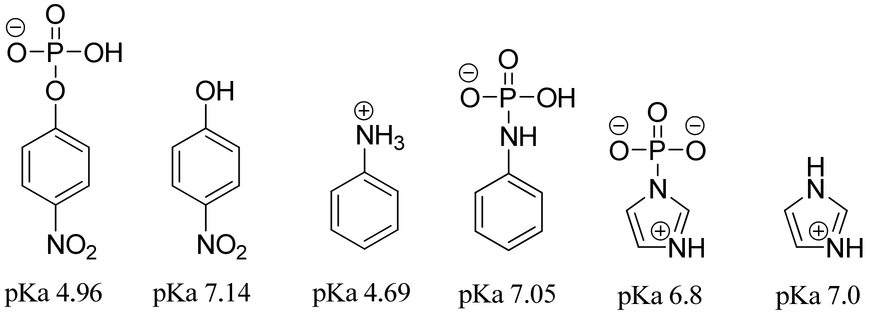

Figure 1-45. Substrates and leaving groups with pK_as.

Comparing the rate constants of the three substrates provides insight to the relative ability of a particular motif to hydrolyze bonds similar those found in phosphorylated proteins. The ability of a motif to catalyze hydrolysis of various substrates is a demonstration of catalytic promiscuity. Catalytic promiscuity may exist even if there are differences in the rate constants with the different substrates.

1.3.8 Considerations for Benchtop Handling of Phosphoramidates

As discussed above, phosphoramidates are several orders of magnitude more labile than phosphate monoesters. Experience with *N*-phPAM demonstrates that even under alkaline solutions significant hydrolysis occurs.

To minimize contact with water the compounds were isolated in the solid form. Storing under inert gas and at cold temperatures was also done to slow degradation. When preparing the compounds for use, they were dissolved in alkali media. The minimum concentration of hydroxide was used to maintain high pH while not causing high ionic strength of enzymatic reaction mixtures. With the general concepts of bench top handling of the compounds in hand, synthetic routes, isolation, and storage can be examined.

CHAPTER 2

MATERIALS AND METHODS

2.1 Initial Considerations

Kinetic constants were obtained by fitting kinetic data to the Michaelis-Menton equation (2.1) to determine V_{max} and K_M.

$$V_{obs} \quad \frac{(V_{max})[S]}{K_M + [S]} \qquad (2.1)$$

V_{obs} is the observed velocity in units of Ms^{-1}, [S] is the substrate concentration in units of M, K_M is the Michaelis constant in units of M, and V_{max} is the velocity of the reaction when all active sites of the enzyme are occupied by substrate. The value of k_{cat}, units of s^{-1}, is given by

$$V_{max} = k_{cat}[E] \qquad (2.2)$$

where [E] is the enzyme concentration. A second order rate constant is given from the ratio of k_{cat}/K_M, units of $M^{-1}s^{-1}$. Comparing the enzymatic rate constant against the un-catalyzed rate constant provides a measure of the enzymes catalytic efficiency.

The Michaelis-Menton equation is based upon consumption of a substrate as represented by equation (2.3). In order to satisfy the assumptions of steady-state kinetics typically less than 5% of the reaction is measured. The initial rate data obtained is used to fit to equation 2.1.

$$E + S \underset{k_{-1}}{\overset{k_1}{\rightleftharpoons}} ES \xrightarrow{k_2} E + P \qquad (2.3)$$

Preconditions to this *modus operandi* are that the substrate can be synthesized and isolated in reasonably pure form; that the substrate will not spontaneously and rapidly hydrolyze, masking enzymatic hydrolysis while also generating significant concentrations of inhibitor; and that there is a way to monitor the reaction for a mere 5% of the reaction. Phosphoramidates challenge all of these preconditions, likely explaining why such experiments are scant in the literature.

With phosphatase assays a common contaminant that will cause difficulties is inorganic phosphate, P_i. Phosphatases can have low inhibition constants, K_i, with P_i, so elimination of P_i from the substrate preparation is critical (Table 2-1). For the three substrates used in this study, different protocols were employed to isolate the products and control concentrations of P_i.

Table 2-1. Published inhibition values, K_i, with P_i for enzymes used in this study.

Enzyme	Phosphate K_i (mM)	Ref
AP	0.0143, 0.001	37,111
λPP	0.71	58
PAcP	0.8	112,113
VHR	0.97	42
YopH	6.1, 5.5	26,27
PHPT1	1.1	20

2.2 Synthetic Protocols

2.2.1 General Procedures

Pyridine and methylene chloride were distilled after being refluxed over CaH_2 and used immediately. Methanol was sparged with nitrogen gas for an hour and used immediately. Diethyl ether was distilled after being refluxed over sodium and used immediately. Aniline was purchased from Fisher. It was purified by simple distillation, followed by storage in the dark under nitrogen gas. Acetone and ethyl acetate were purchased from Fisher and used as supplied. Phosphorus oxychloride, para-nitro phenol, benzyl alcohol, trichloro phosphite, palladium on carbon, and imidazole were purchased from Aldrich and used as supplied. Triethyl amine was purchased from Fisher. It was kept over sodium hydroxide and distilled prior to use. ^{1}H NMR spectra were obtained at 300 MHz (JEOL, Tokyo, Japan) with TMS as an internal standard in $CDCl_3$; external standard, when used, was pyrazine. ^{31}P NMR spectra were obtained at 122 MHz (JEOL, Tokyo, Japan). UV/Vis spectra requiring 1 or 0.1 cm path length cells were obtained on a Cary 50 (Agilent Technologies, agilent.com/chem); assays suitable for 96 well plates used Costar 96 well flat-bottomed 330 μL plates read in a Molecular Devices VERSAMax microplate reader.

2.2.2 *p*NPP, disodium salt.

The disodium salt of *p*NPP was prepared following literature procedures (Figure 2-1).[114] Phosphorus oxychloride (30 mL, 320 mmol, 1.5 eq) was dissolved in freshly distilled anhydrous pyridine (205 mL) to make a 1.6 M solution. pNP, (27.8 g, 200 mmol, 1 eq) was dissolved in pyridine (100 mL) to make a 2 M solution and placed in an addition funnel. The reaction was run under dry nitrogen at 0 ^oC. After slow addition of pNP with stirring, the mixture stood for 30 minutes, upon which the mixture was slowly poured into 400 mL of cold water. The resulting solution was titrated to pH 7~8 with 4 N NaOH. The product was isolated by evaporation under reduced pressure and purified by crystallization.[115] After dissolving the crude product in 90% cold methanol (20 mL MeOH per 1 g crude) and filtering, an equal volume of acetone was added to the filtrate. The solution stood at 4 ^oC overnight, whereupon the resultant crystals were filtered and washed with acetone. The crystals were air-dried on a Buchner funnel for thirty minutes. The product was kept at 4 ^oC.

While it would seem counterintuitive to not dry the product as thoroughly as possible, literature precedent indicated complete removal of water caused more hydrolysis than leaving the product as a hydrate.[115] The product was stored both as a hydrate and after removing water via high vacuum with moderate heat. NMR confirms that less hydrolysis was obtained with air drying. Further, storage at 4 °C was sufficient to minimize hydrolysis in the solid state, and made handling easier when introducing the product to the bench.

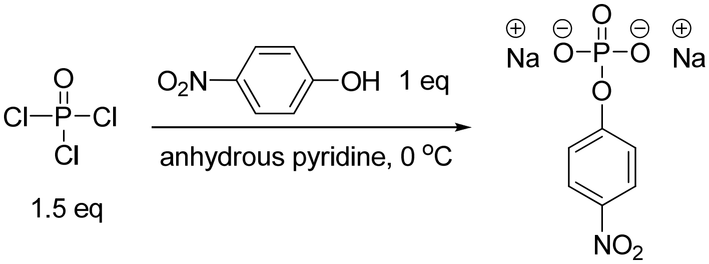

Figure 2-1. Synthesis of *p*NPP.

^{1}H NMR (300 MHz, D_2O): δ 7.2 (d, J=7.6 Hz, 2H), 8.1 (d, J=9.4 Hz, 2H); ^{31}P NMR (122 MHz, D_2O) δ 0.24 (Figures A1 and A2).

2.2.3 *N*-phenyl phosphoramidate

N-phenyl phosphoramidate was synthesized following the general scheme depicted in Figure 2-2.

2.2.4 Tribenzyl phosphite, (Figure 2-3)[116]

Trichloro phosphite (2.56 mL, 29 mmol, 1 eq) and triethyl amine (12.5 mL, 89 mmol, 3.1 eq) were dissolved in freshly distilled anhydrous diethyl ether (150 mL) for a 0.2 M PCl_3 solution in a round bottom flask with stir bar. Benzyl alcohol (8.9 mL, 86 mmol, 3 eq) was dissolved in 30 mL ether for a 2.9 M solution that was placed in an

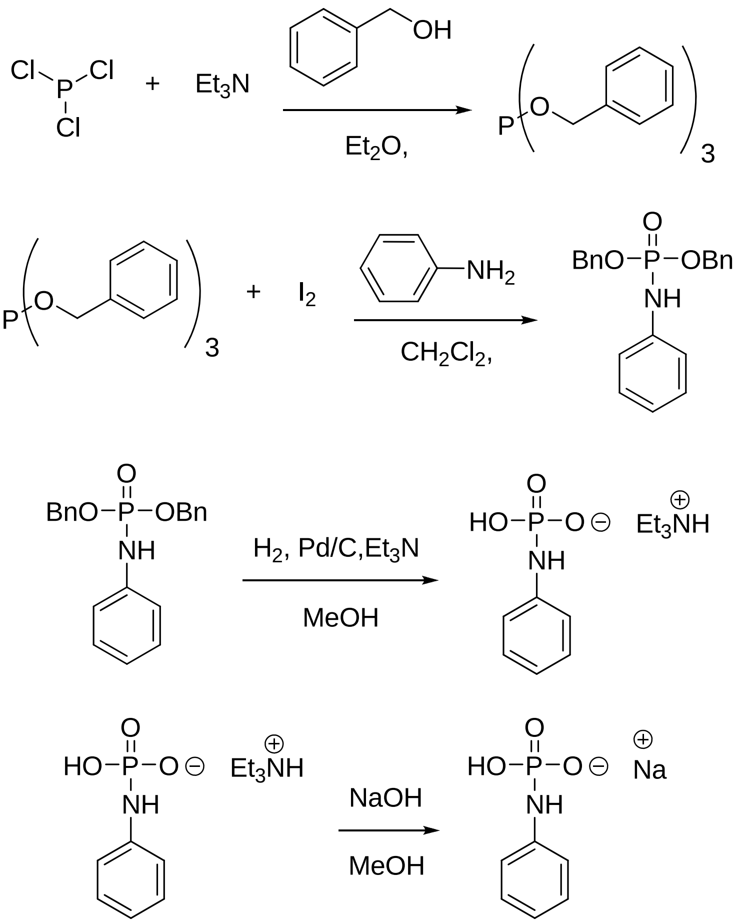

Figure 2-2. General synthetic scheme for *N*-phenyl phosphoramidate. Literature protocols[116,117] did not provide a direct route to the product.

addition funnel. The apparatus was purged with and reaction maintained under nitrogen. The round bottom flask was cooled to -78 °C in a dry ice/acetone bath. The benzyl alcohol was slowly added to completion. The mixture was brought to room temperature over a 14 hour period and filtered. The filtrate was evaporated under reduced pressure. The clear-colorless, oily product was used without purification. It was maintained under nitrogen, in dark, at room temperature. The product rapidly degrades on normal phase silica gel, even if triethylamine is added to the eluent, precluding purification in this manner. NMR indicated the product was reasonably clean after high vacuum and was used as is for the next step.

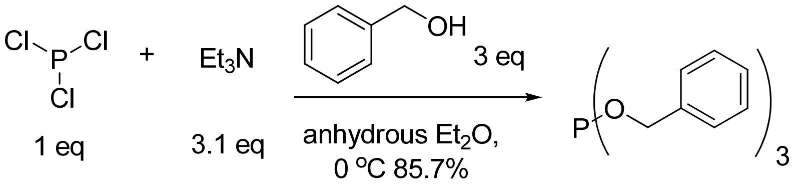

Figure 2-3. Synthesis of tribenzyl phosphite.

^{1}H NMR (300 MHz, $CDCl_3$): δ 4.9 (d, *J* =7.9 Hz, 6H), 7.3 (m, 15H); ^{31}P NMR (122 MHz, $CDCl_3$) δ 140.2 (Figures A3 through A5).

2.2.5 **Dibenzyl *N*-phenyl phosphoramidate** (Figure 2-4)[117]

Iodine (0.51 g, 1.95 mmol, <1 eq) was dissolved in 5 mL methylene chloride for a 0.4 M solution and placed in an addition funnel; it takes several hours for the iodine to completely dissolve. Freshly distilled aniline (0.28 g, 3 mmol, 1.5 eq) was dissolved in 5 mL methylene chloride for a 0.6 M solution and placed in an addition funnel.

Tribenzyl phosphite (0.67 g, 2 mmol, 1 eq) was dissolved in 3 mL methylene chloride for a 0.6 M solution. The addition funnels were placed over a round bottom flask holding the tribenzyl phosphite, the system flushed with nitrogen, and cooled to 0 °C. The iodine solution was slowly added with stirring to the tribenzyl phosphite. Less than 1 eq of iodine was used, keeping the reaction clear and colorless. Excessive iodine causes the reaction mixture to turn pink, lowers yield, and makes clean-up difficult. The mixture was maintained at 0 °C for one hour, whereupon aniline was slowly added with stirring. The reaction was maintained at 0 °C for twenty minutes, brought to room temperature, kept for two hours, and evaporated under reduced pressure. The crude product was partitioned between 25 mL of diethyl ether and 25 mL 2 N HCl. The organic layer was washed twice with 25 mL of 2 N HCl, once with 25 mL of brine, dried over magnesium sulfate, filtered, and evaporated under reduced pressure. Purification was completed isocratically by normal phase silica chromatography (50/50 Hex/EtOAc). The product, a white solid, was further purified by recrystallization (80/20 hexane/ethylene chloride). Crystals were dried under vacuum and kept at -10 °C under nitrogen.

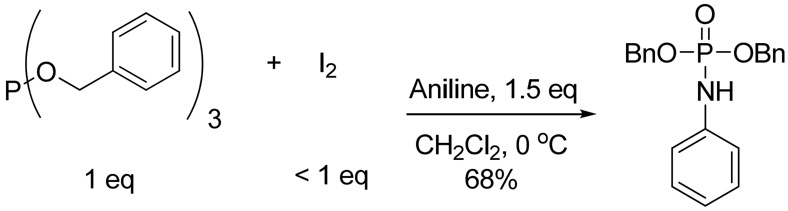

Figure 2-4. Synthesis of dibenzyl *N*-phenyl phosphoramidate.

^{1}H NMR (300 MHz, $CDCl_3$): δ 5.1 (m, 4H), 7.0 (t, *J* =7.6, 3H), 7.2 (m, 2H), 7.3 (m, 10H); ^{31}P NMR (122 MHz, $CDCl_3$) δ 3.1 (Figures A6 through A8).

2.2.6 *N*-phPAM triethyl ammonium salt (Figure 2-5)[117]

Dibenzyl *N*-phenyl phosphoramidate (2.2 g, 6.1 mmol, 1 eq), triethylamine (2.2 mL, 15 mmol, 2.5 eq), palladium on carbon (0.86 g of 5%), 40 mL of methanol, and a stir bar were placed in a three neck flask fitted with a hydrogen filled balloon. The vessel was evacuated three times followed by flushing with nitrogen. Hydrogen gas supplied by balloon and vigorous stirring initiated. After thirty minutes, one benzyl group was removed and the palladium had become poisoned. The reaction was quenched by filtration of the palladium catalyst over celite. Repeating the above procedure using the same quantities removed the second benzyl group. The solid white precipitate was isolated by evaporation under reduced pressure. Recrystallization was effected using 85/10/5 hexane/dichloro ethane/ethyl acetate. The product is stored at -10 °C under N_2.

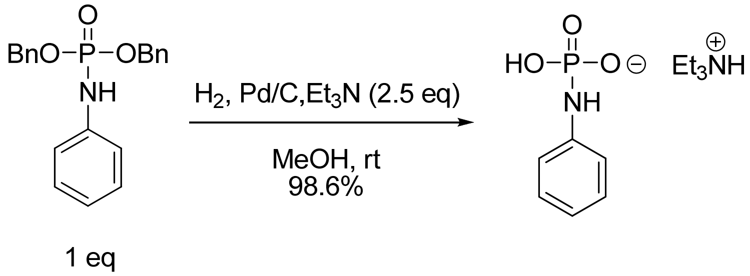

Figure 2-5. Synthesis of *N*-phPAM triethyl ammonium salt.

^{1}H NMR (300 MHz, $CDCl_3$): δ 1.2 (t, *J* =7.2, 9H), 2.9 (q, *J* =7.2, 6H) 6.7 (m, 1H) 7.1 (m, 4H); ^{31}P NMR (122 MHz, $CDCl_3$) δ 0.9 (Figures A9 and A10).

2.2.7 *N*-phPAM sodium salt

The triethylammonium salt of *N*-phenyl phosphoramidate (2.2 g, 6.1 mol, 1 eq), was dissolved in freshly sparged methanol (2.2 mL, 15 mmol, 2.5 eq). An equal volume of 2 N NaOH was added, and the aqueous layer washed three times with ethyl acetate. The aqueous layer was brought to neutral pH with 2 N HCl and frozen with liquid nitrogen. After lyophilization, the product was dissolved with methylene chloride followed by evaporation under reduced pressure.

^{1}H NMR (300 MHz, D_2O): δ 6.7 (t, *J* =7.2, 1H), 6.9 (d, *J* =7.5, 2H) 7.1 (m, 2H); ^{31}P NMR (122 MHz, D_2O) δ 1.1 (Figures A11 and A12).

2.2.8 Phosphoimidazole

Phosphoimidazole was synthesized following the general scheme depicted in Figure 2-6.

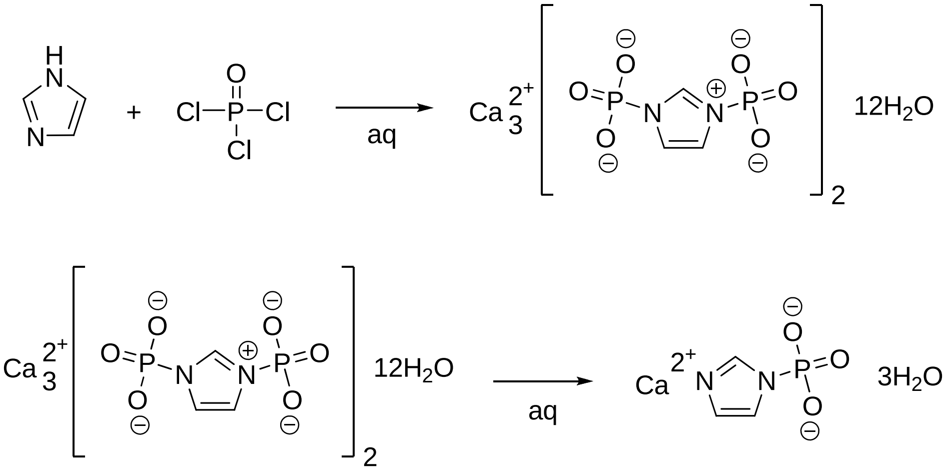

Figure 2-6. General synthetic scheme for phosphoimidazole.

2.2.9 Diphosphoimidazole (Figure 2-7)[118]

Diphosphoimidazole was prepared according to a literature method with modifications. Imidazole (4 g, 58 mmol, 1 eq) was dissolved in 40 mL water in an Erlenmeyer flask. The flask was kept at 0 °C throughout the reaction. The pH was adjusted to 11 using 5 N potassium hydroxide. A pH probe and thermometer were placed in the vessel. Phosphoryl chloride (23 mL, 240 mmol, 4.2 eq) was added in 150 μL increments using a pipette. The pipette tip was placed under the level of the solvent when adding the phosphoryl chloride. Vigorous stirring was maintained throughout the addition. After addition of each phosphoryl chloride aliquot, the temperature was allowed to return to 0 °C and the pH was adjusted to 11 using 5 N KOH. After complete addition of the phosphoryl chloride, the temperature and pH were maintained for 30 min., after which the reaction was kept at room temperature for 20 hours. The pH was adjusted to 9.5 with 2 N HCl. Ethanol (45 mL) was added. The mixture was allowed to stand for 18 hours at 4 °C, whereupon the product and contaminating phosphate were filtered. The product with contaminant was stored at -10 °C under N_2.

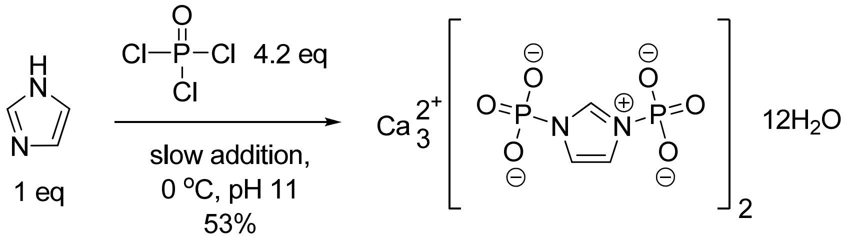

Figure 2-7. Synthesis of diphosphoimidazole.

^{1}H NMR (300 MHz, D$_2$O): δ7.3 (s, 2H), 8.3 (s, 1H); ^{31}P NMR (122 MHz, D$_2$O) δ-3.8 (Figures A13 and A14).

2.2.10 **Monophosphoimidazole** (Figure 2-8)[119]

Monophosphoimidazole was prepared according to a literature method with modifications. Diphosphoimidazole (2.1 g, 0.0027 mol, 1 eq) was dissolved in 140 mL water, the pH brought to 12.5, and the solution kept at 50 °C for 12 hours. Monitoring the reaction via chromatography is problematic. The reaction was monitored by ^{1}H NMR. As the reaction progresses, starting material, product, and any contaminating Im can be seen (Figures 2-21 and 2-22). When the reaction was complete the mixture was cooled to 0 °C and filtered. The filtrate was adjusted to pH 8.5 with 5 M HCl. Calcium chloride dihydrate (1.41 g, 0.0096 mol, 3.6 eq) was dissolved in the minimum quantity of water and the pH was adjusted to pH 8.5. This was added to the filtrate, and the resulting mixture filtered; the filtered precipitate was discarded. Three volumes of ethanol were added to the filtrate, and the mixture was cooled to 4 °C for 4 hours. The resulting monophosphoimidazole was filtered, washed with 75% ethanol, ethanol, and diethyl ether. It was dried via high vacuum, placed in a 50 mL cylindrical vial, flushed with dry nitrogen, and stored as the calcium salt. The calcium salt is insoluble in water and is stable at room temperature. Prior to use, the calcium must be exchanged for sodium.

This is effected by incubating the calcium salt with Amberlite IRC 748 cation exchange resin at a ratio of 20 g resin for 1 g phosphoimidazole at pH 8.5 for exactly 30 minutes. The resulting PIm concentration was determined via NMR using a pyrazine standard of known concentration.

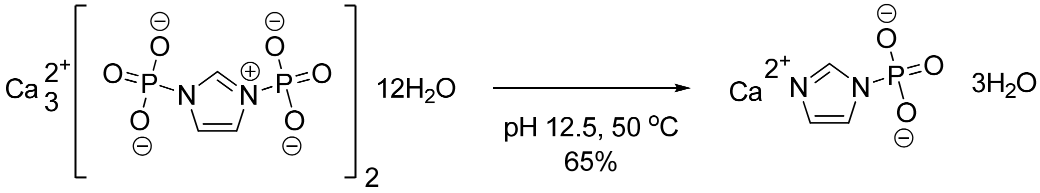

Figure 2-8. Synthesis of monophosphoimidazole.

^{1}H NMR (300 MHz, D_2O): δ 6.9 (s, 1H), 7.1 (s, 1H), 7.7 (s, 1H); ^{31}P NMR (122 MHz, D_2O) δ -4.0 (Figures A15 and A16).

2.3 Enzyme Preparation

2.3.1 Human PHPT1

The pNIC28-Bsa4 vector containing the human PHPT1 gene with His tag was a gift from Martin Hammarstrom, M. Sc., Ph.D., Karolinska Institutet Structural Genomics Consortium. Expression and purification were as described in the literature.[20,120] DH-5α cells (0.5 mL) were transformed with 2 μL of vector at 42 °C for 1 minute. The cells were then placed on ice for 30 minutes. The cells were placed in 400 μL of growth media (10 g/L tryptone, 5 g/L yeast extract, 5 g/L NaCl), and shaken at 37 °C for 1.5 hours. They were plated on growth media containing kanamycin (0.035 g/L) and grown at 37 °C for 24 hours. A small scale growth was completed by selecting colonies and inoculating two 50 mL tubes of growth media with kanamycin. DNA was removed via a

QIApre Spin Miniprep Kit (250). Concentration was determined by a Nanodrop ND-1000 spectrophotometer from Thermo Fisher Scientific. An aliquot of DNA was sent to USU's Center for Integrated Biotechnology, CIB, for sequencing, which confirmed vector contained the desired gene.

BL21 (DE3) cells were transformed with 2 μL of vector at 42 ^{o}C for 1 minute. The cells were then placed on ice for 30 minutes. The cells were placed in 400 μL of growth media (10 g/L tryptone, 5 g/L yeast extract, 5 g/L NaCl), and shaken at 37 ^{o}C for 1.5 hours. They were plated on growth media containing kanamycin (0.035 g/L) and grown at 37 ^{o}C for 24 hours. A small scale growth was completed by selecting colonies and inoculating two 50 mL tubes of growth media with kanamycin. After completing a small scale growth, a large scale growth was completed using 3 L of growth media. After inoculating the media, cells were grown at 37 ^{o}C until the OD_{600} was 1.8~2, whereupon protein expression was induced by the addition of 0.5 mM isopropyl thiogalactaside, IPTG. After overnight incubation, cells were harvested by centrifugation, RCF (g) 6816, 25 minutes at 4 ^{o}C. Cells were frozen at -80 ^{o}C.

Cells were placed in 40 mL lysis buffer (0.05 M sodium phosphate, 0.5 M NaCl, 0.01 M Im., 0.0005 M TCEP, 10% glycerol, 0.3 μM aprotinin, 4 μM leupeptin, 4 μM pepstatin, titrated to pH 7.5) and thawed. Lysis was completed with ten iterations, seven cycles per iteration, of sonication. The lysate was centrifuged, RCF (g) 52648, for 45 minutes at 4 ^{o}C.

The supernatant was added to nickel resin (10 mL) and mixed on a rotator-mixer for an hour at 4 ^{o}C. The solution was centrifuged at 1,500 rpm for 10 minutes, whereupon the supernatant was discarded. Bind/wash buffer (0.05 M sodium phosphate, 0.5 M NaCl, 0.01 M Im., 0.0005 M TCEP, 10% glycerol, pH 7.5) was added, mixed for ten minutes, centrifuged, and the supernatant discarded; this step was repeated. Protein was eluted isocratically from a 25 mL column at 4 ^{o}C (0.05 M sodium phosphate, 0.5 M NaCl, 0.5 M Im., 0.0005 M TCEP, 10% glycerol, pH 7.5). Fractions were pooled and dialyzed for 2 hours in dialysis buffer (0.05 M Tris, 0.5 mM EDTA, 10% glycerol, 10 mM DTT, pH 8.0).

Fresh dialysis buffer was added and TEV cleavage protease was added to the dialysis bag. The solution was kept overnight at 4 ^{o}C, whereupon new dialysis buffer was added (0.05 M sodium phosphate, 0.5 M NaCl, 10% glycerol, 10 mM Im., 0.5 mM TCEP, pH 8.0); dialysis was run for 2 hours. The solution was equilibrated with the nickel resin again. TEV protease, cleaved His tags, and un-cleaved protein stick to the resin, leaving the protein in the supernatant. Protein was concentrated using an Amicon 10,000 MW membrane. Pressure for the concentrator was 20 psi.

The protein was purified by size exclusion chromatography using a SUPERDEX column (0.02 M HEPES, 0.3 M NaCl, 10% glycerol, 0.5 mM DTT, pH 7.5). Concentration was accomplished as indicated above (final concentration 300 μmol/L) and checked using a Nanodrop ND-1000 spectrophotometer from Thermo Fisher Scientific. Extinction coefficient was determined using protein sequence. Purity was checked by SDS-PAGE (Figure 2-9). Protein was dialyzed (0.05 M HEPES, 0.3 M NaCl, 10% glycerol, 0.5 mM DTT), concentrated, the concentration checked (ε 26088 $cm^{-1}M^{-1}$), and flash frozen in liquid nitrogen. The protein was stored at -80 ^{o}C.

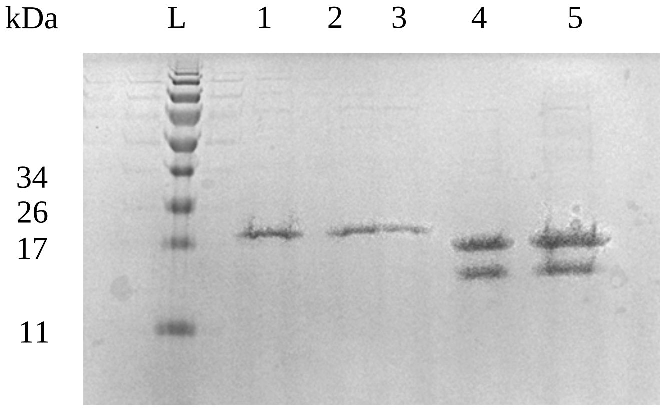

Figure 2-9. SDS-PAGE of PHPT1. Lanes 1, 2 and 3 are final product. Lanes 4 and 5 are after cleavage with TEV protease.

2.3.2 YopH

BL21 cells with the YopH gene were obtained from lab cell stocks. Expression and purification were as described in literature.[22,35] Pin-head sized aliquots of frozen cell stocks were used to inoculate small scale (40 mL) growth media (8 g bacto tryptone, 5 g yeast extract, 5 g NaCl, pH 7.0, 100 μg/mL ampicillin). Cells were grown at 37 ^{o}C until OD660 was ~1, whereupon protein expression was inducted with IPTG (400 μM). After expression was continued overnight, cells were harvested by centrifugation, RCF (g) 6816, 25 minutes at 4 ^{o}C. Cells were frozen at -80 ^{o}C.

Cells were placed in 40 mL lysis buffer (100 mM sodium acetate, 100 mM NaCl, 1 mM EDTA, 10% glycerol, 0.3 μM aprotinin, 4 μM leupeptin, 4 μM pepstatin, titrated to pH 5.7) and thawed. Lysis was completed with ten iterations, seven cycles per iteration, of sonication. The lysate was centrifuged, RCF (g) 52648, for 45 minutes at 4 ^{o}C.

Lysate was bound to a Sephadex C-25 cation exchange column (100 mM sodium acetate, 100 mM NaCl, 1 mM EDTA, pH 5.7) at 4 ^{o}C for 1 hour. Protein was removed using gradient elution with increasing concentration of NaCl (100 mM NaCl to 500 mM NaCl, 100 mM sodium acetate, 1 mM EDTA, pH 5.7).

The protein was purified by size exclusion chromatography using a SUPERDEX column (100 mM sodium acetate, 100 mM NaCl, 1 mM EDTA, pH 5.7) and concentrated (final concentration 332 μmol/L) using an Amicon 10,000 MW membrane under 20 psi of pressure. Purity was confirmed by SDS-PAGE (Figure 2-10). Concentration was determined using a Nanodrop ND-1000 spectrophotometer from Thermo Fisher Scientific using an extinction coefficient determined using the protein sequence. (ε 19348 cm^{-1}M^{-1}), and flash frozen in liquid nitrogen. Purified protein was stored at -80 ^{o}C.

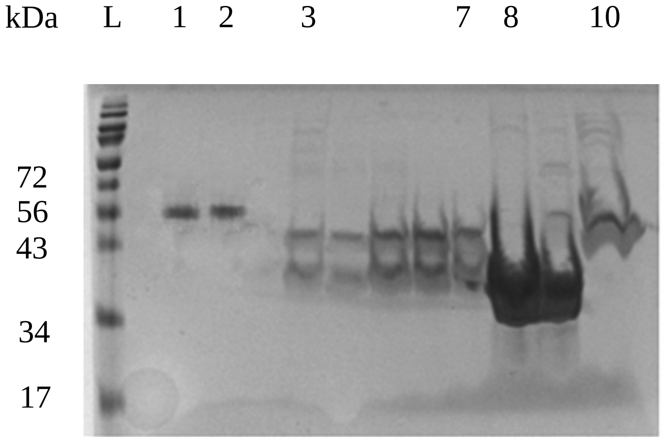

Figure 2-10. SDS-PAGE of YopH. Lanes 1 and 2 are final product. Lanes 3 through 7 and 8 through 10 are before chromatography.

2.3.3 Alkaline Phosphatase

The pEK154 vector containing the *E. coli* AP gene was a gift from Prof. John Peters, Montana State University. Expression and purification were as described in the literature.[111,121] *Escherichia coli* DH-5α cells (0.5 mL) were transformed by heating with

2 μL of vector at 42 °C for 1 minute. The cells were then placed on ice for 30 minutes. The cells were placed in 400 μL of growth media (8 g/L tryptone, 5 g/L yeast extract, 5 g/L NaCl, pH 7.5), and shaken at 37 °C for 1.5 hours. They were plated on growth media with ampicillin (0.035 g/L) and grown at 37 °C for 24 hours. A small scale growth was completed by selecting colonies and inoculating two 50 mL tubes of growth media with ampicillin. DNA was isolated via a QIAprep Spin Miniprep Kit (250). Concentration was determined by a Nanodrop ND-1000 spectrophotometer from Thermo Fisher Scientific.

Escherichia coli BL21 (DE3) cells were transformed following the above protocol. After completing a small scale growth, a large scale growth was completed using 3 L of the same growth media. After inoculating the media, cells were grown at 37 °C until the OD_{600} was 0.5,[71] whereupon protein expression was induced by the addition of 0.5 mM IPTG. After overnight incubation, cells were harvested by centrifugation RCF (g) 6816, 25 minutes at 4 °C. Cells were frozen at -80 °C.

Cells were thawed in 75 mL of wash buffer (10 mM Tris, 10 mM $MgCl_2$, pH 7.6), centrifuged RCF (g) 6816, 25 minutes at 4 °C. Washing was repeated once, whereupon the cells were suspended in 30 mM Tris, pH 7.6. Using the cells in wash buffer, sucrose was added to 20% weight/volume. EDTA was added to make the solution 5 mM. Cells were gently stirred for 10 minutes at room temperature. The solution was centrifuged RCF (g) 6816, 25 minutes at 4 °C. Cells were resuspended in ice water, shaken vigorously for 10 minutes, and centrifuged, RCF (g) 6816, 25 minutes at 4 °C.

Stock solutions of Tris, $MgCl_2$, $ZnCl_2$ were added to make a final concentration of 10 mM, 100 mM, and 10 mM, respectively, with the final pH being 7.0. The mixture was heated to 80 °C for 10 minutes, cooled in an ice bath, and centrifuged, RCF (g) 6816, for 15 minutes at 4 °C. Ammonium sulfate was added to the supernatant to 85% of saturation, followed by centrifugation RCF (g) 6816, 25 minutes at 4 °C. The pellet was placed in 10 mL of dialysis buffer and dialyzed overnight with two changes of dialysis buffer (10 mM Tris, 1 mM $MgCl_2$, 0.1 mM NaH_2PO_4, 0.1 mM $ZnSO_4$, pH 7.0).

Purity was checked by SDS-PAGE (Figure 2-11). The protein was concentrated (final concentration 49 umol/L) using an Amicon 10,000 MW membrane. Pressure for the concentrator was 20 psi. Concentration was determined with a Nanodrop ND-1000 spectrophotometer from Thermo Fisher Scientific using an extinction coefficient determined from the protein sequence (ε 31390 $cm^{-1}M^{-1}$). Concentrated protein was flash frozen in liquid nitrogen and stored at -80 °C.

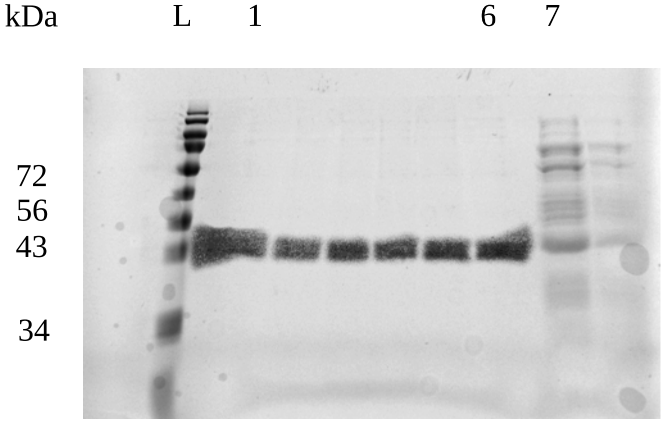

Figure 2-11. SDS-PAGE of AP. Lanes 1 through 6 are final product. Lane 7 is before purification and concentration.

2.3.4 λPP

The T7-7 vector containing the λPP gene with His tag was a gift from Amy Rosenzweig and Nicholas Reiter, Northwestern University. Expression and purification were as described in literature.[54,58-60] *Escherichia coli* DH-5α cells (0.5 mL) were transformed by heating with 2 μL of vector at 42 °C for 1 minute. The cells were then placed on ice for 30 minutes. The cells were placed in 400 μL of growth media (8 g/L tryptone, 5 g/L yeast extract, 5 g/L NaCl, pH 7.5) and shaken at 37 °C for 1.5 hours. They were plated on growth media containing ampicillin (0.4 mg/L) and grown at 37 °C for 24 hours. A small scale growth was completed by selecting colonies and inoculating two 50 mL tubes of growth media with ampicillin (0.4 mg/L). DNA was isolated via a QIAprep Spin Miniprep Kit (250). Concentration was determined by a Nanodrop ND-1000 spectrophotometer from Thermo Fisher Scientific. An aliquot of DNA was sent to USU's Center for Integrated Biotechnology, CIB, for sequencing, which confirmed the isolated DNA contained the desired gene.

BL21 (DE3) cells were transformed following the above protocol. After completing a small scale growth, a large scale growth was completed using 3 L of growth media. After inoculating the media, cells were grown at 37 °C until the OD_{600} was 0.7~1, whereupon protein expression was induced by the addition of 0.3 mM IPTG. After overnight incubation, cells were harvested by centrifugation, RCF (g) 6816, 25 minutes at 4 °C. Cells were frozen at -80 °C.

Cells were placed in 40 mL lysis buffer (0.025 M Tris, 0.002 M EDTA, 20% glycerol, 0.3 μM aprotinin, 4 μM leupeptin, 4 μM pepstatin, titrated to pH 7.8) and thawed. Lysis was completed with ten iterations, seven cycles per iteration, of sonication. The lysate was centrifuged, RCF (g) 52648, for 45 minutes at 4 °C.

The supernatant was loaded to 250 mL of DEAE Sephadex (25 mM Tris, pH 7.8, 2 mM EDTA) and eluted isocratically while maintaining 4 °C (25 mM Tris, pH 7.8, 100 mM NaCl, 2 mM EDTA). Fractions were pooled based upon phosphatase activity with *p*NPP. The pooled active fractions were loaded to 100 mL of phenyl Sepharose fast flow (25 mM Tris, pH 7.8, 500 mM NaCl) and eluted isocratically while maintaining 4 °C (25 mM Tris, pH 7.8, 50% glycerol). Fractions were pooled based upon phosphatase activity and SDS-PAGE (Figure 2-12), and subsequently dialyzed (9 mM Tris, pH 7.8, 10% glycerol, 1 mM DTT). The dialysalate was concentrated (final concentration 0.35 μmol/L) using an Amicon 10,000 MW membrane at a pressure of 20 psi. Concentration was determined with a Nanodrop ND-1000 spectrophotometer from Thermo Fisher Scientific (ε 40450 $cm^{-1}M^{-1}$), the concentrated protein was flash frozen in liquid nitrogen and stored at -80 °C.

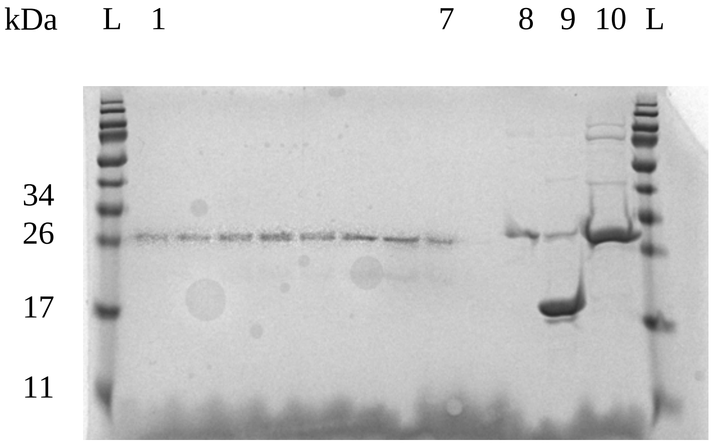

Figure 2-12. SDS-PAGE of λPP. Lanes 1 through 7 are final product. Lanes 8 through 10 are before chromatography

2.4 Substrate-Dependent Experimental Techniques and Mathematical Analysis

2.4.1 *p*NPP

Several techniques were employed to monitor *p*NPP hydrolysis. When the assay was conducted under alkaline conditions, the hydrolysis product p-nitrophenolate was detected directly by UV/Vis (ε p-nitrophenolate 18,300 λ_{max} = 405 nm).[122,123] For reactions at mildly acidic conditions hydroxide was added to quench the reaction and produce fully ionized p-nitrophenolate.

Enzymatic rates were measured as a function of substrate concentration, followed by a computerized least squares fit to the Michaelis-Menton equation, to yield V_{max} and K_M. The value of k_{cat} was then obtained from V_{max}, and the second order rate constant was had from k_{cat}/K_M.

2.4.2 *N*-phPAM

While a sufficient difference exists between the absorbance spectra of *N*-phPAM and aniline to facilitate direct read assays, the difference is small. When using this technique with *N*-phPAM, several runs must be made to reduce standard deviation to acceptable levels. The change in absorbance is a reflection of the change in concentration of product, or substrate (2.4).

$$\frac{\Delta A_{ttl}}{\Delta t} = l \quad \mathrm{x} \quad \frac{\Delta C_{prod}}{\Delta t} \quad \mathrm{x} \quad (\varepsilon_{prod} - \varepsilon_{SM}) \qquad (2.4)$$

The challenge in the technique is had by considering an example. At pH 7.5 the difference in extinction coefficient is 415 $M^{-1}cm^{-1}$. If a 5 mM solution of *N*-phPAM is enzymatically hydrolyzed to 5% in a 1 cm cell, the change in absorbance is 0.1 AU. While this change is small, it is within the ability of the lab's instrument to detect.

Each enzyme was treated with different concentrations of *N*-phPAM. Upon mixing, the absorbance was read. Plots of concentration versus rate, were made, and least-squares fitted to the Michaelis-Menton equation.

2.4.3 PIm

Enzymatic assays were conducted at, or near, the pH optimum for the enzyme (see chapter 1). Because of this, assays were conducted at pH 5.5, 6.5, 7.8, and pH 8.0. A method was needed to detect hydrolysis of PIm at these four pH conditions.

At pH 5.5 the absorbance spectra for PIm and Im are nearly identical making it impractical to monitor the enzymatic reaction spectrophotometrically (Figure 2-13). Although at pH 8.0 some absorbance difference existed between PIm and Im, buffers absorb strongly in the region where the absorbance difference was greatest.

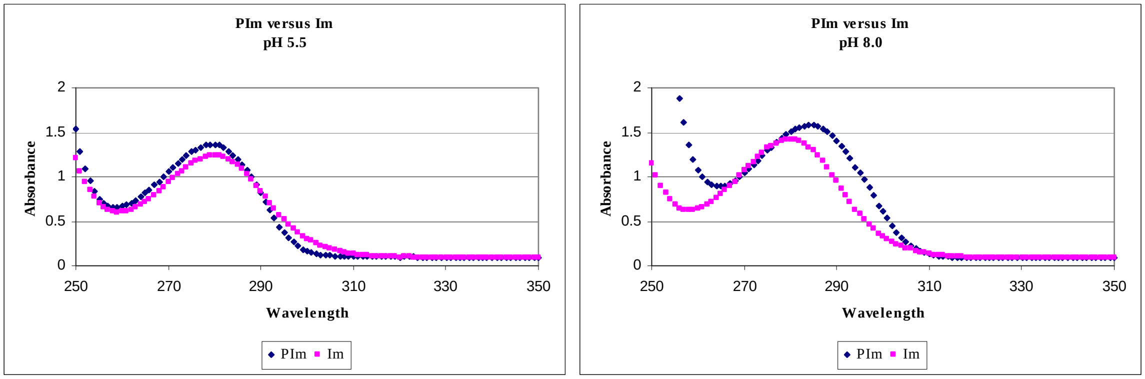

Figure 2-13. UV/Vis profile for PIm versus Im, both at 1 mM.

Molybdate assays of inorganic phosphate require acidic pH[124-132] which result in significant hydrolysis of PIm; this prohibited their use. Proton NMR was found to be able to detect hydrolysis of PIm. NMR is not well suited to initial rate methods because the sensitivity necessary to accurately quantify the first few percent of reaction is lacking. For this reason, full time course kinetics were carried out.

During full time course experiments significant concentrations of inhibitor P_i are produced. The Michaelis-Menton equation may be used if modified to account for the inhibitor concentration (2.5).

$$V_{obs} = \frac{(V_{max})[S]}{K_M(1 + [I]/K_i) + [S]} \qquad (2.5)$$

I is the inhibitor, K_i is the inhibition constant.

Duplicate NMR experiments set at equal time intervals are run until an enzyme consumes 90% of a substrate, or until the instrument cannot detect an integratable signal (Figure 2-14). As substrate is converted to product and monitored over time, each NMR spectrum yields three variables, [S], [I], and V_{obs}. Reactions are typically assayed at 5 minute intervals for 60 minutes. Least squares fitting of data is accomplished using the Scientist program by Micromath. A similar technique has been reported.[2]

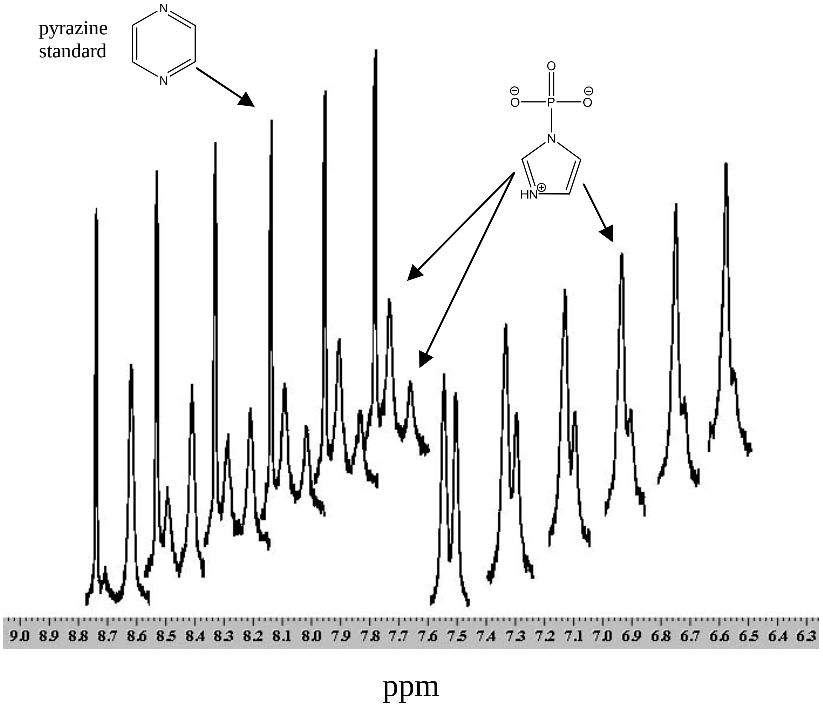

Figure 2-14. ^{1}H NMR time course for the hydrolysis of PIm by PAcP at pH 5.5, $\Delta t_{interval}$ = 7 min. Full course not shown for clarity. At the start of the course, unhydrolyzed substrate is indicated by a maximum signal at 8.6 ppm. As substrate is hydrolyzed, the

signal at 8.6 ppm disappears, and a new signal appears at 8.7 ppm indicating formation of free imidazole. The net integration of the signals at 7.5 to 7.6 ppm will remain unchanged as these signals are the same for the imidazole moiety of PIm and free imidazole.

When least squares fitting full time course NMR data, the validity of allowing the computer algorithm to determine the K_i is compared to the published K_i values (Table 2-1). The same values for V_{max} and K_M are obtained whether K_i is fixed to the literature value or allowed to float during the fit.

Substrate and protein concentrations that result in 90% completion within two hours provide the best results. Consistent with literature precedent, substrate concentrations greater than the obtained K_M yielded the lowest standard deviation.[133,134]

2.4.3.1 Specific Protocols for PIm Assays

A 0.1 M pyrazine standard was made by dissolving 0.0404 g pyrazine in 5.0 mL D_2O. After incubating the calcium salt of PIm with Amberlite, see section **2.2.10**, the concentration of the PIm was determined by mixing 150 μL of pyrazine standard with 300 μL of PIm, final [pyrazine] = 0.033M, and integrating the proton signals, ^{1}H NMR (300 MHz, D_2O): pyrazine, δ 8.5 (s, 4H); PIm δ 6.9 (s, 1H), 7.1 (s, 1H), 7.7 (s, 1H). During the determination of PIm concentration a ^{31}P experiment was run to determine if any contaminating phosphate existed. In all cases, the substrate demonstrated no contaminating phosphate. With the concentration of the sodium salt of PIm known, the desired dilution for an enzymatic assay was made; specific concentrations are listed by enzyme in section **2.5**.

A 5 mM pyrazine standard was made by diluting 500 μL of 0.1 M pyrazine to 10 mL using D_2O. 100 μL of this 5 mM standard was placed into a NMR coaxial tube. Enzyme, buffer, and PIm were mixed and placed into the NMR tube, see section **2.5**, the coaxial tube placed into the NMR tube, and a series of duplicate NMR experiments run.

Concentrations of buffer varied by enzyme, but always greatly exceeded PIm and pyrazine concentrations. To mitigate deleterious effects on the signals, offset was 8.1 ppm, and sweep was 3 ppm; pre-saturation of H_2O was at 4.7 ppm and 35 db. Other instrument settings were: scans – 32; prescans – 1; relaxation delay – 1.8 s; scans – 32; x points – 4096. During the course of a reaction, loss of signal at 6.9 ppm was followed (Figure 2-14) (Figures A17 through A20).

2.5 Enzymatic Assays

2.5.1 PHPT1

PHPT1 was tested with the substrates *p*NPP, *N*-phPAM, and PIm. *p*NPP assays were conducted in a 96 well microplate, 330 μL total volume per well, 23 ^oC, [PHPT1] = 2.41 μM, μ 200 mM, in either 150 mM MES buffer at pH 5.5, or 150 mM EPPS buffer at pH 8.0. Reactions at pH 5.5 were quenched after 10 minutes with 2N NaOH and read at λ_{405}. Reactions at pH 8.0 were monitored directly by UV/Vis (ε p-nitrophenolate at pH 8.0 = 16200, λ_{max} = 405nm). *p*NPP concentrations at both pH conditions were 1, 2.5, 5, 8, 12, and 15 mM.

N-phPAM assays were conducted in quartz cuvettes via direct read, 23 ^oC, [PHPT1] = 2 μM, μ 200 mM, 150 mM MES buffer at pH 5.5, λ_{295}, 150 mM EPPS buffer at pH 8.0, λ_{295}. *N*-phPAM concentrations at both pH conditions were 1 mM, using a 1 cm quartz cell with a reaction volume of 1300 μL, and 4, 8, 12, and 14 mM using 0.1 cm quartz cells with a reaction volume of 330 μL.

PIm assays were conducted by NMR using tube with coaxial insert holding the external standard pyrazine, 23 °C, [PHPT1] = 2 μM, μ 100 mM, 150 mM MES buffer at pH 5.5, or 150 mM EPPS buffer at pH 8.0. PIm concentration at both pH conditions was 6 mM with a total reaction volume of 550 μL. The ^{1}H NMR signals $\delta = 8.4$ ppm at pH 5.5 and $\delta = 7.9$ ppm at pH 8.0 were followed during the time course. Integration was against pyrazine at $\delta = 8.5$.

2.5.2 YopH

YopH was tested with the substrates *p*NPP, *N*-phPAM, and PIm. *p*NPP assays were conducted in a 96 well microplate, 330 μL total volume per well, 23 °C, [YopH] = 2.5 nM, μ 200 mM, 150 mM MES buffer at pH 5.5. Reactions were quenched after 1 minute with 2N NaOH and read at 405 nm. *p*NPP concentrations were 1, 2.5, 5, 7.5, 10, and 15 mM.

N-phPAM assays were conducted in quartz cuvettes monitored at 295 nm, 23 °C, [YopH] = 25 nM, μ 200 mM, 150 mM MES buffer at pH 5.5. *N*-phPAM concentrations were 1 mM, using a 1 cm quartz cell with a reaction volume of 1300 μL, and 4, 8, 12, and 14 mM using 0.1 cm quartz cells with a reaction volume of 330 μL.

PIm assays were conducted by NMR using a coaxial insert holding the external standard pyrazine, 23 °C, [YopH] = 120 nM, μ 100 mM, 150 mM MES buffer at pH 5.5. PIm concentration was 5.5 mM with a total reaction volume of 550 μL. The ^{1}H NMR signal at δ = 8.4 ppm was followed during the time course and integrated relative to the pyrazine standard at δ = 8.5 ppm.

2.5.3 VHR

VHR was tested with the substrates *p*NPP, *N*-phPAM, and PIm. *p*NPP assays were conducted in a 96 well microplate, 330 μL total volume per well, 23 °C, [VHR] = 10 nM, μ 200 mM, 150 mM acetate buffer at pH 5.5. Reactions were quenched after 8 minutes with 2N NaOH and read at 405 nm. *p*NPP concentrations were 1, 2.5, 5, 7.5, 10, and 15 mM.

N-phPAM assays were conducted in quartz cuvettes monitored at 295 nm, 23 °C, [VHR] = 300 nM, μ 200 mM, 150 mM acetate buffer at pH 5.5. *N*-phPAM concentrations were 1 mM, using a 1 cm quartz cell with a reaction volume of 1300 μL, and 4, 8, 12, and 14 mM using 0.1 cm quartz cells with a reaction volume of 330 μL.

PIm assays were conducted by NMR using a coaxial insert holding the external standard pyrazine, 23 °C, [VHR] = 300 nM, μ 200 mM, 150 mM acetate buffer at pH 5.5. PIm concentration was 5.5 mM with a total reaction volume of 550 μL. The ^{1}H NMR signal at δ = 8.4 ppm was followed during the time course. Integration was against pyrazine at δ = 8.5 ppm.

2.5.4 PAcP

PAcP was tested with the substrates *p*NPP, *N*-phPAM, and PIm. *p*NPP assays were conducted in a 96 well microplate, 330 μL total volume per well, 23 °C, [PAcP] = 500 nM, μ 150 mM, 50 mM acetate buffer at pH 5.5. Reactions were quenched after 6 minutes with 2N NaOH and read at 405 nm. *p*NPP concentrations were 32, 200, 400, 600, and 800 μM.

N-phPAM assays were conducted in quartz cuvettes monitored at 295 nm, 23 ^{o}C, [PAcP] = 81.6 nM, μ 150 mM, 50 mM acetate buffer at pH 5.5. *N*-phPAM concentrations were 86, 200, 400, and 600 μM, using a 1 cm quartz cell with a reaction volume of 1300 μL.

PIm assays were conducted by NMR using a coaxial insert holding the external standard pyrazine, 23 ^{o}C, [PAcP] = 500 nM, μ 150 mM, 50 mM acetate buffer at pH 5.5. PIm concentration was 3.0 mM with a total reaction volume of 550 μL. The ^{1}H NMR signal at $\delta = 8.4$ ppm was followed during the time course and integrated relative to the pyrazine standard at $\delta = 8.5$ ppm.

2.5.5 λPP

λPP was tested with the substrates *p*NPP, *N*-phPAM, and PIm. λPP's behavior with *p*NPP followed normal Michaelis-Menton kinetics, but it did not for PIm. To validate the results with PIm, both NMR and HPLC were used. Because k_{cat} and K_M could not be obtained with PIm, percent hydrolysis after a single fixed time period was obtained using HPLC. To make a side-by-side comparison of the enzyme's behavior with *p*NPP and PIm, percent *p*NPP hydrolysis after the same fixed time period was obtained using HPLC.

Additionally, inhibition assays were conducted with PIm as inhibitor and *p*NPP as substrate. Inhibition assays were conducted in a 96 well microplate, 330 μL total volume per well, [λPP] = 1 nM, μ 200 mM, 150 mM Tris, pH 7.8, 1 mM $MnCl_2$, 10 mM DTT, 10% glycerol, 30 ^{o}C. *p*NPP concentrations were 1, 2.5, 5, 10, 15, and 20 mM. PIm concentrations were 3, 6, 12, 18, and 24 mM. Reactions were monitored at 405 nm. Data were least squares fitted using the Visual Enzymics Program by SoftZymics.

*p*NPP activity assays were conducted in a 96 well microplate, 330 μL total volume per well, [λPP] = 1 nM, μ 200 mM, 150 mM Tris, pH 7.8, 1 mM $MnCl_2$, 10 mM DTT, 10% glycerol, 30 ^{o}C. *p*NPP concentrations were 1, 2.5, 5, 10, 15, and 20 mM. Reactions were monitored at 405 nm.

HPLC assays to detect percent *p*NPP hydrolysis after a single fixed time period were conducted in 500 μL Eppendorf tubes, [λPP] = 100 nM, μ 150 mM, 1 mM $MnCl_2$, 10% glycerol, 10 mM DTT, 100 mM Tris buffer, pH 7.8, 30 ^{o}C. Concentration of *p*NPP was 1 mM. Reactions were injected directly into an Agilent Technologies Zorbax Eclipse Plus C18 column and analyzed by an Agilent 1200 HPLC. The mobile phase consisted of 42.5% 1 M NH_4OH, pH 8.0, and 57.5% MeOH run isocratically at a flow rate of 1 mL/min. UV/Vis detection was used at 410 nm. Retention time was 6.9 min. The reference wavelength was 510 nm. Integration was against a calibration curve developed using the same HPLC settings.

N-phPAM assays were conducted in quartz cuvettes monitored at 295 nm, [λPP] = 100 nM, μ 200 mM, 1 mM $MnCl_2$, 10% glycerol, 10 mM DTT, 150 mM Tris buffer, pH 7.8, 30 ^{o}C. *N*-phPAM concentrations were 1 mM, using a 1 cm quartz cell with a reaction volume of 1300 μL, and 4, 8, 12, and 14 mM using 0.1 cm quartz cells with a reaction volume of 330 μL.

HPLC assays to detect percent PIm hydrolysis after a single fixed time period were conducted in 500 μL Eppendorf tubes, [λPP] = 100 nM, μ 150 mM, 1 mM $MnCl_2$, 10% glycerol, 10 mM DTT, 100 mM Tris buffer, pH 7.8, 30 ^{o}C. Concentration of PIm was 1 mM. Reactions were injected directly into an Agilent Technologies Zorbax Eclipse Plus C18 column and analyzed by an Agilent 1200 HPLC. Elution was run stepwise at a flow rate of 1 mL/min. From 0 to 12 minutes the mobile phase consisted of 42.5% 1 M NH_4OH, pH 8.0, and 57.5% MeOH. During the time period from 12 to 16 minutes, the composition of eluent was gradually changed to 100% MeOH. It was held at 100% MeOH for an additional 2 minutes. UV/Vis detection was used at 209 nm. Retention time was 15.2 min. The reference wavelength was 360 nm. Integration was against a calibration curve developed using the same HPLC settings.

Percent hydrolysis for PIm was verified by NMR. Manganese was precipitated prior to conducting the NMR experiment by EDTA.

2.5.6 PP1γ

Inhibition assays with PIm as inhibitor and *p*NPP as substrate were conducted in a 96 well microplate, 330 μL total volume per well, [PP1] = 400 nM, 50 mM Tris, 50 mM Bis-Tris, 100 mM acetate, 0.05 mM $MnCl_2$, pH 6.5, 23 ^{o}C. *p*NPP concentrations were 1, 2.5, 5, 7.5, 10, and 12.5 mM. PIm concentrations were 1, 5, and 10 mM. Reactions were monitored at 405 nm.

N-phPAM assays were conducted in quartz cuvettes monitored at 293 nm, [PP1] = 375 nM, 50 mM Tris, 50 mM Bis-Tris, 100 mM acetate, 0.05 mM $MnCl_2$, pH 6.5, 23 ^{o}C. *N*-phPAM concentrations were 1 mM, using a 1 cm quartz cell with a reaction volume of 1300 μL, and 4, 8, 12, and 14 mM using 0.1 cm quartz cells with a reaction volume of 330 μL.

PIm assays were conducted in 500 μL Eppendorf tubes, [PP1] = 400 nM, 50 mM Tris, 50 mM Bis-Tris, 100 mM acetate, 0.05 mM $MnCl_2$, pH 6.5, 23 ^oC. Concentration of PIm was 1 mM. Reaction progress was analyzed by NMR.

2.5.7 AP

*p*NPP assays were conducted in a 96 well microplate monitored at 405 nm, 330 μL total volume per well, [AP] = 5 nM, μ 100 mM, 75 mM MOPS at pH 8.0, 23 ^oC. *p*NPP concentrations were 1, 10, 50, 100, 200, 300, 400, and 500 μM.

N-phPAM assays were conducted in quartz cuvettes monitored at 295 nm, [AP] = 1 μM, μ 200 mM, 150 mM MOPS, pH 8.0, 23 ^oC. *N*-phPAM concentrations were 0.75 and 1 mM, using a 1 cm quartz cell with a reaction volume of 1300 μL, and 2.5, 5, 7.5, 10, and 15 mM, using a 1 cm quartz cell with a reaction volume of 1300 μL.

PIm assays were conducted using a NMR tube with coaxial insert holding the external standard pyrazine, [AP] = 500 nM, IS 200 mM, 150 mM MOPS, pH 8.0, 23 ^oC. PIm concentration was 15 mM with a total reaction volume of 550 μL. ^1H NMR δ 7.9 followed during time course. Integration was against pyrazine, δ 8.5.

2.6 Titration of *N*-phPAM

The pK_a of *N*-phPAM was determined by ^{31}P NMR titration.[110] A coaxial tube with methylphosphonic acid in D_2O was used as an internal chemical shift standard. *N*-phPAM was dissolved in buffer (50mM Tris, 50 mM Bis-Tris, 100 mM acetate) and brought to pH 9.2. The pH of the buffered solution was lowered stepwise using 0.1 M HCl. ^{31}P NMR chemical shifts were obtained as a function of pH, and the data least squares fitted against equation 2.6.

$$\delta = \delta_p + \frac{\delta u - \delta p}{1 + 10^{(pKa - pH)}} \tag{2.6}$$

where δ is the observed ^{31}P shift in ppm, and δ_p and δ_u are the chemical shifts of the fully protonated and un-protonated states. A plot of the data and the resulting fit is shown in Figure 2-15. The fit yielded $pK_a = 7.05 \pm 0.02$.

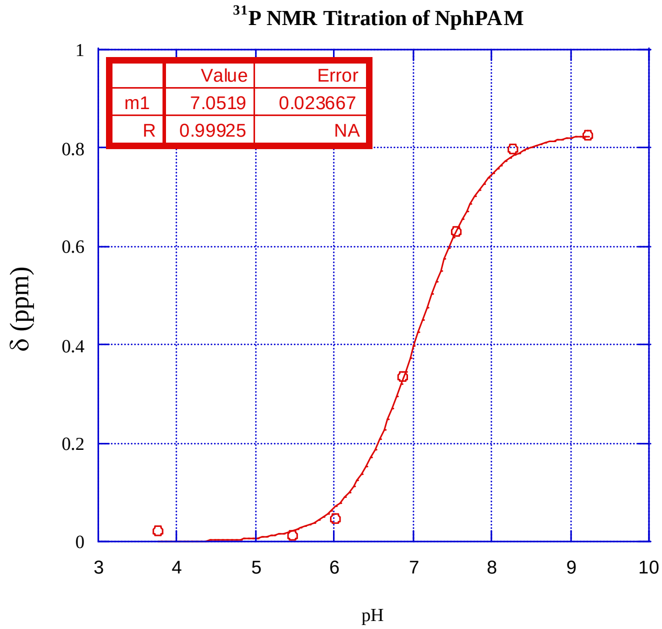

Figure 2-15. Titration curve showing ^{31}P shift (ppm) of *N*-phPAM as a function of pH.

2.7 Computer Modeling of Substrates into Active Sites

Additional evidence to validate the results of the kinetic experiments herein was attempted using computer modeling. Generally, computer models were used to assess differences in the initially bound orientations of *p*NPP versus PIm for each of the enzymes. Comparisons could be made between the known rate limiting step of catalysis, k_{cat} values, and the computer generated binding modes.

Kinetic experiments with λPP and PP1 showed significantly different results with the substrates *p*NPP versus PIm. The geometric and charge differences between these substrates are also significant, and computer modeling presented another possibility to determine if these differences may be the cause for the kinetic results.

Protein Data Bank crystallographic files 2OZW (PHPT1 with phosphate bound), 2I42 (YopH with vanadate bound), 1VHR (VHR with sulfate bound in one structure and 4-(2-hydroxyethyl)-1-piperazine ethanesulfonic acid bound in another), 1ND6 (PAcP with phosphate bound), 1ED8 (AP with phosphate bound), 1G5B (λPP with sulfate bound), and 1IT6 (PP1γ with phosphocalyculin A bound) were used for computer modeling. The files were loaded into Acclerys Design Studio Viewer Pro, version 5.0.

For each enzyme, PIm and *p*NPP were placed in the active site using the bound tetrahedral compound shown in the crystal structure as the basis for substrate orientation. Where multiple possibilities for the bridging atom were possible, all options were tried. Once the substrates were emplaced, energy was minimized using the Dreiding model.[135-137] Such minimization was attempted in two manners: with just the active site and with the entire enzyme. Minimization operations were conducted using 200 to 4000 iterations.

CHAPTER 3

RESULTS

3.1 Overall Experimental Results

Kinetic data were collected for hydrolysis of the substrates *p*NPP, *N*-phPAM, and PIm for six of seven enzymes assayed (Table 3-1). For each enzyme, kinetic results will be discussed along with the results of computer modeled fitting of the substrates.

Table 3-1. The k_{cat}, K_M, and k_{cat}/K_M values for enzymatic substrate hydrolysis.

Enzyme	Substrate	k_{cat} (s^{-1})	K_M (mM)	$k_{cat}/K_M \times 10^{-3}$ * ($M^{-1}s^{-1}$)
pH 5.5				
PHPT1	*p*NPP	0.00407 ±0.00007	2.7 ±0.2	0.0015
	N-phPAM	0.26 ±0.06	5 ±3	0.05
	PIm	2.70 ±0.04	0.13 ±0.02	21
YopH	*p*NPP	610 ±30	3.1 ±0.4	200
	N-phPAM	530 ±70	4 ±2	100
	PIm	34 ±2	4.9 ±0.5	7
VHR	*p*NPP	5.9 ±0.2	2.0 ±0.2	3.0
	N-phPAM	5.8 ±0.6	0.8 ±0.2	7
	PIm	7.8 ±0.6	0.58 ±0.09	13
PAcP	*p*NPP	2.13 ±0.02	0.23 ±0.04	9.3
	N-phPAM	2.5 ±0.1	0.07 ±0.01	40
	PIm	6.0 ±0.4	1.01 ±0.09	5.9
pH 8.0				
PHPT1	*p*NPP	0.0106 ±0.0004	6.3 ±0.6	0.0017
	N-phPAM	2.6 ±0.1	10 ±1	0.26
	PIm	2.31 ±0.05	0.10 ±0.02	23
AP	*p*NPP	27.3 ±0.8	0.0070 ±0.0008	3900
	N-phPAM	1.30 ±0.09	0.0021 ±0.0002	620
	PIm	18 ±2	0.0020 ±0.0003	9000
pH 7.8				
λPP	*p*NPP[138]	390 ±10	11 ±1	35
	N-phPAM	Not detected		
	PIm	Not determined		
pH 6.5				
PP1γ	*N*-phPAM	Not detected		
	PIm	Not detected		

*Values in the column k_{cat}/K_M were multiplied by 10^{-3} for ease of display. Thus, the first value of 0.0015 $M^{-1}s^{-1}$ for PHPT1 is actually 1.5 $M^{-1}s^{-1}$.

The pH optima for the enzymes were reviewed in section **1.2** and are shown in Table 3-2. Enzymatic assays in this research were conducted at or near the pH optimum.

Table 3-2. Literature values for the pH optimum for catalysis of the substrate shown by the enzymes used in this study.

Enzyme	pH Optimum	Substrate
PHPT1[20]	8.0	*p*NPP
YopH[26]	5.0~5.5	*p*NPP
VHR[44]	5.5~6.0	*p*NPP
PAcP[47,48,51]	3~5.5	*p*NPP
AP[78]	8.0~8.5	*N*-naphthyl-phosphoramidate
AP[78]	9.0~9.5	*p*NPP
λPP[56]	7.8	*p*NPP
PP1γ[63]	6.5	*p*NPP

For YopH, VHR, PAcP, and λPP the shape of the pH rate profile is affected by the ionization states of active site residues. The pH rate profiles for PAcP and AP are affected by the ionization state of the substrate. Comparing the substrates used in this study, the ionization states may be different or similar depending upon the pH (Figure 3-1).

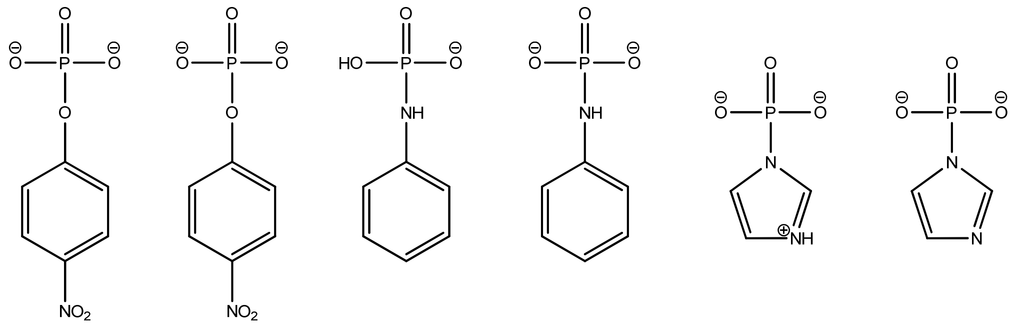

pH 5.5, % A^{2-} = 77.6%

pH 8.0, % A^{2-} = 99.9%

pH 5.5, % A^{-} = 97.2%

pH 8.0, % A^{2-} = 90.1%

pH 5.5, % A^{-} = 95.2%

pH 8.0, % A^{2-} = 94.1%

Figure 3-1. Predominant protonation states of the substrates at the experimental pH. A^{-} is the monoanion; A^{2-} is the dianion.

3.2 Results by Enzyme

3.2.1 PHTP1

The substrate PIm exhibited the greatest k_{cat}, lowest K_M, and greatest catalytic efficiency (k_{cat}/K_M). The lowest k_{cat} and highest K_M with this enzyme were observed with *p*NPP, while *N*-phPAM exhibited intermediate values. Kinetic values for PIm were remarkably similar at both pH 8.0 and pH 5.5. The enzyme preparation for this project had k_{cat} and k_{cat}/K_M values with *p*NPP that were about an order of magnitude lower than reported; literature values were k_{cat} ($0.35\ s^{-1}$) and k_{cat}/K_M ($47\ M^{-1}s^{-1}$).[20] Two enzyme preparations were made with the same result. No explanation is provided for this discrepancy.

Computer modeling found P_i, PIm, and *p*NPP bind in the active site in the same orientation, but with different hydrogen bonding and electrostatic interaction distances (Figures 3-2 through 3-4). This result is consistent with the enzyme hydrolyzing both PIm and *p*NPP; both substrates can bind, completing the first step in catalysis. PHPT1's binding motif was reviewed in section **1.2.1**.

3.2.2 YopH

Catalysis of phosphomonoesters by YopH is one of the fastest displayed by phosphatases.[35] This project is the first to examine YopH's ability to hydrolyze phosphoramidates. In this study, YopH showed the highest k_{cat} with *p*NPP and the lowest k_{cat} with PIm. It also showed a lower second order rate constant with PIm than with *p*NPP.

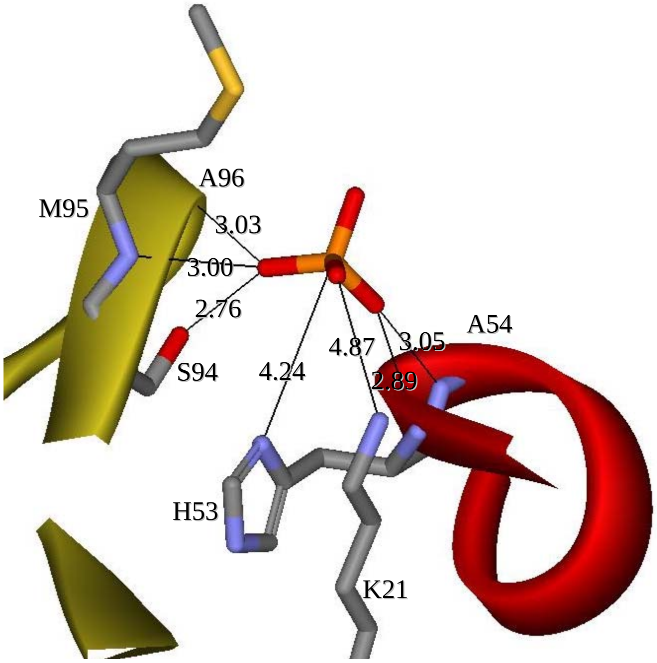
A96
M95
3.03
3.00
2.76
S94
4.24
4.87
3.05
A54
2.89
H53
K21

Figure 3-2. Phosphate bound in the active site of PHPT1. Distances are in Å and are taken directly from crystal structure without modification (PDB 2OZW).

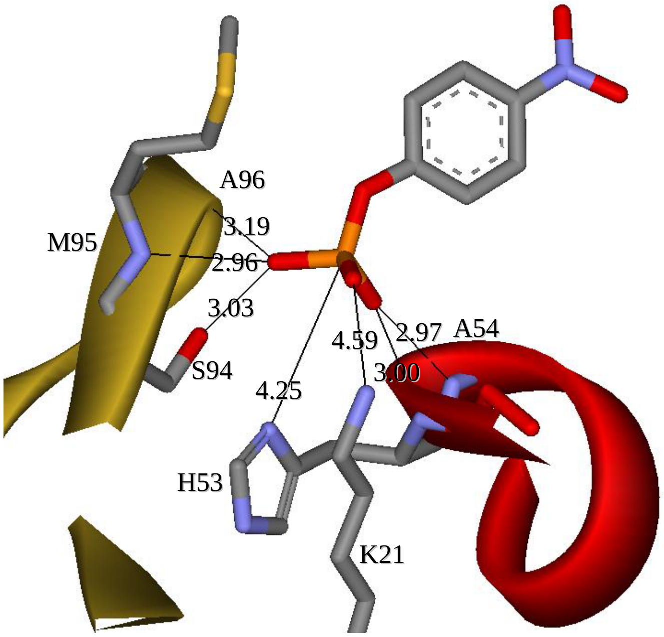
A96
M95
3.19
2.96
3.03
S94
4.25
4.59
2.97
A54
3.00
H53
K21

Figure 3-3. *p*NPP bound in the active site of PHPT1 as modeled in Acclerys.

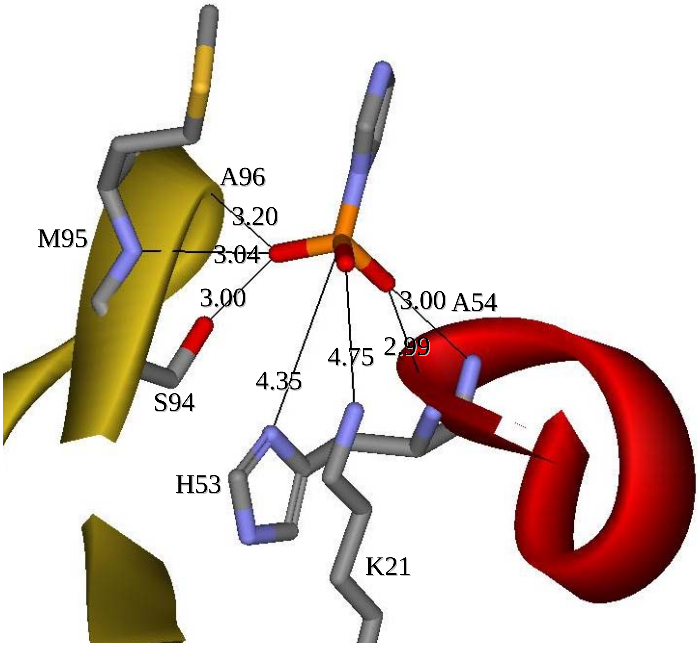

Figure 3-4. PIm bound in the active site of PHPT1 as modeled in Acclerys.

Differences in k_{cat} between *p*NPP and PIm were not only large, but the values for *p*NPP and *N*-phPAM were the highest displayed by any of the enzymes assayed in this study. In contrast, values for K_M were of equal order of magnitude. Thus, variation in the second order rate constants was driven predominantly by differences in k_{cat}. YopH's second order rate constants varied in the order *p*NPP>*N*-phPAM>PIm.

Computer modeling found P_i, PIm, and *p*NPP fit in the active site in the same orientation, but with different hydrogen bonding distances (Figures 3-5 through 3-9). This result is consistent with the observed ability of the enzyme to hydrolyze both PIm and *p*NPP. YopH's binding motif was reviewed in section **1.2.2**.

The computer models indicate a 1.94 Å distance between PIm's phosphorus and the nucleophilic cystein's sulfur (Figure 3-7). Since this distance is likely too short to represent the position of the substrate and nucleophile prior to catalysis, amino acids Asn353 through Ala359 were removed from the computer model and the distances recalculated for both PIm and *p*NPP (Figures 3-8 and 3-9). Removal of the sequences eliminated the flexible WPD loop and any clashes between the loop and substrate. A phosphorus-sulfur distance of 3.59 Å was found for PIm.

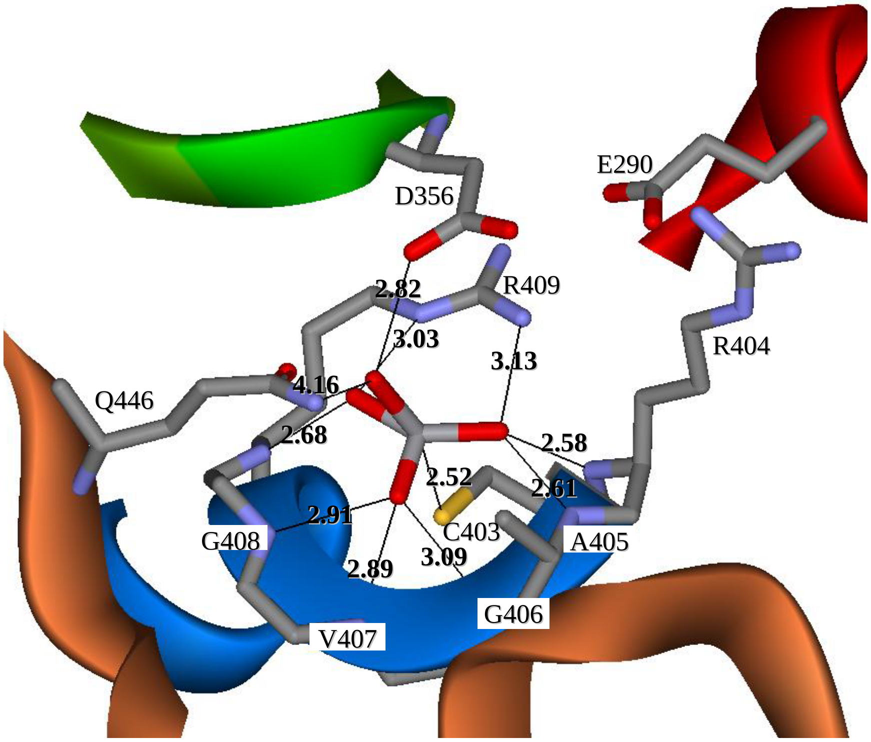
E290
D356
R409
2.82
3.03
3.13
R404
Q446
4.16
2.68
2.58
2.52
2.61
2.91
G408
C403
A405
2.89
3.09
G406
V407

Figure 3-5. Vanadate bound in the active site of YopH. Distances are taken directly from crystal structure without modification (PDB 2I42).

3.2.3 VHR.

VHR's k_{cat} values for the three substrates were of the same order of magnitude. In comparison to the other PTP used in this study, YopH, VHR's k_{cat} values for *p*NPP and *N*-phPAM were lower by two orders of magnitude, and for PIm was lower by one order of magnitude. While K_M for *p*NPP was similar between the enzymes, VHR's K_M values with the phosphoramidates were an order of magnitude lower than for YopH. VHR's

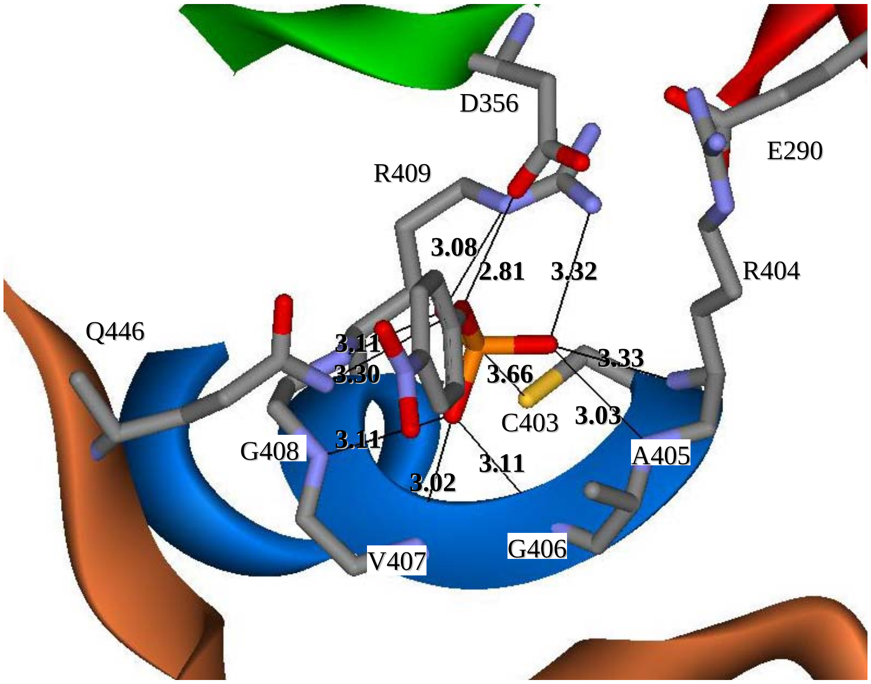
D356
E290
R409
3.08
2.81
3.32
R404
Q446
3.11
3.30
3.66
3.33
C403
3.03
G408
3.11
A405
3.02
3.11
V407
G406

Figure 3-6. *p*NPP bound in the active site of YopH as modeled in Acclerys.

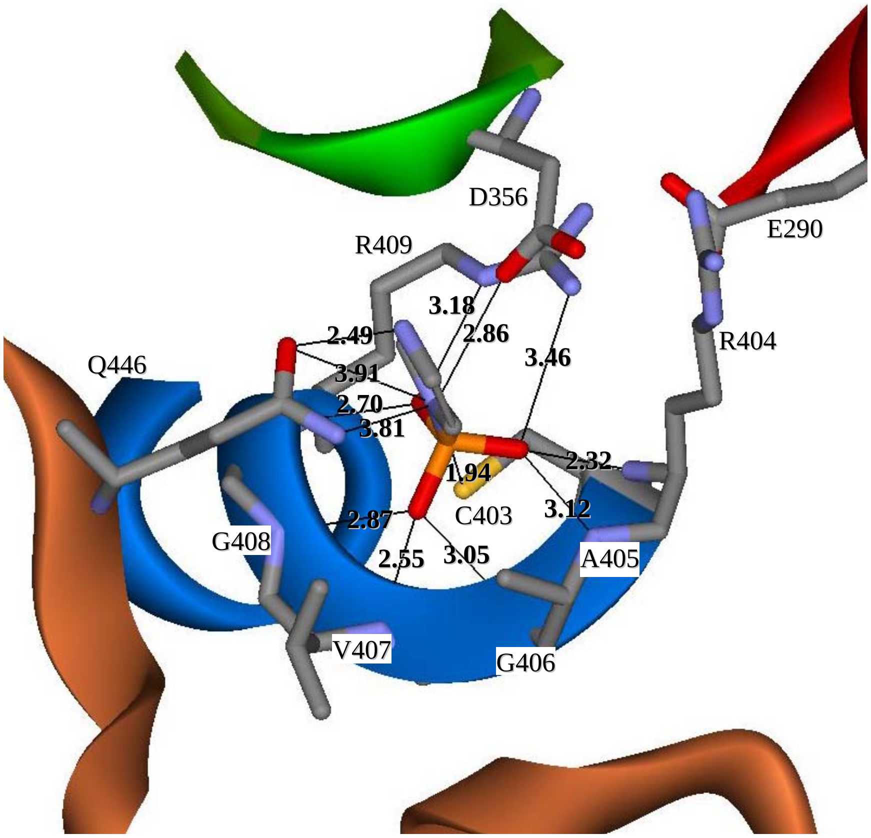
D356
E290
R409
3.18
2.86
3.46
R404
2.49
Q446
3.91
2.70
3.81
2.32
1.94
C403
3.12
2.87
G408
2.55
3.05
A405
V407
G406

Figure 3-7. PIm bound in the active site of YopH as modeled in Acclerys.

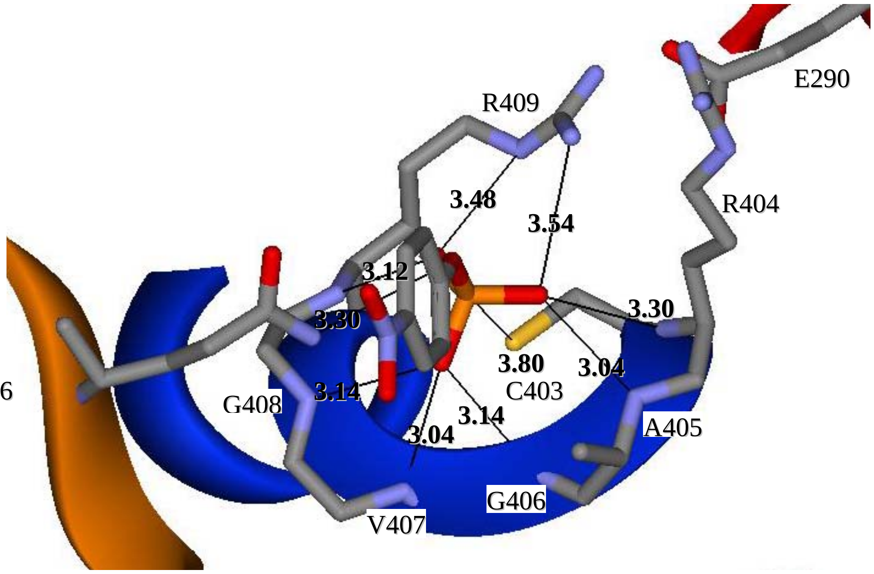
R409
E290
3.48
3.54
R404
3.12
3.30
3.30
Q446
G408
3.14
3.80
C403
3.04
3.14
A405
3.04
G406
V407

Figure 3-8. *p*NPP bound in the active site of YopH with the WPD loop removed as modeled in Acclerys.

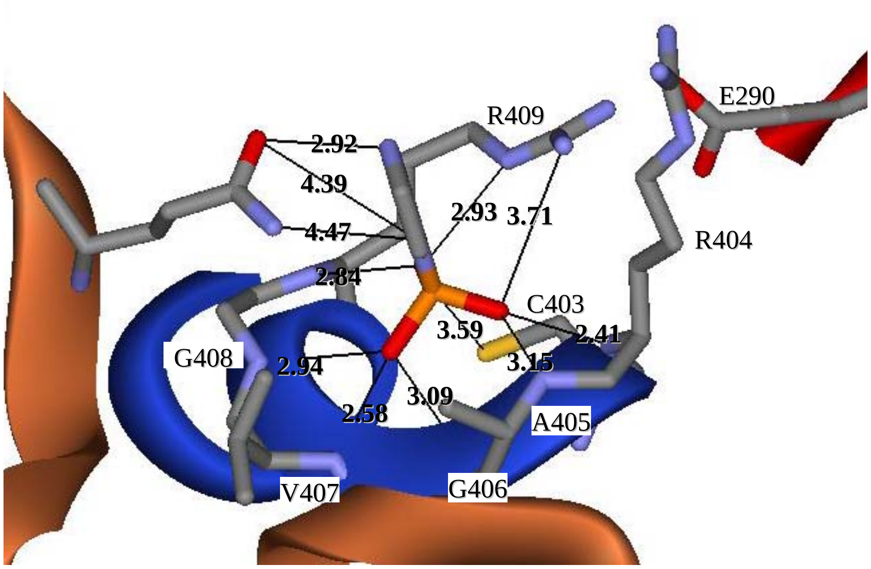
2.92
R409
E290
4.39
2.93
3.71
Q446
4.47
R404
2.84
C403
3.59
2.41
G408
2.94
3.15
3.09
2.58
A405
V407
G406

Figure 3-9. PIm bound in the active site of YopH with the WPD loop removed as modeled in Acclerys.

second order rate constants had the order PIm>*N*-phPAM>*p*NPP; this relative efficiency was driven both by differing k_{cat} and K_M values.

Computer modeling found sulfate, PIm and *p*NPP fit in the active site in the same orientation (Figures 3-10 through 3-12). The distance between the substrate's oxyanion and the amide hydrogen of E126 changes from 3.13 in sulfate to 2.46 with *p*NPP and 2.09 with PIm. This change is consistent with the lower K_Ms of the phosphoramidates in comparison to *p*NPP. VHR's binding motif was reviewed in section **1.2.3**.

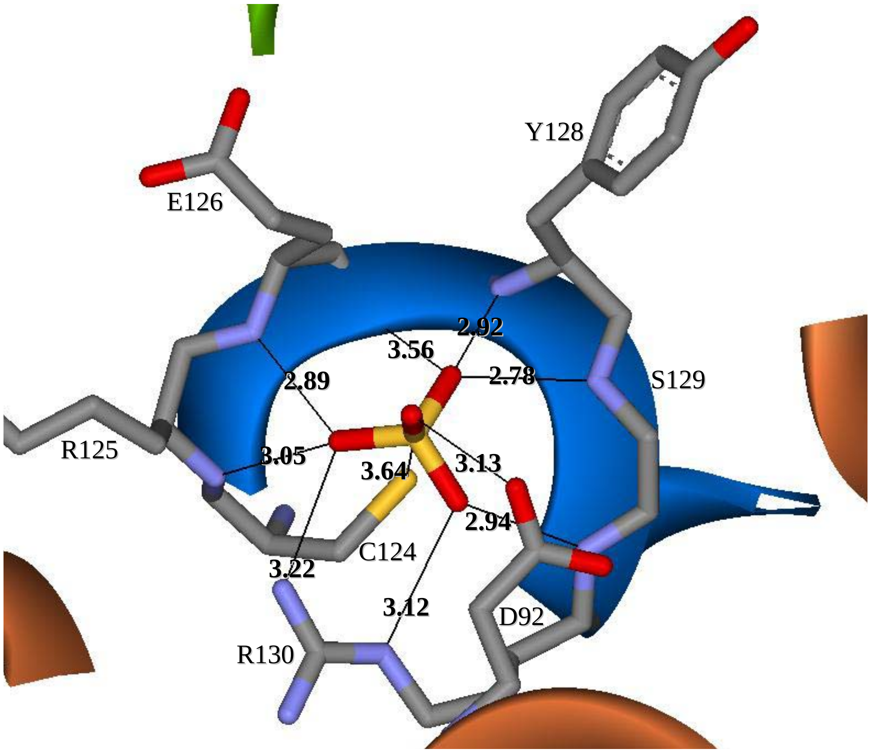

Figure 3-10. Sulfate bound in the active site of VHR. Distances are taken directly from crystal structure without modification (PDB 1VHR).

3.2.4 PAcP.

The non-specific histidine acid phosphatase PAcP displayed the same order of magnitude for k_{cat} with the three substrates. The second order rate constants for *p*NPP and PIm were of the same order of magnitude, while *N*-phPAM had the highest rate

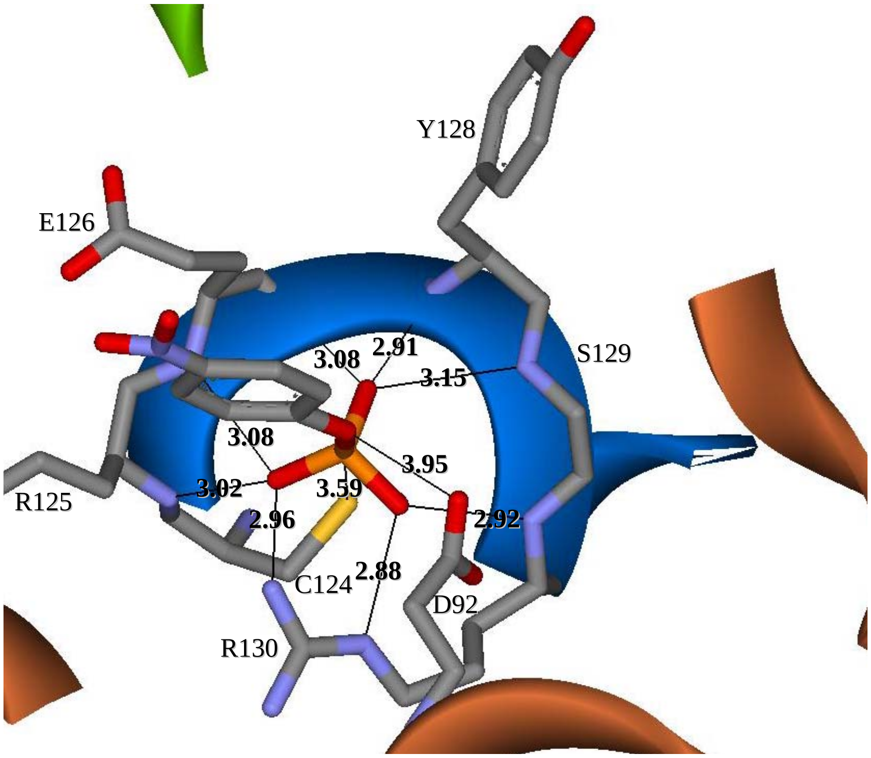
Y128
E126
S129
R125
C124
D92
R130
3.08
2.91
3.15
3.08
3.95
3.02
3.59
2.96
2.92
2.88

Figure 3-11. *p*NPP bound in the active site of VHR as modeled in Acclerys.

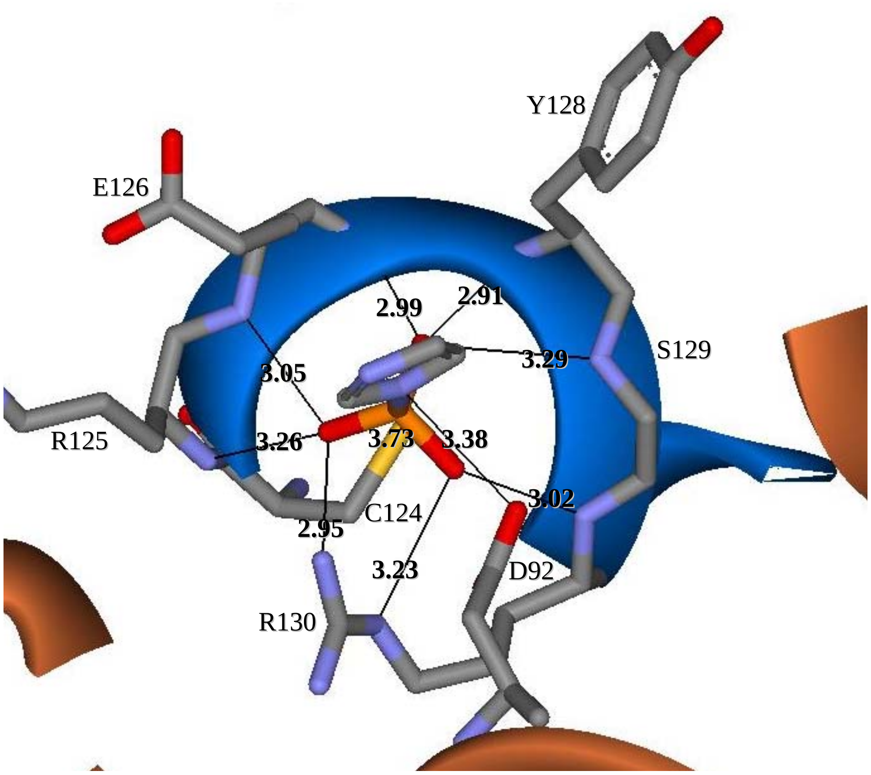
Y128
E126
S129
R125
C124
D92
R130
2.99
2.91
3.29
3.05
3.26
3.73
3.38
3.02
2.95
3.23

Figure 3-12. PIm bound in the active site of VHR as modeled in Acclerys.

constant of the three substrates. Differences in the rate constant were driven predominantly by differences in K_M. Relative K_M values were PIm>*p*NPP>*N*-phPAM, while k_{cat}/K_M values were *N*-phPAM>*p*NPP>PIm.

Computer modeling found P_i, PIm and *p*NPP fit in the active site in the same orientation, but with different hydrogen bond distances (Figures 3-13 through 3-15). This result is consistent with the enzyme hydrolyzing both PIm and *p*NPP; both substrates can bind, completing the first step in catalysis. PAcP's binding motif was reviewed in section **1.2.4**.

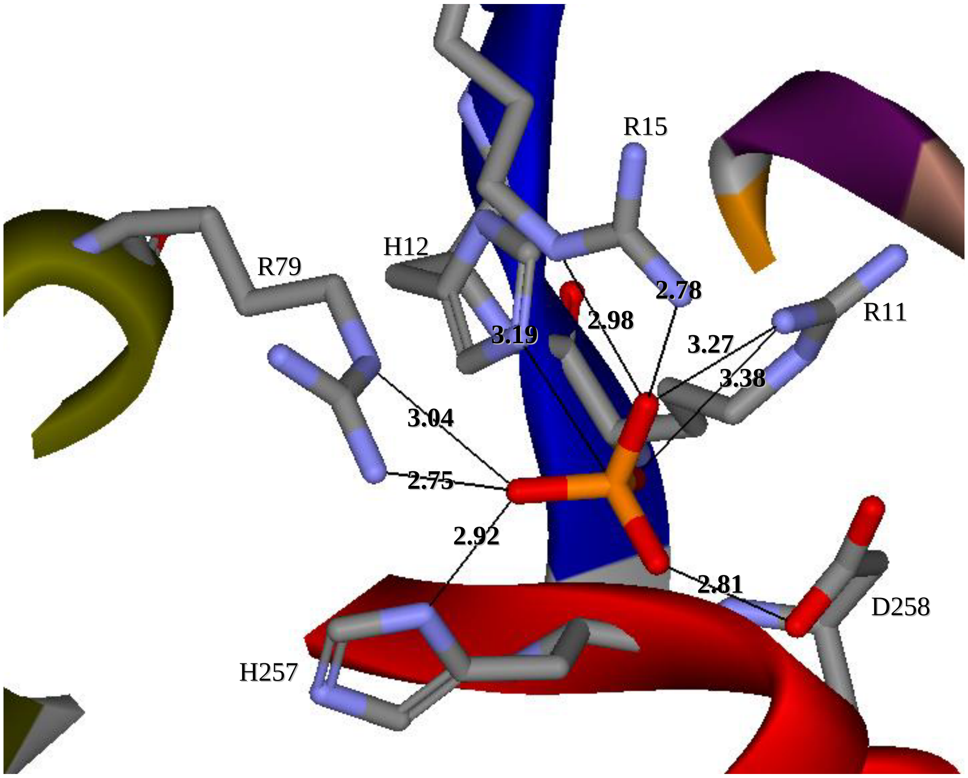

Figure 3-13. Phosphate bound in the active site of PAcP. Distances are taken directly from crystal structure without modification (PDB 1ND6).

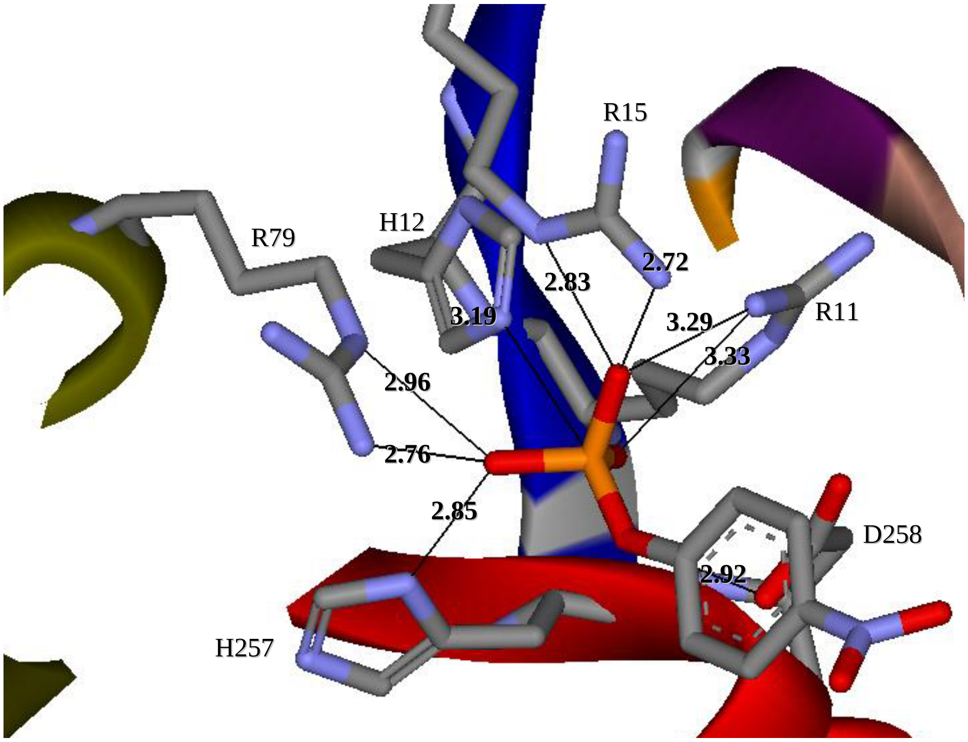
R15
R79
H12
2.72
2.83
3.19
3.29
R11
3.33
2.96
2.76
2.85
D258
2.92
H257

Figure 3-14. *p*NPP bound in the active site of PAcP as modeled in Acclerys.

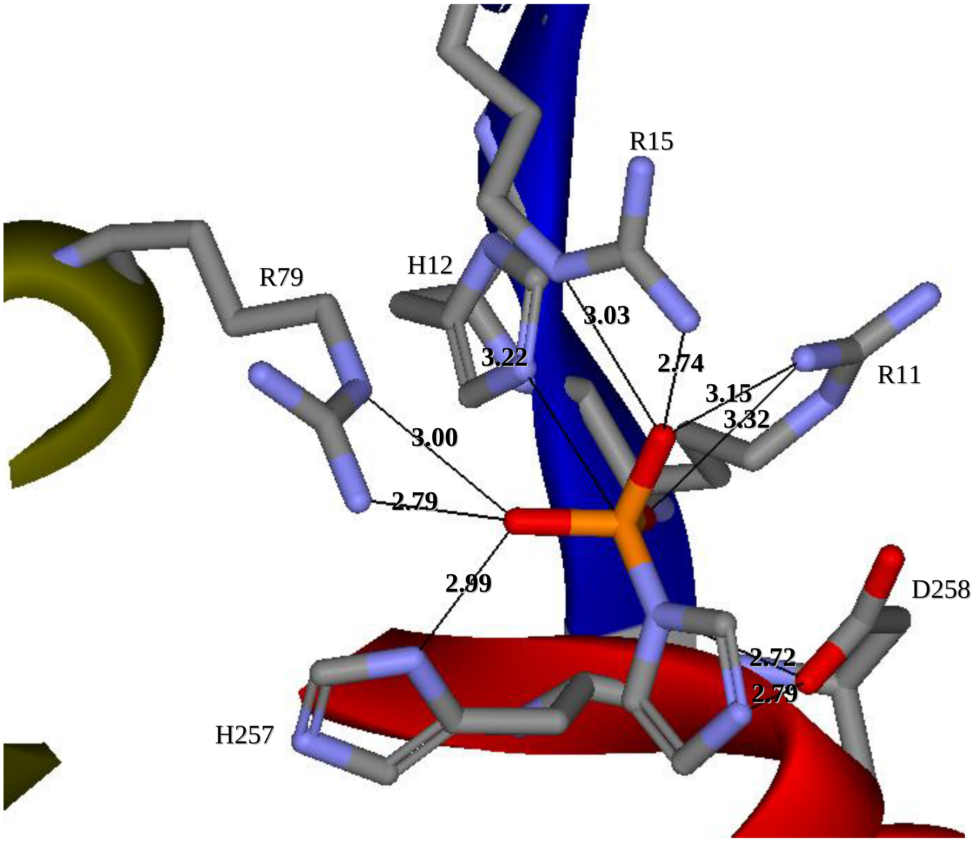
R15
R79
H12
3.03
3.22
2.74
R11
3.15
3.32
3.00
2.79
2.99
D258
2.72
2.79
H257

Figure 3-15. PIm bound in the active site of PAcP as modeled in Acclerys.

3.2.5 λPP and PP1

The two dual-specificity metallophosphatases, λPP and PP1γ, were examined. λPP was able to catalyze the hydrolysis of PIm, whereas PP1 was not. Neither enzyme showed detectable hydrolysis of *N*-phPAM. *N*-phPAM's hydrolysis at pH 5.5 is sufficiently rapid that if the enzymes effected slow catalysis it was undetectable from the background.

During the reaction of λPP with PIm the reaction was found to proceed to 25% hydrolysis of initial starting concentration and proceed no further. This prevented obtaining a full time course for NMR analysis. Therefore, k_{cat} and K_M values could not be obtained. That the reaction would proceed no further was likely due to product inhibition.

An HPLC assay was developed to detect the imidazole product as described section **2.5.5**. The sensitivity was not sufficient to obtain initial rate kinetics, but did permit an assessment of the relative rate of PIm hydrolysis compared to *p*NPP hydrolysis under the same conditions by λPP. After 20 minutes of reaction time, λPP hydrolyzed 75.2% of 1 mM *p*NPP as compared to 10.4% of 1 mM PIm.

In order to determine whether the unusual behavior with PIm was due to improper binding, the mode of inhibition by PIm of *p*NPP hydrolysis was examined. Inhibition data were fitted to an inverse reciprocal plot.[139] Competitive inhibition was found with $K_i = 22 \pm 3$ mM (Figure 3-16). This result means that PIm binds to the same form of the enzyme at the same site as *p*NPP, although with reduced affinity.

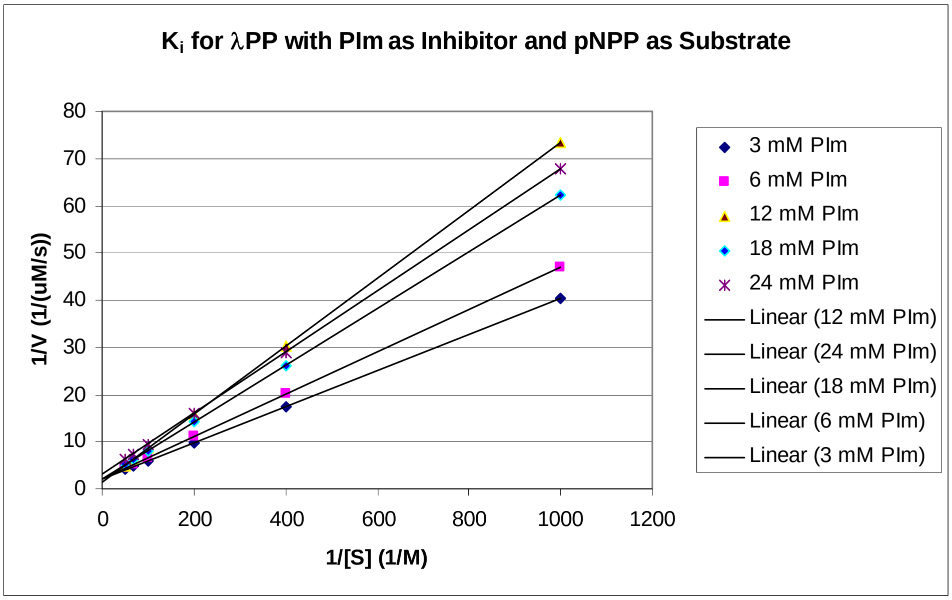

Figure 3-16. Double reciprocal plot to determine the mode of inhibition and the K_i of PIm with *p*NPP as substrate for λPP, 30 °C, pH 7.8.

Additional tests were completed to determine if the enzyme maintained activity over the time course. Loss of activity was not detected up to four hours after frozen enzyme was prepared for kinetic assays. Another test was conducted wherein enzyme that had hydrolyzed PIm to 25%, [λPP] = 100 nM, was then used to hydrolyze *p*NPP, [λPP] = 1 nM; the enzyme displayed full activity with *p*NPP. This verifies that the loss of hydrolysis of PIm after 25% of hydrolysis was not due to loss of enzymatic activity.

λPP's binding motif was reviewed in section **1.2.5**. Computer modeling of the substrates with λPP found sulfate, *p*NPP, and PIm bound in different orientations. This difference was found regardless of the initial coordination mode of the sulfate in the crystal structure, see section **1.2.5**.

Using sulfate bound in coordination mode B as an example (Figures 3-17 through 3-22) illustrates the differences in binding between *p*NPP and PIm. In attaining the lowest energy enzyme-substrate conformation, the computer placed water differently between the modeled *p*NPP bound structure and the modeled PIm bound structure. Further, the general orientation between *p*NPP and PIm was different (Figures 3-18 and 3-19).

Distances between active site residues, the metals, and the substrates are shown (Figures 3-20 through 3-22). The active site metals are crucial for catalytic function, so the metal to metal and phosphoryl group to metal distances were examined.

Metal to metal distance with *p*NPP in the active site was modeled at 4.13 Å in *p*NPP as compared to 4.57 Å with PIm. A single oxyanion of *p*NPP coordinated to just one of the metals, the distance being 3.05 Å. A water molecule was interposed between the other metal and the same oxyanion. A single oxyanion of PIm coordinated to both metals, the distances being 4.17 Å and 4.78 Å. It is apparent that the computer models show a significantly closer distance between *p*NPP and the metals than PIm.

Computer modeling with PP1 provided similar results as with λPP. Placement of water in the active site was different between the crystal structure with phosphate, the model with *p*NPP, and the model with PIm (Figure 3-23 through 3-25). Further, *p*NPP was closer to the metals than PIm.

3.2.6 AP.

AP hydrolyzes both PIm and N-phPAM. Literature reports of kinetic constants for hydrolysis of *p*NPP by AP vary as a result of product inhibition by P_i (Table 3-6). The most accurate values are obtained when substrate concentrations are kept low as this

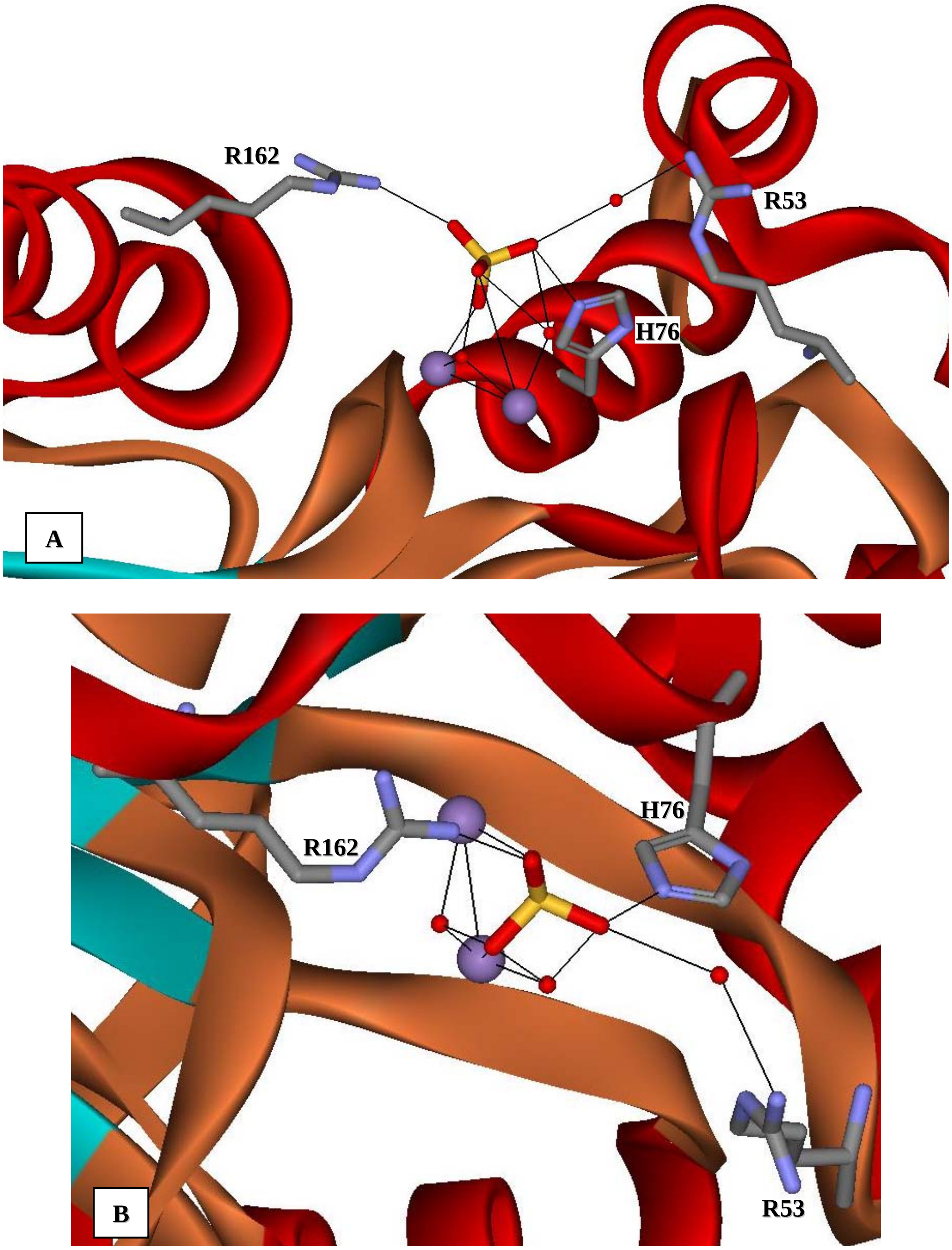
R162
R53
H76
A
H76
R162
R53
B

Figure 3-17. λPP with bound sulfate in coordination mode B, boxes A and B (PDB 1G5B).

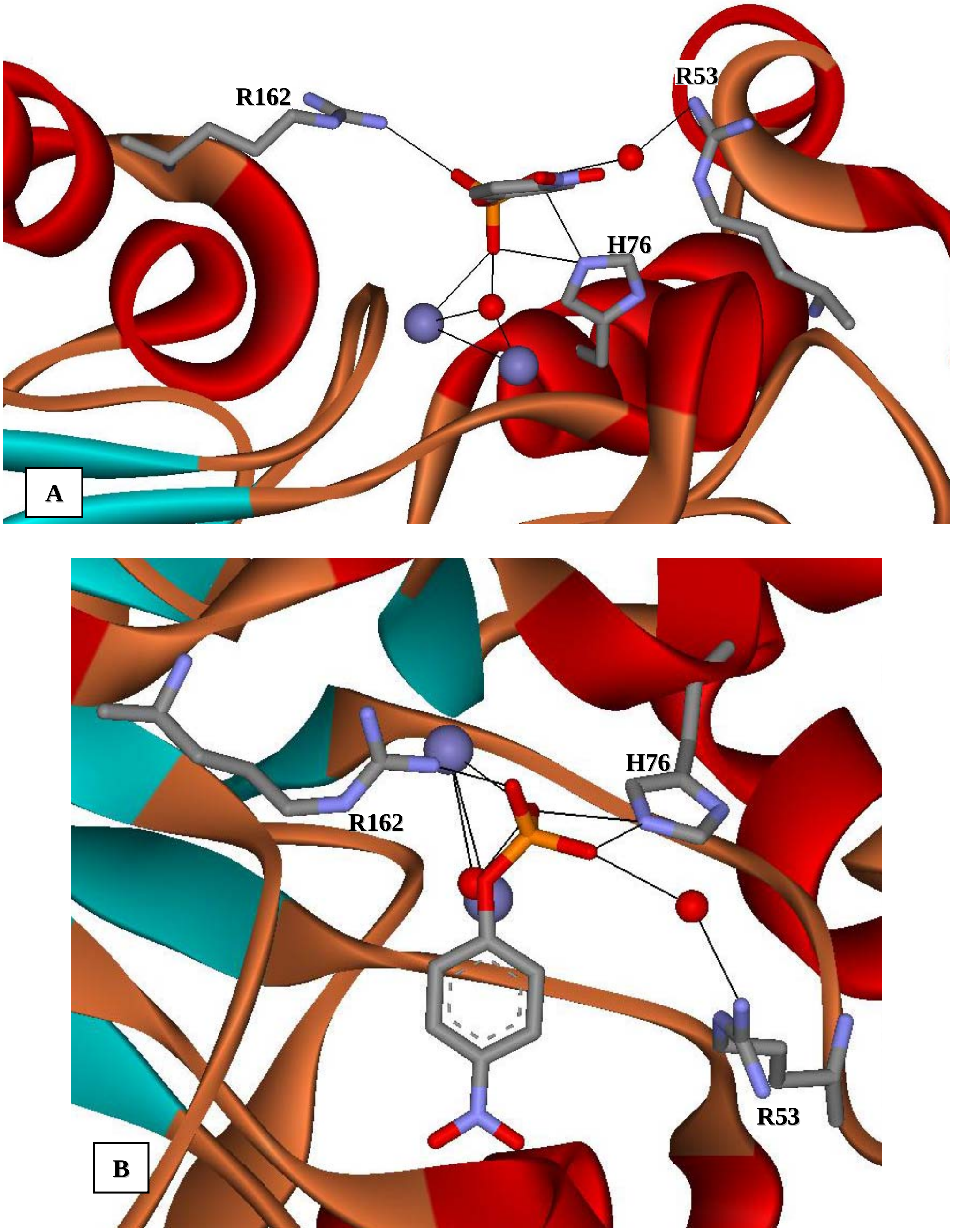
R162
R53
H76
A
H76
R162
R53
B

Figure 3-18. λPP with *p*NPP as modeled in Acclerys, boxes A and B.

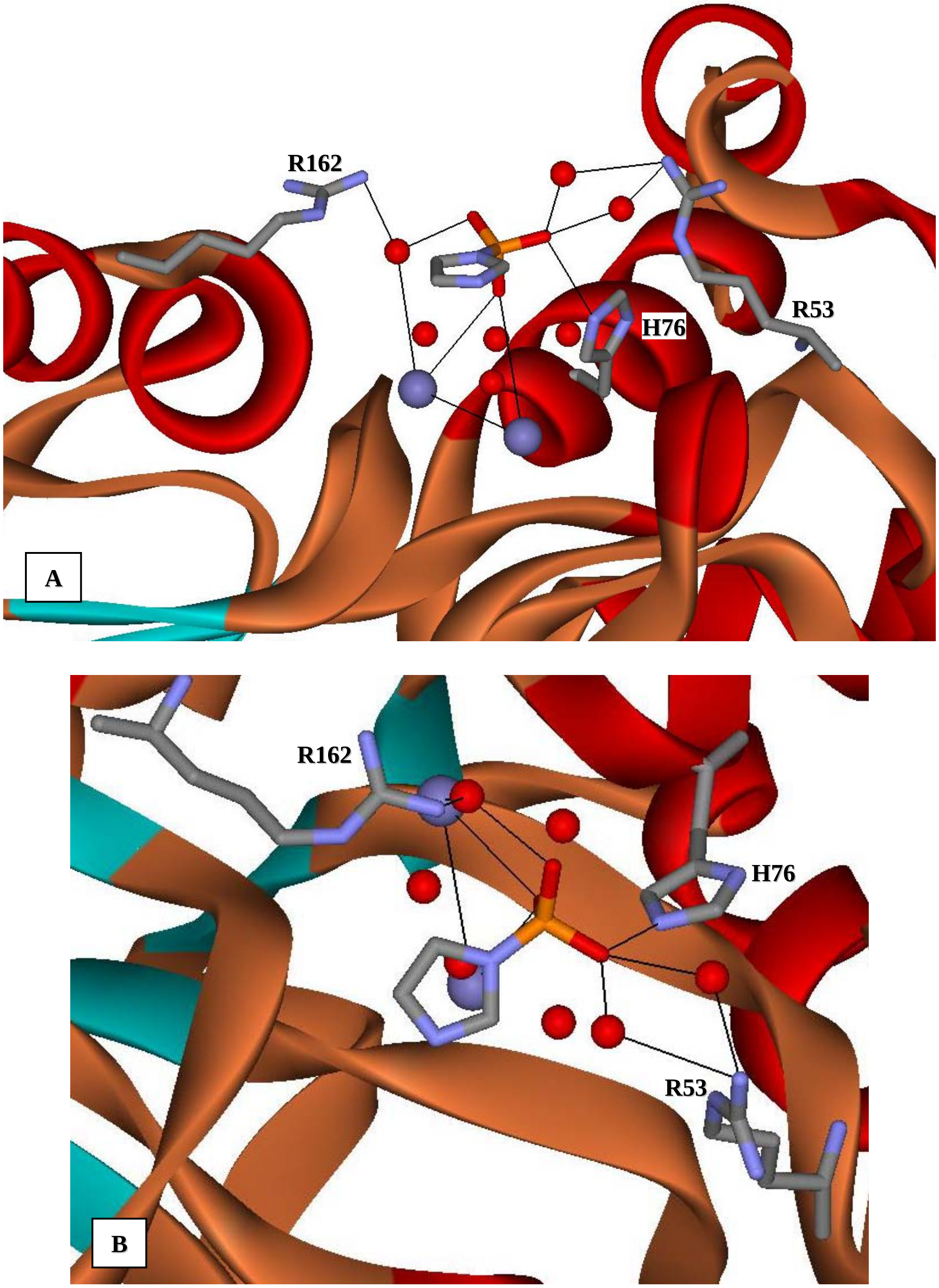
R162
H76
R53
A
R162
H76
R53
B

Figure 3-19. λPP with PIm as modeled in Acclerys, boxes A and B.

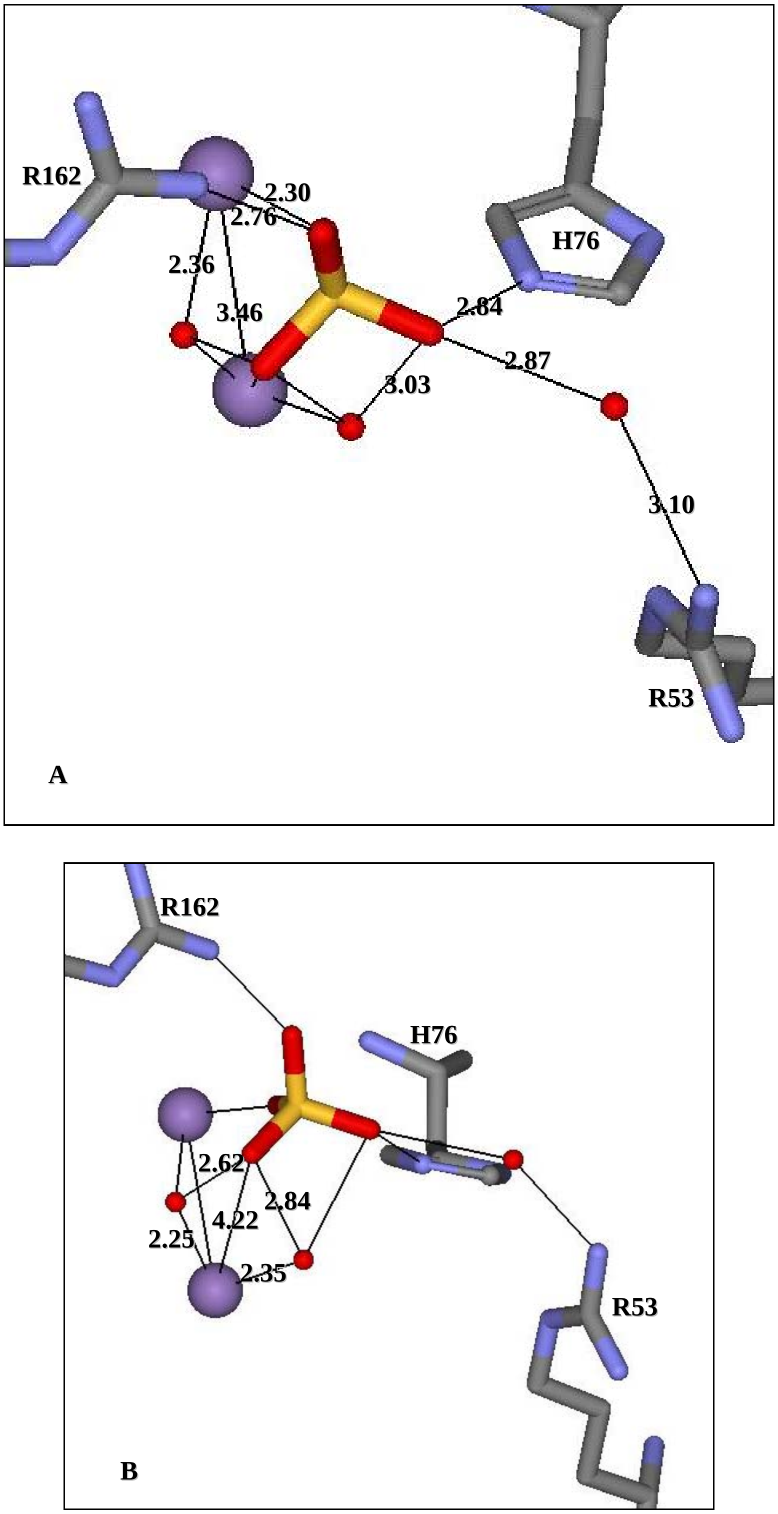
R162
2.30
2.76
H76
2.36
3.46
2.84
2.87
3.03
3.10
R53
A
R162
H76
2.62
2.84
4.22
2.25
2.35
R53
B

Figure 3-20. Sulfate bound in active site. A is the same view as in figure 3-15; B is rotated to view distances. Distances are taken directly from the crystal structure without modification.

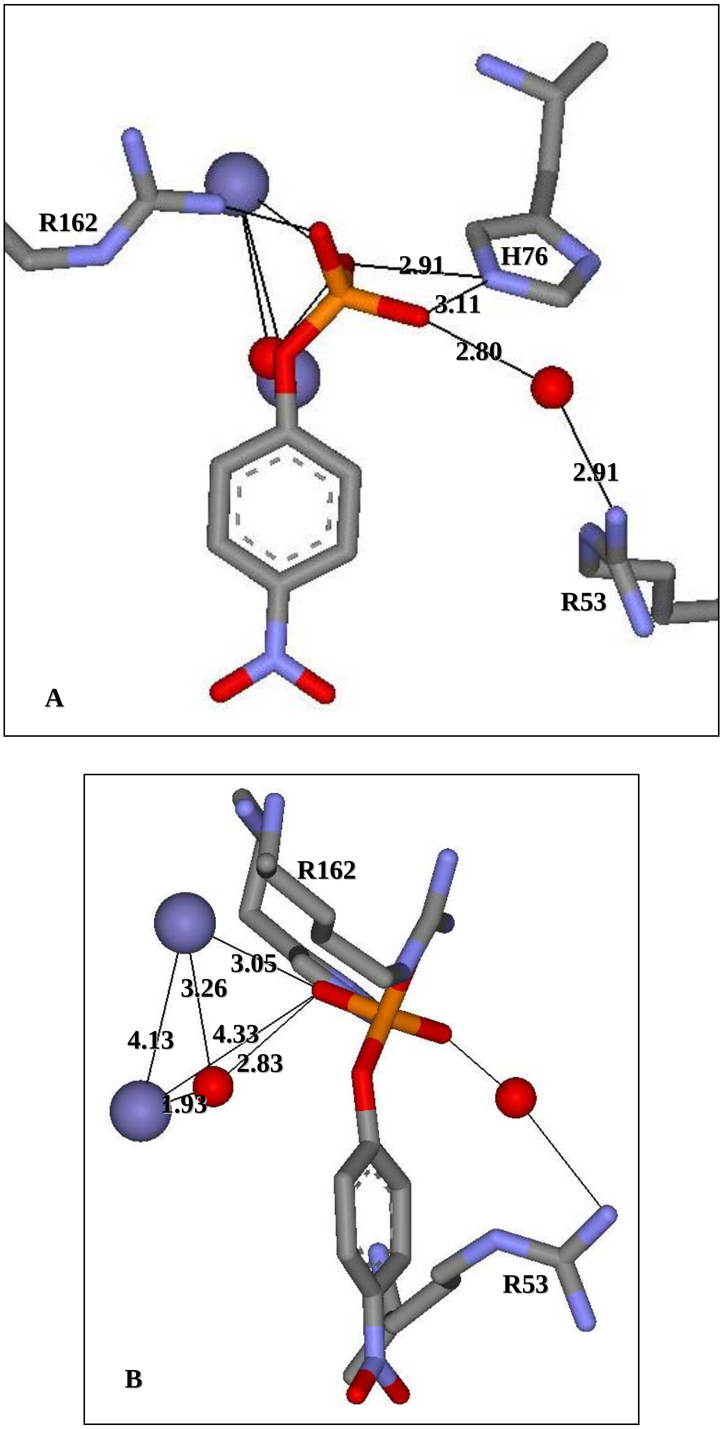
R162
2.91
H76
3.11
2.80
2.91
R53
A
R162
3.05
3.26
4.13
4.33
2.83
1.93
R53
B

Figure 3-21. *p*NPP bound in active site of λPP as modeled in Acclerys. A is the same view as in figure 3-16; B is rotated to view distances.

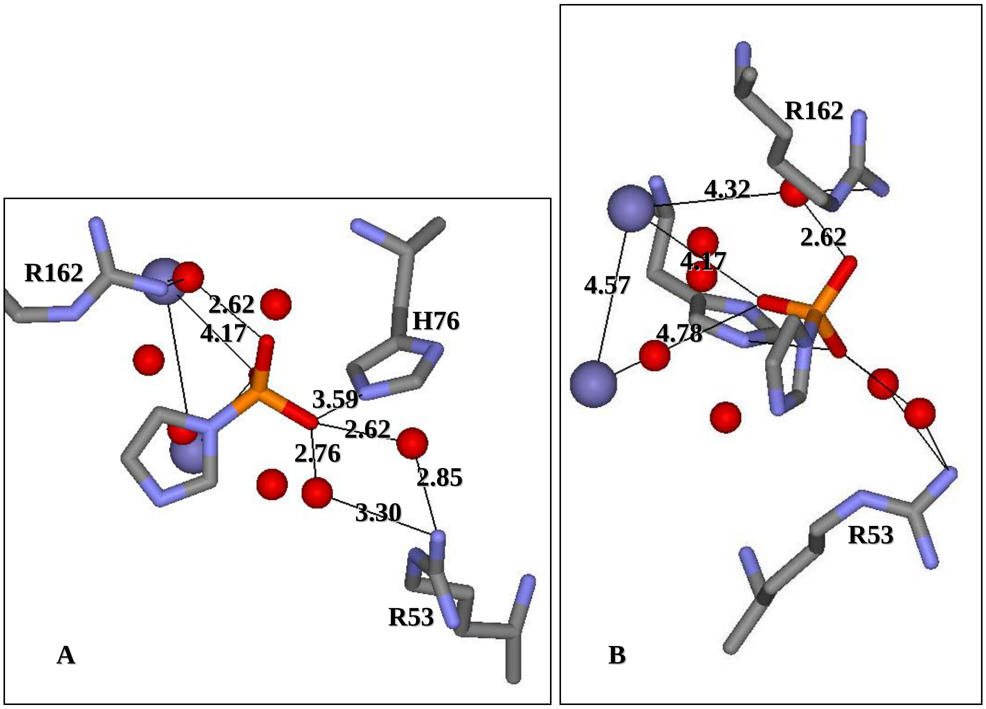
R162
2.62
4.17
H76
3.59
2.62
2.76
2.85
3.30
R53
A
R162
4.32
2.62
4.17
4.57
4.78
R53
B

Figure 3-22. PIm bound in active site of λPP as modeled in Acclerys. A is the same view as in figure 3-17; B is rotated to view distances.

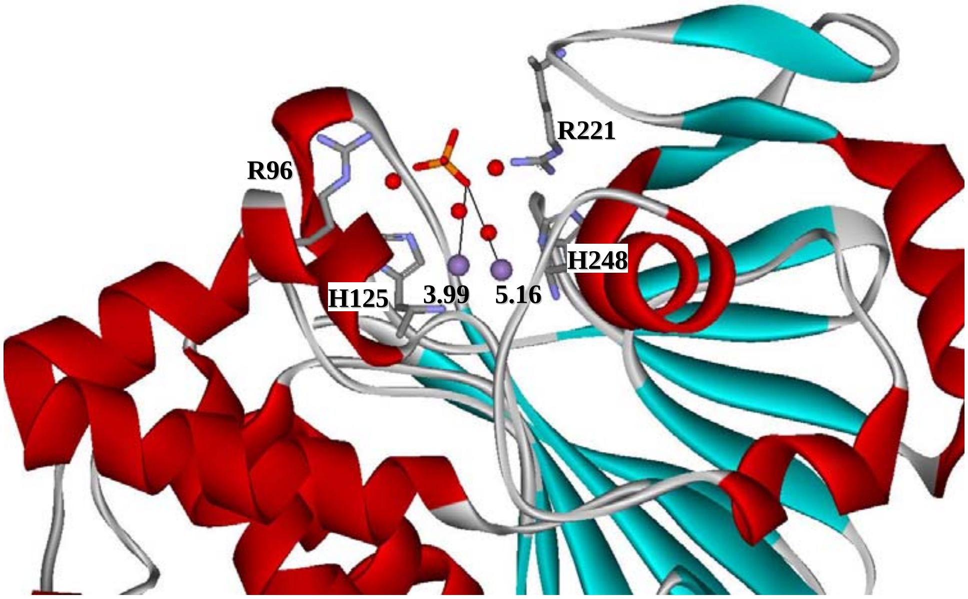
R221
R96
H248
H125
3.99
5.16

Figure 3-23. PP1 active site with phosphate.

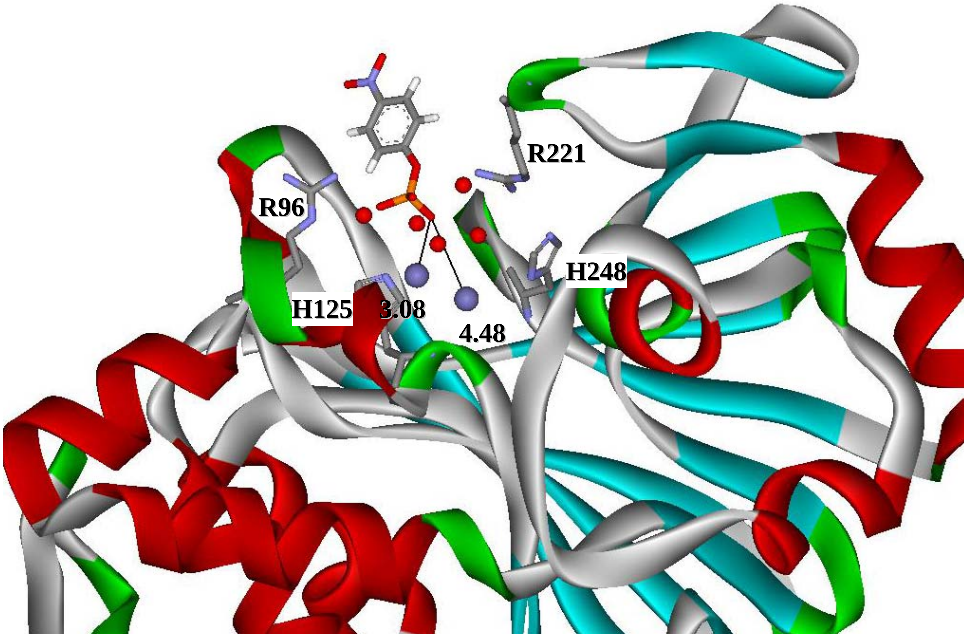
R221
R96
H248
H125
3.08
4.48

Figure 3-24. PP1 active site with *p*NPP as modeled in Acclerys.

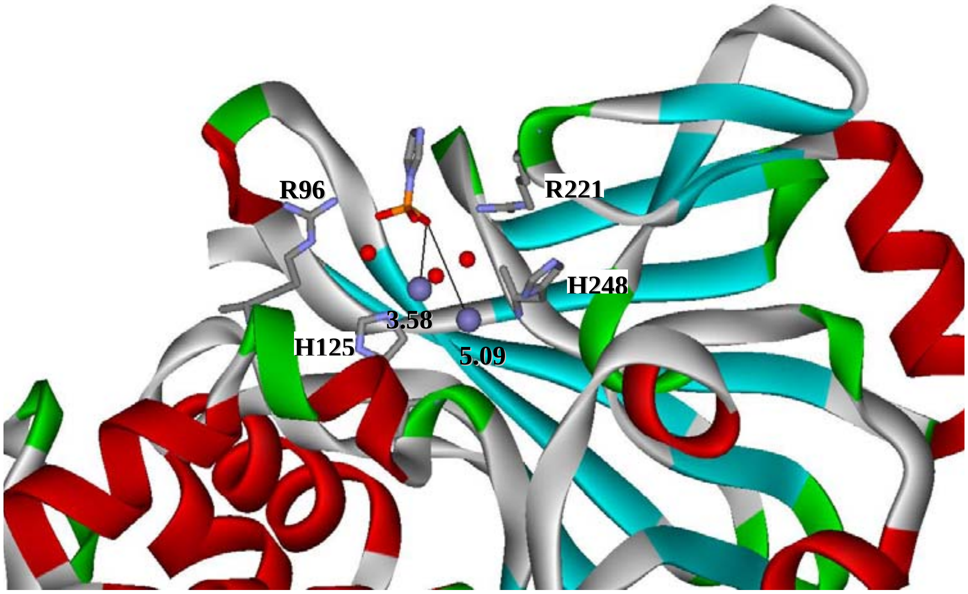
R96
R221
H248
3.58
H125
5.09

Figure 3-25. PP1 active site with PIm as modeled in Acclerys.

keeps generated P_i low; under such conditions micromolar K_M values have been reported. In this study k_{cat} and K_M values for *p*NPP and PIm comparable to those reported in the literature for *p*NPP at low substrate conditions. *N*-phPAM was a slower substrate than either *p*NPP or PIm. Nonetheless, among all of the tested enzymes AP exhibited the highest catalytic efficiencies with all three substrates.

Table 3-3. Kinetic literature values for *E. coli* AP at pH 8.0.

k_{cat} (s^{-1})	K_M (μM)	k_{cat}/K_M ($\times 10^6$) ($M^{-1}s^{-1}$)	Reference
79.8	21	3.8	70
167.5	32.7	5.1	75
175.5	34.9	5.0	140
74.7	21.8	3.4	141
44.4	9.4	4.7	142
13.6	7.4	1.8	111
	1.3		78
		3.3	73

Computer modeling found P_i, PIm and *p*NPP fit in the active site in the same orientation, but with different hydrogen bonding distances (Figures 3-26 through 3-31). This result is consistent with the enzyme's ability to hydrolyze both PIm and *p*NPP. AP's binding motif was reviewed in section **1.2.6**.

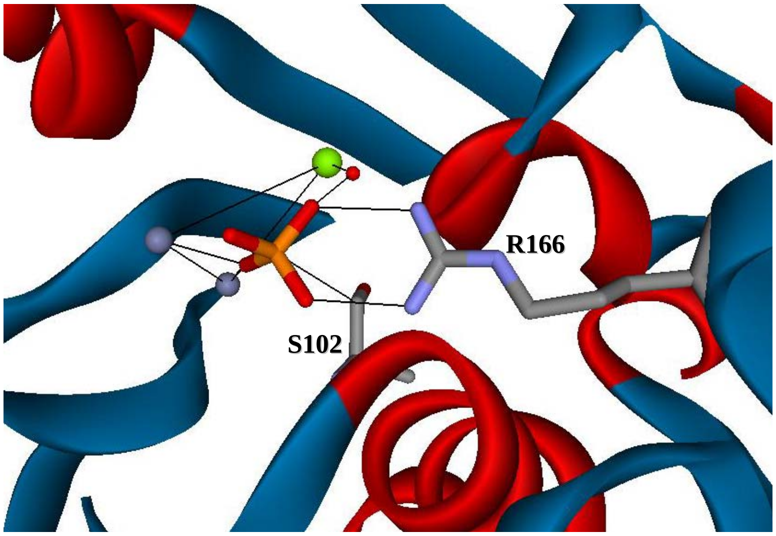

Figure 3-26. Phosphate bound in active site of AP (PDB 1ED8). Color scheme – green is zinc, yellow is magnesium, red sphere is water.

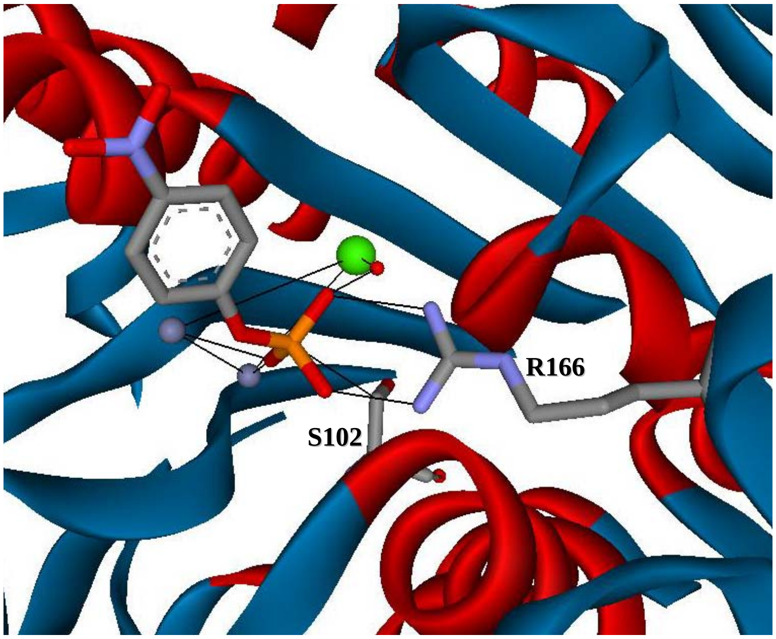

Figure 3-27. *p*NPP bound in active site of AP as modeled in Acclerys.

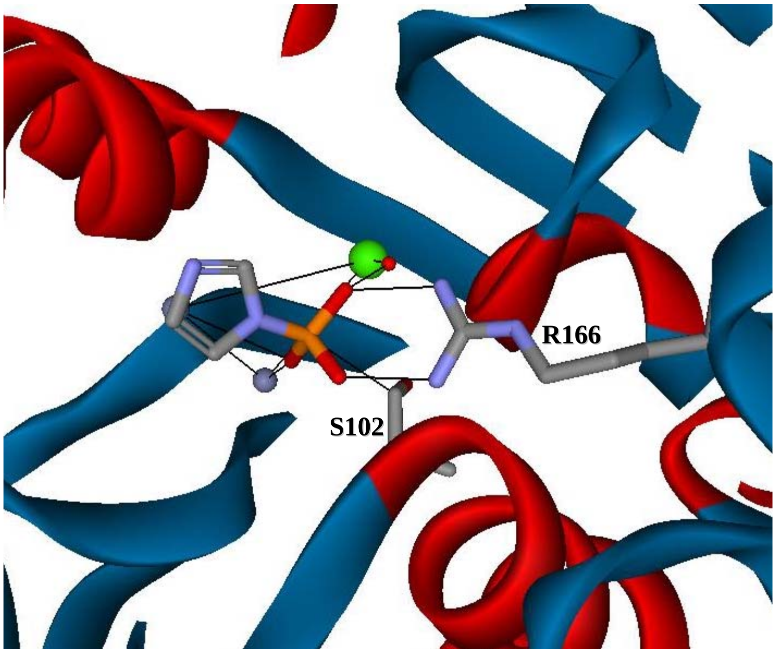

Figure 3-28. PIm bound in active site of AP as modeled in Acclerys.

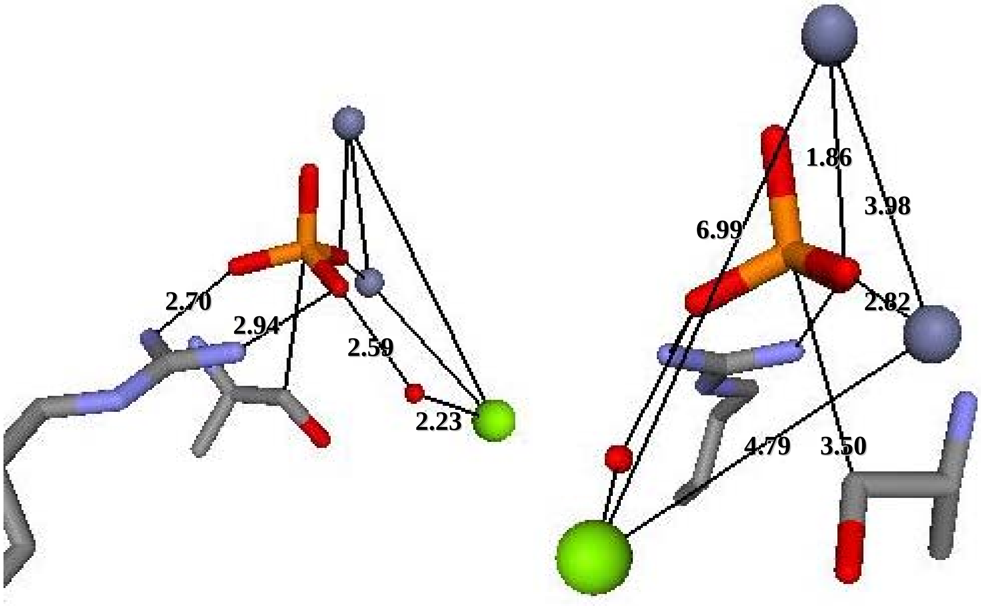
2.70
2.94
2.59
2.23
6.99
1.86
3.98
2.82
4.79
3.50

Figure 3-29. Phosphate bound in active site of AP (PDB 1ED8).

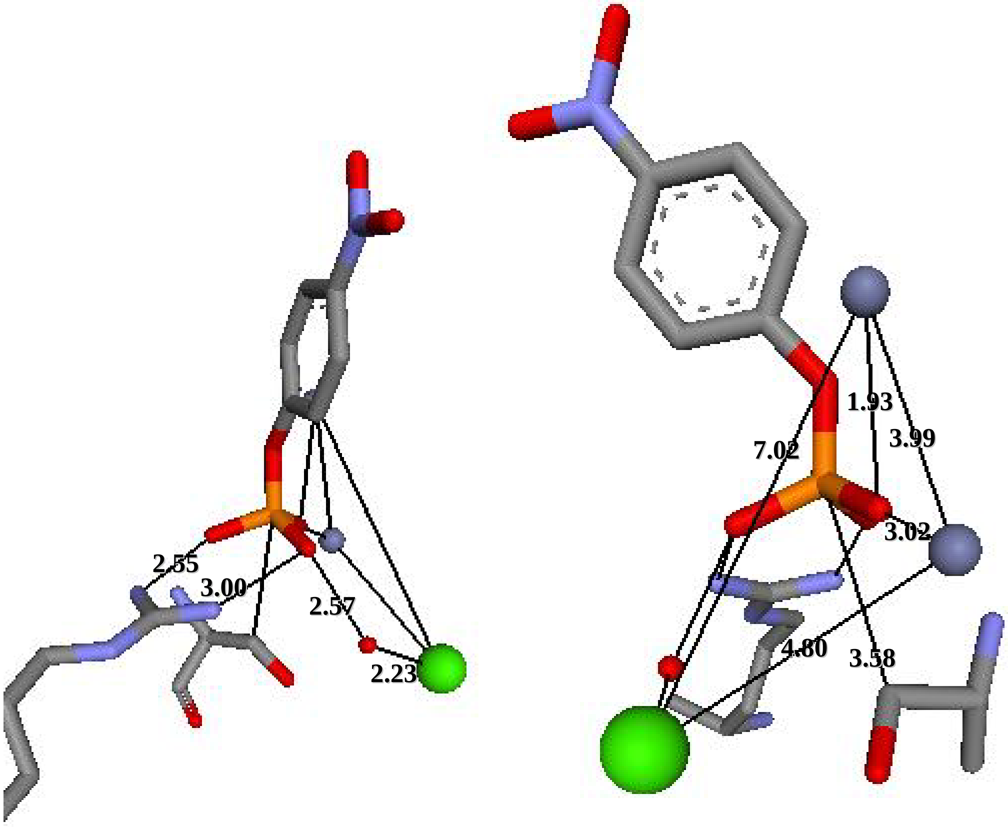
2.55
3.00
2.57
2.23
7.02
1.93
3.99
3.02
4.80
3.58

Figure 3-30. *p*NPP bound in active site of AP as modeled in Acclerys.

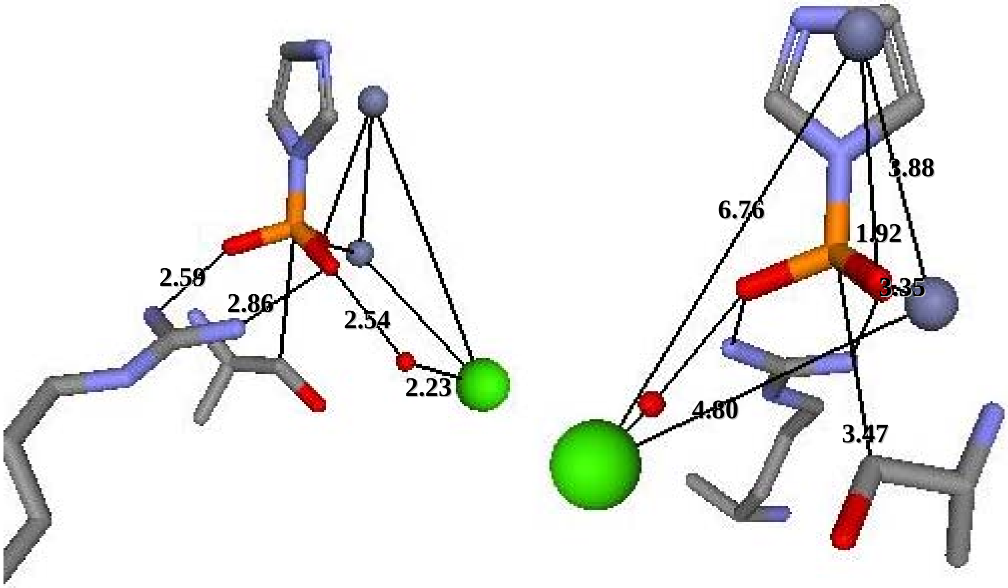
2.59
2.86
2.54
2.23
6.76
3.88
1.92
3.35
4.80
3.47

Figure 3-31. PIm bound in active site of AP as modeled in Acclerys.

CHAPTER 4

DISCUSSION

4.1 Discussion of Overall Experimental Results

The purpose of this research is to determine if known phosphatase motifs cleave both P-O and P-N bonds, or if enzymes must exist specifically with phosphoramidase activity. With the exception of PP1γ, the enzymes in this study catalyze hydrolysis of *p*NPP and PIm (Table 4-1). The known phosphomonoester phosphatases motifs were found to be capable of catalyzing the hydrolysis of both phosphomonoesters and phosphoramidates, albeit with different catalytic constants.

Table 4-1. Ratio of second order rate constants (*p*NPP/PIm) by enzyme.

	$(k_{cat}/K_M)/(k_{cat}/K_M)$	Catalyzes Hydrolysis of		
Enzyme	(*p*NPP)/(PIm)	*p*NPP	*N*-phPAM	PIm
YopH	27	Yes	Yes	Yes
VHR	0.22	Yes	Yes	Yes
PAcP	1.6	Yes	Yes	Yes
PHPT1 at pH 5.5	7.1×10^{-5}	Yes	Yes	Yes
PHPT1 at pH 8.0	7.4×10^{-5}	Yes	Yes	Yes
AP	0.51	Yes	Yes	Yes
λPP		Yes	ND	Yes
PP1γ		Yes	ND	No

In several cases catalytic values with an enzyme are similar with the different substrates, a seeming validation that the substrates are being bound and catalyzed similarly. Nevertheless, to justifiably state that all three substrates are hydrolytically catalyzed in the same manner would require specific experiments and is not the purpose of this study. Even so, there is an experimental result from this study that is consistent with hydrolysis proceeding the same for both phosphomonoesters and phosphoramidates:

during NMR studies with PIm there was no indication of cleavage other than at the P-N bond (see section 1.2). However, the NMR results do not mean that phosphoramidate hydrolysis must follow the same mechanistic pathway as phosphomonoesters.

In addition to the kinetic assays a series of computer experiments was conducted to examine whether there are structural properties of the enzymes that would shed insight into how the substrates bind in the active site. Substrate binding can affect the activity of an enzyme, and computer models have the ability to provide a snapshot of the enzyme-substrate complex before hydrolysis. If the initial placement of phosphomonoesters was different from phosphoramidates, catalysis proceeding via the same mechanism would be in question. In making the models, the differences in charge and geometry were used to assess the initial orientation of the substrate.

Charge may affect binding of the substrate. Inductive effects by the leaving group have the potential to significantly affect charge localization on the non-bridging oxygens. Charge localization might affect formation of the enzyme-substrate complex, and thus K_M. Charge repulsion between the bridging atom and active site residues may also affect formation of the enzyme-substrate complex. Shown in several figures in chapters one and three are active site arginines whose guanidinium groups are positively charged. This positive charge is repulsive to positively charged leaving groups, as with the imidazole moiety of PIm.

Geometric misalignments between the substrate and active site residues may also affect catalysis. The bridging atoms of *p*NPP and PIm exhibit different hybridizations, with *p*NPP's sp^3 bridging oxygen having free rotation around the C-O bond and PIm's sp^2 bridging nitrogen being constrained around the C-N-C bonds. Also, PIm is a smaller substrate than *p*NPP. The different hybridizations and sizes could result in different relative orientations between the enzyme and substrates.

Two significant differences between the phosphate ester and phosphoramidate substrates are the protonation of the phosphate moiety as well as protonation of the leaving group. Location of a proton during hydrolysis is important as it affects electron density on the phosphate moiety and P-X bond strength. Some accounting of proton location may be made by considering the percent protonation of the substrate before catalysis versus percent protonation of the free leaving group (Table 4-2).

Table 4-2. Percent protonation of the substrate before catalysis versus percent protonation of the free leaving group in solvent. Refer to Figure 3-1 for location of protonation.

	pH 5.5		pH 8.0	
	Substrate	Leaving group	Substrate	Leaving group
*p*NPP/pNP	22.4%	97.8%	0.1%	12.1%
N-phPAM/aniline	97.2%	19%	9.9%	0.1%
PIm/Im	95.2%	96.9%	5.9%	8.9%

As the purpose of this project is to determine if known phosphatase motifs can cleave phosphoramidates, the remainder of this chapter will discuss the results obtained from each enzyme with the different substrates. Where relevant, concepts from the introduction regarding the enzyme’s motif as well as uncatalyzed hydrolysis will be applied to the results.

4.2 Discussion of Results by Enzyme

4.2.1 PHPT1

The phosphohistidine phosphatase PHPT1 is believed to selectively cleave phosphohistidine residues in proteins. No explanation has been given for the specificity, but its mechanism employs general base catalysis. This is different from the other non-metallic motifs, in that they employ general acid/base catalysis.

While the enzyme catalyzes hydrolysis of both phosphomonoesters and phosphoramidates, there is a demonstrated preference for the phosphoramidates. The enzyme is able to catalyze hydrolysis of PIm 14,000 times faster than *p*NPP at both acidic and alkaline pH. Of the two phosphoramidate substrates, PHPT1 hydrolyzes PIm faster than *N*-phPAM. The results of this experiment validate PHPT1's assignment as a histidine phosphatase.

At pH 5.5 PIm is predominantly a zwitterionic monoanion with two negative charges on the phosphate moiety (Table 4-2 and Figure 3-1). The leaving group is positively charged and therefore activated. In the zwitterion, the opposite charges are proximal before the substrate enters the active site. After entering the active site the opposite charges become separated due to the negative charge on the non-bridging oxygens hydrogen bonding with the backbone. Intermolecular ionic attraction within the substrate is weakened with the increased distance between the imidazole cation and phosphoryl anions.

The enzyme's crystal structure reveals no amino acids within the active site that can act as a general acid. This was confirmed by mutational studies from the literature.[20] At pH 5.5, the imidazole that was cleaved from the substrate must obtain a proton from the solvent. At pH 8.0 PIm exists primarily as a dianion, again with two negative charges on the phosphate moiety. Again, the imidazole that was cleaved from the substrate must obtain a proton from the solvent.

The striking experimental result with PHPT1 is the similarities in kinetic performance at acidic and alkaline conditions. Comparing catalysis of a substrate at pH 5.5 and pH 8.0 shows that changes in pH do not yield significantly different rates.

The rate limiting step for substrate catalysis by PHPT1 is not known. Values for k_{cat} vary significantly between the three substrates, as do the protonation states of the substrates (Figure 3-1 and Table 4-3). The enzyme's general base, His53, remains unprotonated at pH 5.5 and pH 8.0, and the enzyme performs with similar catalytic values at both conditions. If generation of the base or nucleophilic attack was rate limiting, k_{cat} values between the substrates would be expected to be similar; they are not.

Table 4-3. Kinetic results for PHPT1.

pH 5.5			
	k_{cat} (s^{-1})	K_M (mM)	k_{cat}/K_M ($M^{-1}s^{-1}$)
*p*NPP	0.00407 ±0.00007	2.7 ±0.2	1.5
N-phPAM	0.26 ±0.06	5 ±3	50
PIm	2.70 ±0.04	0.13 ±0.02	21000
pH 8.0			
*p*NPP	0.0106 ±0.0004	6.3 ±0.6	1.7
N-phPAM	2.6 ±0.1	10 ±1	260
PIm	2.31 ±0.05	0.10 ±0.02	23000

The kinetic results are consistent with the rate limiting step is driven by differences in the nature of the substrate's P-X bond. They are also consistent with the rate limiting step is driven by the protonation state of the substrate. A chemical step in catalysis is rate limiting.

Noted in the introduction was that hydrolysis of phosphomonoesters and phosphoramidates proceeded with pre-equilibrium protonation of the leaving group's bridging atom. In uncatalyzed hydrolysis phosphomonoesters rely on protons from the non-bridging oxygens to protonate the bridging oxygen. This explains why phosphomonoester monoanions hydrolyze rapidly. Phosphoramidates more readily hold a proton on the bridging atom, explaining why they hydrolyze more rapidly than phosphomonoesters.

Unlike the other non-metallo enzymes used in this study, PHPT1 does not protonate the bridging atom. The phosphomonoesters should less susceptible to PHPT1's general base mechanism since the phosphomonoesters must rely on the solvent for protonation of the bridging atom; phosphomonoesters bind as the dianion, so the proton source for the bridging oxygen is likely not the phosphoryl oxygens. Conversely, the phosphoramidates may be better able to gain a proton on the bridging nitrogen from the solvent. It must also be noted that pNPP is a dianion at both pH 5.5 and 8.0 and will bind as such. The phosphoramidates can bind as monoanions or dianions. More readily obtaining a proton from the solvent, more readily holding a proton on the bridging nitrogen, or entering the active site with the bridging nitrogen already protonated would explain the greater k_{cat} values of the phosphoramidates versus *p*NPP.

Whether or not protonation of the leaving group is responsible for the change in rate could be determined by generating a pH rate profile of PHPT1 with PIm and *N*-methyl PIm. *N*-methyl PIm's hydrolysis is insensitive to hydrogen ion concentration. If the pH rate profile of *N*-methyl PIm was also insensitive to pH and the rate profile with PIm was sensitive to pH, then it could be discerned that protonation of the leaving group is rate limiting. If the pH rate profile of *N*-methyl PIm was affected by hydrogen ion concentration, then generation of the nucleophile is likely rate limiting.

The kinetic results herein are consistent with a similar mechanism for hydrolysis of phosphoramidates and phosphomonoesters. The alternative possibility of cleavage of the C-N bond has been ruled out by NMR experiments. Additional evidence that the mechanism is similar was found by computer modeling of substrate binding.

Computer models with *p*NPP and PIm in the active site show the phosphate moiety in the same general orientation (Figures 3-3 and 3-4). Hydrogen bonding distances with the backbone and Ser94 were close between the two substrates (Table 4-4). His53 to phosphorus distance varied by 2.4%, while Lys21 to the phosphoryl oxygen distance varied by 3.5%. Both substrates were oriented in the active site essentially the same and key distances exhibited little variation. This is consistent with the catalytic mechanism being the same for the two substrates.

4.2.2 YopH

YopH displays specificity for phosphotyrosine due to the depth of its active site. Peptide substrates with shorter phosphorylated hydroxyl residues are not able to access the active site. Aside from phosphotyrosine, YopH can dephosphorylate *p*NPP, naphthyl phosphate, and nitro-benzyl phosphate, NBP.[30] The ability to catalyze hydrolysis of NBP shows that the ester bond need not involve an aryl ester. The small molecule substrates in this experiment include both sp^2 and sp^3 bridging atoms and are able to access the active site as they are not constrained by a peptide.

YopH catalyzes hydrolysis of *p*NPP with the highest rate constant, followed by *N*-phPAM and PIm (Table 4-5). Although the bridging atom is different, *p*NPP and *N*-

Table 4-4. Comparison of distances between PHPT1 crystal structure with P_i and computer models with *p*NPP and PIm.

	Importance of Amino Acid	Crystal Structure With P_i (Å)	Computer Model With *p*NPP (Å)	Computer Model With PIm (Å)
His53 residue - phosphorus	Generates general base, affects substrate binding	4.24	4.25	4.35
His53 amide backbone – phosphoryl group	Hydrogen bonding for binding	2.89	3.00	2.99
Ala54 amide backbone – phosphoryl group	Hydrogen bonding for binding	3.05	2.97	3.00
Lys21 – phosphoryl group	Hydrogen bonding for binding, stabilize charge on nucleophilic water	4.87	4.59	4.75
Ala96 amide backbone – phosphoryl group	Hydrogen bonding for binding	3.03	3.19	3.20
Met95 amide backbone – phosphoryl group	Hydrogen bonding for binding	3.00	2.96	3.04
Ser94 residue – phosphoryl group	Hydrogen bonding for binding	2.76	3.03	3.00

Table 4-5. Kinetic results for YopH.

pH 5.5			
	k_{cat}(s^{-1})	K_M (mM)	k_{cat}/K_M x 10^{-3} ($M^{-1}s^{-1}$)
*p*NPP	610 ±30	3.1 ±0.4	200
N-phPAM	530 ±70	4 ±2	100
PIm	34 ±2	4.9 ±0.5	7

phPAM are isosteric. PIm differs from *p*NPP and *N*-phPAM in sterics and electronics, and catalysis proceeds with an order of magnitude lower rate constant than either *p*NPP or *N*-phPAM.

The K_M's for the substrates are very similar. Differences in the catalytic efficiency are driven predominantly by differences in k_{cat}, which must be due to the nature of the leaving group. There is little effect on the rate constant by para substituted monoester substrates,[26] and the β_{LG} value for YopH is -0.19.[31]

For all three substrates in this study, the same phosphocysteine intermediate is expected. If hydrolysis of this intermediate is rate limiting with all three substrates, there should be no difference in k_{cat}. There is a significant difference in k_{cat} between *p*NPP and PIm, indicating that the rate limiting step is either different, or the first step is partially rate limiting.

For catalysis, the WPD loop of the enzyme closes over the substrate, bringing the general acid, Asp356, close to the bridging atom, facilitating protonation of the leaving group. The leaving group of *p*NPP and *N*-phPAM can be effectively protonated by Asp356 as they share sterics and electronics. Both enter the active site with a predominantly uncharged leaving group. PIm likely enters the active site of YopH as a monoanionic zwitterion (Figure 3-1 and Table 4-2). The leaving group is positively charged and thus more labile; departure of imidazole need not involve protonation by the general acid.

The kinetic results are consistent with *p*NPP and *N*-phPAM having the same rate-limiting step in YopH catalysis. Cleavage of the C-N bond was not observed in NMR experiments with PIm, which is consistent with the catalytic mechanism being similar for *p*NPP and PIm. Additional insight to the *p*NPP and PIm mechanisms was found by computer modeling.

The crystal structure used as the basis for computer modeling had the WPD loop in the closed position. The advantage in starting with this structure is that it is a close representation of the enzyme during catalysis. An advantage to using a structure with the loop opened would be that such a structure would better represent binding. With the loop open the bound substrate's leaving group is not constrained by the shape or size of the active site. With the loop closed there is constraint (Figures 1-7 and 1-8). The positive charge on the imidazole moiety had the potential to interfere with loop closure, and clashes between the imidazole moiety and WPD loop residues could occur with a loop closed structure.

Computer models of *p*NPP and PIm in the active site show the phosphate moiety in the same general orientation (Figures 3-6 and 3-7). Both substrate's phosphate oxyanions form hydrogen bonds with the same residues when bound. But, the computer determines the distances by minimizing the energy for all distances between the enzyme and substrate. In considering the Cys403 to phosphorus distance in the model with PIm, the computer forced the distance to be 1.94 Å; this reflects the computer's effort to minimize the total energy between PIm and the residues (Table 4-6).

When the WPD loop is removed from the computer models, distances between the enzyme and substrates trend toward lengthening; lengths were greater in all cases with PIm, and the cysteine-phosphorus distance increased 1.65 Å (Table 4-6 and Figures 3-8 and 3-9). The computer modeling is consistent with loop closure creating an unfavorable cysteine-phosphorus distance with PIm whereas no unfavorable distance exists with *p*NPP. The two substrates are geometrically different. PIm's imidazole moiety cannot rotate away from the WPD loop, causing clash. Conversely, *p*NPP's phenol moiety can rotate away from the WPD loop.

The global conformation of the active site residues possesses differences in distances between *p*NPP and PIm. While the general orientation of the substrates was similar, differences in key enzyme-substrate distances indicate differences in the exact orientation. Enzyme-PIm distances tend to be lower than enzyme-*p*NPP distances.

Aside from Cys403, two other important residues exhibit significant variation between the substrates: Asp356, the general acid/base; and Gln446, responsible for orienting the nucleophilic water. Asp356 is 0.37 Å further from PIm than *p*NPP, while Gln446 is 0.51 Å further. These longer distances reflect the loop-closed conformation having some differences between the substrates.

4.2.3 VHR

VHR possesses a catalytic motif similar to YopH. Two important differences between the enzymes' active sites are the position of the general acid/base, and depth. VHR's general acid/base, Asp92, is not on a flexible loop. Additionally, VHR's active site is shallow, approximately 6.4 Å, as compared to YopH's deep active site, approximately 9.5 Å (these values were obtained using VHR crystal structure PDB 1VHR, and YopH crystal structure PDB 1YPT which is a loop open structure).

VHR catalysis of phosphomonoesters shows little dependence on the leaving group, β_{LG} = -0.074 ±0.023.[42] Further, the enzyme displays burst kinetics.[44] The low dependence on the leaving group and burst kinetics are explained by breakdown of the phosphoenzyme intermediate being rate limiting.

Table 4-6. Comparison of distances between YopH crystal structure with vanadate and computer models with *p*NPP and PIm.

	Importance of Amino Acid	Crystal Structure With Vanadate (Å)	Computer Model With *p*NPP (Å)	Computer Model With PIm (Å)	Computer Model With *p*NPP & WPD Loop Removed (Å)	Computer Model With PIm & WPD Loop Removed (Å)
Cys403 residue – vanadate/ phosphorus	Nucleophile, forms covalent bond	2.52	3.66	1.94	3.80	3.59
Arg404 amide backbone – phosphoryl group	Hydrogen bonding for binding	2.58	3.33	2.32	3.12	2.41
Ala405 amide backbone – phosphoryl group	Hydrogen bonding for binding	2.61	3.03	3.12	3.04	3.15
Gly406 amide backbone – phosphoryl group	Hydrogen bonding for binding	3.09	3.11	3.05	3.14	3.09
Val407 amide backbone – phosphoryl group	Hydrogen bonding for binding	2.89	3.02	2.55	3.04	2.58
Gly408 amide backbone – phosphoryl group	Hydrogen bonding for binding	2.91	3.11	2.87	3.14	2.94
Arg409 amide backbone – phosphoryl group	Hydrogen bonding for binding	2.68	3.11	2.70	3.12	2.84
Arg409 residue – phosphoryl group	Hydrogen bonding for binding, stabilize charge on leaving group	3.03/3.13	3.08/3.32	2.86/3.46	3.48/3.54	2.93/3.71
Asp356 residue – bridging atom	General acid/base	2.82	2.81	3.18	N/A	N/A
Gln446 residue – bridging atom	Orient nucleophilic water	4.16	3.30	3.91 from GlnO to bridge N 2.49 from GlnO to non-bridge N 3.81 from GlnN to bridge N	3.30	4.39 from GlnO to bridge N 2.92 from GlnO to non-bridge N 4.47 from GlnN to bridge N

VHR catalyzes hydrolysis of alkyl and aryl phosphomonoesters with similar catalytic efficiency.[42] In this research with VHR, k_{cat} is similar for all three substrates (Table 4-7). The second order rate constants are also similar. These results are consistent with breakdown of the phosphoenzyme intermediate in VHR catalyzed hydrolysis of *N*-phPAM and PIm also being rate limiting.

Table 4-7. Kinetic results for VHR.

pH 5.5			
	$k_{cat}(s^{-1})$	K_M (mM)	$k_{cat}/K_M \times 10^{-3}$ ($M^{-1}s^{-1}$)
*p*NPP	5.9 ±0.2	2.0 ±0.2	3.0
N-phPAM	5.8 ±0.6	0.8 ±0.2	7
PIm	7.8 ±0.6	0.58 ±0.09	13

VHR has lower K_M values for the phosphoramidate substrates than *p*NPP. Literature precedent exists regarding VHR's variation in K_M. Reported catalytic values for β-naphthyl phosphate (**20**) and 4-methyl umbelliferyl phosphate (**21**) at pH 6.0 are $k_{cat} = 6.80 \pm 0.41\ s^{-1}$, $K_M = 0.50 \pm 0.07$ mM, pK_{aLG} 9.38, and $k_{cat} = 6.74 \pm 0.31\ s^{-1}$, $K_M = 0.72 \pm 0.11$ mM, pK_{aLG} 7.80, respectively.[42] These values compare to reported catalytic values for *p*NPP at pH 6.0 of $k_{cat} = 6.0 \pm 0.2\ s^{-1}$, and $K_M = 1.7 \pm 0.1$ mM.[43] The phosphoramidate values obtained herein are within variation reported for phosphomonoesters and are a close match for **20** and **21**.[42]

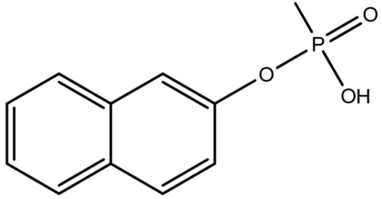

20

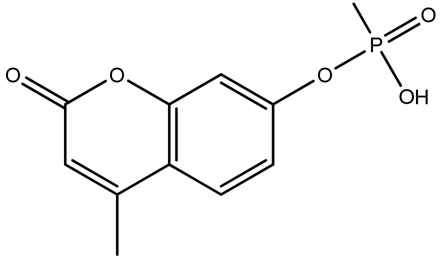

21

Computer models with *p*NPP and PIm in the active site show the phosphate moiety in the same general orientation (Figures 3-11 and 3-12). Both substrates' phosphate oxyanions form hydrogen bonds with the same residues with approximately the same distances when bound (Table 4-8). Variation between enzyme-substrate complexes with *p*NPP and PIm was minimal with two exceptions. The Arg130 to phosphoryl oxygen distance was greater with PIm, while the Asp92 residue to the bridging atom distance was shorter by 0.57 Å with PIm; Asp92 is the general acid/base. Given that PIm is already activated, there may be less importance for Asp92 to be close

Table 4-8. Comparison of distances between VHR crystal structure with sulfate and computer models with *p*NPP and PIm.

	Importance of Amino Acid	Crystal Structure With Sulfate (Å)	Computer Model With *p*NPP (Å)	Computer Model With PIm (Å)
Cys124 residue – sulfate/ phosphorus	Nucleophile	3.64	3.59	3.73
Cys124 amide backbone – phosphoryl group	Hydrogen bonding for binding	3.05	3.02	3.26
Arg125 amide backbone – phosphoryl group	Hydrogen bonding for binding	2.89	3.08	3.05
Glu126 – phosphoryl group	Hydrogen bonding for binding	3.56	3.08	2.99
Tyr128 amide backbone – phosphoryl group	Hydrogen bonding for binding	2.92	2.91	2.91
Ser129 amide backbone – phosphoryl group	Hydrogen bonding for binding	2.78	3.15	3.29
Arg130 backbone – phosphoryl group	Hydrogen bonding for binding	2.94	2.92	3.02
Arg130 residue – phosphoryl group	Hydrogen bonding for binding	3.12/3.22	2.88/2.96	3.23/2.95
Asp92 residue – bridging atom	General acid/base	3.13	3.95	3.38

to PIm as compared to *p*NPP.

The same mechanism of hydrolysis with *p*NPP and PIm is consistent with similar k_{cat} values, similar enzyme-substrate distances in computer models, and only P-N cleavage in NMR experiments. One difference may be that the enzyme does not have to protonate the leaving group to effect hydrolysis.

4.2.4 hPAcP

The histidine acid phosphatases are able to catalyze a variety of substrates, to include phosphotyrosine,[143,144] glycerol phosphate,[51,145,146] acetyl phosphate,[145] adenosine monophosphate,[145] benzyl phosphate,[51] naphthyl phosphate,[144] phytate,[147] and fructose phosphate.[147] Due to the many types of substrates PAcP is able to catalyze it is considered a non-specific phosphatase.

With this enzyme, an interesting situation arises when phosphoimidazole enters the active site. The P-N bond of the substrate is equivalent to the potential P-N bond of the phosphoenzyme intermediate. That PAcP catalyzed hydrolysis of PIm shows that active site must generate a preference for the enzyme’s histidine residue to attack the PIm substrate and preferentially cleave one P-N bond over the other. This may be facilitated by the imidazole moiety of the substrate being protonated during the transition state while the imidazole moiety of His12 is not.

The β_{LG} value with the enzyme and substituted phenyl phosphates was -0.08, showing little dependence of the rate upon the leaving group.[37,113] This is consistent with breakdown of the phosphoenzyme intermediate being rate limiting. In the research here, k_{cat} values were similar for all three substrates, consistent with the same rate limiting step being operative, i.e. breakdown of the phosphoenzyme intermediate (Table 4-9). K_M

values varied significantly, a reflection of changes in formation of the enzyme-substrate complex.

Table 4-9. Kinetic results for PAcP.

pH 5.5			
	$k_{cat}(s^{-1})$	K_M (mM)	$k_{cat}/K_M \times 10^{-3}$ ($M^{-1}s^{-1}$)
*p*NPP	2.13 ±0.02	0.23 ±0.04	9.3
N-phPAM	2.5 ±0.1	0.07 ±0.01	40
PIm	6.0 ±0.4	1.01 ±0.09	5.9

Unlike the other non-metallo enzymes, binding is not accomplished by hydrogen bonds with the protein backbone. PAcP's hydrogen bond network is with three arginines and histidine. Whereas amide backbones have no charge, arginine and protonated histidine have a positive charge. If the Arg11, Arg15, Arg79, and His 257 were protonated, there would be four positive charges in the active site of PAcP (Figure 1-15). This would be expected to be repulsive to the positive charge on the imidazole moiety of PIm. Such repulsion may be the cause of the greater K_M with PIm.

Computer modeling found PIm and *p*NPP bound in the same general orientation (Figures 3-14 and 3-15). Both substrates' phosphate oxyanions form hydrogen bonds with the same residues with approximately the same distances when bound (Table 4-10). There was a 0.2 Å shorter distance between the general acid/base Asp258 and the bridging atom for PIm than for *p*NPP. Given that PIm is already activated, this distance may be of minimal importance.

The same mechanism of hydrolysis with *p*NPP and PIm is consistent with similar k_{cat} values, similar enzyme-substrate distances in computer models, and only P-N cleavage in NMR experiments.

Table 4-10. Comparison of distances between PAcP crystal structure with phosphate and computer models with *p*NPP and PIm.

	Importance of Amino Acid	Crystal Structure With P_i (Å)	Computer Model With *p*NPP (Å)	Computer Model With PIm (Å)
His12 residue – phosphorus	Nucleophile	3.19	3.19	3.22
Arg11 residue – phosphate oxyanion	Hydrogen bonding for binding	3.38/3.27	3.33/3.29	3.32/3.15
Arg15 residue – phosphate oxyanion	Hydrogen bonding for binding	2.78/2.98	2.72/2.83	2.74/3.03
Arg79 residue – phosphate oxyanion	Hydrogen bonding for binding	3.04/2.75	2.96/2.76	3.00/2.79
His257 residue – phosphate oxyanion	Hydrogen bonding for binding	2.92	2.85	2.99
Asp258 residue – bridging atom	General acid/base	2.81	2.92	2.72 bridge N 2.79 non-bridge N

4.2.5 λPP & PP1.

Both λPP and PP1γ are serine/threonine phosphatases. Despite this classification, neither enzyme is able to hydrolyze monomeric serine or threonine phosphate.[60,61,148] The amino acid sequence, as well as the length of the sequence, are crucial for catalytic hydrolysis of phosphopeptide substrates.[60]

Both enzymes have the catalytic core of the serine/threonine phosphatases. Between the two, λPP is the smaller enzyme, 221 amino acids versus 294 for the human PP1γ protein. λPP is the smallest of the cataloged serine/threonine phosphatases.

Phosphohistidine peptides and proteins are substrates for λPP[60] and PP1.[62] Additionally, PP1 catalyzes hydrolysis of aryl methylphosphonates,[63] while λPP catalyzes hydrolysis of phosphodiesters.[66] While the enzymes are classified as serine/threonine phosphatases, their inability to catalyze hydrolysis of phosphoserine or phosphothreonine, while at the same time catalyzing hydrolysis of phosphohistidine, phosphonates, and phosphodiesters, throws into question what their native substrates are and what classification they should be assigned. In the research herein, λPP effected hydrolysis of PIm, while PP1 did not.

Under the same conditions and equal periods of time λPP catalyzes hydrolysis of *p*NPP more than seven times more rapidly than PIm. But, catalysis goes to 25% with PIm and stops. These results provide little insight as to why overall catalysis of *p*NPP was greater than with PIm; kinetic constants cannot be obtained.

Computer models show *p*NPP and PIm bound in significantly different orientations in the active site (Figures 3-18, 3-19, 3-21, and 3-22). Not only are the substrates in different orientations, the location, number and placement of water molecules is different. Since the number of water molecules in the active site varies according to substrate, it is difficult to make comprehensive side by side distance comparisons between computer modeled binding of *p*NPP and PIm. However, proximity of the substrate to the metals must be crucial regardless of which of the three possible mechanisms is operative. Arginines 162 and 53 may be important for binding and/or proper orientation of the substrate.

Key distances between the substrates, metals, and arginines are shown (Table 4-11). Most distances with the PIm model are significantly larger than with the *p*NPP model. Coupled with a PIm K_i of 22 mM, it can be concluded that PIm does not bind well to λPP.

Table 4-11. Comparison of distances between λPP crystal structure with sulfate and computer models with *p*NPP and PIm.

	Crystal Structure With Sulfate (Å)	Computer Model With *p*NPP (Å)	Computer Model With PIm (Å)
Mn^{2+} – Mn^{2+}	3.46	4.13	4.57
Mn_1^{2+} – oxyanion	2.30	3.05	4.17
Mn_2^{2+} – oxyanion	4.22	4.33	4.78
Arg162 – phosphate oxyanion	2.76	2.78	3.69
Arg53 – phosphate oxyanion	5.57	5.35	4.58

Poor binding by PIm cannot be solely responsible for hydrolysis proceeding to 25% and stopping. The different binding orientations and distances may reflect a different catalytic mechanism with PIm as compared to *p*NPP. Insight of the possible mechanism cannot be gleaned from the results herein.

4.2.6 AP.

AP is a non-specific enzyme. It is able to hydrolyze a wide variety of substrates, including phosphopyridines,[76] *N*-phenyl phosphoramidates,[77,78] alkyl phosphoramidates,[78] phenyl phosphate esters,[81,149] alkyl phosphate esters,[81,149] phosphodiesters,[72] phosphorothioates,[80,150] sulfates,[69] and phosphonates.[151]

Diffusion controlled enzymatic reactions have a theoretical upper limit of ~10^9 $M^{-1}s^{-1}$.[152] As a comparison, AP catalyzed reactions have rate constants up to 10^7 with phosphomonoester substrates. Thus, not only does AP catalyze hydrolysis of many different substrates, its motif is able to generate rate increases that approach diffusion control.

At pH 8.0 release of P_i is rate limiting for phosphomonoester substrates as shown by NMR, crystallography, mutagenesis, and β_{LG} studies.[82,153] AP displays burst kinetics, which is also consistent with P_i release being rate limiting.[154]

A similar k_{cat} between the three substrates would be consistent with the same rate limiting step. PIm and *p*NPP have k_{cat} values of the same order of magnitude, consistent with the rate limiting step for the two substrates being the same. Yet, *N*-phPAM has a lower k_{cat} than PIm or *p*NPP. AP catalyzed hydrolysis of *N*-phPAM having a lower k_{cat} than *p*NPP is consistent with literature.[77]

It has been proposed that AP-catalyzed hydrolysis may be limited by substrate binding or some other conformational change.[155] It may be that *N*-phPAM has different binding than the other substrates or otherwise changes the rate limiting step. The latter suggestion has literature precedent that will now be reviewed.

AP catalyzed hydrolysis of phosphorylated pyridines has little dependence upon the leaving group "because the chemical step is not rate limiting for these substrates."[73,76] The rate limiting step for phosphorylated pyridines has been attributed to limitations on substrate binding or conformational changes to the enzyme.[76] If *N*-phPAM had different binding characteristics or required conformational changes to the enzyme, as with the phosphorylated pyridines, it would be expected that k_{cat} values of AP with *N*-phPAM would be lower than with *p*NPP. The $k_{\mathrm{apparent}}^{p\mathrm{NPP}}$ is 7.8 times the $k_{\mathrm{apparent}}^{\mathrm{1\text{-}picoline}}$.[76] The results herein found $k_{cat}^{p\mathrm{NPP}}$ to be 21 times the $k_{cat}^{N\text{-}\mathrm{phPAM}}$ (Table 4-12).

Computer models show *p*NPP and PIm bound in the active site in the same orientation (Figures 3-27, 3-28, 3-30, and 3-31). Both models showed Ser102 with its hydroxyl group facing away from the substrate's phosphorus atom (Figures 3-25 and 3-

Table 4-12. Kinetic results for AP.

pH 8.0			
	$k_{cat}(s^{-1})$	K_M (mM)	$k_{cat}/K_M \times 10^{-3}(M^{-1}s^{-1})$
*p*NPP	27.3 ±0.8	0.0070 ±0.0008	3900
N-phPAM	1.30 ±0.09	0.0021 ±0.0002	620
PIm	18 ±2	0.0020 ±0.0003	9000

26). For this reason, the methylene carbon of Ser102 is the basis for measurement of the distance to the phosphorus atom (Table 4-13).

Table 4-13. Comparison of distances between *E. coli* AP crystal structure with phosphate and computer models with *p*NPP and PIm.

	Crystal Structure With P_i (Å)	Computer Model With *p*NPP (Å)	Computer Model With PIm (Å)
$Zn_1^{2+} – Zn_2^{2+}$	3.98	3.99	3.88
Zn_1^{2+} – phosphate oxyanion	1.86	1.93	1.92
Zn_2^{2+} – phosphate oxyanion	2.82	3.02	3.35
$Zn_1^{2+} – Mg^{2+}$	6.99	7.02	6.76
$Zn_1^{2+} – Mg^{2+}$	4.79	4.80	4.80
Arg166 residue – phosphate oxyanion	2.70/2.94	2.55/3.00	2.59/2.86
Ser102 – phosphorus	3.50	3.58	3.47

There is no apparent trend in key distances of the enzyme-substrate complexes; some are closer for PIm than *p*NPP and vice versa. Distance of the nucleophile, Ser102, is similar between P_i, *p*NPP, and PIm. None of the distances between the bound substrates deviated by more than 5%. The same mechanism of hydrolysis with *p*NPP and PIm is consistent with similar k_{cat} values, similar enzyme-substrate distances in computer models, and only P-N cleavage in NMR experiments.

CHAPTER 5

CONCLUSIONS

5.1 Summary of Phosphoramidase vs. Phosphatase Activities

The two phosphoramidates used in this study were analogs of phosphorylated nitrogenous amino acids. *N*-phPAM possesses a sp^3 hybridized bridging nitrogen as does phospholysine. PIm possess a sp^2 hybridized bridging nitrogen akin to phosphohistidine. All of the motifs assayed in this study are capable of catalyzing hydrolysis of phosphoramidates with sp^2 bridging nitrogens. With the exception of the protein phosphatase motif, the motifs can also catalyze phosphoramidates with sp^3 bridging nitrogens.

PHPT1 has been shown to selectively catalyze phosphohistidine proteins. The results herein show the enzyme is also selective for phosphoimidazole, the phosphohistidine analog. That the enzyme catalyzed PIm 14000 times faster than *p*NPP in acidic and alkaline media shows that selectivity is based upon the P-X bond. That the enzyme catalyzed PIm faster than *N*-phPAM shows hybridization of the nitrogen is important.

Depending upon the PTP, phosphoramidase activity may be the same as phosphatase activity, as with VHR, or it may be less, as with YopH. The hybridization of the bridging atom can affect kinetic values, as demonstrated by YopH catalysis of *N*-phPAM and PIm. Despite the enzymes showing different activities with the substrates, PTPs are able to catalyze hydrolysis of all three substrates in this study with high activity.

While possessing very different motifs and having antipodal pH optima, PAcP and AP are both non-specific phosphatases. Both enzymes were able to catalyze the phosphoramidates with similar activity as the phosphomonoester. Thus, kinetic values showed neither enzyme possessed clear specificity for any of the substrates.

Interpretation of the results from the serine/threonine phosphatases is difficult. Clearly the motif can catalyze hydrolysis of PIm. But, the behavior of the two enzymes with PIm was opposite: λPP catalyzed PIm while PP1 didn't. While λPP catalyzed PIm, it went to 25% and inexplicably stopped. To complicate experiments, small molecules such as phosphorylated serine and threonine are not substrates. Phosphoramidase activity was demonstrated in this study. Considering the inability of the enzymes to catalyze phosphoserine or phosphothreonine as well as the behavior of the enzymes with the phosphoramidate substrates in this study, specificity of the enzymes cannot be determined with small molecule substrates.

5.2 Computer Modeling

The kinetic experiments address the question of whether or not phosphoramidase activity exists in the known phosphatases. The positive results do not specify *per se* whether or not catalysis proceeds with the same mechanism for phosphoramidates or phosphomonoesters, although similar k_{cat} values are consistent with the same rate limiting step. NMR results showing cleavage of the P-N bond are also consistent with the same mechanism. Isotope and LFER experiments would strengthen the proposition that catalysis occurs with the same mechanism. Such experiments are costly in funds and time. In this study, computer models were used to address the matter.

The transition state in enzymatic catalysis occurs in the time span of one vibration. As such, a transition species is too short-lived to be detected. Crystal structures cannot be obtained with an enzyme's substrate as hydrolysis will occur before crystallization. However, a computer can model a substrate in the active site of an enzyme. Such a model provides an examination of the enzyme-substrate complex before the transition state or catalysis.

Enzyme-substrates complexes with the same orientation of different substrates and the same enzyme are consistent with the catalytic mechanism being the same. However, there must be a justification for orienting the substrates. Inhibitors crystallized with enzymes assume a specific orientation that can be a starting point for orienting a substrate in a computer model.

There are two important considerations when placing a substrate into an active site using an inhibitor as a starting point. One, the inhibitor lacks a leaving group, and interactions between a substrate's leaving group and residues are not seen in the crystal structure. Two, the enzyme-inhibitor structure represents a product, or product analog, bound with the enzyme in a specific conformation. This conformation may or may not be a close transition-state analog.

Since the transition state occurs in the time span of one vibration, the enzyme must assume its transition state conformation before catalysis. A model of this conformation is desired. But, the starting point for the model is a crystal structure, and a crystal structure represents a low-energy conformation of an enzyme. However, transition state conformations represent higher-energy global enzyme conformations. Attempts to artificially move residues in the low energy crystal structure to model an enzyme-substrate complex at the high energy transition state would necessarily entail significant assumptions.

A computer model with limited assumptions may be had realizing that the model does not necessarily represent the transition state conformation. If a substrate is placed into the active site in the same orientation as an inhibitor, a computer may modify distances between residues and the substrate to lower the overall energy of the enzyme-substrate complex. While a model so obtained would not necessarily represent the transition state complex, it would show the bound orientation of a substrate before catalysis. By mere orientation and proximity of the catalytic residues and the substrate, the role of the residues could be inferred. This is what was done during this study.

The computer experiments completed in this study examine structure-activity relationships. Significant geometric differences exist between the substrates, which may alter the structure of the enzyme-substrate complex. With PHPT1, VHR, and λPP the leaving group is surrounded predominantly by solvent when the substrate is bound. Little difference is expected in binding distances or orientation between *p*NPP and PIm. This was true for PHPT1 and VHR. λPP's kinetic results indicated phenomena were causing the enzymes to catalyze the substrates with significantly different values. The computer modeling was consistent with the kinetic results in that binding of *p*NPP and PIm were different.

Substrates bound to YopH, PAcP, and AP have leaving groups in greater contact with the enzyme's amino acids. Differences in binding distances and orientation are possible, but not mandated, between *p*NPP and PIm because of the leaving group-amino acid interactions. With the WPD loop closed, there is a difference between distances with YopH. PAcP had little differences, neither did AP. This is an indication that the different leaving groups are not *a priori* indicators that kinetic rates or binding orientation are different.

While it is an equilibrium constant, the Michaelis constant is also a ratio of rates. K_M is not a reflection of binding strength, and there is no associating between binding orientation or binding distances with K_M. The computer modeled structures cannot be directly associated with K_M.

The rate limiting step of catalysis is given by k_{cat}. Structure-activity relationships do not indicate what step of catalysis is rate limiting, and computer modeled structures cannot be directly associated with k_{cat}.

With no direct link to k_{cat} or K_M, the computer models may seem of limited value. However, there is no other technique to examine an enzyme-substrate complex before catalysis. The strength of the method is that it provides a structure comparison between enzyme-substrate complexes with different substrates. It is one more piece of evidence to support a hypothesis that catalysis does, or does not, proceed by the same mechanism.

5.3 Major Conclusions

While phosphoramidases in addition to PHPT1 may be discovered, the existing phosphomonoesterase motifs are capable of hydrolyzing phosphoramidates. The most important result of this study is that there is no prerequisite for the future discovery of additional phosphoramidases.

The results of this study are readily placed into a larger physiological perspective. Proteins are often phosphorylated at multiple sites. With the exception of PHPT1's motif, none of the enzymes studied possess a motif that can selectively dephosphorylate a protein (Figure 5-1). If an enzyme is to selectively dephosphorylate a protein, selection must be accomplished by some property of the phosphatase other than its motif.

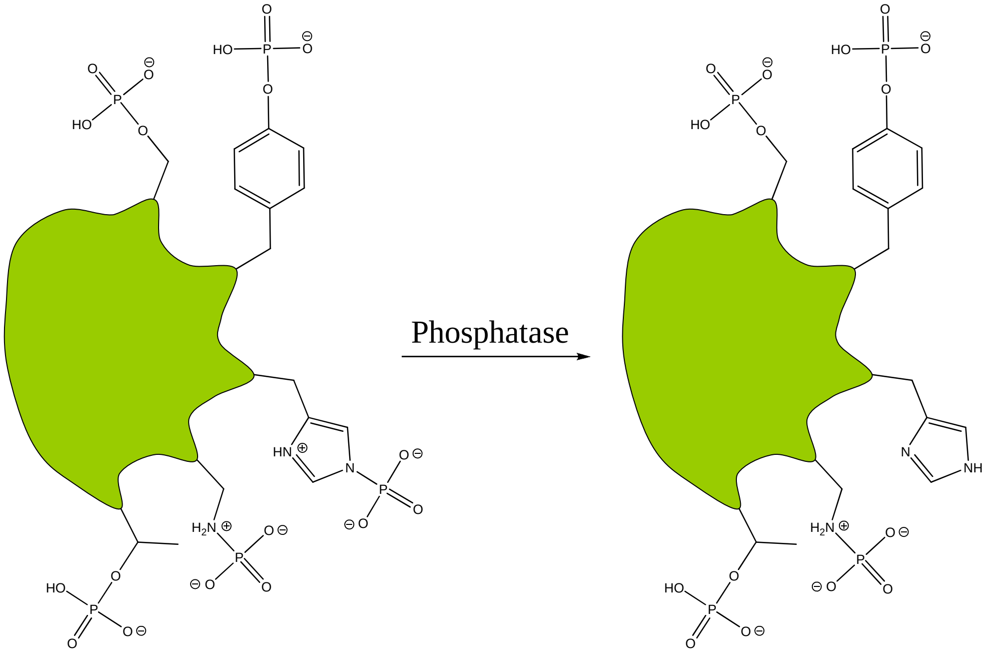

Figure 5-1. Selective dephosphorylation of a protein cannot be accomplished by an enzyme's motif. The exception being PHPT1, that can dephosphorylate phosphohistidine. A generalized protein with multiple phosphorylation sites is shown in green.

PHPT1 has an ability to selectively dephosphorylate phosphohistidine (Figure 5-1). While the rate constant for catalysis of PIm does not appear to be high, the selectivity for PIm over *p*NPP is high. This may be due to the general base catalysis employed by the enzyme. The leaving group of phosphoesters is not especially labile, but can be made so by protonation by a general acid. In comparison, phosphohistidine's leaving group is labile. The differences in leaving groups likely account for substrate susceptibility to general base catalysis.

Proteins may be phosphorylated on lysine or arginine. While such residues would possess labile P-N bonds, the results herein indicate the bonds could be catalytically cleaved by motifs studied. Not only is there no prerequisite for phosphoramidases able to cleave phosphohistidine, there is no prerequisite for phosphoramidases to cleave phospholysine or phosphoarginine.

5.4 Future Study in the Field of Phosphoramidates and Phosphoramidases

In this study, PIm and *N*-phPAM were used as substrates. *In vivo* phosphorylation of lysine and arginine are known. Analogs of such substrates could be made, but the techniques to conduct kinetic assays with such substrates are nascent at best.

The unique nature of phosphoramidates provides an interesting probe for enzymatic action. Charged and uncharged sp^3 nitrogens, as well as charged and uncharged sp^2 nitrogens provide different phosphoramidate substrates. The behavior of enzymes with these substrates *in vitro* can provide insight as to how the enzymes may work *in vivo*.

Presently the field seems to have attracted far less attention than studies with phosphoesters, likely a reflection of the difficulties associated with the substrates. Without more research in this area, an incomplete knowledge of biochemical pathways will remain. This study is a start in understanding the catalyzed hydrolysis of phosphoramidates.

REFERENCES

(1) Huang, J.; Wei, Y.; Kim, Y.; Osterberg, L.; Matthews, H. R. *J. Biol. Chem.* **1991**, *266*, 9023-9031.

(2) Attwood, P. V.; Ludwig, K.; Bergander, K.; Besant, P. G.; Adina-Zada, A.; Krieglstein, J.; Klumpp, S. *Biochim. Biophys. Acta* **2010**, *1804*, 199-205.

(3) Huang, J.; Nasr, M.; Kim, Y.; Matthews, H. R. *J. Biol. Chem.* **1992**, *267*, 15511-15515.

(4) Fujitaki, J. M.; Fung, G.; Oh, E. Y.; Smith, R. A. *Biochemistry* **1981**, *20*, 3658-3664.

(5) Chen, C. C.; Smith, D. L.; Bruegger, B. B.; Halpern, R. M.; Smith, R. A. *Biochemistry* **1974**, *13*, 3785-3787.

(6) Boyer, P. D.; Deluca, M.; Ebner, K. E.; Hultquist, D. E.; Peter, J. B. *J. Biol. Chem.* **1962**, *237*, PC3306-PC3308.

(7) Chen, C. C.; Bruegger, B. B.; Kern, C. W.; Lin, Y. C.; Halpern, R. M.; Smith, R. A. *Biochemistry* **1977**, *16*, 4852-4855.

(8) Steiner, A. W.; Helander, E. R.; Fujitaki, J. M.; Smith, L. S.; Smith, R. A. *J. Chromatogr.* **1980**, *202*, 263-269.

(9) Zetterqvist, O.; Engstrom, L. *Biochim. Biophys. Acta* **1967**, *141*, 523-532.

(10) Wakim, B. T.; Aswad, G. D. *J. Biol. Chem.* **1994**, *269*, 2722-2727.

(11) Nishino, M.; Tsujimura, S.; Kuba, M.; Kumon, A. *Arch. Biochem. Biophys.* **1994**, *312*, 101-106.

(12) Kumon, A.; Kodama, H.; Kondo, M.; Yokoi, F. *J. Biochem* **1996**, *119*, 719-724.

(13) Moller, K. M. *Biochim. Biophys. Acta* **1955**, *16*, 162-165.

(14) Singer, M. F.; Fruton, J. S. *J. Biol. Chem.* **1957**, *229*, 111-119.

(15) Niall, H. D. *Methods Enzymol.* **1973**, *27*, 942-1010.

(16) Blake, C. C. F.; Koenig, D. F.; Mair, G. A.; North, A. C. T.; Phillips, D. C.; Sarma, V. R. *Nature* **1965**, *4986*, 757-761.

(17) Ohmori, H.; Kuba, M.; Kumon, A. *J. Biol. Chem.* **1993**, *268*, 7625-7627.

(18) Khersonsky, O.; Tawfik, D. S. *Annu. Rev. Biochem.* **2010**, *79*, 471-505.

(19) Ek, P.; Pettersson, G.; B., E.; Gong, F.; Li, J.-P.; Zetterqvist, O. *Eur. J. Biochem.* **2002**, *269*, 5016-5023.

(20) Gong, W.; Li, Y.; Cui, G.; Hu, J.; Fang, H.; Jin, C.; Xia, B. *Biochem. J.* **2009**, *418*, 337-344.

(21) Ma, R.; Kanders, E.; Sundh, U. B.; Geng, M.; Ek, P.; Zetterqvist, O.; Li, J.-P. *Biochem. Biophys. Res. Commun.* **2005**, *337*, 887-891.

(22) Zhang, Z.-Y.; Wang, Y.; Dixon, J. E. *Proc. Natl. Acad. Sci. U.S.A.* **1994**, *91*, 1624-1627.

(23) Hoff, R. H.; Hengge, A. C.; Wu, L.; Keng, Y.-F.; Zhang, Z.-Y. *Biochemistry* **2000**, *39*, 46-54.

(24) Stuckey, J. A.; Schubert, H. L.; Fauman, E. B.; Zhang, Z.-Y.; Dixon, J. E.; Saper, M. A. *Nature* **1994**, *370*, 571-575.

(25) Hu, P.; Elliott, J.; McCready, P.; Skowronski, E.; Garnes, J.; Kobayashi, A.; Brubaker, R. R.; Garcia, E. *J. Bacteriol.* **1998**, *180*, 5192-5202.

(26) Zhang, Z.-Y.; Malachowski, W. P.; Van Etten, R. L.; Dixon, J. E. *J. Biol. Chem.* **1994**, *269*, 8140-8145.

(27) Zhang, Z.-Y.; Palfey, B. A.; Wu, L. Z., Y. *Biochemistry* **1995**, *34*, 16389-16396.

(28) Hengge, A. C.; Sowa, G. A.; Wu, L.; Zhang, Z.-Y. *Biochemistry* **1995**, *34*, 13982-13987.

(29) Khajehpour, M.; Wu, L.; Liu, S.; Zhadin, N.; Zhang, Z.-Y.; Callender, R. *Biochemistry* **2007**, *46*, 4370-4378.

(30) McCain, D. F.; Grzyska, P. K.; Wu, L.; Hengge, A. C.; Zhang, Z.-Y. *Biochemistry* **2004**, *43*, 8256-8264.

(31) Zhao, Y.; Wu, L.; Noh, S. J.; Guan, K.-L.; Zhang, Z.-Y. *J. Biol. Chem.* **1998**, *273*, 5484-5492.

(32) Hu, X.; Stebbins, C. E. *Biophys. J.* **2006**, *91*, 948-956.

(33) Guan, K.; Dixon, J. E. *J. Biol. Chem.* **1991**, *266*, 17026-17030.

(34) Sun, J.-P.; Wu, L.; Fedorov, A. A.; Almo, S. C.; Zhang, Z.-Y. *J. Biol. Chem.* **2003**, *278*, 33392-33399.

(35) Zhang, Z.-Y.; Clemens, J. C.; Schubert, H. L.; Stuckey, J. A.; Fischer, M. W. F.; Hume, D. M.; Saper, M. A.; Dixon, J. E. *J. Biol. Chem.* **1992**, *267*, 23759-23766.

(36) Zhang, Z.-Y.; Dixon, J. E. *Biochemistry* **1993**, *32*, 9340-9345.

(37) Hengge, A. C. *Adv. Phys. Org. Chem.* **2005**, *40*, 49-108.

(38) Hengge, A. C.; Denu, J. M.; Dixon, J. E. *Biochemistry* **1996**, *35*, 7084-7092.

(39) Rigas, J. D.; Hoff, R. H.; Rice, A. E.; Hengge, A. C.; Denu, J. M. *Biochemistry* **2001**, *40*, 4398-4406.

(40) Zhao, Y.; Wu, L.; Zhang, Z.-Y. *Biochemistry* **1997**, *36*, 7928-7936.

(41) Zhao, Y.; Zhang, Z.-Y. *Biochemistry* **1996**, *35*, 11797-11804.

(42) Zhang, Z.-Y.; Wu, L.; Chen, L. *Biochemistry* **1995**, *34*, 16088-16096.

(43) Chen, L.; Montserat, J.; Lawrence, D. S.; Zhang, Z.-Y. *Biochemistry* **1996**, *35*, 9349-9354.

(44) Denu, J. M.; Dixon, J. E. *Proc. Natl. Acad. Sci. U.S.A.* **1995**, *92*, 5910-5914.

(45) Zhou, G.; Denu, J. M.; Wu, L.; Dixon, J. E. *J. Biol. Chem.* **1994**, *269*, 28084-28090.

(46) Denu, J. M.; Zhou, G.; Yuping, G.; Dixon, J. E. *Biochemistry* **1995**, *34*, 3396-3404.

(47) Van Etten, R. L.; McTigue, J. J. *Biochim. Biophys. Acta* **1977**, *484*, 386-397.

(48) Ortlund, E.; LaCount, M. W.; Lebioda, L. *Biochemistry* **2003**, *42*, 383-389.

(49) Lindqvist, Y.; Schneider, G.; Vihko, P. *Eur. J. Biochem.* **1994**, *221*, 139-142.

(50) Ostanin, K.; Saeed, A.; Van Etten, R. L. *J. Biol. Chem.* **1994**, *269,* 8971-8978.

(51) Van Etten, R. L. *Ann. N.Y. Acad. Sci.* **1982**, *390*, 27-51.

(52) Lynn, K. R.; Clevette-Radford, N. A.; Chuaqui, C. A. *Bioorg. Chem.* **1981**, *10*, 90-96.

(53) Reiter, T. A.; Reiter, N. J.; Rusnak, F. *Biochemistry* **2002**, *41*, 15404-15409.

(54) Voegtli, W. C.; White, D. J.; Reiter, N. J.; Rusnak, F.; Rosenzweig, A. C. *Biochemistry* **2000**, *39*, 15365-15374.

(55) Barford, D.; Das, A. K.; Egloff, M.-P. *Annu. Rev. Biophys. Biomol. Struct.* **1998**, *27*, 133-164.

(56) Hoff, R. H.; Mertz, P.; Rusnak, F.; Hengge, A. C. *J. Am. Chem. Soc.* **1999**, *121*, 6382-6390.

(57) Mumby, M. C.; Walter, G. *Physiol. Rev.* **1993**, *73*, 673-699.

(58) Reiter, N. J.; White, D. J.; Rusnak, R. *Biochemistry* **2002**, *41*, 1051-1059.

(59) White, D. J.; Reiter, N. J.; Sikkink, R. A.; Yu, L.; Rusnak, F. *Biochemistry* **2001**, *40*, 8918-8929.

(60) Zhuo, S.; Clemens, J. C.; Hakes, D. J.; Barford, D.; Dixon, J. E. *J. Biol. Chem.* **1993**, *268*, 17754-17761.

(61) Ansai, T.; Dupuy, L. C.; Barik, S. *J. Biol. Chem.* **1996**, *271*, 24401-24407.

(62) Kim, Y.; Huang, J.; Cohen, P.; Matthews, H. R. *J. Biol. Chem.* **1993**, *268*, 18513-18518.

(63) McWhirter, C.; Lund, E. A.; Tanifum, E. A.; Feng, G.; Sheikh, Q. I.; Hengge, A. C.; Williams, N. H. *J. Am. Chem. Soc.* **2008**, *130*, 13673-13682.

(64) Xie, X.-J.; Huang, W.; Xue, C.-Z.; Wei, Q. *Mol. Cell. Biochem.* **2009**, *327*, 241-246.

(65) Zhang, L.; Lee, E. Y. C. *Biochemistry* **1997**, *36*, 8209-8214.

(66) Keppetipola, N.; Shuman, S. *Nucleic Acids Res.* **2007**, *35*, 7721-7732.

(67) Rusnak, R.; Yu, L.; Todorovic, S.; Mertz, P. *Biochemistry* **1999**, *38*, 6943-6952.

(68) Mahapatra, P. P.; Dash, A. K.; Chickerur, N. S. *Thermochim. Acta* **1983**, *70*, 163-171.

(69) Catrina, I.; O'Brien, P. J.; Purcell, J.; Nikolic-Hughes, I.; Zalatan, J. G.; Hengge, A. C.; Herschlag, D. *J. Am. Chem. Soc.* **2007**, *129*, 5760-5765.

(70) Wang, J.; Kantrowitz, E. R. *Protein Sci.* **2006**, *15*, 2395-2401.

(71) Nikolic-Hughes, I.; O'Brien, P. J.; Herschlag, D. *J. Am. Chem. Soc.* **2005**, *127*, 9314-9315.

(72) O'Brien, P. J.; Herschlag, D. *Biochemistry* **2001**, *40*, 5691-5699.

(73) O'Brien, P. J.; Herschlag, D. *Biochemistry* **2002**, *41*, 3207-3225.

(74) Stec, B.; Holtz, K. M.; Kantrowitz, E. R. *J. Mol. Biol.* **2000**, *299*, 1303-1311.

(75) Wang, J.; Stieglitz, K. A.; Kantrowitz, E. R. *Biochemistry* **2005**, *44*, 8378-8386.

(76) Labow, B. I.; Herschlag, D.; Jencks, W. P. *Biochemistry* **1993**, *32*, 8737-8741.

(77) Snyder, S. L.; Wilson, I. B. *Biochemistry* **1972**, *11*, 3220-3223.

(78) Snyder, S. L.; Wilson, I. B. *Biochemistry* **1972**, *11*, 1616-1623.

(79) Stec, B.; Hehir, M. J.; Brennan, C.; Nolte, M.; Kantrowitz, E. R. *J. Mol. Biol.* **1998**, *277*, 647-662.

(80) Coleman, J. E. *Annu. Rev. Biophys. Biomol. Struct.* **1992**, *21*, 441-483.

(81) Han, R.; Coleman, J. E. *Biochemistry* **1995**, *34*, 4238-4245.

(82) Holtz, K. M.; Kantrowitz, E. R. *FEBS Lett.* **1999**, *462*, 7-11.

(83) Cox, J. R. J.; Ramsay, O. B. *Chem. Rev.* **1964**, *64*, 317-352.

(84) Barnard, P. W. C.; Bunton, C. A.; Kellerman, D.; Mhala, M. M.; Silver, B.; Vernon, C. A.; Welch, V. A. *J. Chem. Soc.* **1966**, *B*, 227-235.

(85) Bunton, C. A. *Acc. Chem. Res.* **1970**, *3*, 257-265.

(86) Chanley, J. D.; Feageson, E. *J. Am. Chem. Soc.* **1958**, *80*, 2686-2691.

(87) Chanley, J. D.; Feageson, E. *J. Am. Chem. Soc.* **1963**, *85*, 1181-1190.

(88) Desjobert, A. *Bull. Soc. Chim. Fr.* **1964**, 683-688.

(89) Kugel, L.; Halmann, M. *J. Org. Chem.* **1966**, *32*, 642-647.

(90) Kumamoto, J.; Westheimer, F. H. *J. Am. Chem. Soc.* **1955**, *77*, 2515-2518.

(91) Lloyd, G. J.; Cooperman, B. S. *J. Am. Chem. Soc.* **1971**, *93*, 4883-4889.

(92) Jencks, W. P.; Gilchrist, M. *J. Am. Chem. Soc.* **1965**, *87*, 3199-3209.

(93) Lide, D. R. *CRC Handbook of Chemistry and Physics*, 86th ed.; Taylor and Francis Group: Boca Raton, London, New York, Singapore, 2005.

(94) Bunton, C. A.; Llewellyn, D. R.; Oldham, K. G.; Vernon, C. A. *J. Chem. Soc.* **1958**, 3574-3594.

(95) Levine, D.; Wilson, I. B. *Inorg. Chem.* **1968**, *7*, 818-820.

(96) Grzyska, P. K.; Czyryca, P. G.; Golightly, J.; Small, K.; Larsen, P.; Hoff, R. H.; Hengge, A. C. *J. Org. Chem.* **2002**, *67*, 1214-1220.

(97) Kirby, A. J.; Jencks, W. P. *J. Am. Chem. Soc.* **1965**, *87*, 3209-3216.

(98) Kirby, A. J.; Varvoglis, A. G. *J. Am. Chem. Soc.* **1967**, *89*, 415-423.

(99) Herschlag, D.; Jencks, W. P. *J. Am. Chem. Soc.* **1987**, *109*, 4665-4674.

(100) Benkovic, S. J.; Sampson, E. J. *J. Am. Chem. Soc.* **1971**, *93*, 4009-4016.

(101) Kirby, A. J.; Varvoglis, A. G. *J. Chem. Soc.* **1968**, *B*, 135-141.

(102) Herschlag, D.; Jencks, W. P. *J. Am. Chem. Soc.* **1989**, *111*, 7587-7596.

(103) Buchwald, S. L.; Friedman, J. M.; Knowles, J. R. *J. Am. Chem. Soc.* **1984**, *106*, 4911-4916.

(104) Lad, C.; Williams, N. H.; Wolfenden, R. *Proc. Natl. Acad. Sci. U.S.A.* **2003**, *100*, 5607-5610.

(105) Herschlag, D.; Jencks, W. P. *J. Am. Chem. Soc.* **1989**, *111*, 7579-7586.

(106) Herschlag, D.; Jencks, W. P. *Biochemistry* **1990**, *29*, 5172-5179.

(107) Lloyd, G. J.; Hsu, C.-M.; Cooperman, B. S. *J. Am. Chem. Soc.* **1971**, *93*, 4889-4892.

(108) Page, M. I.; Badarau, A. *Bioinorg. Chem. Appl.* **2008**, *2008*, 1-14.

(109) Ibrahim, M. M.; Shimomura, N.; Ichikawa, K.; Shiro, M. *Inorg. Chim. Acta* **2001**, *313*, 125-136.

(110) Moody, E. M.; Brown, T. S.; Bevilacqua, P. C. *J. Am. Chem. Soc.* **2004**, *126*, 10200-10201.

(111) Chaidaroglou, A.; Brezinski, D. J.; Middleton, S. A.; Kantrowitz, E. R. *Biochemistry* **1988**, *27*, 8338-8343.

(112) VanEtten, R. L.; Waymack, P. P.; Rehkop, D. M. *J. Am. Chem. Soc.* **1974**, *96*, 6782-6785.

(113) Ostanin, K.; Van Etten, R. L. *J. Biol. Chem.* **1993**, *268*, 20778-20784.

(114) Bessey, O. A.; Love, R. H. *J. Biol. Chem.* **1952**, *196*, 175-178.

(115) Aschaffenburg, R. *Science* **1953**, *117*, 611.

(116) Saady, M.; Lebeau, L.; Mioskowski, C. *Helv. Chim. Acta* **1995**, *78*, 670-678.

(117) Burlingham, B. T.; Widlanski, T. S. *J. Org. Chem.* **2001**, *66*, 7561-7567.

(118) Rosenberg, T. *Arch. Biochem. Biophys.* **1964**, *105*, 315-318.

(119) van Dijk, A. A.; De Lange, L. C. M.; Bachovchin, W. W.; Robillard, G. T. *Biochemistry* **1990**, *29*, 8164-8171.

(120) Busam, R. D.; Thorsell, A.-G. T.; Flores, A.; Hammarstrom, M.; Persson, C.; Hallberg, B. M. *J. Biol. Chem.* **2006**, *281*, 33830-33834.

(121) Sadeghi, H. M. M.; Rabbani, M.; Fazeli, S. *Res. Pharmaceut. Sci.* **2008**, *3*, 35-39.

(122) Zhang, Z.-Y.; VanEtten, R. L. *J. Biol. Chem.* **1991**, *266*, 1516-1525.

(123) Kezdy, F.; Bender, M. L. *Biochemistry* **1962**, *1*, 1097-1106.

(124) Hess, H. H.; Derr, J. E. *Anal. Biochem.* **1975**, *63*, 607-613.

(125) Lowry, O. H.; Lopez, J. A. *J. Biol. Chem.* **1946**, *162*, 421-428.

(126) Sjosten, A.; Blomqvist, S. *Water Res.* **1997**, *31*, 1818-1823.

(127) Taussky, H. H.; Shorr, E. *J. Biol. Chem.* **1953**, *202*, 675-685.

(128) Wu, H. *J. Biol. Chem.* **1920**, *43*, 189-220.

(129) Lanzetta, P. A.; Alvarez, L. J.; Reinach, P. S.; Candia, O. A. *Anal. Biochem.* **1979**, *100*, 95-97.

(130) Kallner, A. *Clin. Chim. Acta* **1975**, *59*, 35-39.

(131) Parvin, R.; Smith, R. A. *Anal. Biochem.* **1969**, *27*, 65-72.

(132) Saheki, S.; Takeda, A.; Shimazu, T. *Anal. Biochem.* **1985**, *148*, 277-281.

(133) Duggleby, R. G. *Methods* **2001**, *24*, 168-174.

(134) Duggleby, R. G.; Clarke, R. B. *Biochim. Biophys. Acta* **1991**, *1080*, 231-236.

(135) Mayo, S. L.; Olafson, B. D.; Goddard, I., W. A. *J. Phys. Chem.* **1990**, *94*, 8897-8909.

(136) Eliel, E. L.; Wilen, S. H. *Stereochemistry of Organic Compounds*; John Wiley & Sons: New York, 1994.

(137) Tollenaere, J. P.; Janssen, P. A. J. *Med. Res. Rev.* **1988**, *8*, 1-25.

(138) Mertz, P.; Yu, L.; Sikkink, R.; Rusnak, F. *J. Biol. Chem.* **1997**, *272*, 21296-21302.

(139) Copeland, R. A. *Enzymes, A Practical Introduction to Structure, Mechanism, and Data Analysis*; John Wiley & Sons: New York, 2000.

(140) Wojciechowski, C. L.; Kantrowitz, E. R. *J. Biol. Chem.* **2002**, *277*, 50476-50481.

(141) Boulanger, R. R.; Kantrowitz, E. R. *J. Biol. Chem.* **2003**, *278*, 23497-23501.

(142) Hehir, M. J.; Murphy, J. E.; Kantrowitz, E. R. *J. Mol. Biol.* **2000**, *304*, 645-656.

(143) Lin, M.-F.; Clinton, G. M. *Biochem. J.* **1986**, *235*, 351-357.

(144) Luchter-Wasylewska, E. *Biochim. Biophys. Acta* **2001**, *1548*, 257-264.

(145) Kilsheimer, G. S.; Axelrod, B. *J. Biol. Chem.* **1957**, *227*, 879-890.

(146) Nigam, V. N.; Davidson, H. M.; Fishman, W. H. *J. Biol. Chem.* **1959**, *234*, 1550-1554.

(147) Oh, B.-C.; Choi, W.-C.; Park, S.; Kim, Y.-o.; Oh, T.-K. *Appl. Microbiol. Biotechnol.* **2004**, *63*, 362-372.

(148) Barik, S. *Proc. Natl. Acad. Sci. U.S.A.* **1993**, *90*, 10633-10637.

(149) Hall, A. D.; Williams, A. *Biochemistry* **1986**, *25*, 4784-4790.

(150) Hollfelder, F.; Herschlag, D. *Biochemistry* **1995**, *34*, 12255-12264.

(151) Kelly, S. J.; Dardinger, D. E.; Butler, L. G. *Biochemistry* **1975**, *14*, 4983-4988.

(152) Alberty, R. A.; Hammes, G. G. *J. Phys. Chem.* **1958**, *62*, 154-159.

(153) Runyu, H.; Coleman, J. E. *Biochemistry* **1995**, *34*, 4238-4245.

(154) Bloch, W.; Schlesinger, M. J. *J. Biol. Chem.* **1974**, *6*, 1760-1768.

(155) Hengge, A. C.; Edens, W. A.; Elsing, H. *J. Am. Chem. Soc.* **1994**, *116*, 5045-5049.

APPENDIX

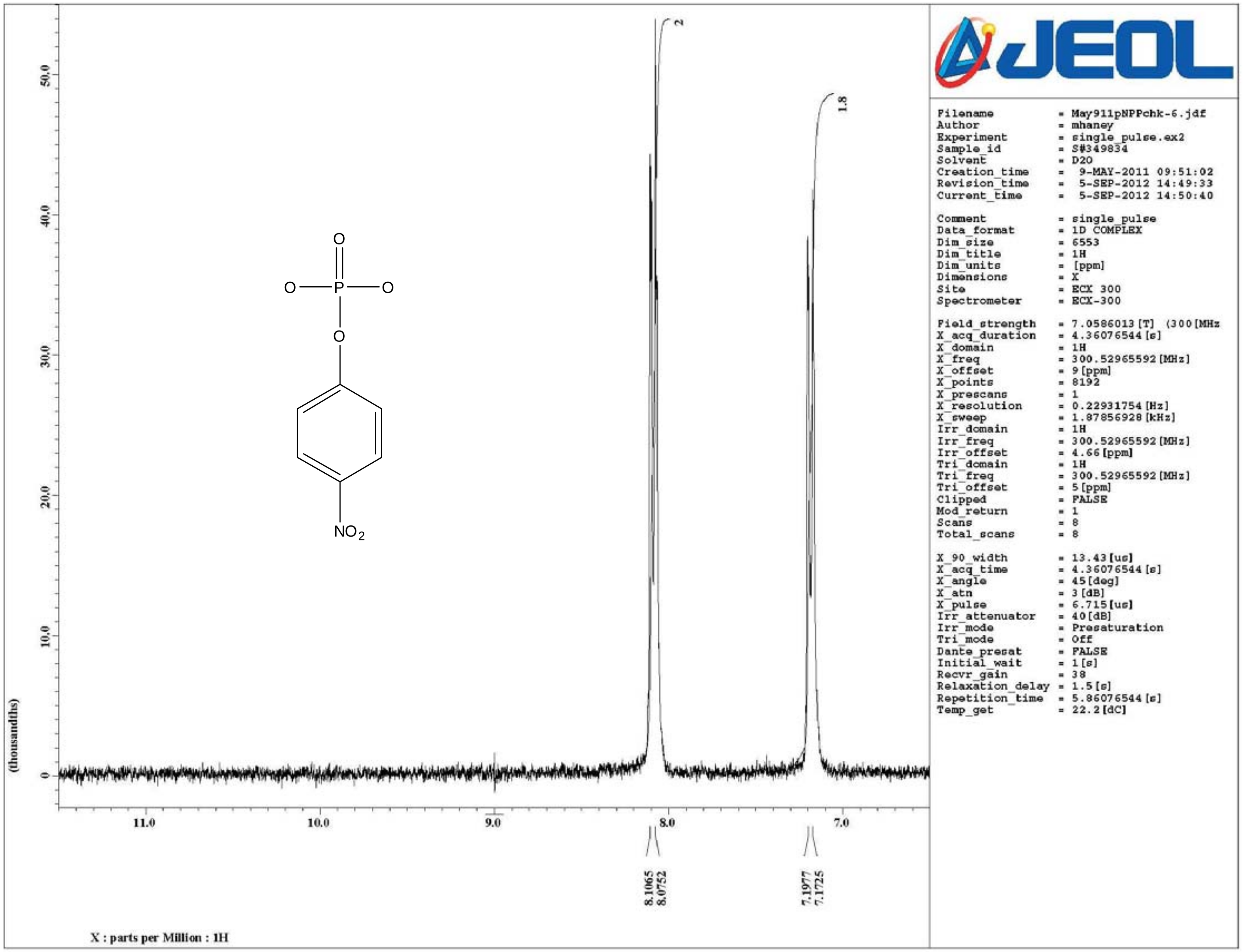

```
Filename            = May911pNPPchk-6.jdf
Author              = mhaney
Experiment          = single_pulse.ex2
Sample_id           = S#349834
Solvent             = D2O
Creation_time       =  9-MAY-2011 09:51:02
Revision_time       =  5-SEP-2012 14:49:33
Current_time        =  5-SEP-2012 14:50:40

Comment             = single_pulse
Data_format         = 1D COMPLEX
Dim_size            = 6553
Dim_title           = 1H
Dim_units           = [ppm]
Dimensions          = X
Site                = ECX 300
Spectrometer        = ECX-300

Field_strength      = 7.0586013[T] (300[MHz
X_acq_duration      = 4.36076544[s]
X_domain            = 1H
X_freq              = 300.52965592[MHz]
X_offset            = 9[ppm]
X_points            = 8192
X_prescans          = 1
X_resolution        = 0.22931754[Hz]
X_sweep             = 1.87856928[kHz]
Irr_domain          = 1H
Irr_freq            = 300.52965592[MHz]
Irr_offset          = 4.66[ppm]
Tri_domain          = 1H
Tri_freq            = 300.52965592[MHz]
Tri_offset          = 5[ppm]
Clipped             = FALSE
Mod_return          = 1
Scans               = 8
Total_scans         = 8

X_90_width          = 13.43[us]
X_acq_time          = 4.36076544[s]
X_angle             = 45[deg]
X_atn               = 3[dB]
X_pulse             = 6.715[us]
Irr_attenuator      = 40[dB]
Irr_mode            = Presaturation
Tri_mode            = Off
Dante_presat        = FALSE
Initial_wait        = 1[s]
Recvr_gain          = 38
Relaxation_delay    = 1.5[s]
Repetition_time     = 5.86076544[s]
Temp_get            = 22.2[dC]
```

A1. Proton NMR spectrum of *p*NPP.

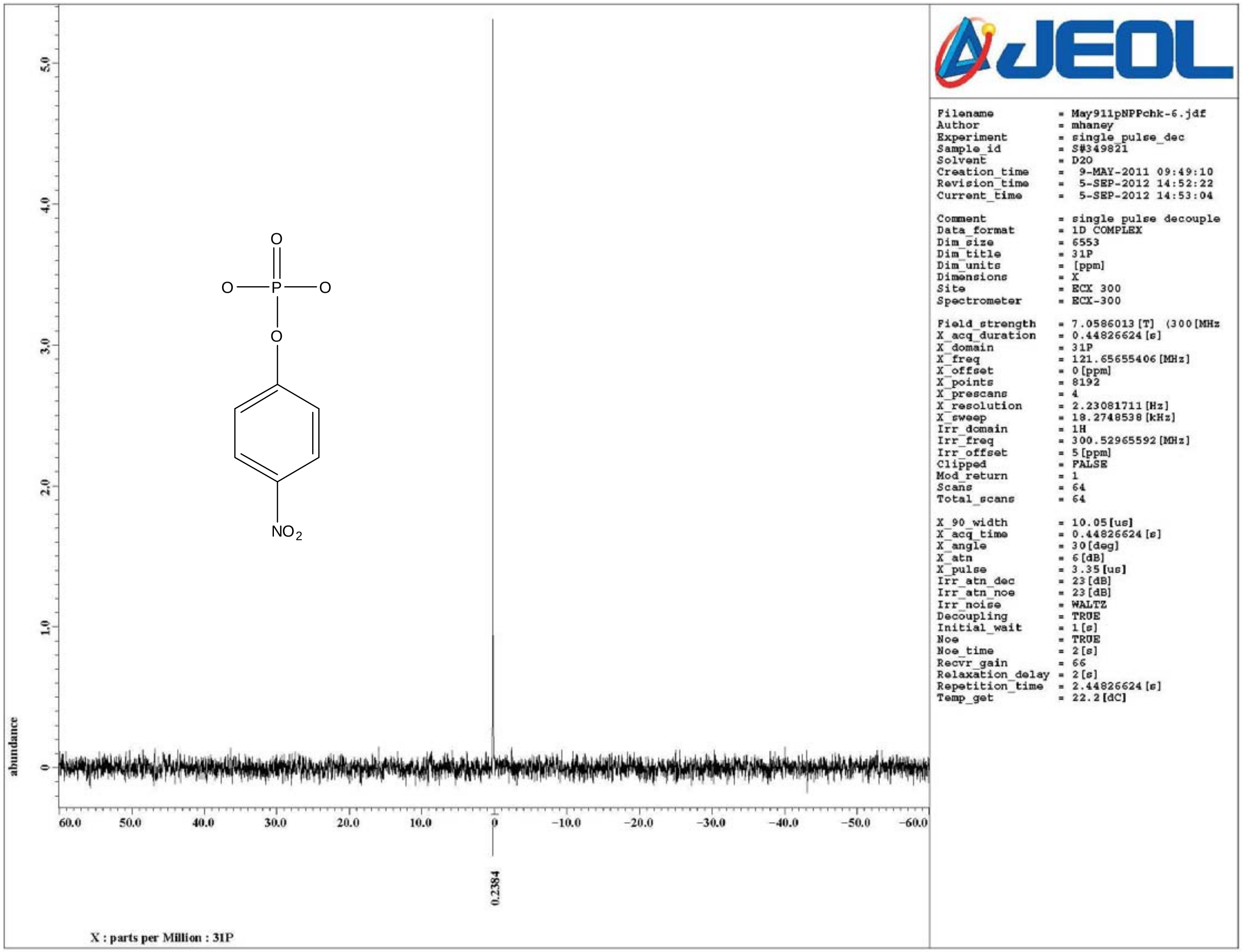

```
Filename            = May911pNPPchk-6.jdf
Author              = mhaney
Experiment          = single_pulse_dec
Sample_id           = S#349821
Solvent             = D2O
Creation_time       =  9-MAY-2011 09:49:10
Revision_time       =  5-SEP-2012 14:52:22
Current_time        =  5-SEP-2012 14:53:04

Comment             = single pulse decouple
Data_format         = 1D COMPLEX
Dim_size            = 6553
Dim_title           = 31P
Dim_units           = [ppm]
Dimensions          = X
Site                = ECX 300
Spectrometer        = ECX-300

Field_strength      = 7.0586013[T] (300[MHz
X_acq_duration      = 0.44826624[s]
X_domain            = 31P
X_freq              = 121.65655406[MHz]
X_offset            = 0[ppm]
X_points            = 8192
X_prescans          = 4
X_resolution        = 2.23081711[Hz]
X_sweep             = 18.2748538[kHz]
Irr_domain          = 1H
Irr_freq            = 300.52965592[MHz]
Irr_offset          = 5[ppm]
Clipped             = FALSE
Mod_return          = 1
Scans               = 64
Total_scans         = 64

X_90_width          = 10.05[us]
X_acq_time          = 0.44826624[s]
X_angle             = 30[deg]
X_atn               = 6[dB]
X_pulse             = 3.35[us]
Irr_atn_dec         = 23[dB]
Irr_atn_noe         = 23[dB]
Irr_noise           = WALTZ
Decoupling          = TRUE
Initial_wait        = 1[s]
Noe                 = TRUE
Noe_time            = 2[s]
Recvr_gain          = 66
Relaxation_delay    = 2[s]
Repetition_time     = 2.44826624[s]
Temp_get            = 22.2[dC]
```

A2. ^{31}P NMR spectrum of *p*NPP.

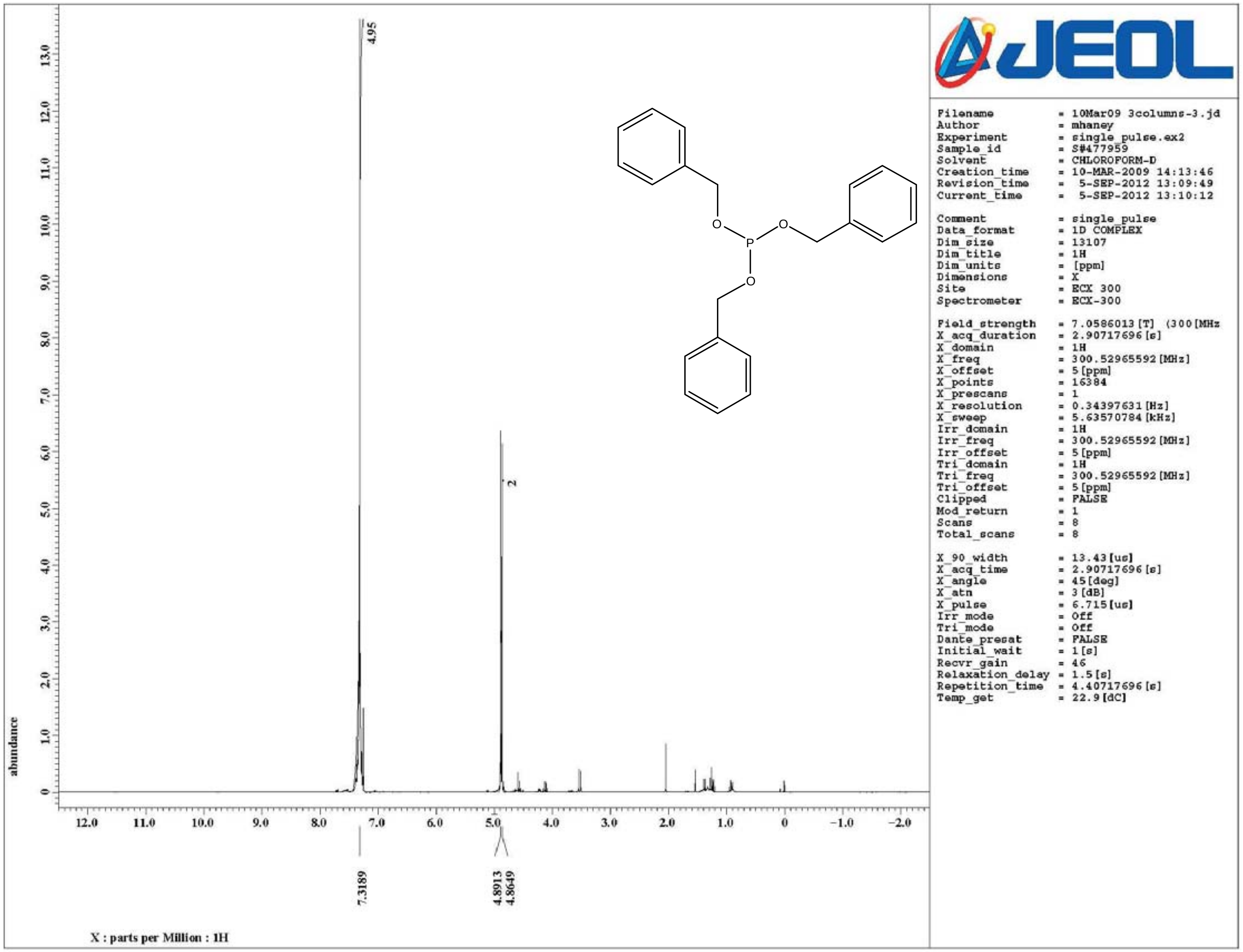

```
Filename          = 10Mar09 3columns-3.jd
Author            = mhaney
Experiment        = single_pulse.ex2
Sample_id         = S#477959
Solvent           = CHLOROFORM-D
Creation_time     = 10-MAR-2009 14:13:46
Revision_time     =  5-SEP-2012 13:09:49
Current_time      =  5-SEP-2012 13:10:12

Comment           = single_pulse
Data_format       = 1D COMPLEX
Dim_size          = 13107
Dim_title         = 1H
Dim_units         = [ppm]
Dimensions        = X
Site              = ECX 300
Spectrometer      = ECX-300

Field_strength    = 7.0586013[T] (300[MHz
X_acq_duration    = 2.90717696[s]
X_domain          = 1H
X_freq            = 300.52965592[MHz]
X_offset          = 5[ppm]
X_points          = 16384
X_prescans        = 1
X_resolution      = 0.34397631[Hz]
X_sweep           = 5.63570784[kHz]
Irr_domain        = 1H
Irr_freq          = 300.52965592[MHz]
Irr_offset        = 5[ppm]
Tri_domain        = 1H
Tri_freq          = 300.52965592[MHz]
Tri_offset        = 5[ppm]
Clipped           = FALSE
Mod_return        = 1
Scans             = 8
Total_scans       = 8

X_90_width        = 13.43[us]
X_acq_time        = 2.90717696[s]
X_angle           = 45[deg]
X_atn             = 3[dB]
X_pulse           = 6.715[us]
Irr_mode          = Off
Tri_mode          = Off
Dante_presat      = FALSE
Initial_wait      = 1[s]
Recvr_gain        = 46
Relaxation_delay  = 1.5[s]
Repetition_time   = 4.40717696[s]
Temp_get          = 22.9[dC]
```

A3. Proton NMR spectrum of tri-benzyl phosphite.

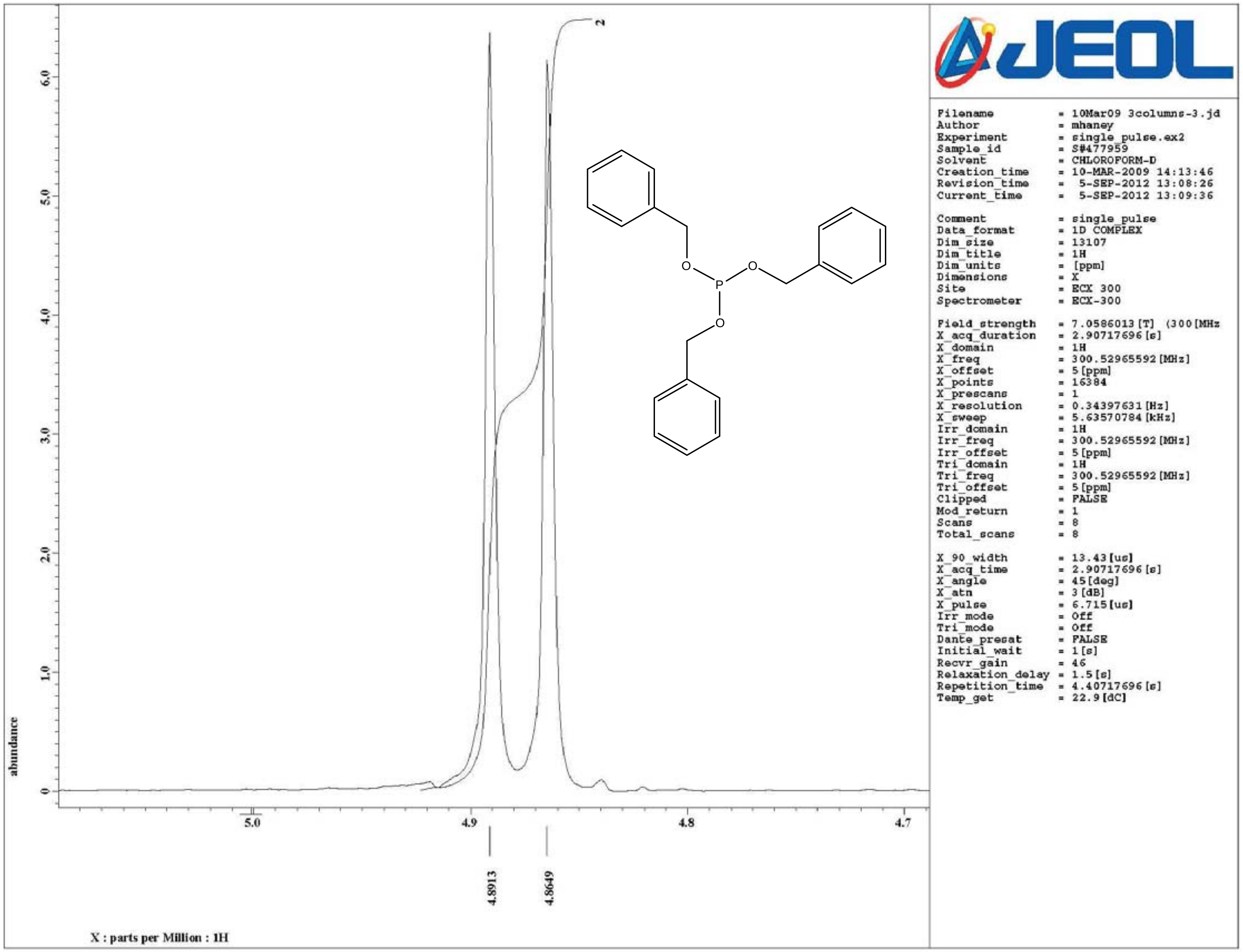

```
Filename            = 10Mar09 3columns-3.jd
Author              = mhaney
Experiment          = single_pulse.ex2
Sample_id           = S#477959
Solvent             = CHLOROFORM-D
Creation_time       = 10-MAR-2009 14:13:46
Revision_time       =  5-SEP-2012 13:08:26
Current_time        =  5-SEP-2012 13:09:36

Comment             = single_pulse
Data_format         = 1D COMPLEX
Dim_size            = 13107
Dim_title           = 1H
Dim_units           = [ppm]
Dimensions          = X
Site                = ECX 300
Spectrometer        = ECX-300

Field_strength      = 7.0586013[T] (300[MHz
X_acq_duration      = 2.90717696[s]
X_domain            = 1H
X_freq              = 300.52965592[MHz]
X_offset            = 5[ppm]
X_points            = 16384
X_prescans          = 1
X_resolution        = 0.34397631[Hz]
X_sweep             = 5.63570784[kHz]
Irr_domain          = 1H
Irr_freq            = 300.52965592[MHz]
Irr_offset          = 5[ppm]
Tri_domain          = 1H
Tri_freq            = 300.52965592[MHz]
Tri_offset          = 5[ppm]
Clipped             = FALSE
Mod_return          = 1
Scans               = 8
Total_scans         = 8

X_90_width          = 13.43[us]
X_acq_time          = 2.90717696[s]
X_angle             = 45[deg]
X_atn               = 3[dB]
X_pulse             = 6.715[us]
Irr_mode            = Off
Tri_mode            = Off
Dante_presat        = FALSE
Initial_wait        = 1[s]
Recvr_gain          = 46
Relaxation_delay    = 1.5[s]
Repetition_time     = 4.40717696[s]
Temp_get            = 22.9[dC]
```

A4. ^{31}P NMR spectrum of tri-benzyl phosphite.

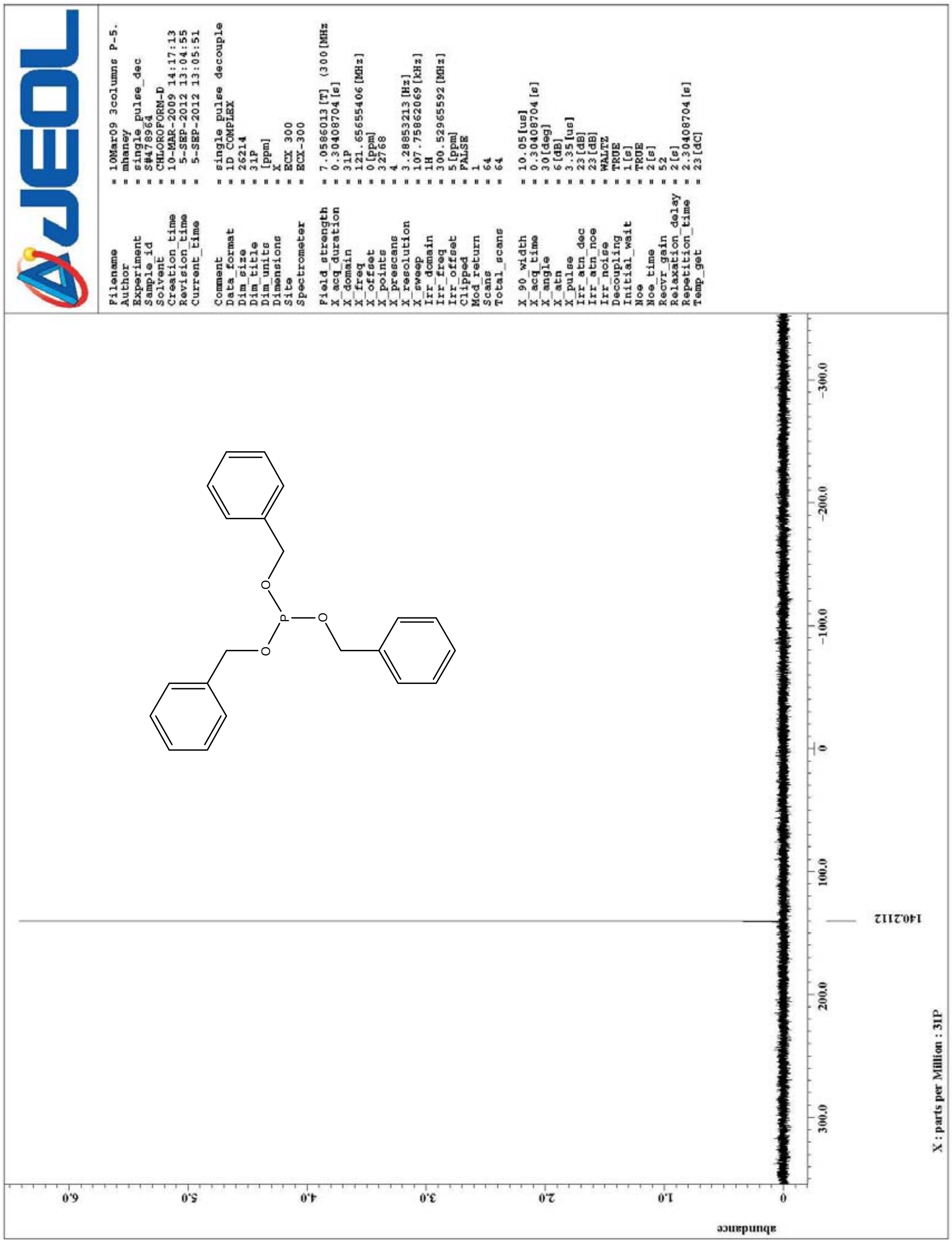

```
Filename            = 10Mar09 3columns P-5.
Author              = mhaney
Experiment          = single_pulse_dec
Sample_id           = S#478964
Solvent             = CHLOROFORM-D
Creation_time       = 10-MAR-2009 14:17:13
Revision_time       =  5-SEP-2012 13:04:55
Current_time        =  5-SEP-2012 13:05:51

Comment             = single pulse decouple
Data_format         = 1D COMPLEX
Dim_size            = 26214
Dim_title           = 31P
Dim_units           = [ppm]
Dimensions          = X
Site                = ECX 300
Spectrometer        = ECX-300

Field_strength      = 7.0586013[T] (300[MHz
X_acq_duration      = 0.30408704[s]
X_domain            = 31P
X_freq              = 121.65655406[MHz]
X_offset            = 0[ppm]
X_points            = 32768
X_prescans          = 4
X_resolution        = 3.28853213[Hz]
X_sweep             = 107.75862069[kHz]
Irr_domain          = 1H
Irr_freq            = 300.52965592[MHz]
Irr_offset          = 5[ppm]
Clipped             = FALSE
Mod_return          = 1
Scans               = 64
Total_scans         = 64

X_90_width          = 10.05[us]
X_acq_time          = 0.30408704[s]
X_angle             = 30[deg]
X_atn               = 6[dB]
X_pulse             = 3.35[us]
Irr_atn_dec         = 23[dB]
Irr_atn_noe         = 23[dB]
Irr_noise           = WALTZ
Decoupling          = TRUE
Initial_wait        = 1[s]
Noe                 = TRUE
Noe_time            = 2[s]
Recvr_gain          = 52
Relaxation_delay    = 2[s]
Repetition_time     = 2.30408704[s]
Temp_get            = 23[dC]
```

A5. ^{31}P NMR spectrum of tribenzyl phosphite.

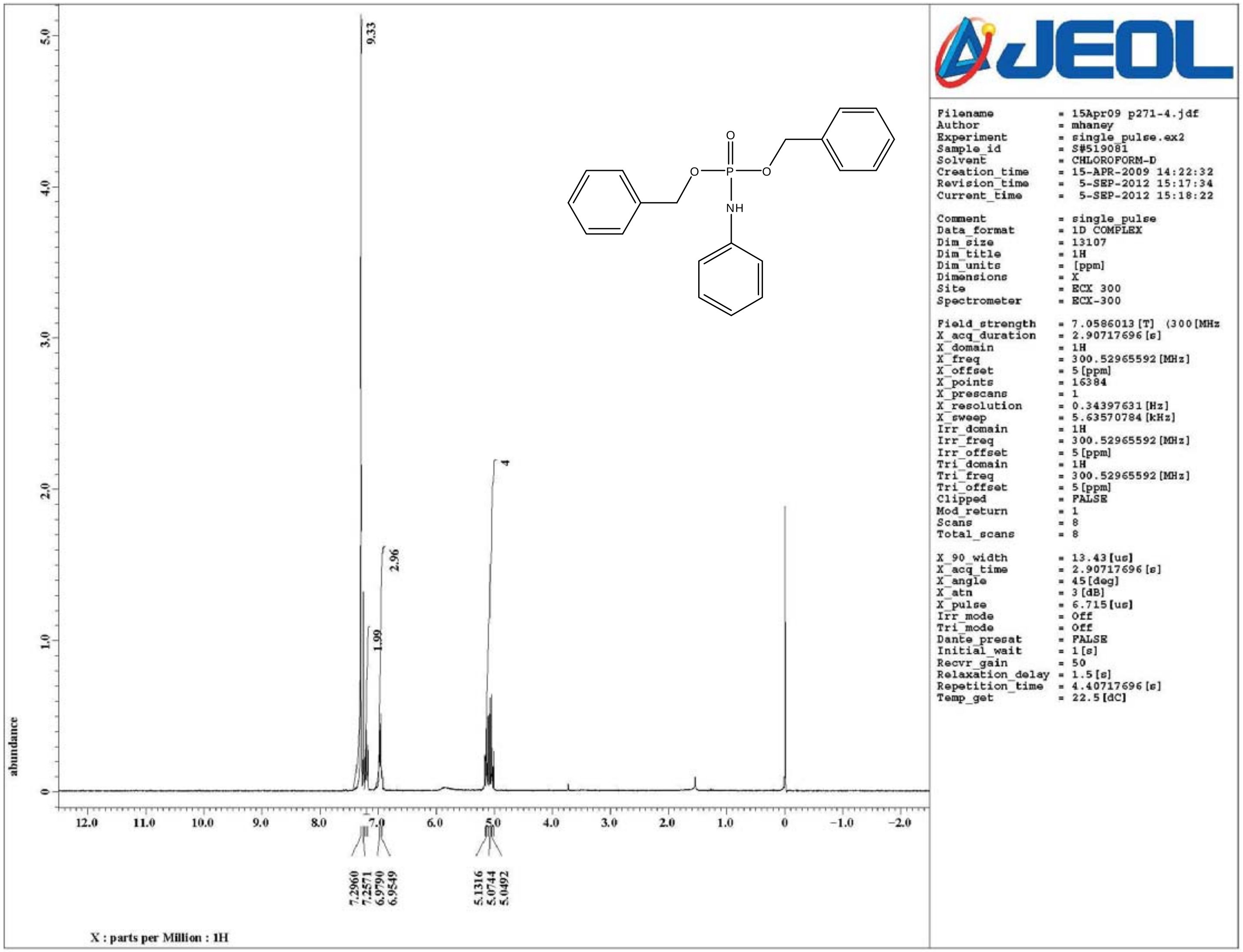

```
Filename          = 15Apr09 p271-4.jdf
Author            = mhaney
Experiment        = single_pulse.ex2
Sample_id         = S#519081
Solvent           = CHLOROFORM-D
Creation_time     = 15-APR-2009 14:22:32
Revision_time     =  5-SEP-2012 15:17:34
Current_time      =  5-SEP-2012 15:18:22

Comment           = single_pulse
Data_format       = 1D COMPLEX
Dim_size          = 13107
Dim_title         = 1H
Dim_units         = [ppm]
Dimensions        = X
Site              = ECX 300
Spectrometer      = ECX-300

Field_strength    = 7.0586013[T] (300[MHz
X_acq_duration    = 2.90717696[s]
X_domain          = 1H
X_freq            = 300.52965592[MHz]
X_offset          = 5[ppm]
X_points          = 16384
X_prescans        = 1
X_resolution      = 0.34397631[Hz]
X_sweep           = 5.63570784[kHz]
Irr_domain        = 1H
Irr_freq          = 300.52965592[MHz]
Irr_offset        = 5[ppm]
Tri_domain        = 1H
Tri_freq          = 300.52965592[MHz]
Tri_offset        = 5[ppm]
Clipped           = FALSE
Mod_return        = 1
Scans             = 8
Total_scans       = 8

X_90_width        = 13.43[us]
X_acq_time        = 2.90717696[s]
X_angle           = 45[deg]
X_atn             = 3[dB]
X_pulse           = 6.715[us]
Irr_mode          = Off
Tri_mode          = Off
Dante_presat      = FALSE
Initial_wait      = 1[s]
Recvr_gain        = 50
Relaxation_delay  = 1.5[s]
Repetition_time   = 4.40717696[s]
Temp_get          = 22.5[dC]
```

A6. Proton NMR spectrum of dibenzyl *N*-phPAM.

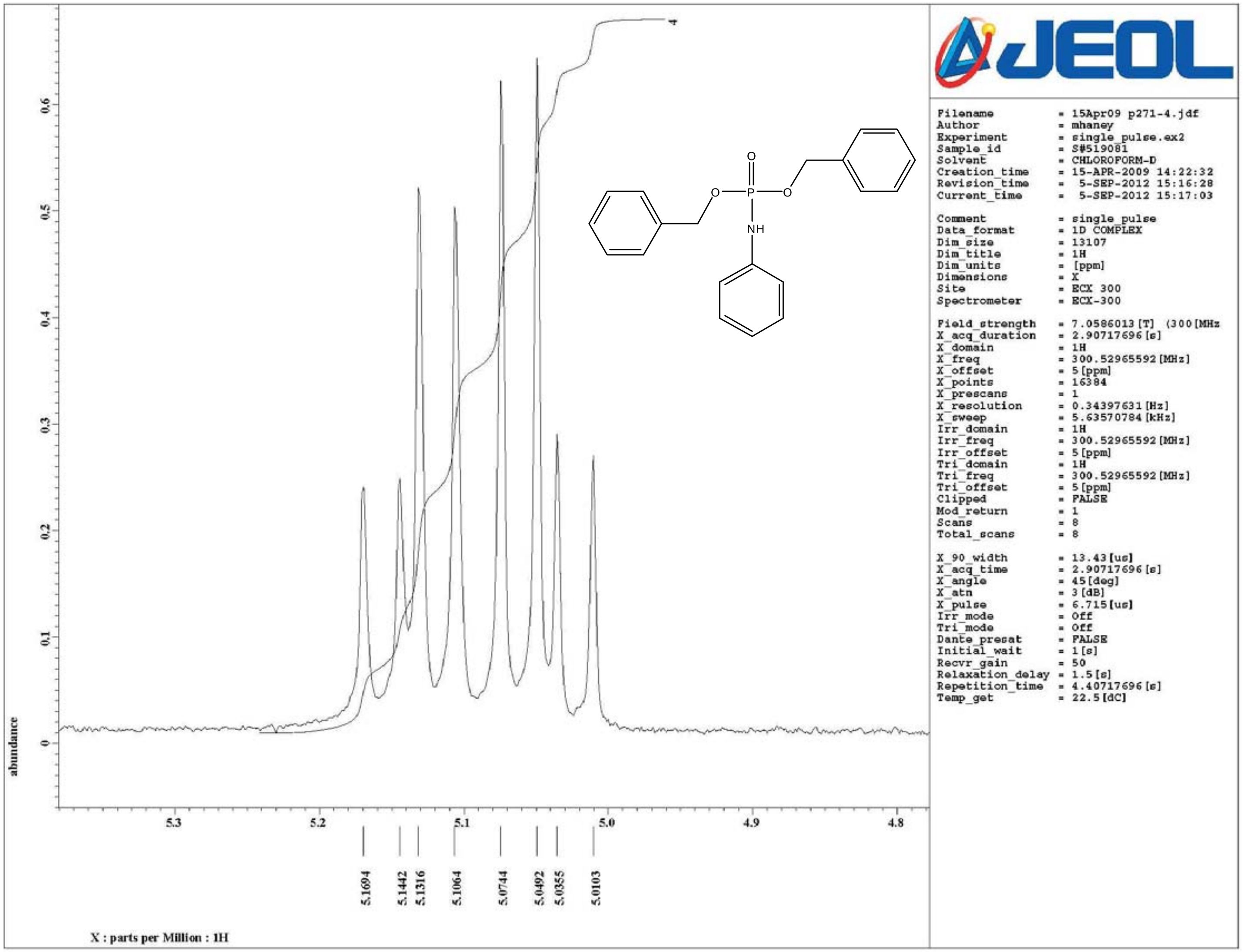

```
Filename          = 15Apr09 p271-4.jdf
Author            = mhaney
Experiment        = single_pulse.ex2
Sample_id         = S#519081
Solvent           = CHLOROFORM-D
Creation_time     = 15-APR-2009 14:22:32
Revision_time     =  5-SEP-2012 15:16:28
Current_time      =  5-SEP-2012 15:17:03

Comment           = single_pulse
Data_format       = 1D COMPLEX
Dim_size          = 13107
Dim_title         = 1H
Dim_units         = [ppm]
Dimensions        = X
Site              = ECX 300
Spectrometer      = ECX-300

Field_strength    = 7.0586013[T] (300[MHz
X_acq_duration    = 2.90717696[s]
X_domain          = 1H
X_freq            = 300.52965592[MHz]
X_offset          = 5[ppm]
X_points          = 16384
X_prescans        = 1
X_resolution      = 0.34397631[Hz]
X_sweep           = 5.63570784[kHz]
Irr_domain        = 1H
Irr_freq          = 300.52965592[MHz]
Irr_offset        = 5[ppm]
Tri_domain        = 1H
Tri_freq          = 300.52965592[MHz]
Tri_offset        = 5[ppm]
Clipped           = FALSE
Mod_return        = 1
Scans             = 8
Total_scans       = 8

X_90_width        = 13.43[us]
X_acq_time        = 2.90717696[s]
X_angle           = 45[deg]
X_atn             = 3[dB]
X_pulse           = 6.715[us]
Irr_mode          = Off
Tri_mode          = Off
Dante_presat      = FALSE
Initial_wait      = 1[s]
Recvr_gain        = 50
Relaxation_delay  = 1.5[s]
Repetition_time   = 4.40717696[s]
Temp_get          = 22.5[dC]
```

A7. Proton NMR spectrum of dibenzyl *N*-phPAM

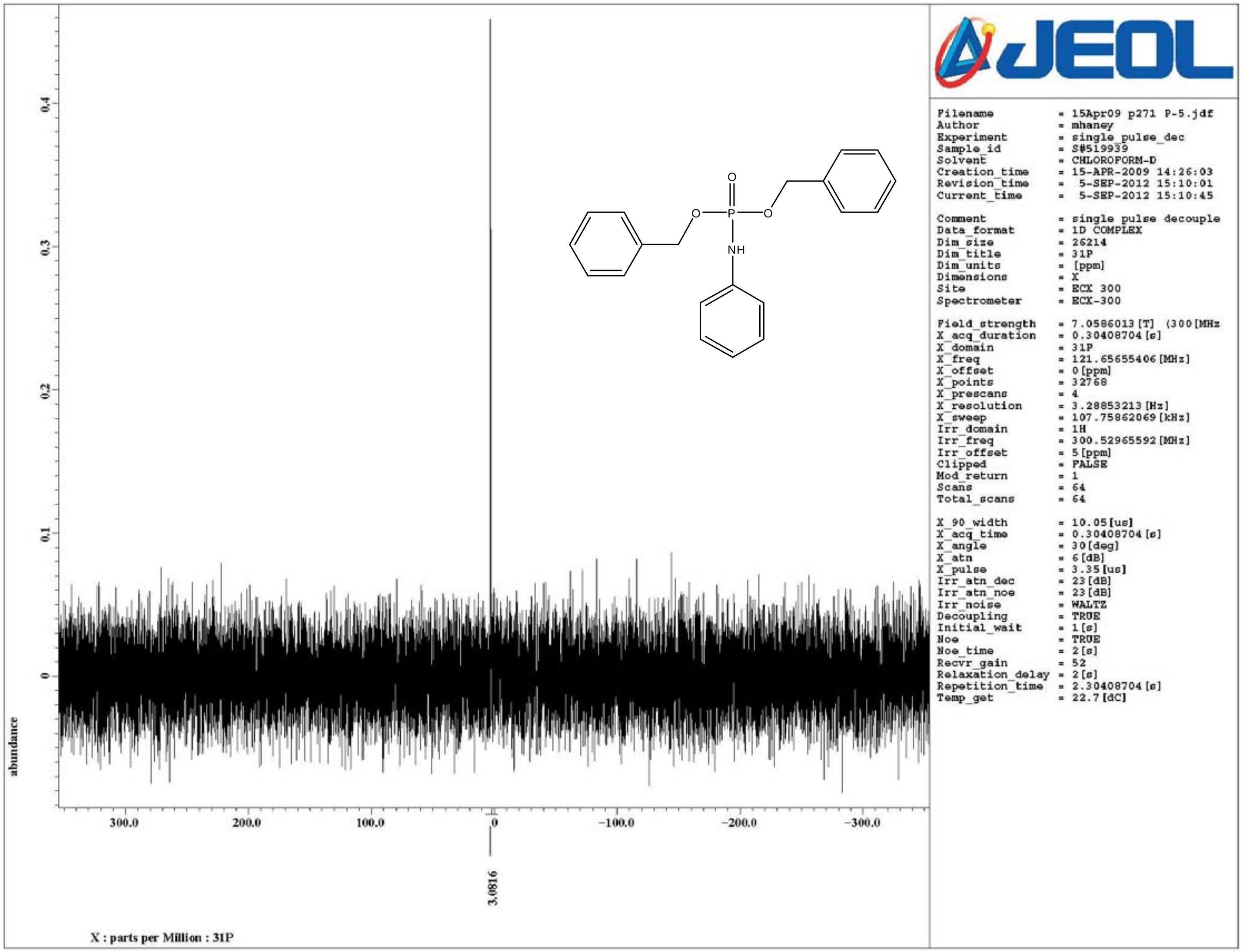

```
Filename          = 15Apr09 p271 P-5.jdf
Author            = mhaney
Experiment        = single_pulse_dec
Sample_id         = S#519939
Solvent           = CHLOROFORM-D
Creation_time     = 15-APR-2009 14:26:03
Revision_time     =  5-SEP-2012 15:10:01
Current_time      =  5-SEP-2012 15:10:45

Comment           = single pulse decouple
Data_format       = 1D COMPLEX
Dim_size          = 26214
Dim_title         = 31P
Dim_units         = [ppm]
Dimensions        = X
Site              = ECX 300
Spectrometer      = ECX-300

Field_strength    = 7.0586013[T] (300[MHz
X_acq_duration    = 0.30408704[s]
X_domain          = 31P
X_freq            = 121.65655406[MHz]
X_offset          = 0[ppm]
X_points          = 32768
X_prescans        = 4
X_resolution      = 3.28853213[Hz]
X_sweep           = 107.75862069[kHz]
Irr_domain        = 1H
Irr_freq          = 300.52965592[MHz]
Irr_offset        = 5[ppm]
Clipped           = FALSE
Mod_return        = 1
Scans             = 64
Total_scans       = 64

X_90_width        = 10.05[us]
X_acq_time        = 0.30408704[s]
X_angle           = 30[deg]
X_atn             = 6[dB]
X_pulse           = 3.35[us]
Irr_atn_dec       = 23[dB]
Irr_atn_noe       = 23[dB]
Irr_noise         = WALTZ
Decoupling        = TRUE
Initial_wait      = 1[s]
Noe               = TRUE
Noe_time          = 2[s]
Recvr_gain        = 52
Relaxation_delay  = 2[s]
Repetition_time   = 2.30408704[s]
Temp_get          = 22.7[dC]
```

A8. ^{31}P NMR spectrum of dibenzyl *N*-phPAM.

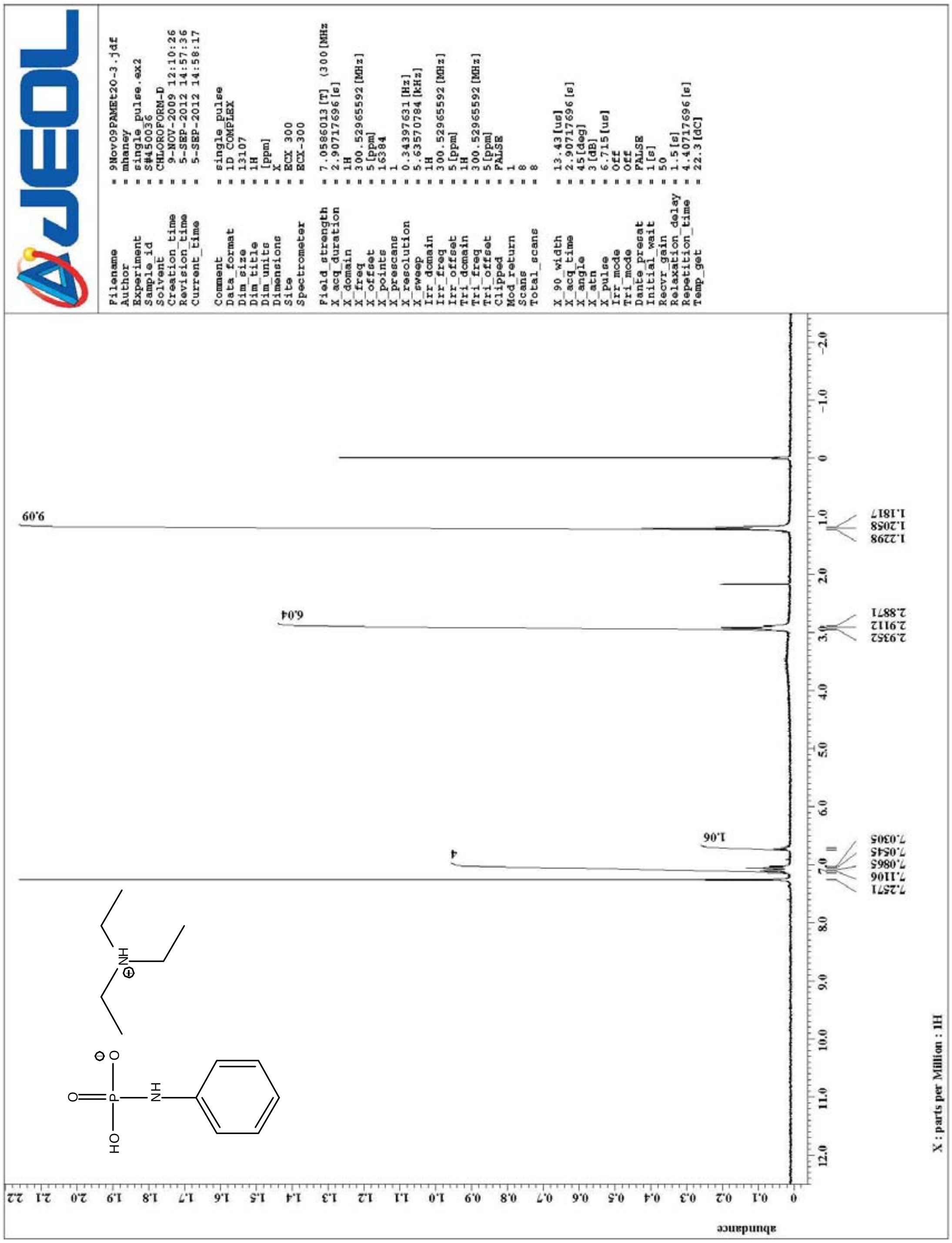

A9. Proton NMR spectrum of *N*-phPAM triethyl ammonium salt.

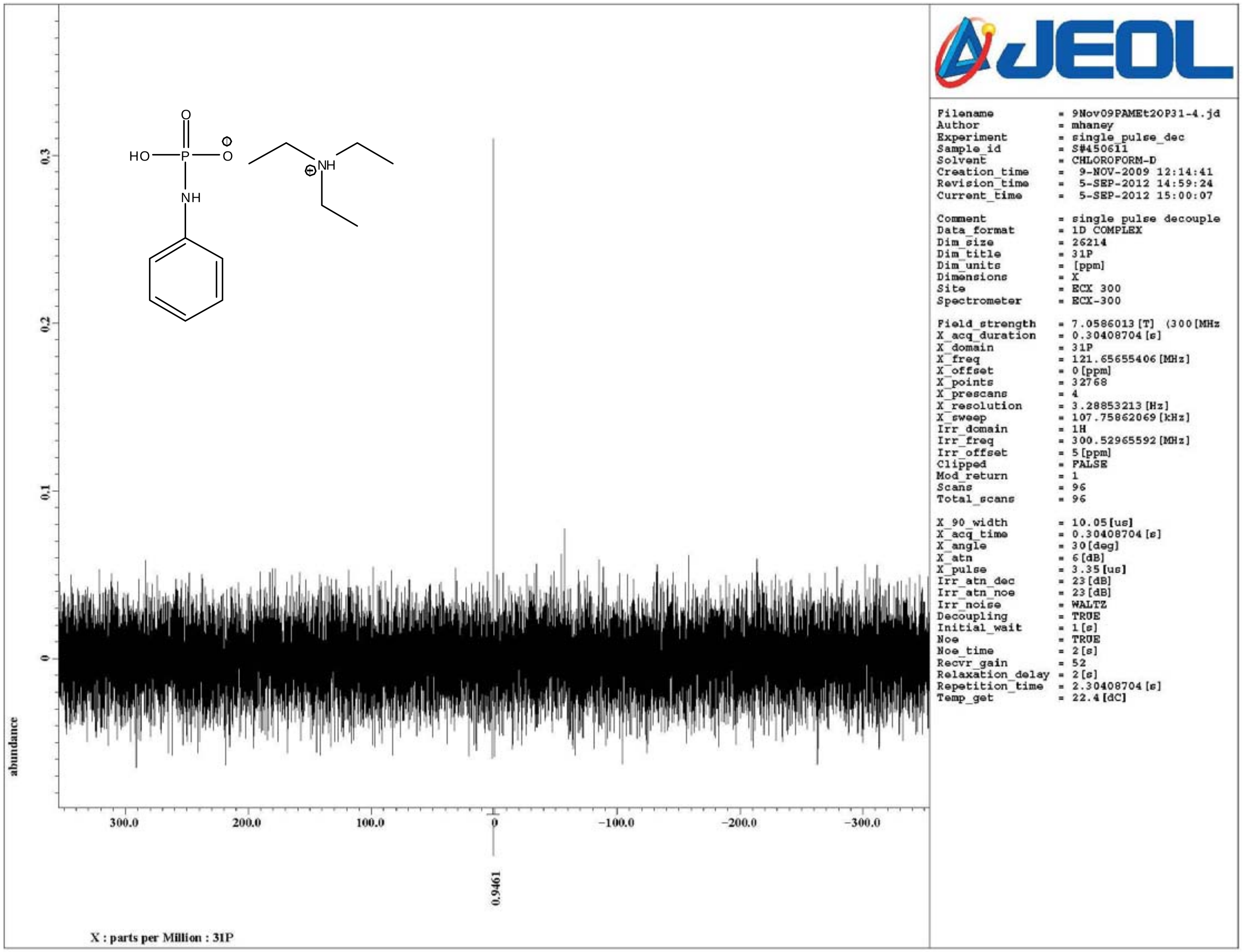

```
Filename            = 9Nov09PAMEt2OP31-4.jd
Author              = mhaney
Experiment          = single_pulse_dec
Sample_id           = S#450611
Solvent             = CHLOROFORM-D
Creation_time       =  9-NOV-2009 12:14:41
Revision_time       =  5-SEP-2012 14:59:24
Current_time        =  5-SEP-2012 15:00:07

Comment             = single pulse decouple
Data_format         = 1D COMPLEX
Dim_size            = 26214
Dim_title           = 31P
Dim_units           = [ppm]
Dimensions          = X
Site                = ECX 300
Spectrometer        = ECX-300

Field_strength      = 7.0586013[T] (300[MHz
X_acq_duration      = 0.30408704[s]
X_domain            = 31P
X_freq              = 121.65655406[MHz]
X_offset            = 0[ppm]
X_points            = 32768
X_prescans          = 4
X_resolution        = 3.28853213[Hz]
X_sweep             = 107.75862069[kHz]
Irr_domain          = 1H
Irr_freq            = 300.52965592[MHz]
Irr_offset          = 5[ppm]
Clipped             = FALSE
Mod_return          = 1
Scans               = 96
Total_scans         = 96

X_90_width          = 10.05[us]
X_acq_time          = 0.30408704[s]
X_angle             = 30[deg]
X_atn               = 6[dB]
X_pulse             = 3.35[us]
Irr_atn_dec         = 23[dB]
Irr_atn_noe         = 23[dB]
Irr_noise           = WALTZ
Decoupling          = TRUE
Initial_wait        = 1[s]
Noe                 = TRUE
Noe_time            = 2[s]
Recvr_gain          = 52
Relaxation_delay    = 2[s]
Repetition_time     = 2.30408704[s]
Temp_get            = 22.4[dC]
```

A10. ^{31}P NMR spectrum of *N*-phPAM triethyl ammonium salt.

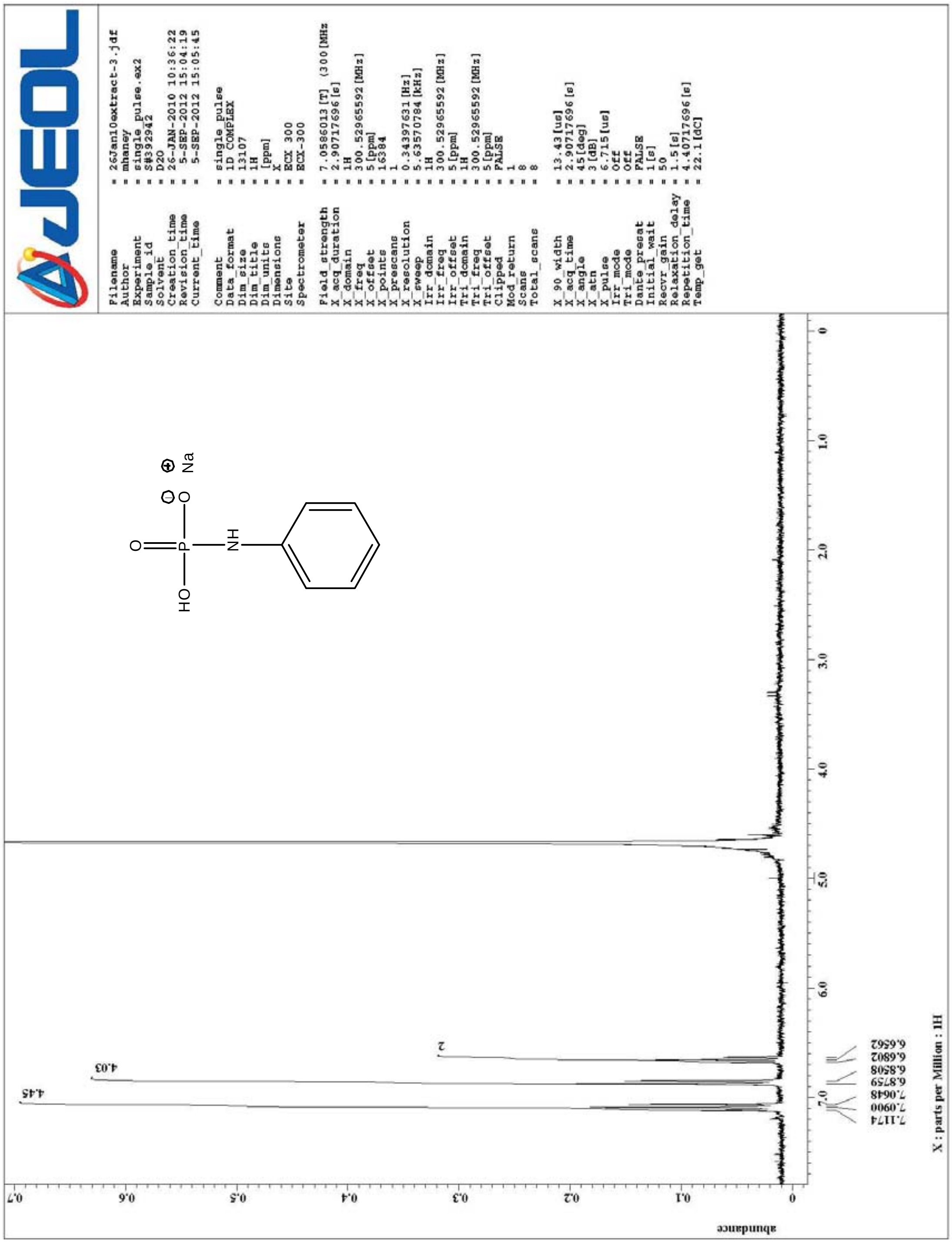

```
Filename          = 26Jan10extract-3.jdf
Author            = mhaney
Experiment        = single_pulse.ex2
Sample_id         = S#392942
Solvent           = D2O
Creation_time     = 26-JAN-2010 10:36:22
Revision_time     =  5-SEP-2012 15:04:19
Current_time      =  5-SEP-2012 15:05:45

Comment           = single_pulse
Data_format       = 1D COMPLEX
Dim_size          = 13107
Dim_title         = 1H
Dim_units         = [ppm]
Dimensions        = X
Site              = ECX 300
Spectrometer      = ECX-300

Field_strength    = 7.0586013[T] (300[MHz
X_acq_duration    = 2.90717696[s]
X_domain          = 1H
X_freq            = 300.52965592[MHz]
X_offset          = 5[ppm]
X_points          = 16384
X_prescans        = 1
X_resolution      = 0.34397631[Hz]
X_sweep           = 5.63570784[kHz]
Irr_domain        = 1H
Irr_freq          = 300.52965592[MHz]
Irr_offset        = 5[ppm]
Tri_domain        = 1H
Tri_freq          = 300.52965592[MHz]
Tri_offset        = 5[ppm]
Clipped           = FALSE
Mod_return        = 1
Scans             = 8
Total_scans       = 8

X_90_width        = 13.43[us]
X_acq_time        = 2.90717696[s]
X_angle           = 45[deg]
X_atn             = 3[dB]
X_pulse           = 6.715[us]
Irr_mode          = Off
Tri_mode          = Off
Dante_presat      = FALSE
Initial_wait      = 1[s]
Recvr_gain        = 50
Relaxation_delay  = 1.5[s]
Repetition_time   = 4.40717696[s]
Temp_get          = 22.1[dC]
```

A11. Proton NMR spectrum of *N*-phPAM sodium salt.

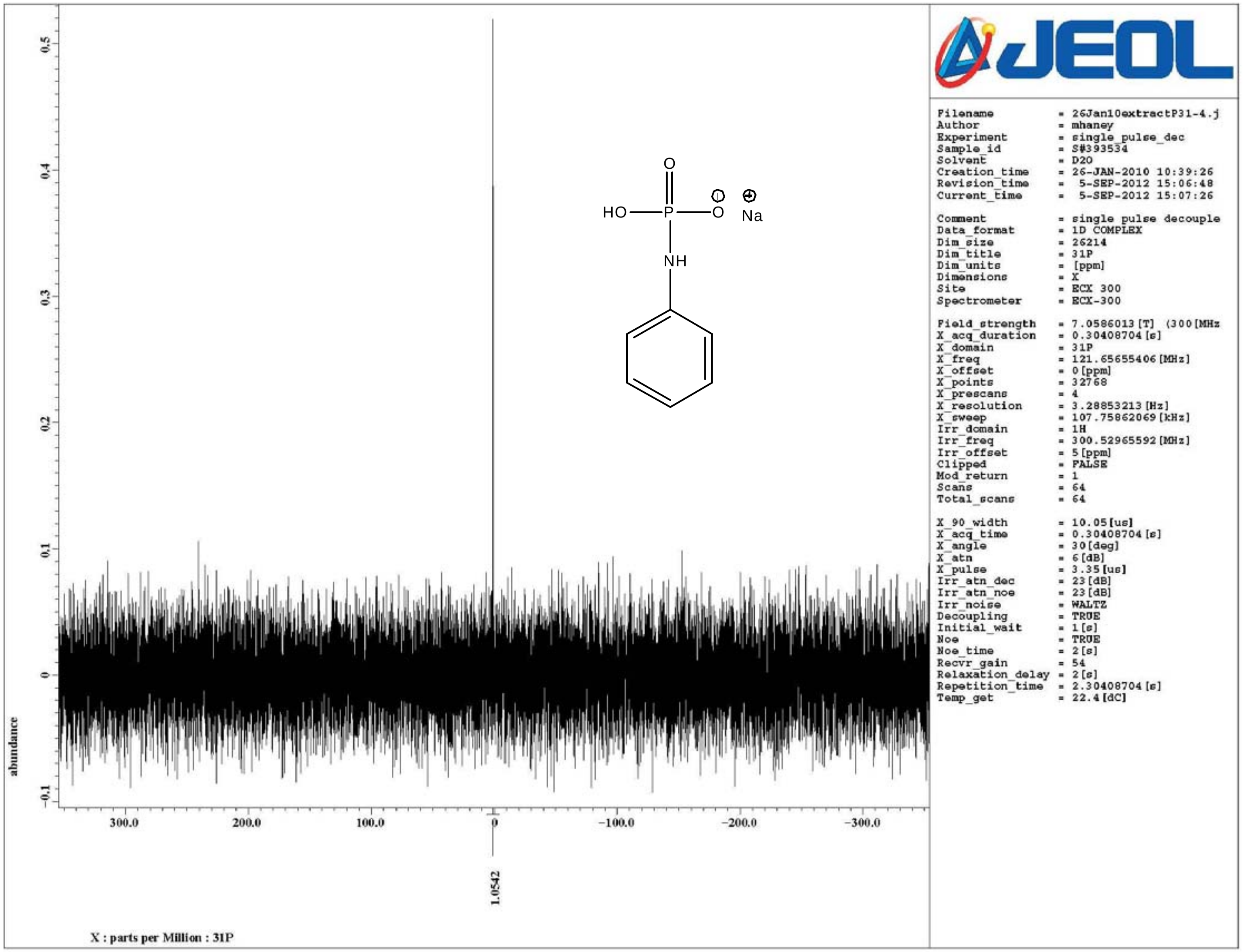

```
Filename            = 26Jan10extractP31-4.j
Author              = mhaney
Experiment          = single_pulse_dec
Sample_id           = S#393534
Solvent             = D2O
Creation_time       = 26-JAN-2010 10:39:26
Revision_time       =  5-SEP-2012 15:06:48
Current_time        =  5-SEP-2012 15:07:26

Comment             = single pulse decouple
Data_format         = 1D COMPLEX
Dim_size            = 26214
Dim_title           = 31P
Dim_units           = [ppm]
Dimensions          = X
Site                = ECX 300
Spectrometer        = ECX-300

Field_strength      = 7.0586013[T] (300[MHz
X_acq_duration      = 0.30408704[s]
X_domain            = 31P
X_freq              = 121.65655406[MHz]
X_offset            = 0[ppm]
X_points            = 32768
X_prescans          = 4
X_resolution        = 3.28853213[Hz]
X_sweep             = 107.75862069[kHz]
Irr_domain          = 1H
Irr_freq            = 300.52965592[MHz]
Irr_offset          = 5[ppm]
Clipped             = FALSE
Mod_return          = 1
Scans               = 64
Total_scans         = 64

X_90_width          = 10.05[us]
X_acq_time          = 0.30408704[s]
X_angle             = 30[deg]
X_atn               = 6[dB]
X_pulse             = 3.35[us]
Irr_atn_dec         = 23[dB]
Irr_atn_noe         = 23[dB]
Irr_noise           = WALTZ
Decoupling          = TRUE
Initial_wait        = 1[s]
Noe                 = TRUE
Noe_time            = 2[s]
Recvr_gain          = 54
Relaxation_delay    = 2[s]
Repetition_time     = 2.30408704[s]
Temp_get            = 22.4[dC]
```

A12. ^{31}P NMR spectrum of *N*-phPAM sodium salt.

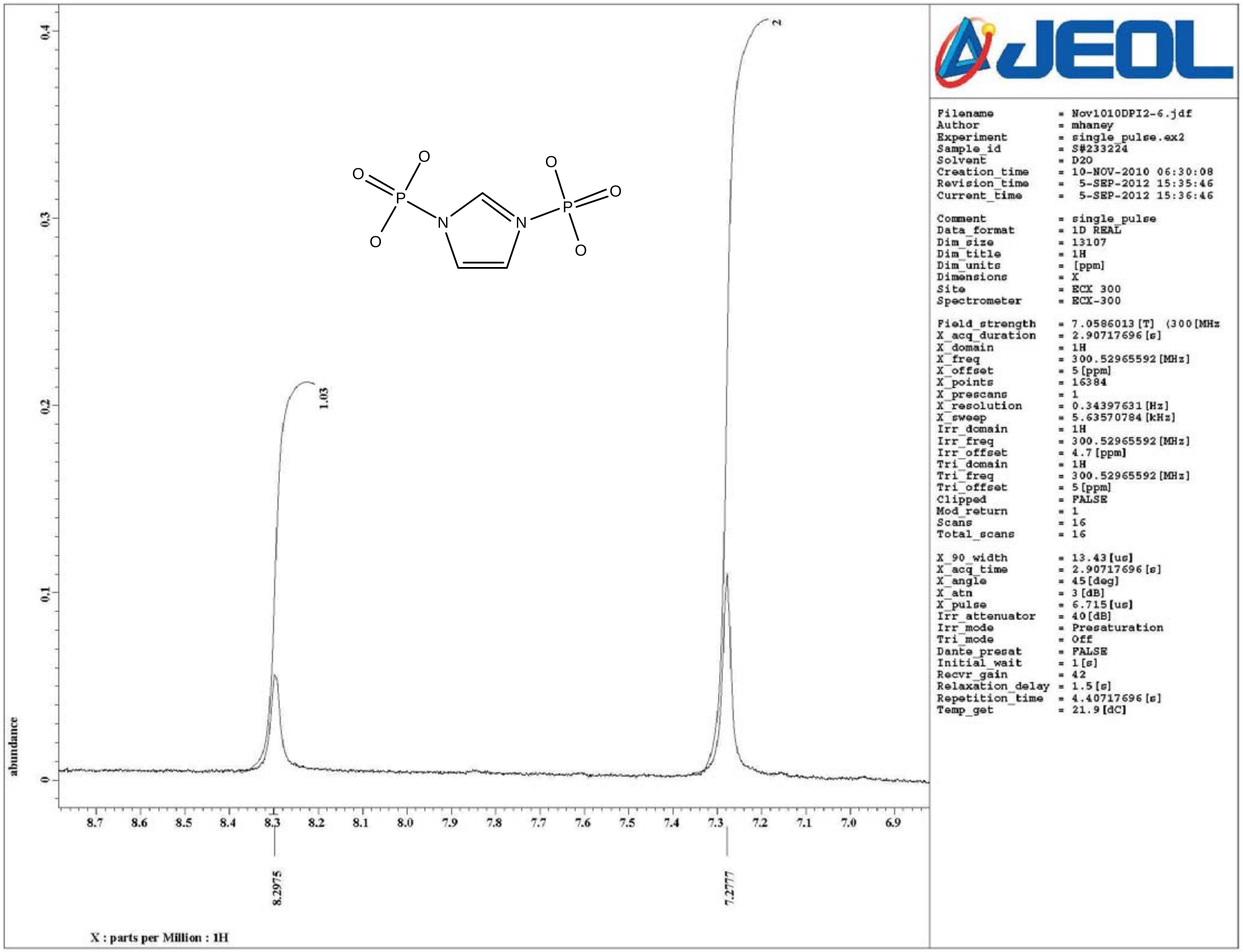

```
Filename           = Nov1010DPI2-6.jdf
Author             = mhaney
Experiment         = single_pulse.ex2
Sample_id          = S#233224
Solvent            = D2O
Creation_time      = 10-NOV-2010 06:30:08
Revision_time      =  5-SEP-2012 15:35:46
Current_time       =  5-SEP-2012 15:36:46

Comment            = single_pulse
Data_format        = 1D REAL
Dim_size           = 13107
Dim_title          = 1H
Dim_units          = [ppm]
Dimensions         = X
Site               = ECX 300
Spectrometer       = ECX-300

Field_strength     = 7.0586013[T] (300[MHz
X_acq_duration     = 2.90717696[s]
X_domain           = 1H
X_freq             = 300.52965592[MHz]
X_offset           = 5[ppm]
X_points           = 16384
X_prescans         = 1
X_resolution       = 0.34397631[Hz]
X_sweep            = 5.63570784[kHz]
Irr_domain         = 1H
Irr_freq           = 300.52965592[MHz]
Irr_offset         = 4.7[ppm]
Tri_domain         = 1H
Tri_freq           = 300.52965592[MHz]
Tri_offset         = 5[ppm]
Clipped            = FALSE
Mod_return         = 1
Scans              = 16
Total_scans        = 16

X_90_width         = 13.43[us]
X_acq_time         = 2.90717696[s]
X_angle            = 45[deg]
X_atn              = 3[dB]
X_pulse            = 6.715[us]
Irr_attenuator     = 40[dB]
Irr_mode           = Presaturation
Tri_mode           = Off
Dante_presat       = FALSE
Initial_wait       = 1[s]
Recvr_gain         = 42
Relaxation_delay   = 1.5[s]
Repetition_time    = 4.40717696[s]
Temp_get           = 21.9[dC]
```

A13. Proton NMR spectrum of di-phospho imidazole.

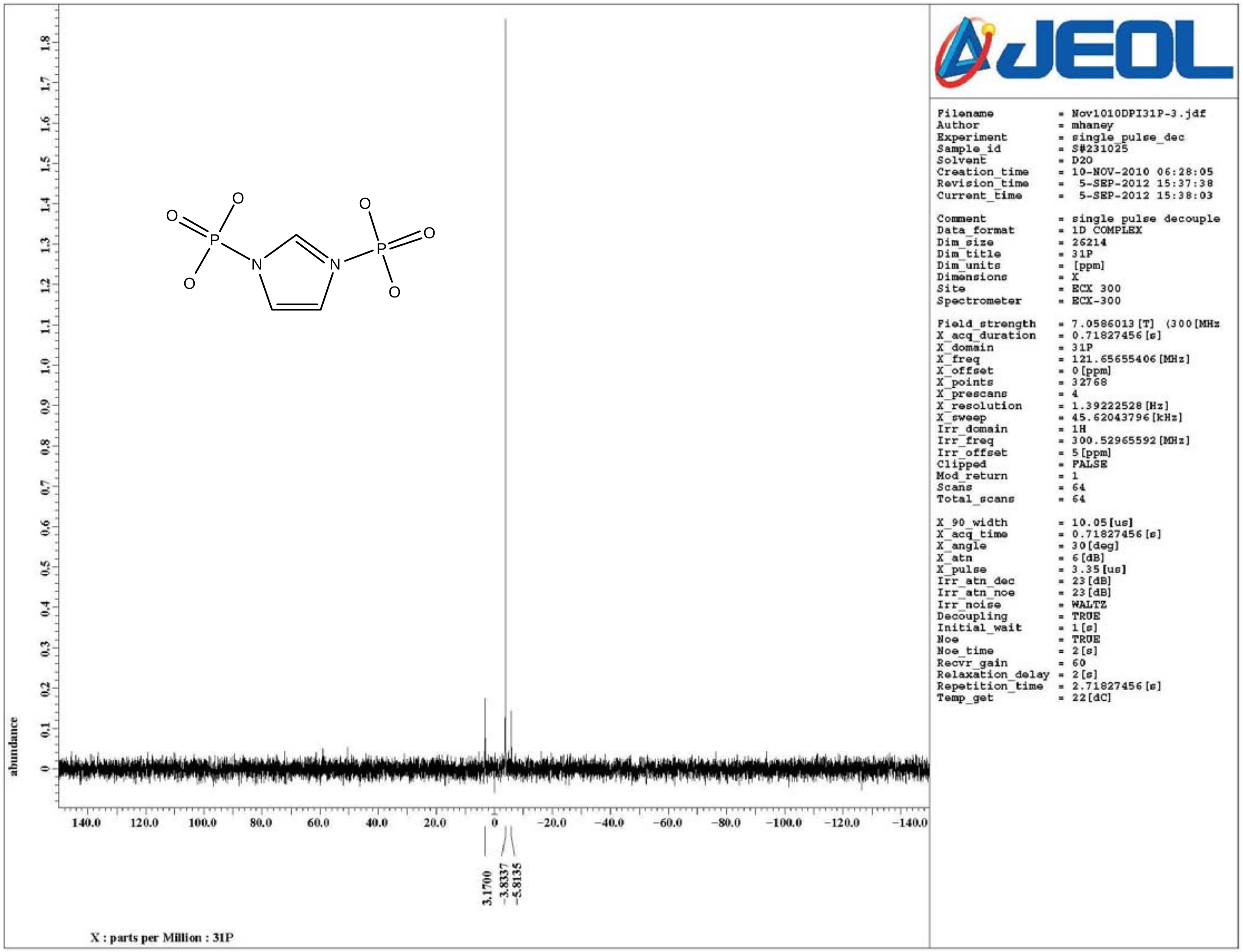

```
Filename            = Nov1010DPI31P-3.jdf
Author              = mhaney
Experiment          = single_pulse_dec
Sample_id           = S#231025
Solvent             = D2O
Creation_time       = 10-NOV-2010 06:28:05
Revision_time       =  5-SEP-2012 15:37:38
Current_time        =  5-SEP-2012 15:38:03

Comment             = single pulse decouple
Data_format         = 1D COMPLEX
Dim_size            = 26214
Dim_title           = 31P
Dim_units           = [ppm]
Dimensions          = X
Site                = ECX 300
Spectrometer        = ECX-300

Field_strength      = 7.0586013[T] (300[MHz
X_acq_duration      = 0.71827456[s]
X_domain            = 31P
X_freq              = 121.65655406[MHz]
X_offset            = 0[ppm]
X_points            = 32768
X_prescans          = 4
X_resolution        = 1.39222528[Hz]
X_sweep             = 45.62043796[kHz]
Irr_domain          = 1H
Irr_freq            = 300.52965592[MHz]
Irr_offset          = 5[ppm]
Clipped             = FALSE
Mod_return          = 1
Scans               = 64
Total_scans         = 64

X_90_width          = 10.05[us]
X_acq_time          = 0.71827456[s]
X_angle             = 30[deg]
X_atn               = 6[dB]
X_pulse             = 3.35[us]
Irr_atn_dec         = 23[dB]
Irr_atn_noe         = 23[dB]
Irr_noise           = WALTZ
Decoupling          = TRUE
Initial_wait        = 1[s]
Noe                 = TRUE
Noe_time            = 2[s]
Recvr_gain          = 60
Relaxation_delay = 2[s]
Repetition_time     = 2.71827456[s]
Temp_get            = 22[dC]
```

O
O
P
O
N
N
O
P
O
O
abundance
1.8
1.7
1.6
1.5
1.4
1.3
1.2
1.1
1.0
0.9
0.8
0.7
0.6
0.5
0.4
0.3
0.2
0.1
0
140.0
120.0
100.0
80.0
60.0
40.0
20.0
0
−20.0
−40.0
−60.0
−80.0
−100.0
−120.0
−140.0
3.1700
−3.8337
−5.8135
X : parts per Million : 31P

A14. ^{31}P NMR spectrum of di-phospho imidazole.

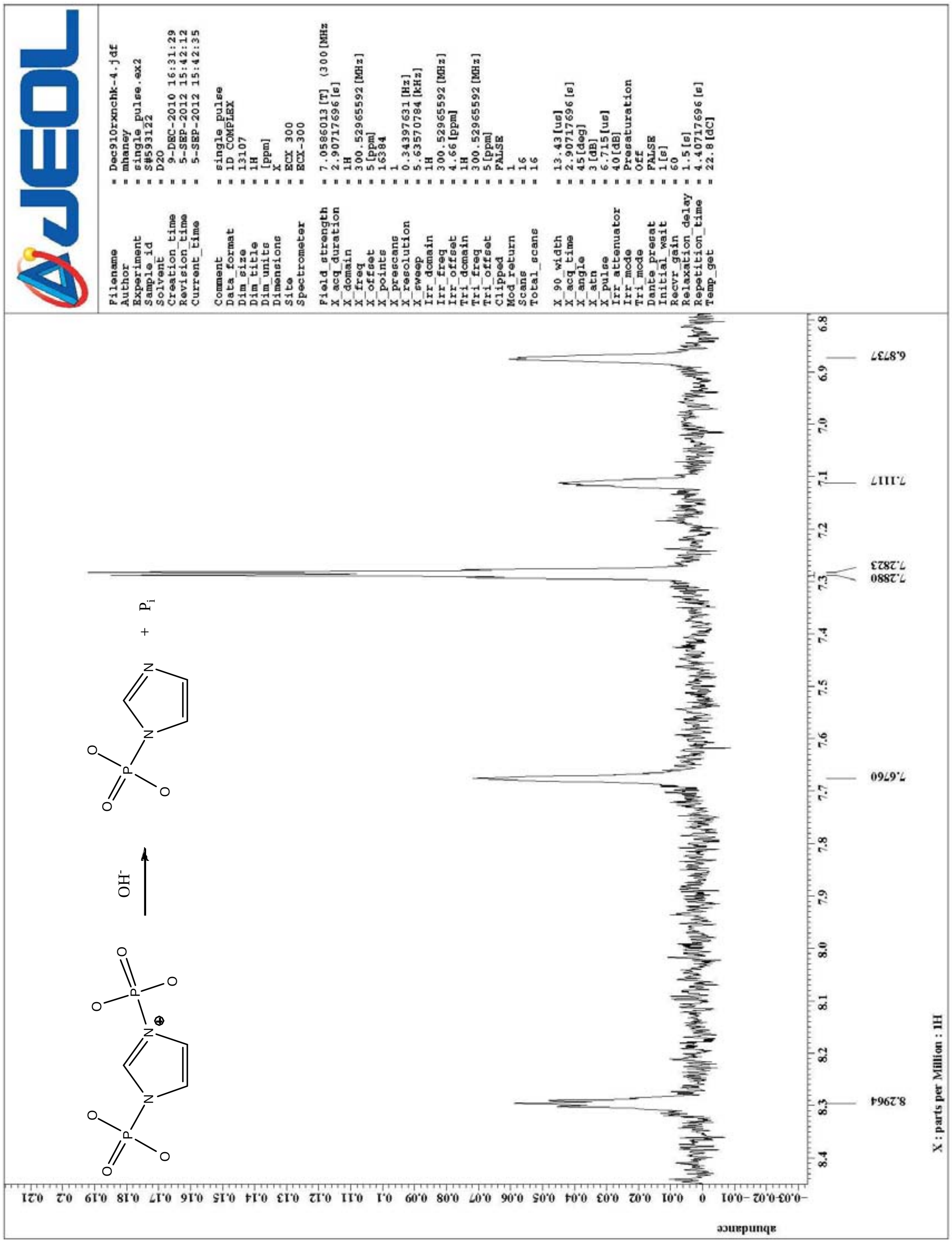

```
Filename             = Dec910rxnchk-4.jdf
Author               = mhaney
Experiment           = single_pulse.ex2
Sample_id            = S#593122
Solvent              = D2O
Creation_time        =  9-DEC-2010 16:31:29
Revision_time        =  5-SEP-2012 15:42:12
Current_time         =  5-SEP-2012 15:42:35

Comment              = single_pulse
Data_format          = 1D COMPLEX
Dim_size             = 13107
Dim_title            = 1H
Dim_units            = [ppm]
Dimensions           = X
Site                 = ECX 300
Spectrometer         = ECX-300

Field_strength       = 7.0586013[T] (300[MHz
X_acq_duration       = 2.90717696[s]
X_domain             = 1H
X_freq               = 300.52965592[MHz]
X_offset             = 5[ppm]
X_points             = 16384
X_prescans           = 1
X_resolution         = 0.34397631[Hz]
X_sweep              = 5.63570784[kHz]
Irr_domain           = 1H
Irr_freq             = 300.52965592[MHz]
Irr_offset           = 4.66[ppm]
Tri_domain           = 1H
Tri_freq             = 300.52965592[MHz]
Tri_offset           = 5[ppm]
Clipped              = FALSE
Mod_return           = 1
Scans                = 16
Total_scans          = 16

X_90_width           = 13.43[us]
X_acq_time           = 2.90717696[s]
X_angle              = 45[deg]
X_atn                = 3[dB]
X_pulse              = 6.715[us]
Irr_attenuator       = 40[dB]
Irr_mode             = Presaturation
Tri_mode             = Off
Dante_presat         = FALSE
Initial_wait         = 1[s]
Recvr_gain           = 60
Relaxation_delay     = 1.5[s]
Repetition_time      = 4.40717696[s]
Temp_get             = 22.8[dC]
```

O
P
O
O
N
N
⊕
P
O
O
O
OH⁻
O
P
O
O
N
N
+ P$_i$
abundance
0.21
0.2
0.19
0.18
0.17
0.16
0.15
0.14
0.13
0.12
0.11
0.1
0.09
0.08
0.07
0.06
0.05
0.04
0.03
0.02
0.01
0
-0.01
-0.02
-0.03
8.4
8.3
8.2
8.1
8.0
7.9
7.8
7.7
7.6
7.5
7.4
7.3
7.2
7.1
7.0
6.9
6.8
8.2964
7.6760
7.2880
7.2823
7.1117
6.8737
X : parts per Million : 1H

A15. Proton NMR spectrum showing the reaction of DPI to PIm.

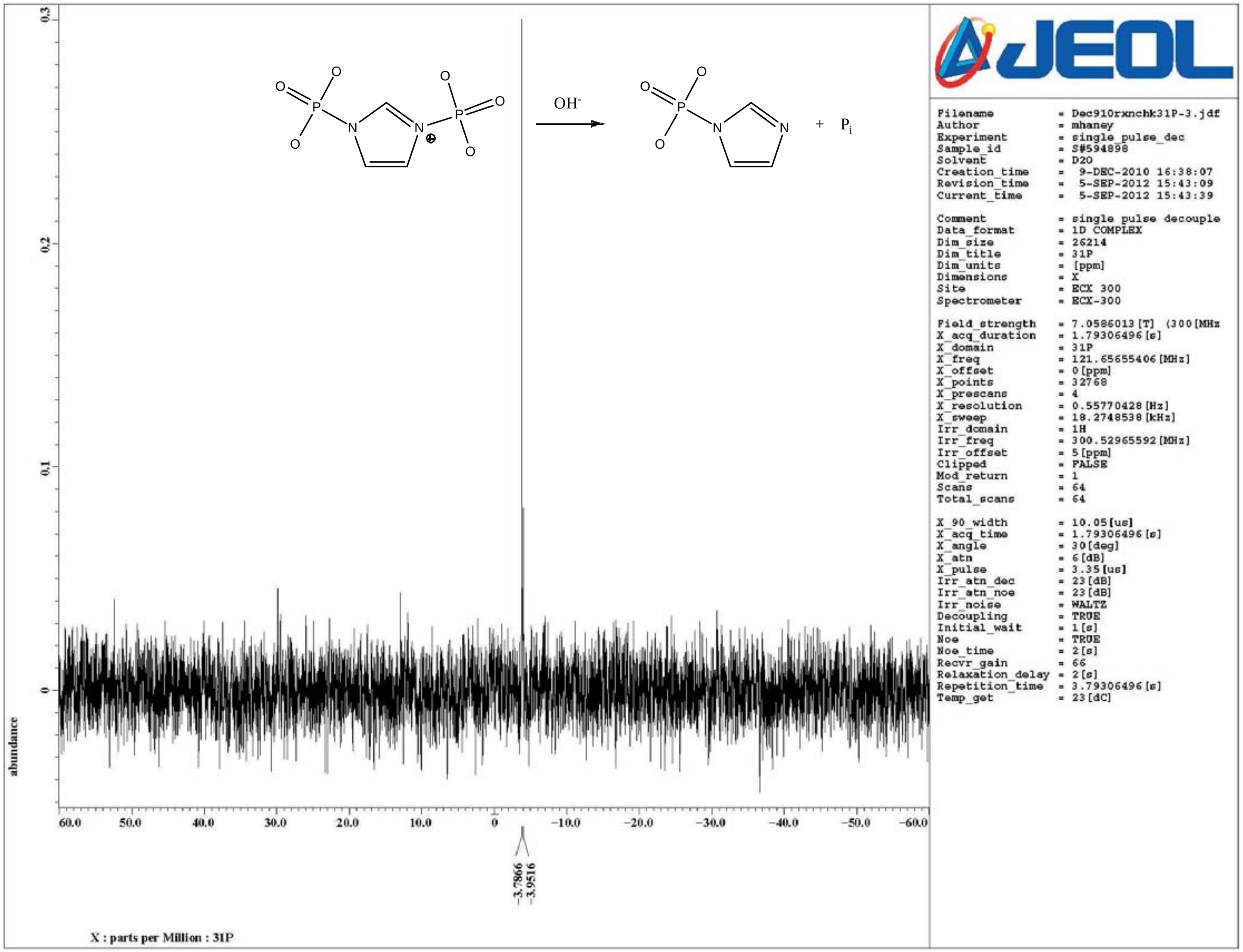

```
Filename            = Dec910rxnchk31P-3.jdf
Author              = mhaney
Experiment          = single_pulse_dec
Sample_id           = S#594898
Solvent             = D2O
Creation_time       =  9-DEC-2010 16:38:07
Revision_time       =  5-SEP-2012 15:43:09
Current_time        =  5-SEP-2012 15:43:39

Comment             = single pulse decouple
Data_format         = 1D COMPLEX
Dim_size            = 26214
Dim_title           = 31P
Dim_units           = [ppm]
Dimensions          = X
Site                = ECX 300
Spectrometer        = ECX-300

Field_strength      = 7.0586013[T] (300[MHz
X_acq_duration      = 1.79306496[s]
X_domain            = 31P
X_freq              = 121.65655406[MHz]
X_offset            = 0[ppm]
X_points            = 32768
X_prescans          = 4
X_resolution        = 0.55770428[Hz]
X_sweep             = 18.2748538[kHz]
Irr_domain          = 1H
Irr_freq            = 300.52965592[MHz]
Irr_offset          = 5[ppm]
Clipped             = FALSE
Mod_return          = 1
Scans               = 64
Total_scans         = 64

X_90_width          = 10.05[us]
X_acq_time          = 1.79306496[s]
X_angle             = 30[deg]
X_atn               = 6[dB]
X_pulse             = 3.35[us]
Irr_atn_dec         = 23[dB]
Irr_atn_noe         = 23[dB]
Irr_noise           = WALTZ
Decoupling          = TRUE
Initial_wait        = 1[s]
Noe                 = TRUE
Noe_time            = 2[s]
Recvr_gain          = 66
Relaxation_delay    = 2[s]
Repetition_time     = 3.79306496[s]
Temp_get            = 23[dC]
```

A16. ^{31}P NMR spectrum showing the reaction of DPI to MPI.

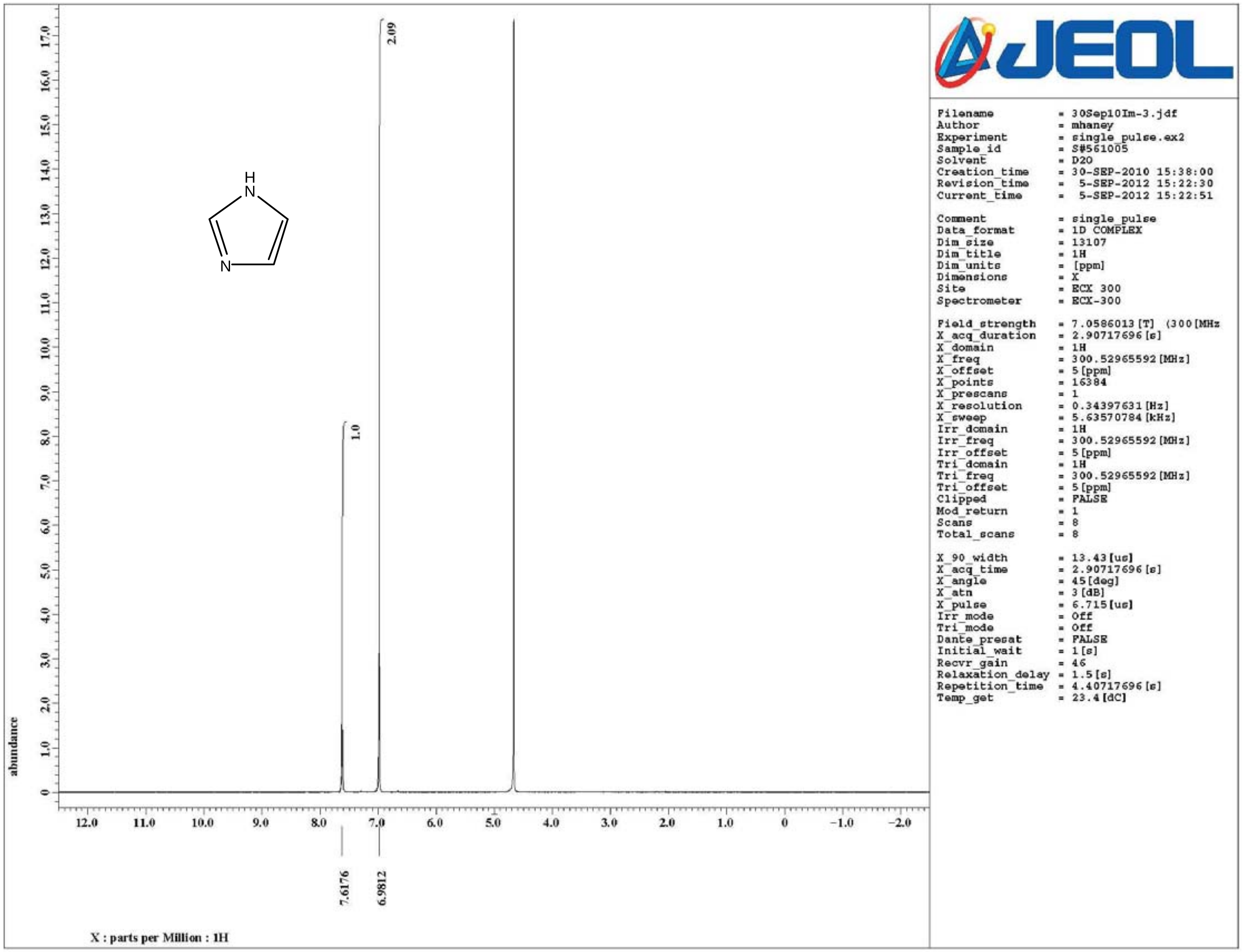

```
Filename            = 30Sep10Im-3.jdf
Author              = mhaney
Experiment          = single_pulse.ex2
Sample_id           = S#561005
Solvent             = D2O
Creation_time       = 30-SEP-2010 15:38:00
Revision_time       =  5-SEP-2012 15:22:30
Current_time        =  5-SEP-2012 15:22:51

Comment             = single_pulse
Data_format         = 1D COMPLEX
Dim_size            = 13107
Dim_title           = 1H
Dim_units           = [ppm]
Dimensions          = X
Site                = ECX 300
Spectrometer        = ECX-300

Field_strength      = 7.0586013[T] (300[MHz
X_acq_duration      = 2.90717696[s]
X_domain            = 1H
X_freq              = 300.52965592[MHz]
X_offset            = 5[ppm]
X_points            = 16384
X_prescans          = 1
X_resolution        = 0.34397631[Hz]
X_sweep             = 5.63570784[kHz]
Irr_domain          = 1H
Irr_freq            = 300.52965592[MHz]
Irr_offset          = 5[ppm]
Tri_domain          = 1H
Tri_freq            = 300.52965592[MHz]
Tri_offset          = 5[ppm]
Clipped             = FALSE
Mod_return          = 1
Scans               = 8
Total_scans         = 8

X_90_width          = 13.43[us]
X_acq_time          = 2.90717696[s]
X_angle             = 45[deg]
X_atn               = 3[dB]
X_pulse             = 6.715[us]
Irr_mode            = Off
Tri_mode            = Off
Dante_presat        = FALSE
Initial_wait        = 1[s]
Recvr_gain          = 46
Relaxation_delay    = 1.5[s]
Repetition_time     = 4.40717696[s]
Temp_get            = 23.4[dC]
```

A17. Proton NMR spectrum of imidazole.

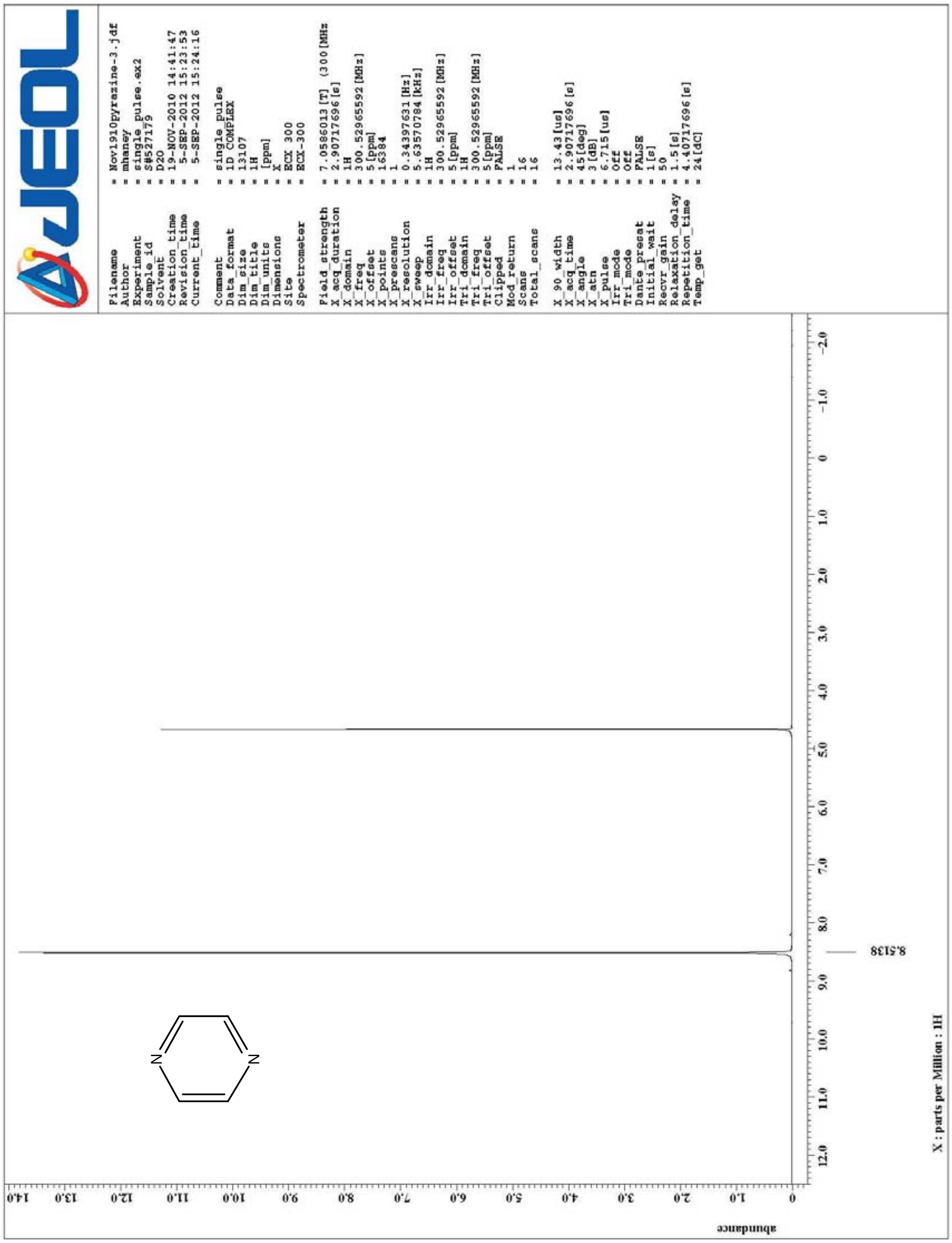

```
Filename          = Nov1910pyrazine-3.jdf
Author            = mhaney
Experiment        = single_pulse.ex2
Sample_id         = S#527179
Solvent           = D2O
Creation_time     = 19-NOV-2010 14:41:47
Revision_time     =  5-SEP-2012 15:23:53
Current_time      =  5-SEP-2012 15:24:16

Comment           = single_pulse
Data_format       = 1D COMPLEX
Dim_size          = 13107
Dim_title         = 1H
Dim_units         = [ppm]
Dimensions        = X
Site              = ECX 300
Spectrometer      = ECX-300

Field_strength    = 7.0586013[T] (300[MHz
X_acq_duration    = 2.90717696[s]
X_domain          = 1H
X_freq            = 300.52965592[MHz]
X_offset          = 5[ppm]
X_points          = 16384
X_prescans        = 1
X_resolution      = 0.34397631[Hz]
X_sweep           = 5.63570784[kHz]
Irr_domain        = 1H
Irr_freq          = 300.52965592[MHz]
Irr_offset        = 5[ppm]
Tri_domain        = 1H
Tri_freq          = 300.52965592[MHz]
Tri_offset        = 5[ppm]
Clipped           = FALSE
Mod_return        = 1
Scans             = 16
Total_scans       = 16

X_90_width        = 13.43[us]
X_acq_time        = 2.90717696[s]
X_angle           = 45[deg]
X_atn             = 3[dB]
X_pulse           = 6.715[us]
Irr_mode          = Off
Tri_mode          = Off
Dante_presat      = FALSE
Initial_wait      = 1[s]
Recvr_gain        = 50
Relaxation_delay  = 1.5[s]
Repetition_time   = 4.40717696[s]
Temp_get          = 24[dC]
```

JEOL
N
N
abundance
0
1.0
2.0
3.0
4.0
5.0
6.0
7.0
8.0
9.0
10.0
11.0
12.0
13.0
14.0
12.0
11.0
10.0
9.0
8.0
7.0
6.0
5.0
4.0
3.0
2.0
1.0
0
-1.0
-2.0
8.5138
X : parts per Million : 1H

A18. Proton NMR spectrum of pyrazine.

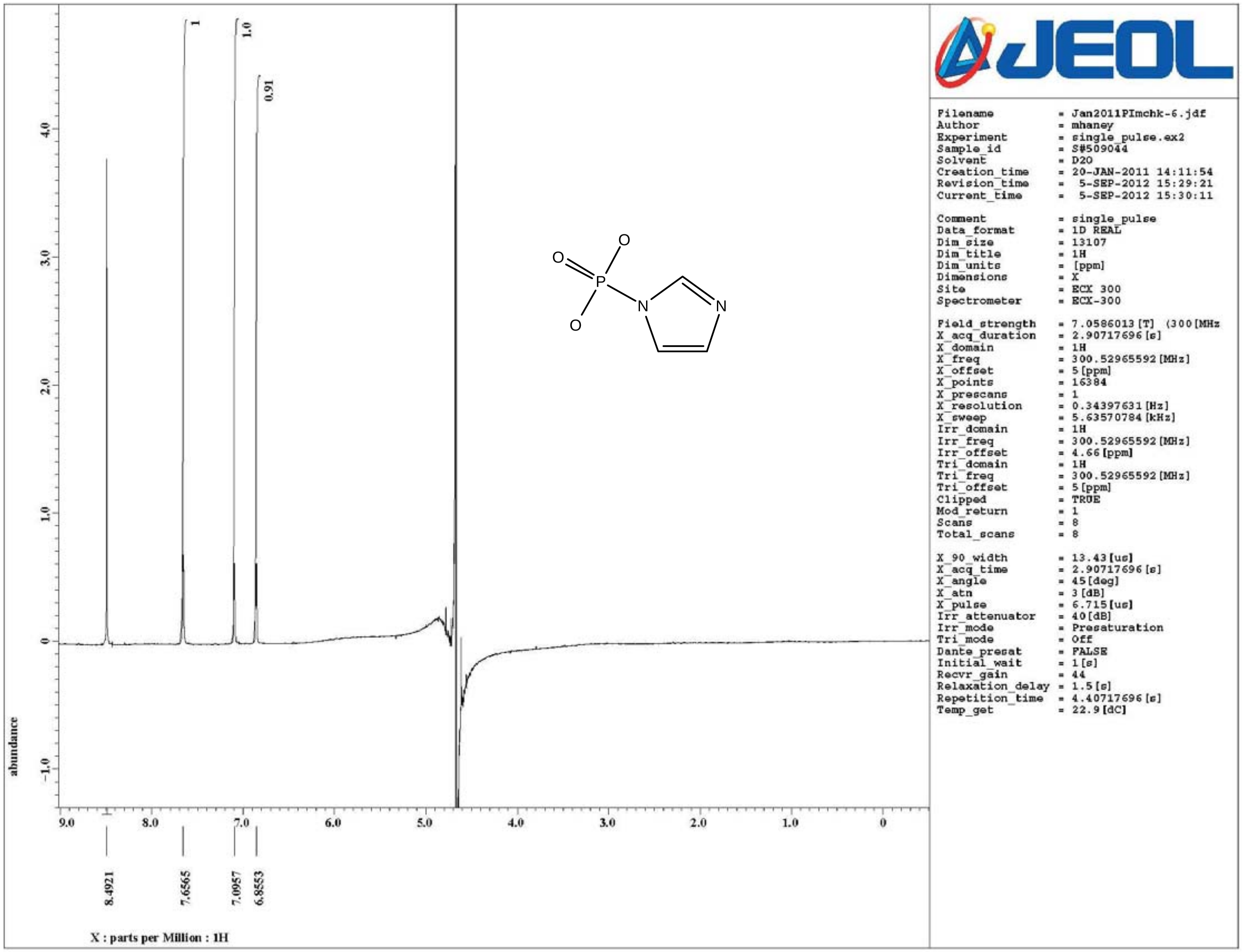

```
Filename           = Jan2011PImchk-6.jdf
Author             = mhaney
Experiment         = single_pulse.ex2
Sample_id          = S#509044
Solvent            = D2O
Creation_time      = 20-JAN-2011 14:11:54
Revision_time      =  5-SEP-2012 15:29:21
Current_time       =  5-SEP-2012 15:30:11

Comment            = single_pulse
Data_format        = 1D REAL
Dim_size           = 13107
Dim_title          = 1H
Dim_units          = [ppm]
Dimensions         = X
Site               = ECX 300
Spectrometer       = ECX-300

Field_strength     = 7.0586013[T] (300[MHz
X_acq_duration     = 2.90717696[s]
X_domain           = 1H
X_freq             = 300.52965592[MHz]
X_offset           = 5[ppm]
X_points           = 16384
X_prescans         = 1
X_resolution       = 0.34397631[Hz]
X_sweep            = 5.63570784[kHz]
Irr_domain         = 1H
Irr_freq           = 300.52965592[MHz]
Irr_offset         = 4.66[ppm]
Tri_domain         = 1H
Tri_freq           = 300.52965592[MHz]
Tri_offset         = 5[ppm]
Clipped            = TRUE
Mod_return         = 1
Scans              = 8
Total_scans        = 8

X_90_width         = 13.43[us]
X_acq_time         = 2.90717696[s]
X_angle            = 45[deg]
X_atn              = 3[dB]
X_pulse            = 6.715[us]
Irr_attenuator     = 40[dB]
Irr_mode           = Presaturation
Tri_mode           = Off
Dante_presat       = FALSE
Initial_wait       = 1[s]
Recvr_gain         = 44
Relaxation_delay   = 1.5[s]
Repetition_time    = 4.40717696[s]
Temp_get           = 22.9[dC]
```

A19. Proton NMR spectrum of PIm with pyrazine standard in coaxial tube.

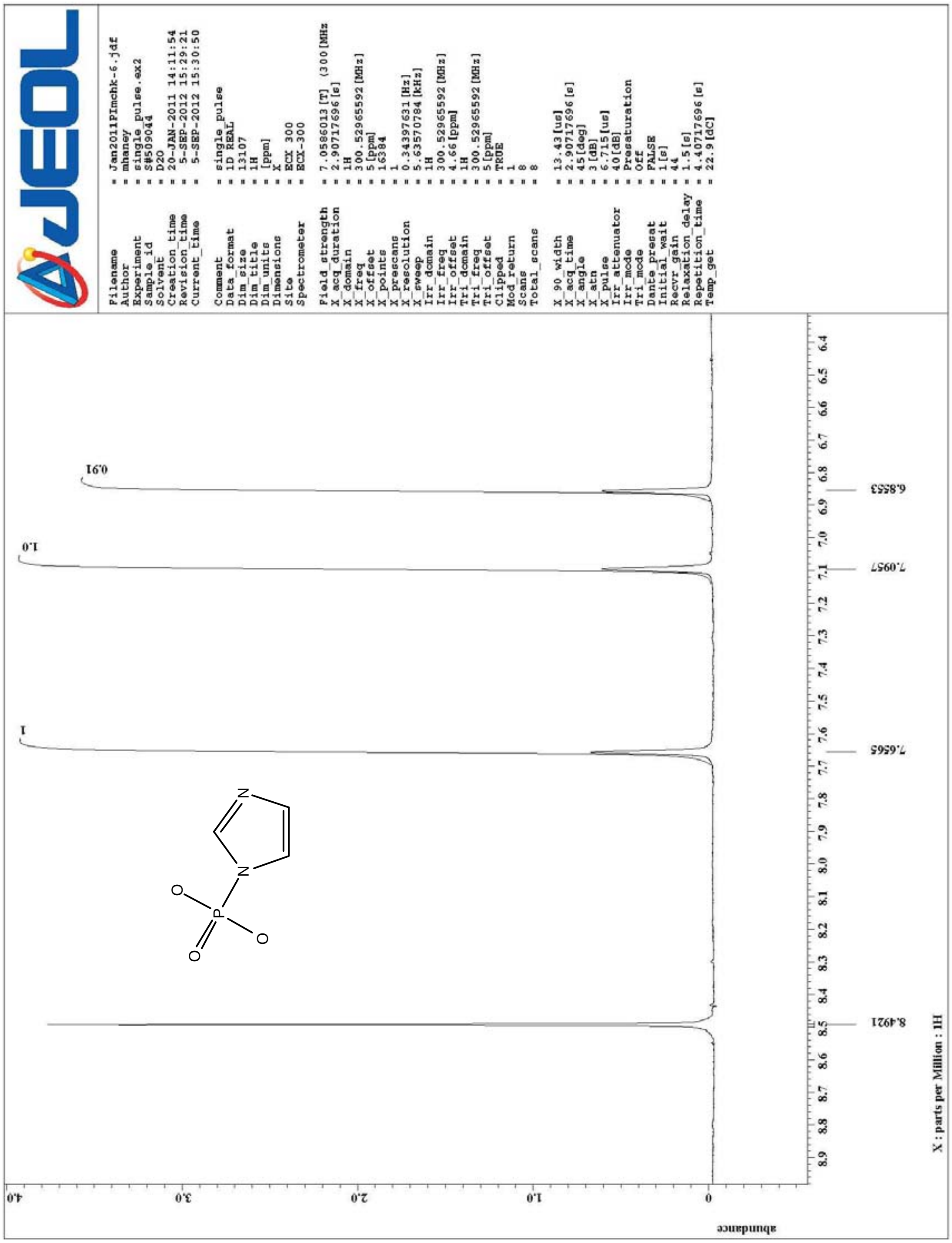

```
Filename          = Jan2011PImchk-6.jdf
Author            = mhaney
Experiment        = single_pulse.ex2
Sample_id         = S#509044
Solvent           = D2O
Creation_time     = 20-JAN-2011 14:11:54
Revision_time     =  5-SEP-2012 15:29:21
Current_time      =  5-SEP-2012 15:30:50

Comment           = single_pulse
Data_format       = 1D REAL
Dim_size          = 13107
Dim_title         = 1H
Dim_units         = [ppm]
Dimensions        = X
Site              = ECX 300
Spectrometer      = ECX-300

Field_strength    = 7.0586013[T] (300[MHz
X_acq_duration    = 2.90717696[s]
X_domain          = 1H
X_freq            = 300.52965592[MHz]
X_offset          = 5[ppm]
X_points          = 16384
X_prescans        = 1
X_resolution      = 0.34397631[Hz]
X_sweep           = 5.63570784[kHz]
Irr_domain        = 1H
Irr_freq          = 300.52965592[MHz]
Irr_offset        = 4.66[ppm]
Tri_domain        = 1H
Tri_freq          = 300.52965592[MHz]
Tri_offset        = 5[ppm]
Clipped           = TRUE
Mod_return        = 1
Scans             = 8
Total_scans       = 8

X_90_width        = 13.43[us]
X_acq_time        = 2.90717696[s]
X_angle           = 45[deg]
X_atn             = 3[dB]
X_pulse           = 6.715[us]
Irr_attenuator    = 40[dB]
Irr_mode          = Presaturation
Tri_mode          = Off
Dante_presat      = FALSE
Initial_wait      = 1[s]
Recvr_gain        = 44
Relaxation_delay  = 1.5[s]
Repetition_time   = 4.40717696[s]
Temp_get          = 22.9[dC]
```

JEOL
0.91
1.0
1
N
N
P
O
O
O
6.8553
7.0957
7.6565
8.4921
6.4
6.5
6.6
6.7
6.8
6.9
7.0
7.1
7.2
7.3
7.4
7.5
7.6
7.7
7.8
7.9
8.0
8.1
8.2
8.3
8.4
8.5
8.6
8.7
8.8
8.9
X : parts per Million : 1H
4.0
3.0
2.0
1.0
0
abundance

A20. Proton NMR spectrum of PIm with pyrazine standard in coaxial tube.

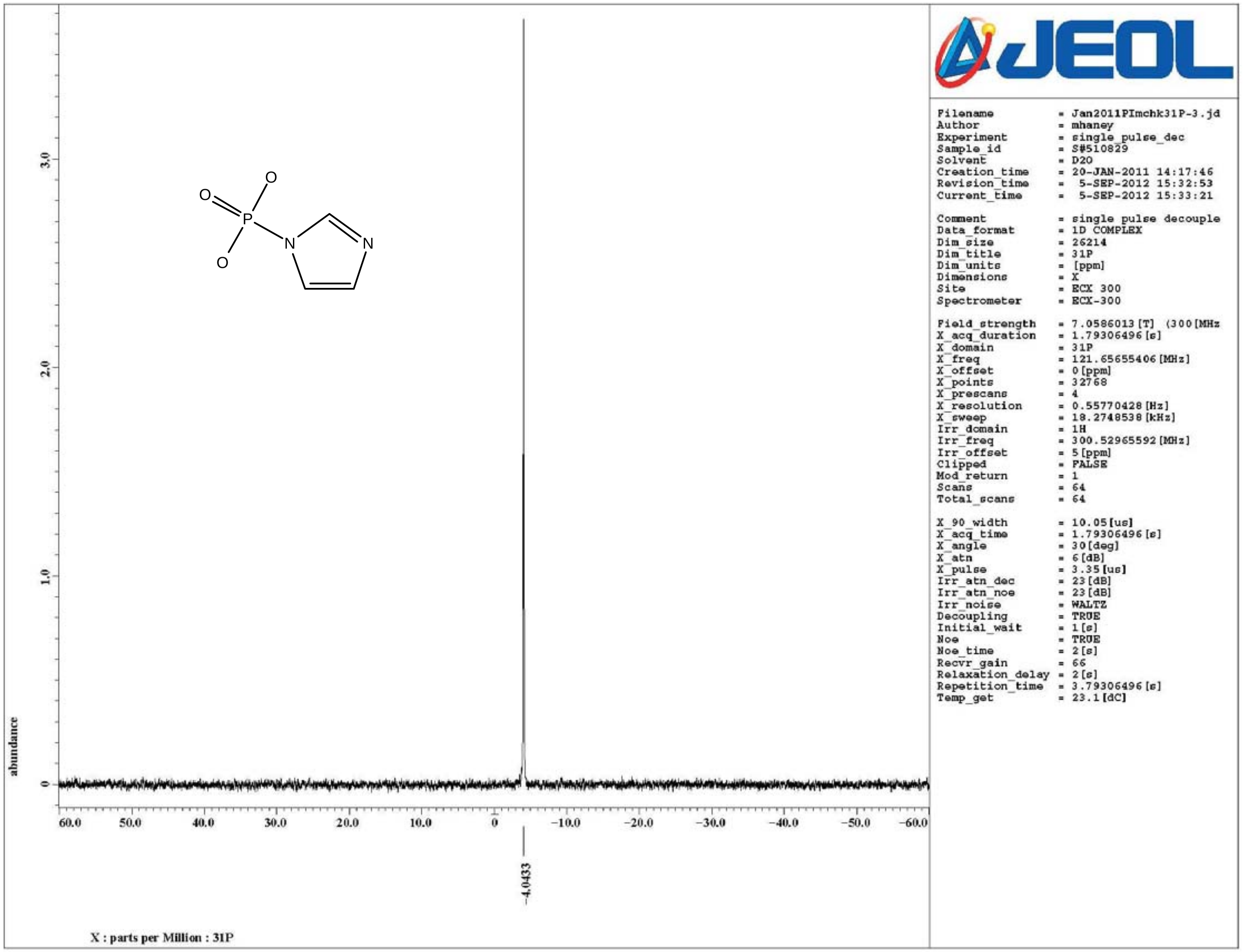

```
Filename            = Jan2011PImchk31P-3.jd
Author              = mhaney
Experiment          = single_pulse_dec
Sample_id           = S#510829
Solvent             = D2O
Creation_time       = 20-JAN-2011 14:17:46
Revision_time       =  5-SEP-2012 15:32:53
Current_time        =  5-SEP-2012 15:33:21

Comment             = single pulse decouple
Data_format         = 1D COMPLEX
Dim_size            = 26214
Dim_title           = 31P
Dim_units           = [ppm]
Dimensions          = X
Site                = ECX 300
Spectrometer        = ECX-300

Field_strength      = 7.0586013[T] (300[MHz
X_acq_duration      = 1.79306496[s]
X_domain            = 31P
X_freq              = 121.65655406[MHz]
X_offset            = 0[ppm]
X_points            = 32768
X_prescans          = 4
X_resolution        = 0.55770428[Hz]
X_sweep             = 18.2748538[kHz]
Irr_domain          = 1H
Irr_freq            = 300.52965592[MHz]
Irr_offset          = 5[ppm]
Clipped             = FALSE
Mod_return          = 1
Scans               = 64
Total_scans         = 64

X_90_width          = 10.05[us]
X_acq_time          = 1.79306496[s]
X_angle             = 30[deg]
X_atn               = 6[dB]
X_pulse             = 3.35[us]
Irr_atn_dec         = 23[dB]
Irr_atn_noe         = 23[dB]
Irr_noise           = WALTZ
Decoupling          = TRUE
Initial_wait        = 1[s]
Noe                 = TRUE
Noe_time            = 2[s]
Recvr_gain          = 66
Relaxation_delay    = 2[s]
Repetition_time     = 3.79306496[s]
Temp_get            = 23.1[dC]
```

A21. ^{31}P NMR spectrum of PIm.

Full Time-Course Kinetics

The inability to follow the hydrolysis of PIm by UV/Vis spectroscopy drove development of a full time-course analytical technique using NMR spectrometry. The disadvantage of following a full time-course is that it requires most, if not all of the initial substrate to be consumed for reliable mathematical analysis. Disadvantages of using NMR spectrometry to follow enzymatic reactions are the slow acquisition time and minimal concentration of substrate detectable by the instrument.

Full time-course assays using NMR were conducted using the following steps: 1) converting the calcium salt of PIm to the sodium salt; 2) determining the concentration of the stock PIm solution using a 0.1M pyrazine standard and NMR, while in the process adjusting instrument parameters for the subsequent enzymatic assay; 3) mixing a buffered solution of PIm; mixing enzyme with the buffered solution of PIm, placing this mixture in the NMR tube and placing a coaxial tube with pyrazine standard in the tube; 4) loading the instrument queue with duplicate experiments; 5) processing each spectra; and 6) inputting data from the processed spectra into a least-squares or simplex fitting program to determine V_{max}, K_M, and K_i. Each step is covered below.

PIm is isolated as the insoluble calcium salt. It is made soluble by exchanging the calcium for sodium with IRC 748 cation exchange resin (section **2.2.10**). Minor changes in incubation time with the resin or incubation temperature can affect the concentration of sodium PIm in solution. For this reason, the concentration of the PIm should be checked whenever a new stock solution is made (section **2.4.3.1**). Mixing an aliquot of the sodium PIm (Figures A19 and A20) with an aliquot of pyrazine of known concentration yields the concentration of PIm by integrating the relative proton signals (section **2.4.3.1**).

When integrating spectra, better accuracy is had by limiting the instrument's acquisition of proton signals to those of interest. Pyrazine, PIm, and imidazole have signals in the aromatic region, whereas water and buffer have no signals in the aromatic region. Water and buffer signals must be addressed before obtaining spectra.

The water signal will be much greater in intensity than the substrates. It should be suppressed with pre-saturation. After the sample with mixed pyrazine and PIm is placed in the instrument, an NMR experiment should be run with a sweep of from 9 to 0 ppm. The resultant spectrum should be processed to determine the shift of the water signal; it usually showed at 4.7 ppm but may vary based upon the instrument's shims. The water signal at the determined ppm was suppressed with pre-saturation at 35 decibels. While 35 decibels was used, the NMR manager should be consulted for the maximum suppression power to minimize risk to the instrument.

With the water signal suppressed, the buffer will still be in much greater concentration than the substrate and will obscure substrate signals. The instrument sweep and offset should be adjusted to show only the aromatic region which will mitigate interference of the buffer signals (section **2.4.3.1**). The x-points should be reduced since the sweep will be greatly reduced. Suppression of the water signal, adjustment of the sweep, offset, and x-points will change a spectrum of a pyrazine/PIm mixture from that shown in Figure A19 to that shown in Figure A20. At this point, the signals can be integrated and the concentration of the stock solution determined. The instrument's settings are now adjusted to conduct the enzymatic assays. The purity of the stock PIm solution may be ascertained at this point by obtaining a ^{31}P spectrum (Figure A21).

The instrument should be prepared for an enzymatic assay. The spinner should be turned off since the motion of the spinner may affect the enzyme. The time span between data points is adjusted changing the number of scans. For example, if each scan takes 5 seconds and an experiment is set for 30 scans, the experiment will take 150 seconds. With the spinner off and the time span adjusted, the instrument is ready for an enzymatic assay.

Stock PIm and buffer can be mixed in a small microcentrifuge tube. Enzyme can be added to the PIm/buffer mix, and the buffered solution placed into the NMR tube. A coaxial tube containing pyrazine is inserted into the NMR tube, the NMR tube is inserted into the instrument, and a series of duplicate NMR experiments are loaded into the queue to be run automatically.

The intensity of the pyrazine signal should neither obscure the PIm signals by being too great nor be obscured by the PIm signals by being too small (Figure A-19). The purpose of the pyrazine standard during an enzymatic assay is to provide a standard signal during the time-course. If the instrument’s shimming should vary, the intensities of the signals will vary. Normalizing the PIm signals against the pyrazine signal accounts for any variation in the shims. If the PIm concentration needs to be increased or decreased, the pyrazine concentration in the coaxial tube may be increased or decreased. Since the pyrazine in the coaxial tube’s purpose is to provide a normalized signal, it’s concentration does not have to be known.

Spectra should be processed as NMR experiments from the queue are completed. The phase and baseline should be adjusted on each spectra. The substrate (PIm) signals and product (imidazole) signals should be integrated against the pyrazine standard (section **2.4.3.1**).

Since the initial concentration of PIm was known, each NMR experiment will yield the concentration of PIm, or imidazole, at a specific time. Changes in concentration of PIm, or imidazole, coupled with the time span between each NMR experiment will give the observed velocity, V_{obs}. Upon addition of enzyme to the substrate hydrolysis will begin immediately. The first data point will not be detected directly by the instrument; the NMR tube holding the enzyme/substrate mixture will be in the experimentalist’s hand. But, the substrate concentration at the first point will be known since stock solution of known concentration was used to make the buffered solution.

For the substrates used in this study, a 1 to 1 ratio of substrate to P_i is maintained during an assay. Specifically, for each mole of PIm hydrolyzed, a mole of P_i is formed. This allows use of the below equation which accounts for generation of inhibitor concentration during the time-course..

$$V_{obs} = \frac{(V_{max})[S]}{K_M(1 + [I]/K_i) + [S]} \qquad \text{(A1)}$$

If the full time-course is followed using proton spectrometry concentrations of P_i will not be directly detected. The instrument will provide the concentration of PIm, or [S], at a given time point. Knowing the starting concentration of substrate, the concentration of inhibitor, or P_i, is determined by $[I] = [S]_{initial} - [S]_{remaining}$. This assumes P_i is not precipitating or otherwise being consumed.

Upon completion of a full time-course enzymatic assay monitored by NMR, V_{obs}, [S], and [I] at a series of time points are known. These data are then fitted to equation A1 using the program Micomath by Scientist to determine V_{max} and K_M. Fits during this study were completed using least squares. Simplex fitting was tried as well and gave the same results as least squares.

Fitting the data involved converting the time of the experiment from hr:min:sec to an elapsed ΔTime. This was done by assuming the first time period to be time t = 0. In Table A1 it can be seen that the time of the first experiment was 3:12:08 a.m. This was the first data point and was taken to be time t = 0. The initial concentration at time t = 0 was 3 mM PIm, 0 mM P_i, and the percent hydrolysis was 0. The data inputted into the spreadsheet were the hours, minutes, seconds, initial concentration of PIm, and concentration of PIm at the time point as determined by integration of the signal. Concentration of P_i was determined as indicated above.

Inputting data into Excel before fitting the data in Scientist by Micromath is necessary to convert the instrument's output time to ΔTime and to determine the concentration of PIm and P_i at each time point. Additionally, Excel will provide instant confirmation that curvature is shown in the resulting plot and that hydrolysis has proceeded to 90%.

A challenge in fitting the data to Equation A1 is having curvature to the plot. During the initial phases of an enzymatic reaction it may visually appear that the rate stays unchanged, even up to 50% or more of the reaction. Not only can the data (V_{obs} vs time, [S] vs time, or [I] vs time) appear linear over the time-course to the eye, the data can appear linear to the computer. If the algorithm does not have the expected curvature to the data it cannot properly fit the data. Error in V_{max} and/or K_M will be larger than that obtained values.

Table A1. Excel spreadsheet for the data entry of the hydrolysis of PIm by PAcP at pH 5.5.

Time hr	min	sec	∆ Time (h:m:s)	∆ Time (min)	PIm Peak at 7.3	PIm Peak at 7.9	[PIm]	[Pi]	by [PIm] % Hydrolysis
3	12	8	192.13	0.00	1	0.47	0.003	0	0%
3	15	10	195.17	3.03	1	0.41	0.002617	0.000383	13%
3	18	10	198.17	6.03	1	0.39	0.002489	0.000511	17%
3	21	12	201.20	9.07	1	0.36	0.002298	0.000702	23%
3	24	13	204.22	12.08	1	0.31	0.001979	0.001021	34%
3	27	15	207.25	15.12	1	0.31	0.001979	0.001021	34%
3	30	16	210.27	18.13	1	0.28	0.001787	0.001213	40%
3	33	18	213.30	21.17	1	0.24	0.001532	0.001468	49%
3	36	18	216.30	24.17	1	0.25	0.001596	0.001404	47%
3	39	20	219.33	27.20	1	0.21	0.00134	0.00166	55%
3	42	21	222.35	30.22	1	0.19	0.001213	0.001787	60%
3	45	23	225.38	33.25	1	0.16	0.001021	0.001979	66%
3	48	25	228.42	36.28	1	0.17	0.001085	0.001915	64%
3	51	25	231.42	39.28	1	0.15	0.000957	0.002043	68%
3	54	27	234.45	42.32	1	0.14	0.000894	0.002106	70%
3	57	28	237.47	45.33	1	0.13	0.00083	0.00217	72%
4	0	30	240.50	48.37	1	0.13	0.00083	0.00217	72%
4	3	30	243.50	51.37	1	0.09845	0.000628	0.002372	79%
4	6	32	246.53	54.40	1	0.1	0.000638	0.002362	79%
4	9	33	249.55	57.42	1	0.1	0.000638	0.002362	79%
4	12	35	252.58	60.45	1	0.09586	0.000612	0.002388	80%
4	15	35	255.58	63.45	1	0.0706	0.000451	0.002549	85%
4	18	37	258.62	66.48	1	0.07124	0.000455	0.002545	85%
4	21	38	261.63	69.50	1	0.06547	0.000418	0.002582	86%
4	24	40	264.67	72.53	1	0.04949	0.000316	0.002684	89%
4	27	40	267.67	75.53	1	0.07169	0.000458	0.002542	85%
4	30	42	270.70	78.57	1	0.05319	0.00034	0.00266	89%
4	33	43	273.72	81.58	1	0.04319	0.000276	0.002724	91%
4	36	44	276.73	84.60	1	0.03854	0.000246	0.002754	92%
4	39	46	279.77	87.63	1	0.03266	0.000208	0.002792	93%

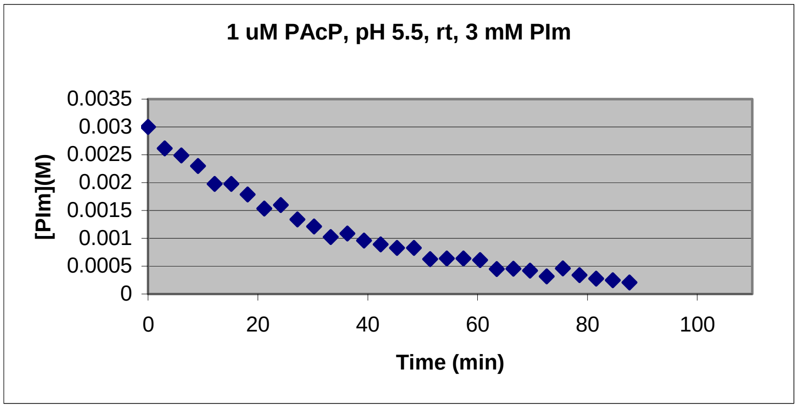

Figure A22. Plot of the data in Table A1. Curvature can be seen in the data.

Literature reports that if a time-course proceeds to 90% or more reliable data can be had.[1,2] This matches attempts herein to least-squares fit time-courses. Shorter time-courses may not display curvature. In nearly all cases attainment of 90% hydrolysis yields visible curvature and good fit of the data to the Michaelis-Menton equation with inhibition.

Experiments must be conducted with different concentrations of enzyme and substrate that yield curvature to the hydrolysis plot (Figure A22). Too little substrate concentration or too high an enzyme concentration and the reaction will be completed before enough data points are collected. Further, the rates between data points will be too great to represent instantaneous data points; no curvature will be seen (Figure A23).

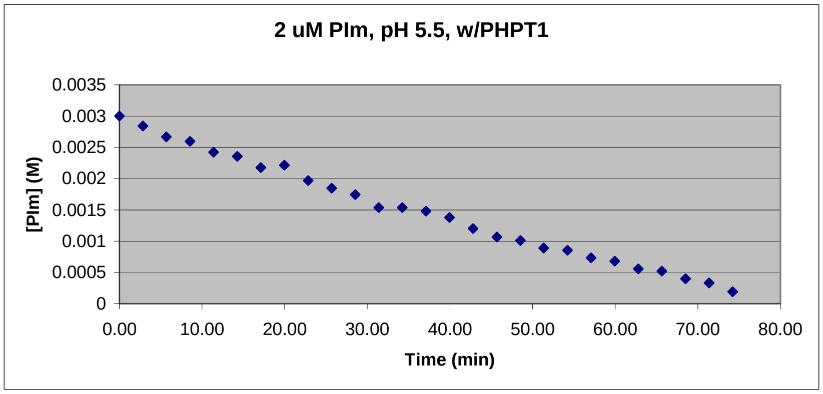

Figure A23. The hydrolysis of PIm by PHPT1 at pH 8.5. No curvature in seen in the plot. Enzyme concentration could be reduced or substrate concentration could be increased to create curvature.

For the enzymes used in this study, it was observed that hydrolysis proceeded rapidly until 50~70% consumption, whereupon the rate rapidly declined. Whereas 70% hydrolysis may be obtained in 30 minutes, the remaining 20% could take an hour. Issues of enzyme stability, instrument shimming, and instrument reservation time become important. Several experiments are necessary to find a suitable concentration of substrate and enzyme. Experience indicates that a full time-course reactions conducted by NMR can be completed in an hour to an hour and a half with curvature to the plot and 90% hydrolysis.

If the results of the NMR experiment meet the curvature and 90% hydrolysis requirements, data may be moved from Excel to Scientist. To do so, the Excel data is imported directly into a Scientist dataset (Figure A24). A mathematical model is entered (Figure A25). Scientist has mathematical models that may be obtained from the “model” menu; one of these models is the Michaelis-Menton equation. This model was used as the starting equation and was modified on the computer screen to equation A1, the

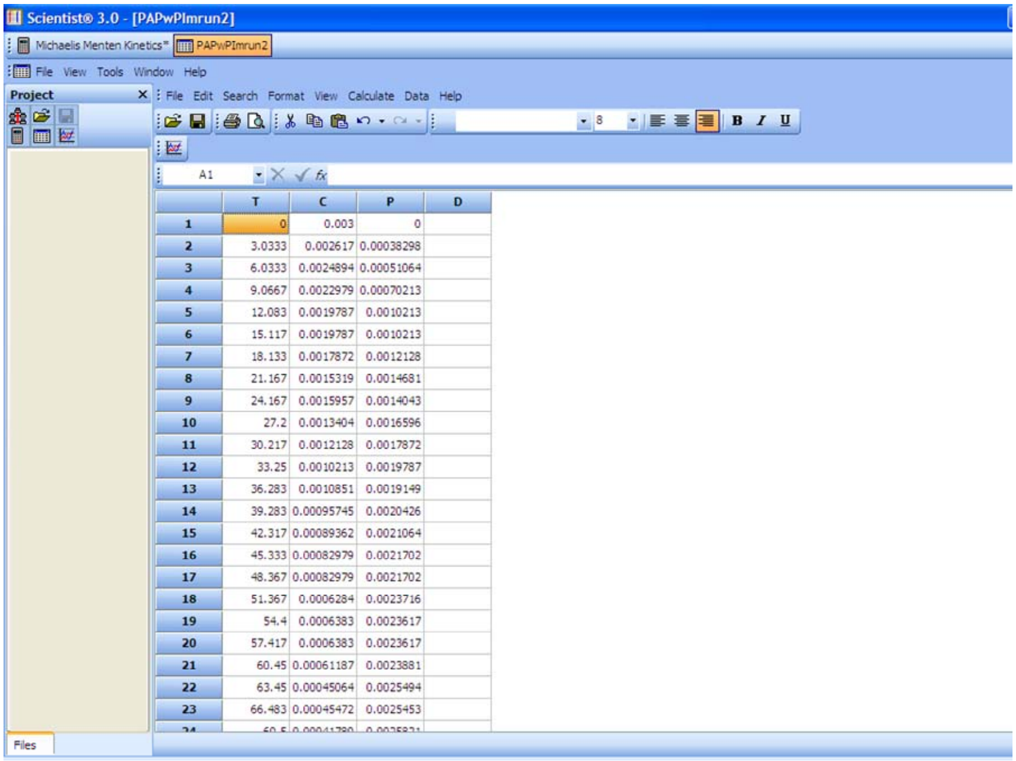
Scientist® 3.0 - [PAPwPImrun2]
Michaelis Menten Kinetics*
PAPwPImrun2
File View Tools Window Help
Project
File Edit Search Format View Calculate Data Help
A1
Files

	T	C	P	D
1	0	0.003	0	
2	3.0333	0.002617	0.00038298	
3	6.0333	0.0024894	0.00051064	
4	9.0667	0.0022979	0.00070213	
5	12.083	0.0019787	0.0010213	
6	15.117	0.0019787	0.0010213	
7	18.133	0.0017872	0.0012128	
8	21.167	0.0015319	0.0014681	
9	24.167	0.0015957	0.0014043	
10	27.2	0.0013404	0.0016596	
11	30.217	0.0012128	0.0017872	
12	33.25	0.0010213	0.0019787	
13	36.283	0.0010851	0.0019149	
14	39.283	0.00095745	0.0020426	
15	42.317	0.00089362	0.0021064	
16	45.333	0.00082979	0.0021702	
17	48.367	0.00082979	0.0021702	
18	51.367	0.0006284	0.0023716	
19	54.4	0.0006383	0.0023617	
20	57.417	0.0006383	0.0023617	
21	60.45	0.00061187	0.0023881	
22	63.45	0.00045064	0.0025494	
23	66.483	0.00045472	0.0025453	

Figure A24. A dataset entered into Scientist. This data is that from Table A1.

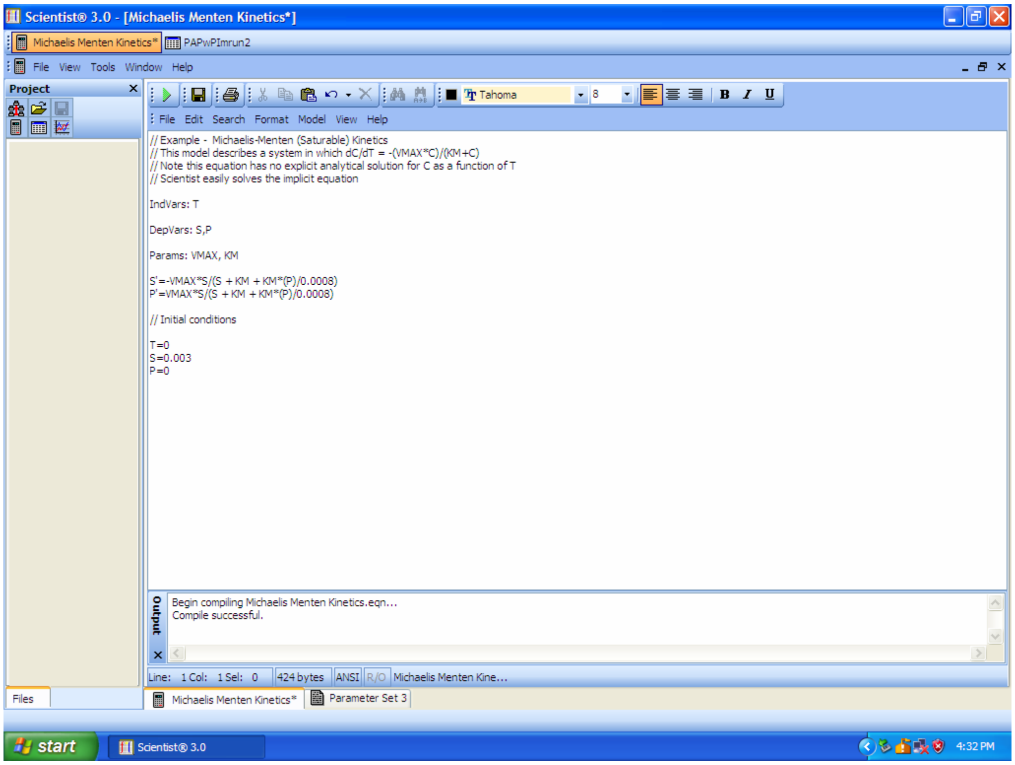
Scientist® 3.0 - [Michaelis Menten Kinetics*]
Michaelis Menten Kinetics*
PAPwPImrun2
File View Tools Window Help
Project
Tahoma
8
File Edit Search Format Model View Help
Output
Line: 1 Col: 1 Sel: 0
424 bytes
ANSI
R/O
Michaelis Menten Kine...
Files
Michaelis Menten Kinetics*
Parameter Set 3
start
Scientist® 3.0
4:32 PM

```
// Example -  Michaelis-Menten (Saturable) Kinetics
// This model describes a system in which dC/dT = -(VMAX*C)/(KM+C)
// Note this equation has no explicit analytical solution for C as a function of T
// Scientist easily solves the implicit equation

IndVars: T

DepVars: S,P

Params: VMAX, KM

S'=-VMAX*S/(S + KM + KM*(P)/0.0008)
P'=VMAX*S/(S + KM + KM*(P)/0.0008)

// Initial conditions

T=0
S=0.003
P=0
```

```
Begin compiling Michaelis Menten Kinetics.eqn...
Compile successful.
```

Figure A25. A mathematical model inputted into Scientist.

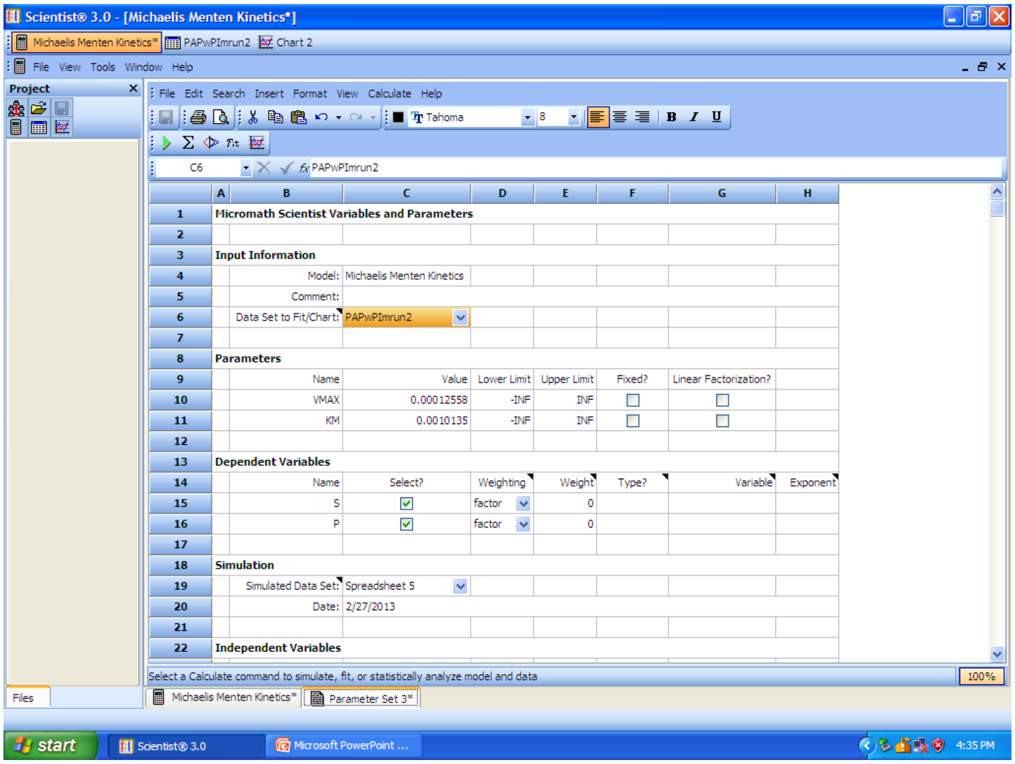
Scientist® 3.0 - [Michaelis Menten Kinetics*]
Michaelis Menten Kinetics*
PAPwPImrun2
Chart 2
File View Tools Window Help
Project
File Edit Search Insert Format View Calculate Help
Tahoma
8
C6
PAPwPImrun2
Files
Michaelis Menten Kinetics*
Parameter Set 3*
start
Scientist® 3.0
Microsoft PowerPoint ...
4:35 PM
100%

	A	B	C	D	E	F	G	H
1	Micromath Scientist Variables and Parameters							
2								
3	Input Information							
4		Model:	Michaelis Menten Kinetics					
5		Comment:						
6		Data Set to Fit/Chart:	PAPwPImrun2					
7								
8	Parameters							
9		Name	Value	Lower Limit	Upper Limit	Fixed?	Linear Factorization?	
10		VMAX	0.00012558	-INF	INF	☐	☐	
11		KM	0.0010135	-INF	INF	☐	☐	
12								
13	Dependent Variables							
14		Name	Select?	Weighting	Weight	Type?	Variable	Exponent
15		S	☑	factor	0			
16		P	☑	factor	0			
17								
18	Simulation							
19		Simulated Data Set:	Spreadsheet 5					
20		Date:	2/27/2013					
21								
22	Independent Variables							

Select a Calculate command to simulate, fit, or statistically analyze model and data

Figure A26. A Scientist parameter set.

Michaelis-Menton equation with inhibition. A blank parameter set is generated using the "New parameter set" command from the pull-down menu (Figure A26). Menus on the parameter set link the parameter set to the data and the mathematical model. The parameter set is "compiled" using the "compile" function from the pull-down menu, followed by "least squares fitting" from the pull down menu. Micromath will then fit the data from the menu and return values for the independent parameters, V_{max} and K_M. Returning to Micromath's data spreadsheet will reveal the program's calculated values at each data point based upon the fit (Figure A27). A chart may be generated in the program to display the raw data and the fitted data (Figure A28).

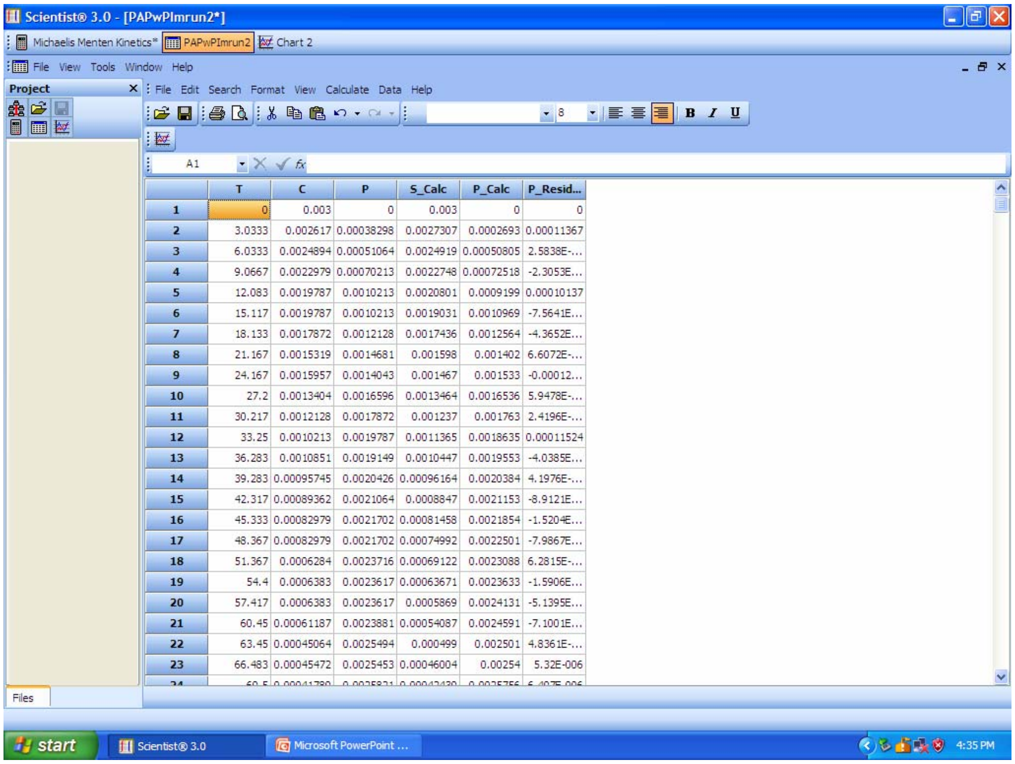
Scientist® 3.0 - [PAPwPImrun2*]
Michaelis Menten Kinetics*
PAPwPImrun2
Chart 2
File View Tools Window Help
Project
File Edit Search Format View Calculate Data Help
A1
Files
start
Scientist® 3.0
Microsoft PowerPoint ...
4:35 PM

	T	C	P	S_Calc	P_Calc	P_Resid...
1	0	0.003	0	0.003	0	0
2	3.0333	0.002617	0.00038298	0.0027307	0.0002693	0.00011367
3	6.0333	0.0024894	0.00051064	0.0024919	0.00050805	2.5838E-...
4	9.0667	0.0022979	0.00070213	0.0022748	0.00072518	-2.3053E...
5	12.083	0.0019787	0.0010213	0.0020801	0.0009199	0.00010137
6	15.117	0.0019787	0.0010213	0.0019031	0.0010969	-7.5641E...
7	18.133	0.0017872	0.0012128	0.0017436	0.0012564	-4.3652E...
8	21.167	0.0015319	0.0014681	0.001598	0.001402	6.6072E-...
9	24.167	0.0015957	0.0014043	0.001467	0.001533	-0.00012...
10	27.2	0.0013404	0.0016596	0.0013464	0.0016536	5.9478E-...
11	30.217	0.0012128	0.0017872	0.001237	0.001763	2.4196E-...
12	33.25	0.0010213	0.0019787	0.0011365	0.0018635	0.00011524
13	36.283	0.0010851	0.0019149	0.0010447	0.0019553	-4.0385E...
14	39.283	0.00095745	0.0020426	0.00096164	0.0020384	4.1976E-...
15	42.317	0.00089362	0.0021064	0.0008847	0.0021153	-8.9121E...
16	45.333	0.00082979	0.0021702	0.00081458	0.0021854	-1.5204E...
17	48.367	0.00082979	0.0021702	0.00074992	0.0022501	-7.9867E...
18	51.367	0.0006284	0.0023716	0.00069122	0.0023088	6.2815E-...
19	54.4	0.0006383	0.0023617	0.00063671	0.0023633	-1.5906E...
20	57.417	0.0006383	0.0023617	0.0005869	0.0024131	-5.1395E...
21	60.45	0.00061187	0.0023881	0.00054087	0.0024591	-7.1001E...
22	63.45	0.00045064	0.0025494	0.000499	0.002501	4.8361E-...
23	66.483	0.00045472	0.0025453	0.00046004	0.00254	5.32E-006

Figure A27. The data spreadsheet will display calculated values.

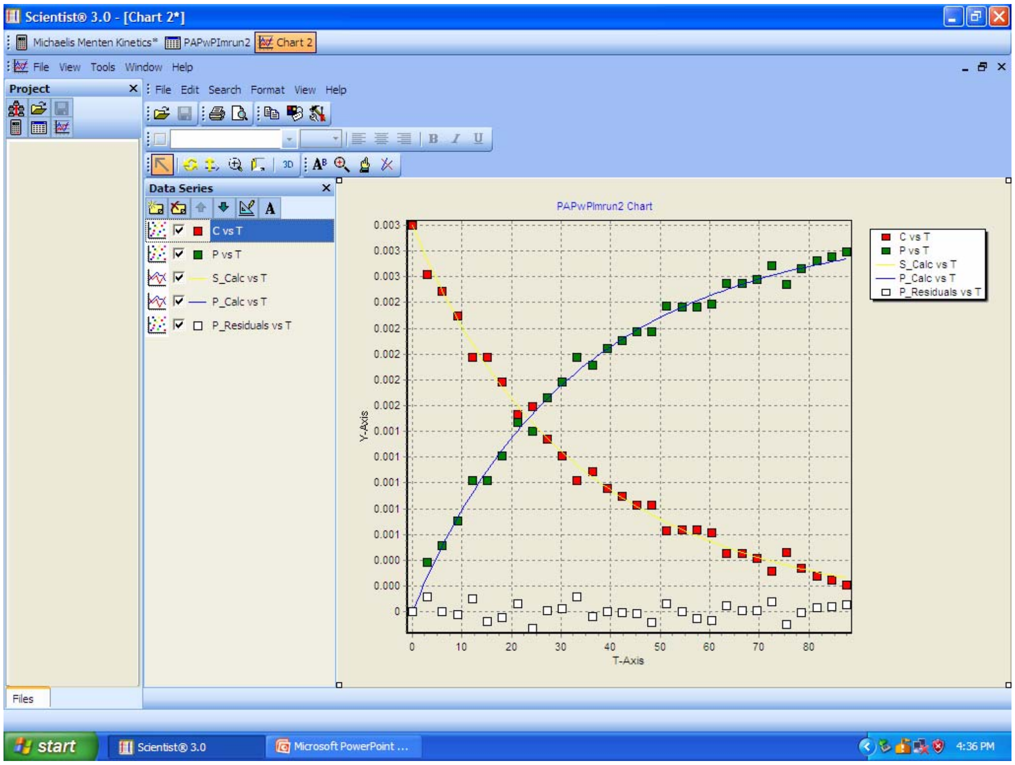
Scientist® 3.0 - [Chart 2*]
Michaelis Menten Kinetics*
PAPwPImrun2
Chart 2
File View Tools Window Help
Project
File Edit Search Format View Help
Data Series
☑ C vs T
☑ P vs T
☑ S_Calc vs T
☑ P_Calc vs T
☑ P_Residuals vs T
PAPwPImrun2 Chart
0.003
0.003
0.003
0.002
0.002
0.002
0.002
0.002
0.001
0.001
0.001
0.001
0.001
0.000
0.000
0
Y-Axis
0
10
20
30
40
50
60
70
80
T-Axis
C vs T
P vs T
S_Calc vs T
P_Calc vs T
P_Residuals vs T
Files
start
Scientist® 3.0
Microsoft PowerPoint ...
4:36 PM

Figure A28. A Micromath chart of the raw and fitted data.

The Scientist program was purchased from Micromath using funds from the Hengge Lab. Three licenses were purchased, two of which have been installed on desktop computers in the Hengge Lab. One key is unused at the time of this writing. Account information is: user name – Alvan Hengge; HWKEY – 1EC0-FB62; Key – 000015-W9JY7D-A2627V-93UZQD-RKETHQ-QT4UN1-ABA60M-0QUMXA-U1ETYC-K4UZ35. A manual for the program is available using the "Help" menu within the program.

References.

(1) Duggleby, R. G. *Methods* **2001**, *24*, 168-174.

(2) Duggleby, R. G.; Clarke, R. B. *Biochimica et Biophysica Acta* **1991**, *1080*, 231-236.

CURRICULUM VITAE

Mark P. Haney
2013

Curriculum Vitae.

Employment history: USMC, 1983-2003

Education:

Undergraduate school:
B.A., geology, University of Colorado at Boulder, Boulder, CO, 1992.

Graduate school:
Ph.D in chemistry, Utah State University, Logan, UT, 2013.
Dissertation: The Phosphoramidase Competency of Prototypical Catalytic Phosphatase Motifs.

Teaching experience (2007-present):

Teaching assistant for 19 general chemistry recitations, Chem 1210 & 1220, taught over 3 semesters.

Teaching assistant for 3 general chemistry labs, Chem 1215, taught during 1 semester.

Additionally, 3 labs are being taught in the current semester.

Teaching assistant for 4 organic chemistry labs, Chem 2315, taught over 2 semesters.

Taught organic chemistry lecture, Chem 2300, for two weeks while professor was away, Fall 2012.

Currently developing broadcast course for Chem 1010, to be taught 3 Mar to 23 May.

Research skills:

- Organic synthesis
- Synthesis of organo-phosphorus compounds
- Characterization using NMR, UV/Vis, IR, HPLC
- Kinetic assays using NMR, UV/Vis, HPLC
- Able to operate NMR, UV/Vis, IR, HPLC
- Data analysis (least squares fitting using computer software)
- 3D computer modeling using PYMOL and Acclerys viewer pro

- Bacterial cell transformation, growth, and protein expression
- Protein preparation (cell lysis and purification using FPLC or protein precipitation)
- Able to choose appropriate column and operate FPLC

Laboratory skills:

- Inventory and manage storage of chemicals (MSDS, storage compatibility, etc.)
- Order chemicals and supplies
- Store and manage disposal of hazardous waste
- Service laboratory stills, high-vacuum pumps, heating/cooling baths, rotovaps, compressed gas tanks, etc.
- Fill NMR instruments with helium and nitrogen
- Maintain lab's safety program

Computer skills:

- Microsoft Word, Excel, Outlook
- PyMol
- Acclerys Design Studio
- Micromath by Scientist
- VisualEnzymics by SoftZymics
- KaleidaGraph by Synergy
- Agilent HPLC controller and processing software
- JEOL controller and processing software

Presentations:

Presented poster at American Society for Biochemistry and Molecular Biology, San Diego, 2012

Awards:

- USU Presidential Fellowship (2007-2008)
- Poster Award, Hansen Life Sciences Retreat (2012)
- Meritorious Service Medal, USMC (2003)

Professional Memberships:

Member of the American Chemical Society